Development of Fluorescein-Based Fluorescent Chemosensors

and

Convergent Approaches in Solid-Phase Organic Synthesis

by

Amanda L. Garner

Bachelor of Science, Allegheny College, 2003

Submitted to the Graduate Faculty of

Arts and Sciences in partial fulfillment

of the requirements for the degree of

Doctor of Philosophy

University of Pittsburgh

2008

UNIVERSITY OF PITTSBURGH

FACULTY OF ARTS AND SCIENCES

This dissertation was presented

by

Amanda L. Garner

It was defended on

September 25, 2008

and approved by

Kay M. Brummond, Professor, Department of Chemistry

Stephen G. Weber, Professor, Department of Chemistry

Billy W. Day, Professor, Department of Pharmaceutical Sciences

Dissertation Advisor: Kazunori Koide, Associate Professor, Department of Chemistry

Development of Fluorescein-Based Fluorescent Chemosensors

and

Convergent Approaches in Solid-Phase Organic Synthesis

Amanda L. Garner, PhD

University of Pittsburgh, 2008

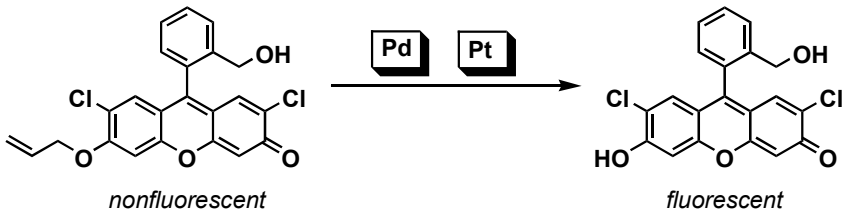

Projects 1,2: Palladium and platinum are widely used precious metals that play a pivotal role in energy, materials and drugs. In collaboration with Dr. Fengling Song, a highly sensitive fluorescent detection method has been developed for these metals based upon the Tsuji-Trost reaction. A key aspect of this method is the amplification of fluorescence signal directly through a catalytic process, which is conceptually new for metal sensors. Using this method, sub-ppb levels of both palladium and platinum can be detected. Importantly, detection of palladium in synthetic samples and detection of cisplatin in serum and crude samples are demonstrated, which have vast applications in the pharmaceutical industry, hospitals and pharmacies. Lastly, selective detection of palladium in the presence of platinum is demonstrated.

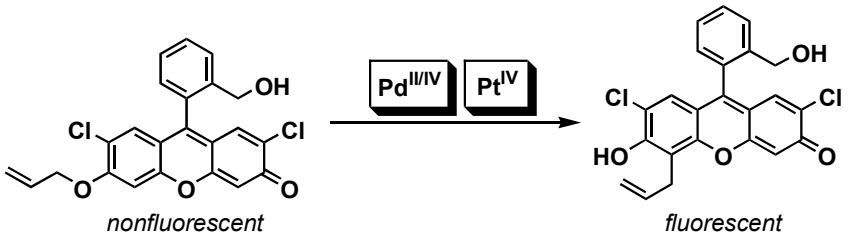

Project 3: Palladium- and platinum-catalyzed reactions are powerful reactions in synthetic organic chemistry. As such, each requires the metal in a specific oxidation state. A convenient fluorogenic probe capable of determining the oxidation state of palladium and platinum has been developed based on the Claisen rearrangement. This probe can fluorescently distinguish Pd^0 from $Pd^{II/IV}$ and Pt^0 from Pt^{IV} in both organic and aqueous solvents. Detection in functionalized organic compounds, reaction mixtures and a spiked platinum drink are demonstrated.

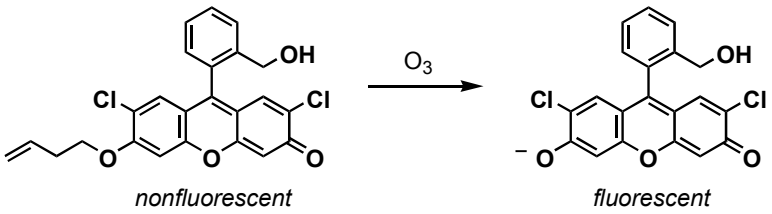

Project 4: Ozone exposure is a significant global health problem, especially in urban areas. While ozone in the stratosphere protects the earth from damaging ultraviolet light, tropospheric or ground level ozone is toxic, resulting in damage to the respiratory tract. The exact mechanism by which ozone damages the respiratory system is poorly understood. It has recently been shown that ozone may be produced endogenously in inflammatory and antibacterial responses of the immune system; however, these results have sparked controversy due to the use of a non-specific colorimetric probe. A fluorescent sensor capable of unambiguously detecting ozone has been

developed. Although many methods exist for ozone detection, this sensor is the first that is specific for ozone and can be used in both biological and atmospheric samples.

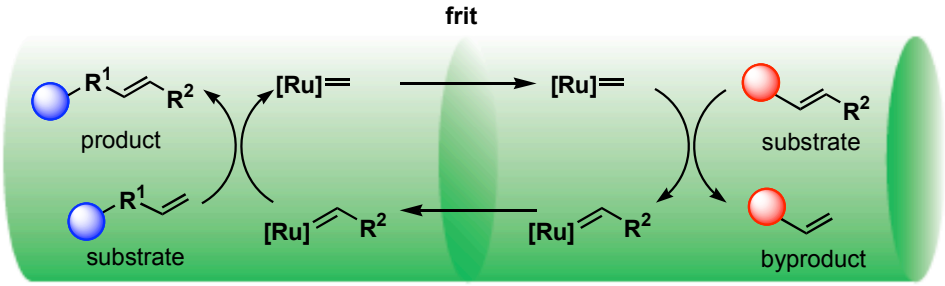

Project 5: Solid-phase organic synthesis is an enabling technology and its automation has profoundly impacted the scientific community and society in general. To date, however, the structural diversity of the molecules that can be synthesized by this technology is limited, partly because current solid-phase organic synthesis relies on linear approaches. Described here are efforts toward the development of an enabling resin-to-resin transfer technology that unites two functionalized fragments to form highly complex small molecules in a convergent manner. Such technology would allow for the synthesis of small molecules possessing natural product- and drug-like functionalities that are not readily accessible by conventional linear approaches.

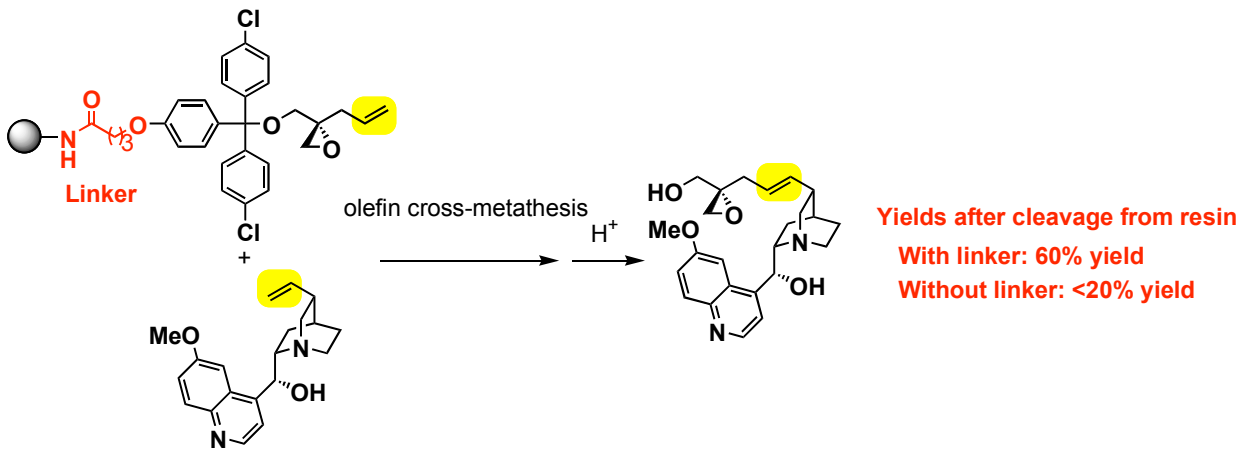

Olefin cross-metathesis couples two alkenes to form complex molecules and has been widely used in solution phase organic synthesis. This powerful method has rarely been used in solid-phase organic synthesis, however. Herein it is reported that olefin cross-metathesis is a synthetically viable method, particularly when a traceless, longer linker is inserted between solid support and reacting olefins.

TABLE OF CONTENTS

LIST OF TABLES

LIST OF FIGURES

ABBREVIATIONS AND ACRONYMS

Ac…….acetyl

API…….active pharmaceutical ingredient

Bn……benzyl

Bu……...butyl

Bz……..benzoyl

°C……..degrees Celsius

DCC…….*N,N'*-dicyclohexylcarbodiimide

DCE…….1,2-dichloroethane

DCF……2',7'-dichlorofluorescein

DDQ…….2,3-dichloro-5,6-dicyano-1,4-benzoquinone

DIBALH……...diisobutylaluminum hydride

DMF…….....dimethylformamide

DMSO……...dimethylsulfoxide

DOS……...diversity-oriented synthesis

Et……ethyl

HOBt……1-hydroxybenzotriazole

HOMO……highest occupied molecular orbital

hpf……..hours post fertilization

HPLC……...high performance liquid chromatography

ICP-MS……...inductively-coupled plasma mass spectrometry

LUMO…….lowest unoccupied molecular orbital

Me……...methyl

Mes……..2,4,6-trimethylphenyl

NMR……..nuclear magnetic resonance

Nu……nucleophile

PeT……photoinduced electron transfer

Ph……phenyl

ppb……parts per billion

ppm……..parts per million

ppt…….parts per trillion

Pr……propyl

ROS……..reactive oxygen species

TFA……..trifluoroacetic acid

TFP……....tri-2-furylphosphine

THF……...tetrahydrofuran

TLC…….thin-layer chromatography

TOF…….turnover frequency

Tr……..triphenylmethyl

Ts…….*para*-toluenesulfonyl

UV…….ultraviolet

Vis……...visible

ACKNOWLEDGEMENTS

I would like to take this opportunity to first thank Professor Kazunori Koide for his constant guidance and support throughout my undergraduate and graduate careers. I would also like to thank my committee members, Professors Kay Brummond and Steve Weber, for their assistance. I thank Dr. Fengling Song for his assistance throughout the palladium sensor development. I thank the NASA Space Grant and Novartis for providing graduate fellowships. I finally thank all of the people who have supported me throughout this journey of chemical exploration.

1.0 INTRODUCTION: SMALL MOLECULE-BASED FLUORESCENT CHEMOSENSORS

Fluorescence spectroscopy is a powerful method used to image otherwise invisible molecules.[1-4] A desirable probe interacts specifically with an analyte and fluoresces or changes color to indicate its presence. Fluorescent probes provide accessibility to real-time imaging in live cells, respond to a wide variety of biological signals and events, target sub-cellular compartments in a broad range of tissues and intact organisms and rarely cause photodynamic toxicity.[1] While many fluorescent sensors are based on green fluorescent protein (GFP) and its variants, small molecule-based fluorescent chemosensors are superior in that they are stable, easier to tune and change emission wavelength, provide faster rates of labeling and are available in large quantities. Thus, such fluorescent chemosensors are indispensable tools in biology.

Small molecule-based fluorescent sensors have provided novel approaches for the detection of metal ions, small organic compounds and biomolecules. These chemosensors are typically derived from a core group of well-known fluorophores, such as coumarin, fluorescein, rhodamine and BODIPY (Figure 1), each emitting in different regions of the electromagnetic spectrum.[4]

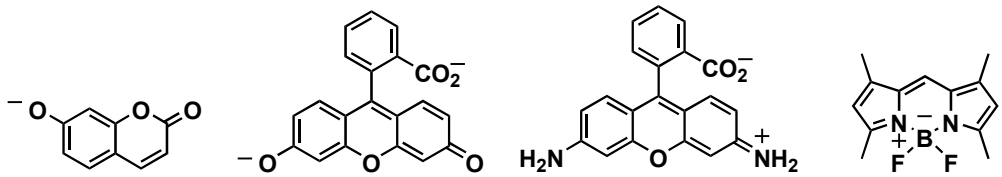

Figure 1. Well-known small molecule fluorophores

Practical fluorescent sensors must possess a few key properties: (1) produce a viable signal with high quantum yield upon selective interaction with the desired analyte; (2) exhibit an excitation wavelength (λ_{ex}) exceeding 340 nm to prevent UV-induced cell damage and an emission wavelength (λ_{em}) approaching 500 nm to avoid autofluorescence issues from species native to the cell; and (3) cell-permeability.[5] As described in Figure 1, the photophysical properties of the fluorophores depicted make them excellent platforms for fluorescent sensor development.

1.1 CHEMICAL PRINCIPLES OF "TURN-ON" FLUORESCENT SENSORS

Fluorescent probes are designed by chemically manipulating the fluorophore scaffold through the addition of side chains specific for the analyte of interest. As such, a variety of chemosensors can be designed simply by changing the attached group. Such modularity has given rise to diverse mechanisms of fluorescence induction, which are derived from two main chemical principles: molecular recognition and chemical reactivity. Descriptions of each principle with key examples follow below.

1.1.1 Molecular Recognition-Based Fluorescent Sensors – Photoinduced Electron Transfer

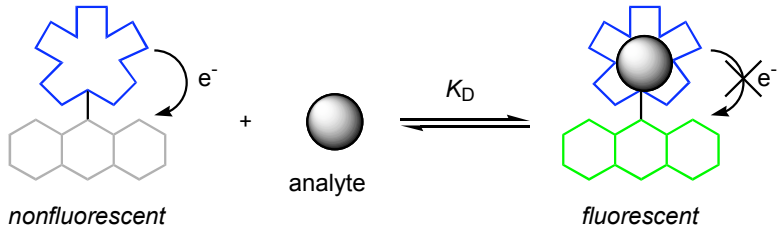

Figure 2. Generic scheme of fluorescent sensors based on a host that serves as a quencher

Many fluorescent sensors rely on molecular recognition whereby a fluorescent compound is covalently linked to a host moiety that also serves as a quencher (blue; Figure 2). In fact, one of the first fluorescent sensors, quin2, was based on this design principle for Ca^{2+} sensing (Figure 3).[6] This type of sensor generates virtually no fluorescence signal when free, while producing strong fluorescence signal when bound to its respective analyte.

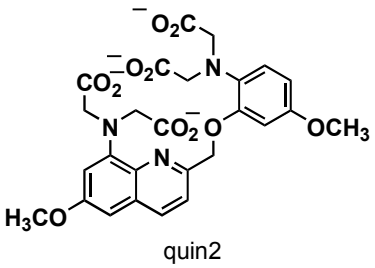

Figure 3. Ca^{2+} sensor based on molecular recognition

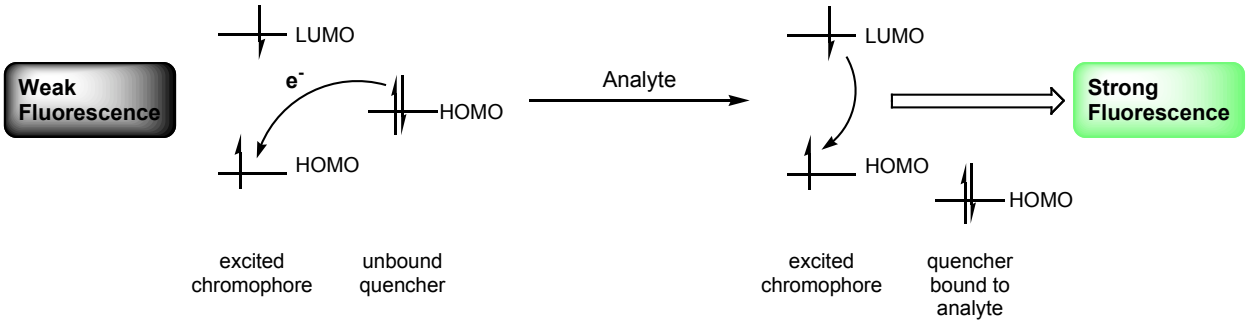

Figure 4. Photoinduced electron transfer (PeT) mechanism

The chemical principle by which these fluorescent off-on switches operate is the photoinduced electron transfer (PeT) mechanism shown in Figure 4.[7] In the weak fluorescence state, the fluorescence emission is quenched via an electron transfer process from the unbound quencher to the excited chromophore. For this electron transfer to occur, the HOMO energy level of the quencher must be higher than that of the chromophore but below the LUMO and in reasonable proximity. If the electrons of the quenchers are used for binding to an analyte, the energy of the quencher is then lowered. This energy lowering suppresses the electron transfer from the quencher to the excited chromophore, thereby restoring fluorescence. Thus, the efficiency of such PeT processes is attributed to the difference in the oxidation potential(s)[8,9] of the quencher(s) (electron donor) and the fluorophore (electron acceptor) and the distance[10] between the two. This principle is well established and numerous studies have been reported on the elucidation of PeT processes.

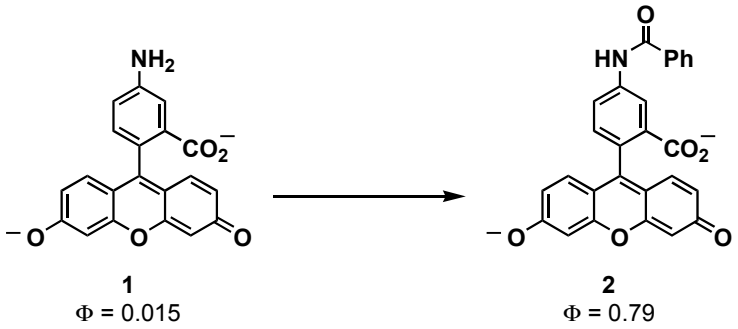

Figure 5. Reversible quenching via oxidation potential

In 1990, the Walt group reported one of the first studies examining the electronic impact on the quenching mechanism;[11] they studied the effect of intramolecular fluorescence self-quenching of fluoresceinamine **1** via covalent bond formation (Figure 5). Compound **1** exhibited a quantum yield (Φ) of 0.015 in pH 7.5 buffer, indicating significant quenching; however, upon amide bond formation to form compound **2**, a considerable increase in fluorescence intensity was

observed (Φ = 0.79), which is likely due to the change in the oxidation potential of the aniline unit (quencher). Thus, this study validates the electronic component of the PeT switch mechanism through π-bonds in the biologically useful fluorescein system.

Other PeT sensors consist of a quencher covalently linked to a fluorophore by a spacer of a certain length, which should also impact the PeT process through space.[7] The kinetics of distance-dependent quenching is expressed as:

$$k(r) = k_a \cdot e^{-\left(\frac{r-a}{r_e}\right)}$$

where k(r) is the rate of quenching at distance r, k_a is the rate of reaction at distance a, and r_e is the characteristic distance (distance where the probability of electron transfer is 50%). Distance a is the distance of closest approach, typically 5–7 Å. The characteristic distance, r_e, is typically 1–2 Å. Thus, as the distance between the quencher and the fluorophore is decreased, the rate of quenching (electron transfer) should increase exponentially. Santa examined this principle and reported a systematic study on the distance-dependent quenching of benzofurazan compounds **3** with linkers ranging from 2 to 12 carbons (Figure 6).[12]

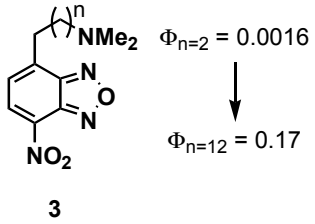

3

Figure 6. Trend in distance-dependent quenching

Not surprisingly, they found that when the quencher was located in closer proximity to the fluorophore (n = 2–4) increased quenching was observed, and when the quencher was located

farther away (n = 5–12) quenching was decreased. A similar trend was also observed in the rate of electron transfer (k_{et}).

Using this PeT process, many practical fluorescent chemosensors have been developed for a number of biologically relevant analytes. PeT sensors have been extensively reviewed.[13–16] A few examples of PeT sensors based on some common design strategies are highlighted below.

For fluorescent sensors to exhibit the greatest signal-to-background ratios in sensing analytes, the fluorescence signals of unbound sensors must be minimized. As a result, many PeT sensors include fluorophores attached to multiple electron donors, typically free amines, in order to achieve this goal. Some examples of sensors designed to include multiple amine quenchers are shown in Figure 7.

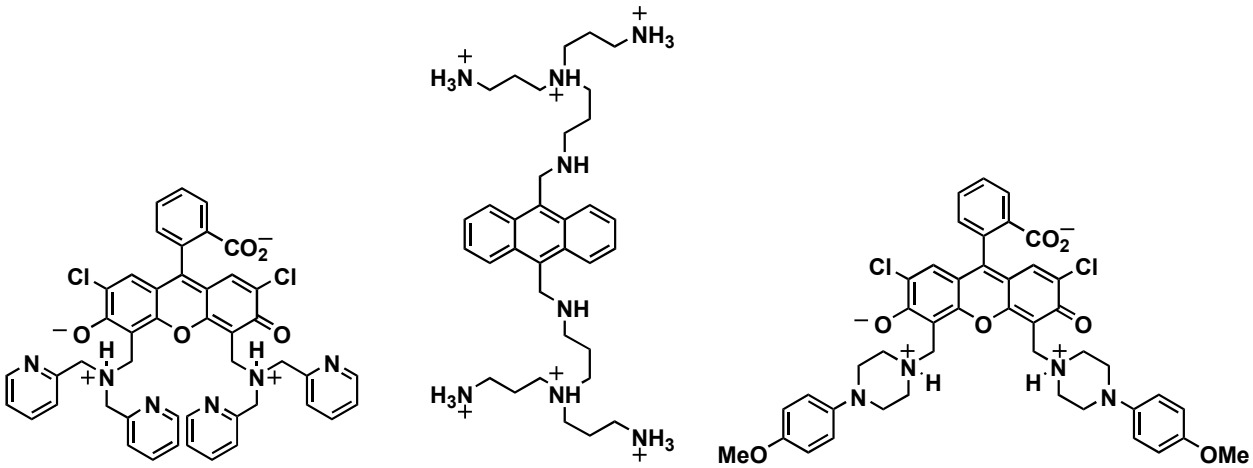

Figure 7. Examples of PeT sensors with multiple electron donors

Zinpyr-1 (**4**) is a fluorescent sensor for intracellular Zn^{2+} and contains two di-(2-picolyl)amine moieties as quenchers.[17,18] This sensor displays an approximate two-fold increase in fluorescence intensity with a Φ_{free} of 0.39 and Φ_{Zn} of 0.89 and is known to form a 1:1 Zn^{2+}:Zinpyr-1 complex. Czarnik developed anthracyl sensor **5** containing protonated polyamine

quenchers, which serves as a sensor for negatively charged phosphate oxygens.[19] The Koide group reported DCF-based sensor **6** using *N*-(*p*-methoxyphenyl)piperazine quenchers, which was used to image specific RNA aptamers.[20–22] Of the aptamers isolated, the best aptamer showed a 13-fold fluorescence enhancement upon binding.

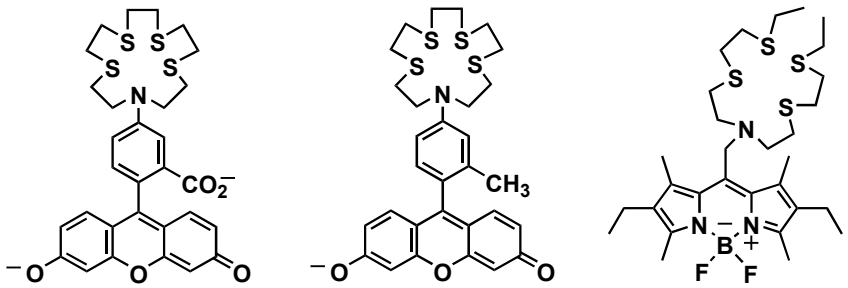

Figure 8. Examples of selective PeT fluorescent sensors

In addition to attaining good signal-to-background and sensitivity, selectivity for the respective analyte is also important in designing a useful PeT sensor. In order to gain selectivity for one analyte over another, a quenching ligand specific for that analyte is required. Three sensors that nicely emulate this concept are Mercuryfluor-1 (**7**),[23] Mercurygreen-1 (**8**)[24] and Coppersensor-1 (**9**),[25] all developed by the Chang group (Figure 8). Each of these sensors possesses thioether ligands selective for Hg^{2+} and Cu^{+}. Sensor **9** is the first fluorescent sensor that is specific for Cu^{+} over Cu^{2+}. Sensors **7** and **8** both selectively and sensitively detect Hg^{2+} in water, cells and tissue; and sensor **8** displays less quenching due to Hg^{2+} and a quantum yield of 0.72.

1.1.2 Molecular Recognition-Based Fluorescent Sensors – Restricted Conformation

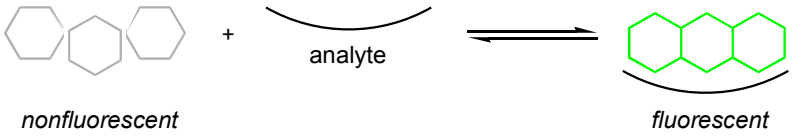

Figure 9. Generic scheme of fluorescent sensors based on conformational rigidity

While PeT sensors induce fluorescence by lowering the energy of the quenching moiety, another class of molecular recognition-based fluorescent sensors operates by affecting the conformation of the probe to produce a fluorescence signal. When free in solution, this type of binding-based sensor emits very low fluorescence due to vibrational deexcitation. Upon binding the analyte, the probe becomes rigid, prohibiting such nonradiative decay and a fluorescence signal is emitted (Figure 9).[26] This type of sensor is frequently used in DNA- and RNA-binding assays and a few examples are shown in Figure 10.

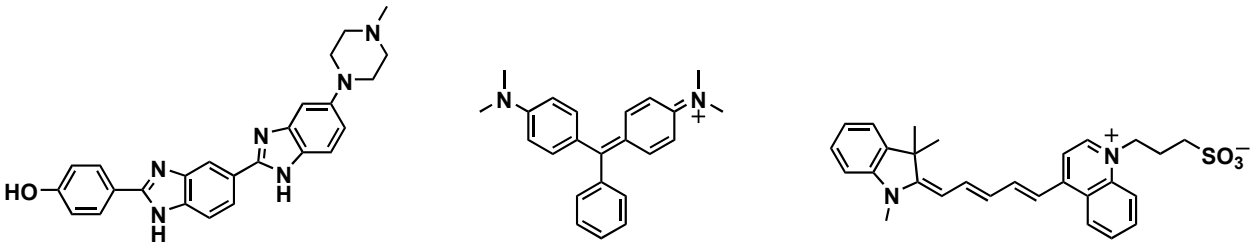

10
Hoechst 33258

11
Malachite Green

12
Dimethylindole Red

Figure 10. Examples of sensors that fluoresce via restricted conformation

Hoechst 33258 (**10**) is a widely used DNA staining reagent.[27] Malachite Green (**11**) was recently utilized as a sensor for a specific RNA aptamer and showed a ~2360-fold enhancement upon binding its specific aptamer.[28] Interestingly, the Tsien group was able to isolate RNA

aptamers specific for Malachite Green and a sulfonated triphenylmethane dye, and this is the first reported example of such specificity. Dimethylindole Red (**12**), an example of an unsymmetrical Cy dye, was recently reported by the Armitage group and is another example of an RNA sensor.[29] An RNA aptamer raised against this fluorophore showed a 60-fold fluorescence enhancement upon binding.

1.1.3 Reactivity-Based Fluorescent Sensors

There are many examples of successful fluorescent sensors based on molecular recognition; however, the binding activity is reversible. An alternative and more effective means of fluorescence induction would utilize the analyte to perform an irreversible chemical reaction that converts a nonfluorescent molecule to a fluorescent molecule. This approach has been used for the detection of metal ions, anions and reactive oxygen species among others, and these sensors have demonstrated enhanced selectivity as compared to their binding counterparts as shown below.

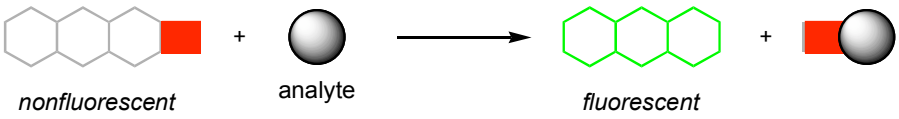

Figure 11. Generic scheme of reactivity-based sensor using a masking group

A common approach of masking a fluorophore (red in Figure 11) is by capping the phenol of fluorescein or coumarin or by forming the nonfluorescent fluorescein lactone by doubly substituting both xanthene oxygen substituents (Figure 12). This chemical principle is well known and originally derived from fluorometric enzyme assays developed in the early

1960's.[30–33] The earliest examples relied on each of these methods and were used to study β-galactosidase and lipase- and esterase-catalyzed hydrolysis reactions (Figure 12), and also applied to release fluorescence immunoassays[34] to study antibody-antigen binding.

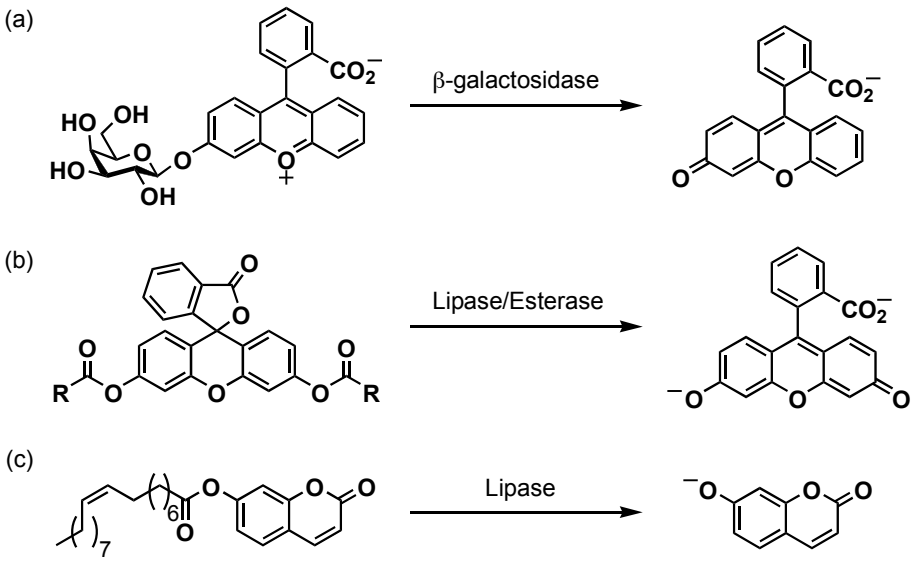

Figure 12. Examples of early fluorometric enzyme assays

Because of the success of this approach, it is still widely used today in biology in reporter gene assays (alkaline phosphatase, luciferase, β-galactosidase),[35] enzyme activity assays[36–38] and cat-ELISA.[39,40] Some more recent examples are shown in Figure 13.

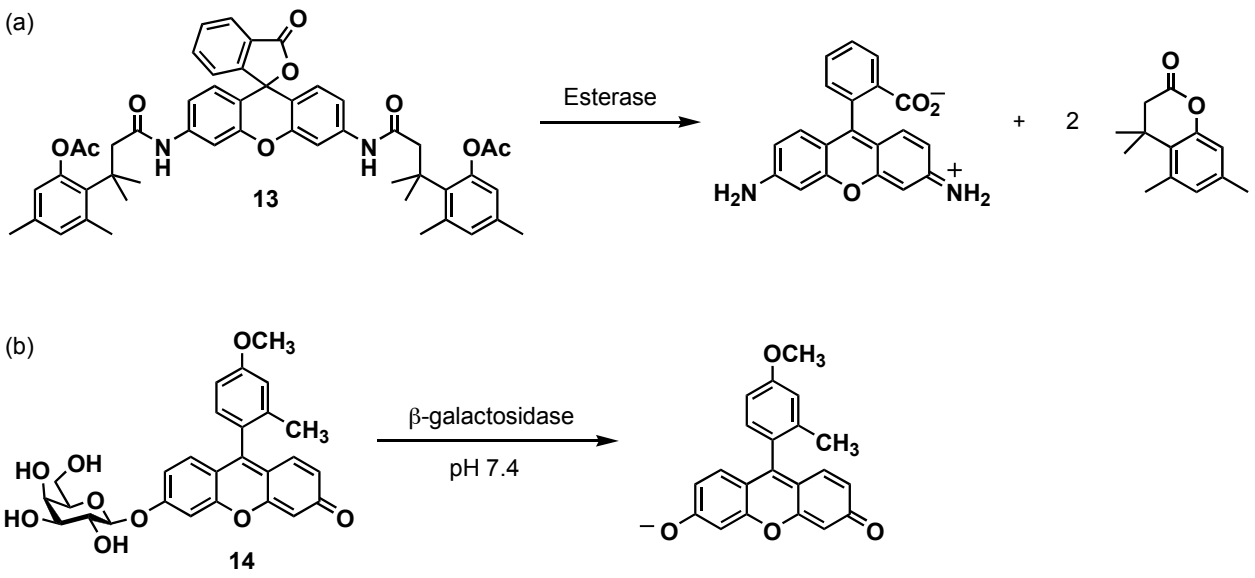

Figure 13. Recent examples of fluorometric enzyme assays

The Raines groups used this chemical principle to design latent rhodamine **13** based on the "trimethyl lock".[41,42] They reasoned that unfavorable steric interactions between the methyl substituents on the reactive side chain would encourage lactonization upon ester hydrolysis to form fluorescent rhodamine. This same "trimethyl lock" approach was recently utilized by the Kiessling group for visualizing the cellular internalization of multivalent ligands for biological analytes.[43] The Nagano group also utilized this approach to design mono-substituted fluorescein **14** based on their Tokyo Green fluorophore scaffold.[44] They demonstrated that this mono-substituted sensor showed many advantages over the di-substituted version in terms of sensitivity and in real-time imaging in live cells.

A key benefit of these fluorometric enzyme assays is the catalytic nature of the analyte, and thus the signal will be amplified dependent upon the efficiency of the catalyst. Most current reactivity-based sensors, however, use the analyte as a stoichiometric reagent, and the signal output for each is dependent upon the effectiveness of the chemical transformation. Examples of

reactivity-based sensors modeled after these similar chemical principles are described below: Figure 14 shows sensors based on the nonfluorescent lactone scaffold and Figure 15 shows sensors based on the phenolic capping scaffold.

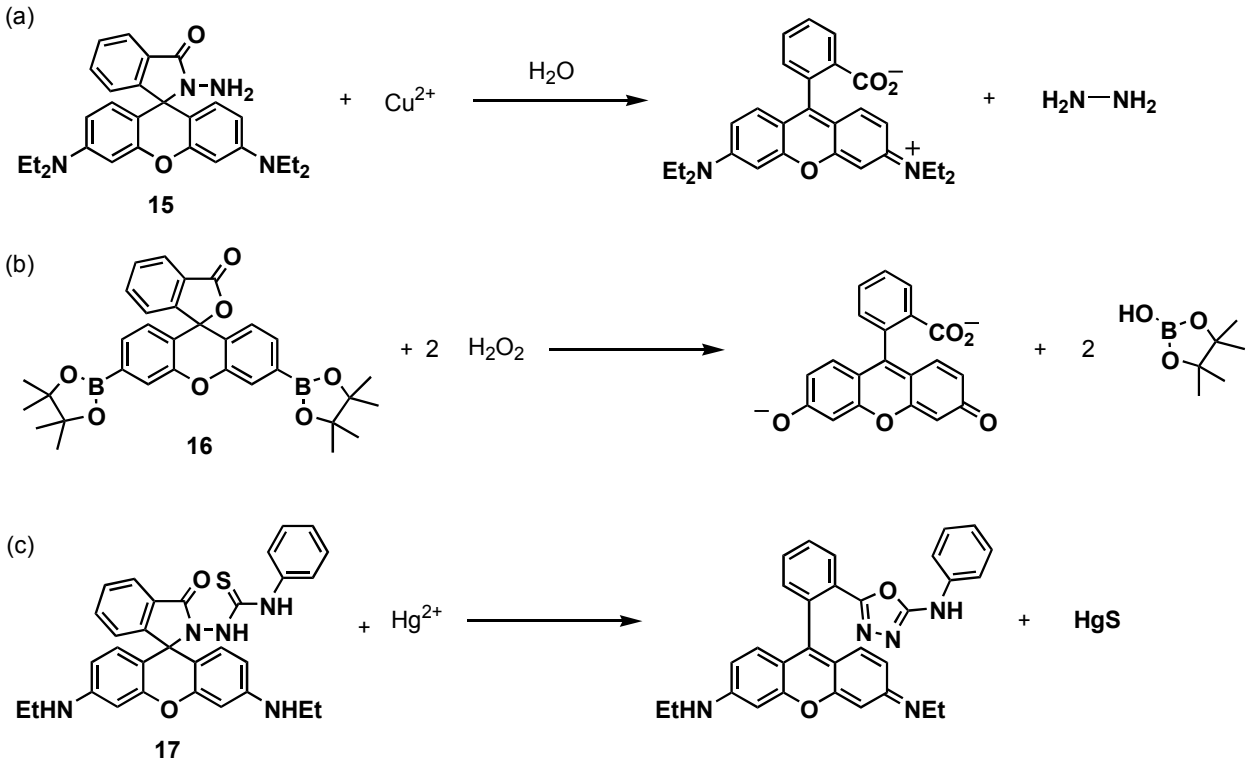

Figure 14. Examples of reactivity-based sensors with nonfluorescent lactone scaffold

Czarnik designed rhodamine hydrazide sensor **15** based on the affinity of Cu^{2+} for α-amino esters, which is the first example utilizing the power of Cu^{2+} to promote hydrolysis reactions.[45] In this case, although the Cu^{2+}-catalyzed ring opening is catalytic, the hydrolysis reaction was dependent upon the hydrazide concentration and nonintegral stoichiometry was observed. This concept has been used in several other more recent Cu^{2+} sensors.[46] Chang recently reported a selective, cell-permeable fluorescent probe for detecting hydrogen peroxide in living cells.[47,48] Sensor **16** is based on the ability of hydrogen peroxide to convert aryl

boronates to phenols, in this case to fluorescent fluorescein, and was recently followed up with a second-generation hydrogen peroxide sensor that specifically targets the mitochondria.[49] A selective probe for Hg^{2+} was developed by the Tae group, which takes advantage of the thiophilicity of this metal ion.[50,51] In this example, Hg^{2+} promotes the conversion of the thiosemicarbazide moiety in **17** to the 1,3,4-oxadiazole with subsequent ring opening and liberation of mercury sulfide to yield a fluorescent compound. This sensor is highly selective and can detect below 2 ppb Hg^{2+} in aqueous solution. In addition, the Kool group recently utilized this approach for fluorescent detection of nucleic acids.[52]

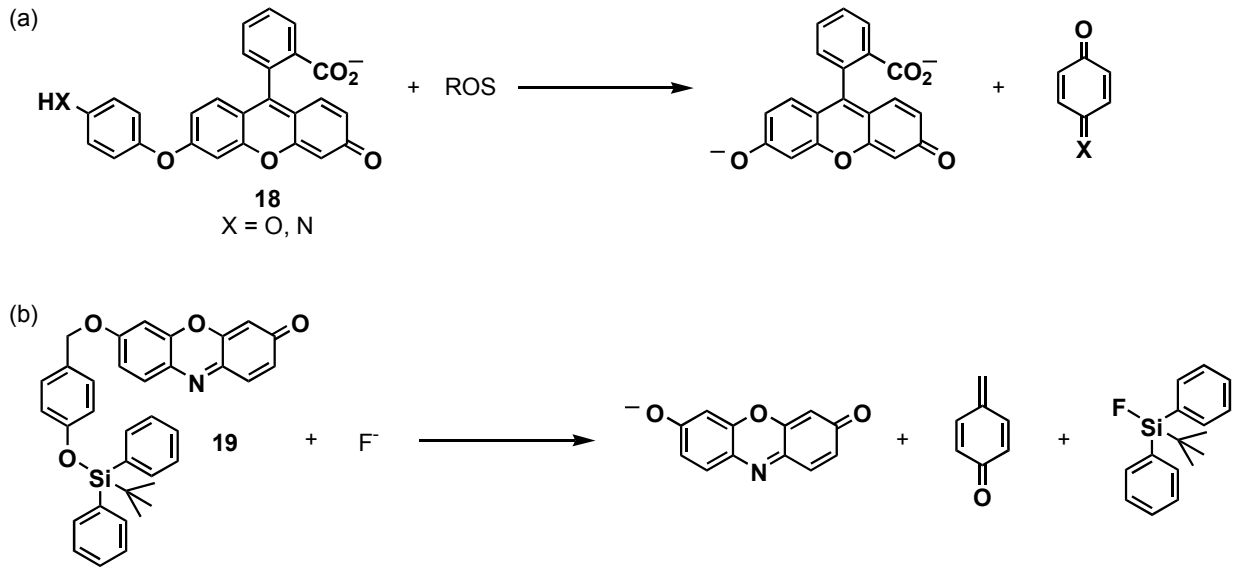

Figure 15. Examples of reactivity-based sensors with phenolic masking group

The Nagano group developed two fluorescein-based fluorescent sensors **18** (Figure 15) to distinguish various reactive oxygen species (ROS).[53] For example, hydroxyl radical can be distinguished from nitric oxide and peroxynitrite can be distinguished from nitric oxide and superoxide, each of which cannot be accomplished with other ROS fluorescent sensors. A

second example is from the Hong group for detecting fluoride.[54] Sensor **19** is based on the resorufin fluorophore and uses fluoride's ability to cleave silylethers to produce a fluorescence signal.

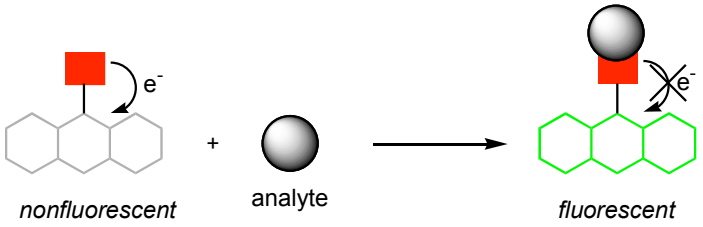

Figure 16. Generic scheme of reactivity-based sensors that operate by modifying a quenching group

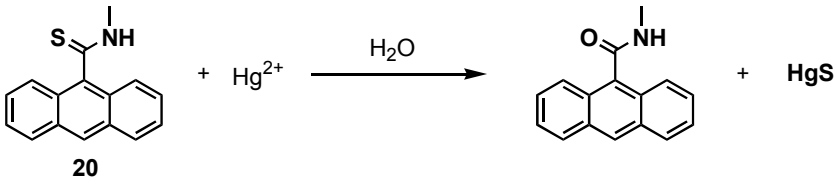

Figure 17. First example of reactivity-based sensor developed by Czarnik

Another principle in which reactivity-based sensors are designed is converting a quenching group (red; Figure 16) to a non-quenching group. In fact, Czarnik designed the first reactivity-based fluorescent sensor for metal ions using this concept in the early 1990's (Figure 17).[55] Anthracene-based sensor **20** showed selectivity toward mercury (87% reaction yield) and to a lesser extent for silver (73% reaction yield). Although the selectivity is lacking, this sensor represents the first example of rational fluorescent sensor design that converts a quenching moiety to a non-quenching moiety. Other examples are shown in Figure 18.

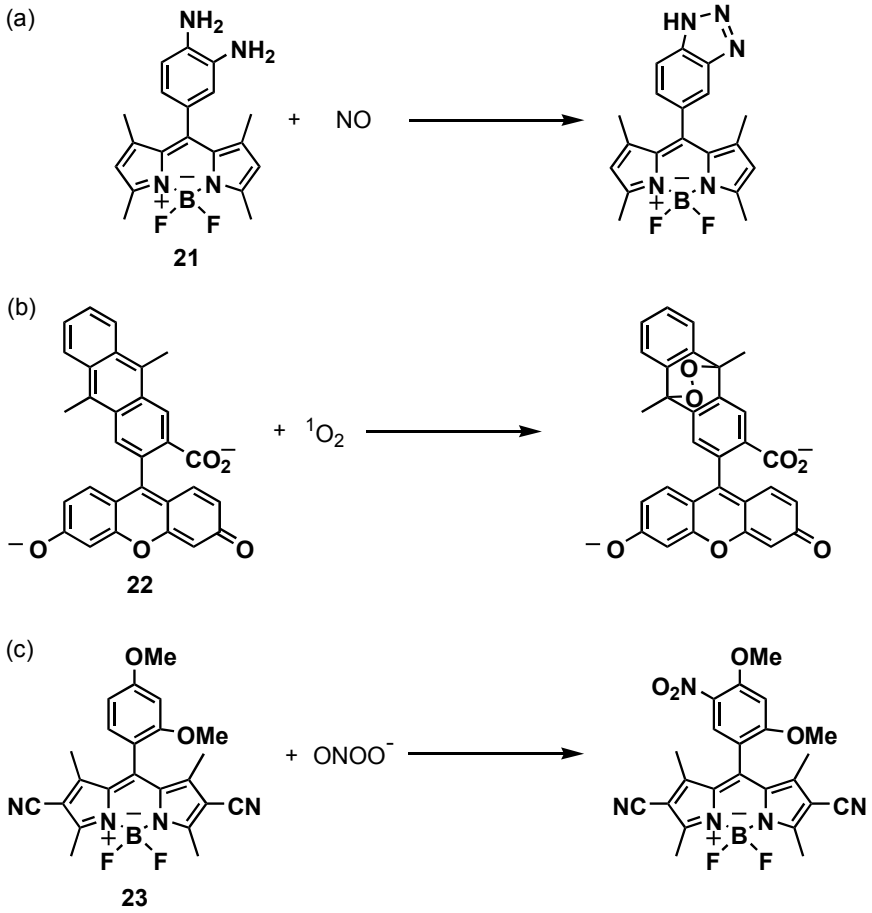

Figure 18. Examples of reactivity-based sensors that convert and quenching group to a non-quenching group

Each one of the sensors depicted in Figure 18 was carefully designed based on PeT to ensure quenching of the parent fluorophore and reactivity to ensure selectivity for the respective analyte by the Nagano group. Sensor **21** was designed to selectively detect nitric oxide based on the reactivity of aromatic amines with nitric oxide in the presence of dioxygen to produce triazenes.[56,57] Thus, by converting quenching adjacent primary amines to an aromatic triazene ring, they are able to selectively and sensitively detect nitric oxide even in living cells. Sensor **22**, which contains a quenching anthracyl moiety as the benzoic acid portion of fluorescein, was designed for selective detection of singlet oxygen.[58,59] The addition of singlet oxygen across the anthracene ring was effective in lowering the HOMO energy to produce a fluorescence signal;

and this sensor was capable of detecting singlet oxygen in both aqueous media and cells. Another mechanism-based probe was developed to detect nitrative stress by peroxynitrite.[60] BODIPY dye **1-23** was shown to selectively detect peroxynitrite by nitrating the di-methoxyphenyl substituent of the sensor to lower the HOMO energy of this quencher. This is the first example of a fluorescent sensor that can monitor aromatic nitration.

1.1.4 Catalytic Signal Amplification via Signal Transduction

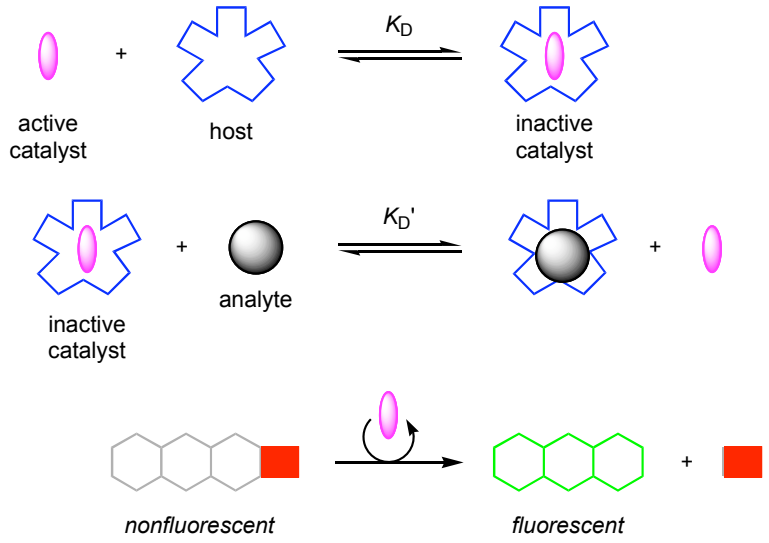

Figure 19. Generic scheme of sensors based on amplification via signal transduction

While the sensitivity of the reactivity-based sensors discussed above is impressive, the emitted signal is stoichiometric with respect to the analyte. To overcome this, the Anslyn group developed an approach for amplifying fluorescence signal (Figure 19).[61] In this approach, a ligand (= host; shown in blue) binds to a catalyst (shown in purple) to mask its reactivity; when an analyte binds to and replaces the catalyst in the ligand host, this complex formation releases the catalyst, which converts fluorogenic molecules to fluorescent molecules and amplifies

fluorescence signal. One drawback, however, is the fact that the binding is inevitably reversible, which generates active catalyst in the absence of the analyte, resulting in amplification of the background fluorescence signal. Additionally, more parameters must be optimized in this approach than in other approaches, presumably requiring laborious work. Although this does not match the catalytic power of fluorometric enzyme assays, it is a clever method of amplifying fluorescence signal. Some examples of sensors based on this principle are shown in Figure 20.

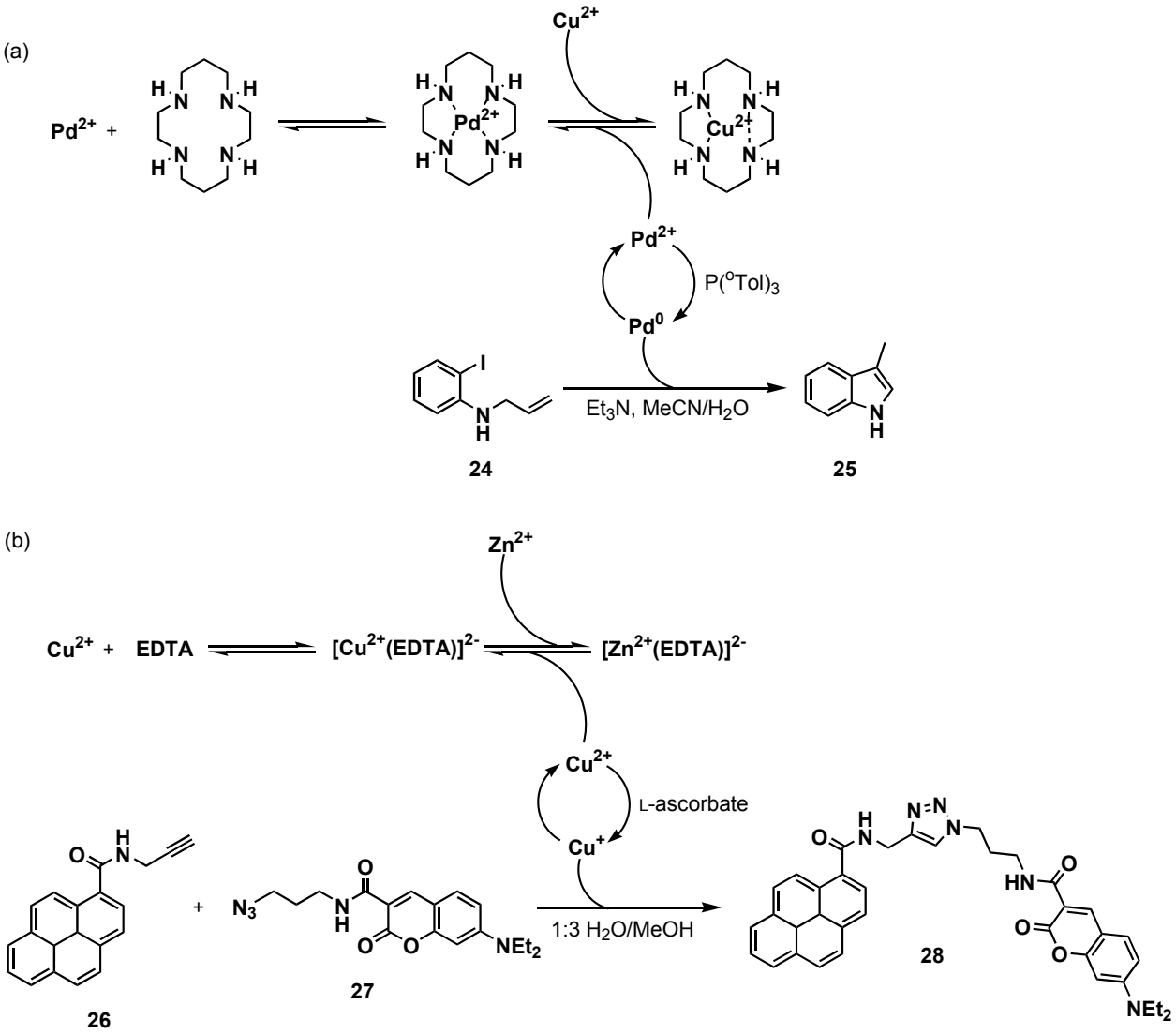

Figure 20. Examples of sensors based on catalytic signal amplification

The first reported example of this approach was a detection method for Cu^{2+} using the Pd-catalyzed Heck reaction shown in Figure 20a.[61] In this case, a cyclam ligand is used to preferentially bind Cu^{2+} to free Pd^{2+}, which after reduction catalyzes the ring closing of compound **24** to form fluorescent indole **25**. The detection limit of this method was 30 nM Cu^{2+} in 1.5 h. Another example from the same group used the copper-catalyzed Huisgen cycloaddition to detect Zn^{2+} and Pb^{2+} (Figure 20b).[62] In this case, the analyte displaces Cu^{2+} from the EDTA ligand for subsequent reduction by L-ascorbate. This Cu^{+} species then catalyzes the cycloaddition reaction between **26** and **27** to produce a ratiometric fluorescence signal (**28**). Although not shown, this system has also been utilized to detect small molecules (ketones and aldehydes)[63] and biomolecules (DNA).[64,65]

1.2 CONCLUSION

A survey of the literature reveals two main chemical principles in which fluorescent sensors are designed: molecular recognition and chemical reactivity. Using these principles, fluorescent sensors for metal ions, biomolecules, small molecules and reactive oxygen species have been designed. Although binding-based sensors and stoichiometric reactivity-based sensors are useful, a more effective method of fluorescence detection would utilize the analyte in catalysis for fluorescence signal amplification. While initial efforts dedicated to this goal are promising, much more work remains to obtain similar signal amplification observed in fluorometric biological assays for metal ion sensing.

1.3 BIBLIOGRAPHY

1. Zhang, J., Campbell, R. E., Ting, A. Y., Tsien, R. Y., "Creating new fluorescent probes for cell biology." *Nat. Rev. Mol. Cell. Biol.* **2002**, *3*, 906–918.

2. Giepmans, B. N. G., Adams, S. R., Ellisman, M. H., Tsien, R. Y., "The fluorescent toolbox for assessing protein location and function." *Science* **2006**, *312*, 217–224.

3. Domaille, D. W., Que, E. L, Chang, C. J., "Synthetic fluorescent sensors for studying the cell biology of metals." *Nat. Chem. Biol.* **2008**, *4*, 168–175.

4. Lavis, L. D., Raines, R. T., "Bright ideas for chemical biology." *ACS Chem. Biol.* **2008**, *3*, 142–155.

5. Czarnik, A. W., "Desperately seeking sensors." *Chem. Biol.* **1995**, *2*, 423–428.

6. Tsien, R. Y., Pozzan, T., Rink, T. J., "Calcium homeostasis in intact lymphocytes: cytoplasmic free calcium monitored with a new, intracellularly trapped fluorescent indicator." *J. Cell Biol.* **1982**, *94*, 325–334.

7. Lakowicz, J. R., "Principles of fluorescence spectroscopy, 3rd ed.", Springer Science+Business Media, New York, 2006.

8. Weller, A., "Electron-transfer and complex formation in the excited state." *Pure Appl. Chem.* **1968**, *16*, 115–123.

9. Rehm, D., Weller, A., "Kinetics of fluorescence quenching by electron and H-atom transfer." *Isr. J. Chem.* **1970**, *8*, 259–271.

10. Barbara, P. F., Meyer, T. J., Ratner, M. A. "Contemporary issues in electron transfer research." *J. Phys. Chem.* **1996**, *100*, 13148–13168.

11. Munkholm, C., Parkinson, D-R., Walt, D. R. "Intramolecular fluorescence self-quenching of fluoresceinamine." *J. Am. Chem. Soc.* **1990**, *112*, 2608–2612.

12. Onoda, M., Uchiyama, S., Santa, T., Imai, K., "The effects of spacer length on the fluorescence quantum yields of the benzofurazan compounds bearing a donor-acceptor system." *Luminescence* **2002**, *17*, 11–14.

13. de Silva, A. P., Gunaratne, H. Q. N., Gunnlaugsson, T., Huxley, A. J. M., McCoy, C. P., Rademacher, J. T., Rice, T. E., "Signaling recognition event with fluorescent sensors and switches." *Chem. Rev.* **1997**, *97*, 1515–1566.

14. Valeur, B., Leray, I., "Design principles of fluorescent molecular sensors for cation recognition." *Coord. Chem. Rev.* **2000**, *205*, 3–40.

15. de Silva, A. P., Fox, D. B., Huxley, A. J. M., Moody, T. S., "Combining luminescence, coordination and electron transfer for signaling purposes." *Coord. Chem. Rev.* **2000**, *205*, 41–57.

16. Callan, J. F., de Silva, A. P., Magri, D. C., "Luminescent sensors and switches in the early 21st century." *Tetrahedron* **2005**, *61*, 8551–8588.

17. Walkup, G. K., Burdette, S. C., Lippard, S. J., Tsien, R. Y., "A new cell-permeable fluorescent probe for Zn^{2+}." *J. Am. Chem. Soc.* **2000**, *122*, 5644–5645.

18. Burdette, S. C., Walkup, G. K., Spingler, B., Tsien, R. Y., Lippard, S. J., "Fluorescent sensors for Zn^{2+} based on a fluorescein platform: synthesis, properties and intracellular distribution." *J. Am. Chem. Soc.* **2001**, *123*, 7831–7841.

19. Huston, M. E., Haider, K. W., Czarnik, A. W., "Chelation-enhanced fluorescence in 9,10-bis(TMEDA)anthracene." *J. Am. Chem. Soc.* **1988**, *110*, 4460–4462.

20. Sparano, B. A., Shahi, S. P., Koide, K., "Effect of binding and conformation on fluorescence quenching in new 2',7'-dichlorofluorescein derivatives." *Org. Lett.* **2004**, *6*, 1947–1949.

21. Sparano, B. A., Koide, K., "A strategy for the development of small-molecule-based sensors that strongly fluoresce when bound to a specfic RNA." *J. Am. Chem. Soc.* **2005**, *127*, 14954–14955.

22. Sparano, B. A., Koide, K., "Fluorescent sensors for specific RNA: a general paradigm using chemistry and combinatorial biology." *J. Am. Chem. Soc.* **2007**, *129*, 4785–4794.

23. Yoon, S., Albers, A. E., Wong, A. P., Chang, C. J, "Screening mercury levels in fish with a selective fluorescent chemosensor." *J. Am. Chem. Soc.* **2005**, *127*, 16030–16031.

24. Yoon, S., Miller, E. W., He, Q., Do, P. H., Chang, C. J., "A bright and specific fluorescent sensor for mercury in water, cells, and tissue." *Angew. Chem. Int. Ed.* **2007**, *46*, 6658–6661.

25. Zeng, L., Miller, E. W., Pralle, A., Isacoff, E. Y., Chang, C. J., "A selective turn-on fluorescent sensor for imaging copper in living cells." *J. Am. Chem. Soc.* **2006**, *128*, 10–11.

26. Oster, G., Nishijima, Y., "Fluorescence and internal rotation: their dependence on viscosity of the medium." *J. Am. Chem. Soc.* **1956**, *78*, 1581–1584.

27. Comings, D. E., "Mechanisms of chromosome banding VIII. Hoechst-33258-DNA interaction." *Chromosoma* **1975**, *52*, 229–243.

28. Babendure, J. R., Adams, S. R., Tsien, R. Y., "Aptamers switch on fluorescence of triphenylmethane dyes." *J. Am. Chem. Soc.* **2003**, *125*, 14716–14717.

29. Constantin, T. P., Silva, G. L., Robertson, K. L., Hamilton, T. P., Fague, K., Waggoner, A. S., Armitage, B. A., "Synthesis of new fluorogenic cyanine dyes and incorporation into RNA fluoromodules." *Org. Lett.* **2008**, *10*, 1561–1564.

30. Rotman, B., "Measurement of activity of single molecules of β-D-galactosidase." *Proc. Natl. Acad. Sci. U. S. A.* **1961**, *47*, 1981–1991.

31. Rotman, B., Papermaster, B. W., "Membrane properties of living mammalian cells as studied by enzymatic hydrolysis of fluorogenic esters." *Proc. Natl. Acad. Sci. U. S. A.* **1966**, *55*, 134–141.

32. Guilbault, G. G., Kramer, D. N., "Lipolysis of fluorescein and eosin esters. Kinetics of hydrolysis." *Anal. Biochem.* **1966**, *14*, 28–40.

33. Jacks, T. J., Kircher, H. W., "Fluorometric assay for the hydrolytic activity of lipase using fatty acyl esters of 4-methylumbelliferone." *Anal. Biochem.* **1967**, *21*, 279–285.

34. Hemmilä, I., "Fluoroimmunoassays and immunofluorometric assays." *Clin. Chem.* **1985**, *31*, 359–370.

35. Alam, J., Cook, J. L., "Reporter genes: application to the study of mammalian gene transcription." *Anal. Biochem.* **1990**, *188*, 245–254.

36. Haugland, R. P., Johnson, I. D., "Detecting enzymes in living cells using fluorogenic substrates." *J. Fluorescence* **1993**, *3*, 119–127.

37. Wahler, D., Reymond, J-L., "High-throughput screening for biocatalysts." *Curr. Opn. Biotech.* **2001**, *12*, 535–544.

38. Goddard, J-P., Reymond, J-L., "Recent advances in enzyme assays." *TRENDS Biotech.* **2004**, *22*, 363–370.

39. Tawfik, D. S., Green, B. S., Chap, R., Sela, M., Eshhar, Z., "catELISA: a facile general route to catalytic antibodies." *Proc. Natl. Acad. Sci. U. S. A.* **1993**, *90*, 373–377.

40. MacBeath, G., Hilvert, D., "Monitoring catalytic activity by immunoassay: implications for screening." *J. Am. Chem. Soc.* **1994**, *116*, 6101–6106.

41. Chandran, S. S., Dickson, K. A., Raines, R. T., "Latent fluorophore based on the trimethyl lock." *J. Am. Chem. Soc.* **2005**, *127*, 1652–1653.

42. Lavis, L. D., Chao, T-Y., Raines, R. T., "Fluorogenic label for biomolecular imaging." *ACS Chem. Biol.* **2006**, *1*, 252–260.

43. Mangold, S. L., Carpenter, R. T., Kiessling, L. L., "Synthesis of fluorogenic polymers for visualizing cellular internalization." *Org. Lett.* **2008**, *10*, 2997–3000.

44. Urano, Y., Kamiya, M., Kanda, K., Ueno, T., Hirose, K., Nagano, T., "Evolution of fluorescein as a platform for finely tunable fluorescence probes." *J. Am. Chem. Soc.* **2005**, *127*, 4888–4894.

45. Dujols, V., Ford, F., Czarnik, A. W., "A long-wavelength fluorescent chemodosimeter selective for Cu(II) ion in water." *J. Am. Chem. Soc.* **1997**, *119*, 7386–7387.

46. For example: Xiang, Y., Tong, A., Jin, P., Ju, Y., "New fluorescent rhodamine hydrazone chemosensor for Cu(II) with high selectivity and sensitivity." *Org. Lett.* **2006**, *8*, 2863–2866.

47. Chang, M. C. Y., Pralle, A., Isacoff, E. Y., Chang, C. J., "A selective, cell-permeable optical probe for hydrogen peroxide in living cells." *J. Am. Chem. Soc.* **2004**, *126*, 15392–15393.

48. Miller, E. W., Albers, A. E., Pralle, A., Isacoff, E. Y., Chang, C. J., "Boronate-based fluorescent probes for imaging cellular hydrogen peroxide." *J. Am. Chem. Soc.* **2005**, *127*, 16652–16659.

49. Dickinson, B. C., Chang, C. J., "A targetable fluorescent probe for imaging hydrogen peroxide in the mitochondria of living cells." *J. Am. Chem. Soc.* **2008**, *130*, 9638–9639.

50. Yang, Y-K., Yook, K-J., Tae, J., "A rhodamine-based fluorescent and colorimetric chemodosimeter for the rapid detection of Hg^{2+} ions in aqueous media." *J. Am. Chem. Soc.* **2005**, *127*, 16760–16761.

51. Ko, S-K., Yang, Y-K., Tae, J., Shin, I., "In vivo monitoring of mercury ions using a rhodamine-based molecular probe." *J. Am. Chem. Soc.* **2006**, *128*, 14150–14155.

52. Franzini, R. M., Kool, E. T., "Organometallic activation of a fluorogen for templated nucleic acid detection." *Org. Lett.* **2008**, *10*, 2935–2938.

53. Setsukinai, K., Urano, Y., Kakinuma, K., Majima, H. J., Nagano, T., "Development of novel fluorescence probes that can reliably detect reactive oxygen species and distinguish specific species." *J. Biol. Chem.* **2003**, *278*, 3170–3175.

54. Kim, S. Y., Hong, J-I., "Chromogenic and fluorescent chemodosimeter for detection of fluoride in aqueous solution." *Org. Lett.* **2007**, *9*, 3109–3112.

55. Chae, M-Y., Czarnik, A. W., "Fluorimetric chemodosimetry. Mercury(II) and silver(I) indication in water via enhanced fluorescence signaling." *J. Am. Chem. Soc.* **1992**, *114*, 9704–9705.

56. Kojima, H., Nakatsubo, N., Kikuchi, K., Kawahara, S., Kirino, Y., Nagoshi, H., Hirata, Y., Nagano, T., "Detection and imaging of nitric oxide with novel fluorescent indicators: diaminofluoresceins." *Anal. Chem.* **1998**, *70*, 2446–2453.

57. Gabe, Y., Urano, Y., Kikuchi, K., Kojima, H., Nagano, T., "Highly sensitive fluorescence probes for nitric oxide based on boron dipyrromethene chromophore – rational design of potentially useful bioimaging fluorescence probe." *J. Am. Chem. Soc.* **2004**, *126*, 3357–3367.

58. Umezawa, N., Tanaka, K., Urano, Y., Kikuchi, K., Higuchi, T., Nagano, T., "Novel fluorescent probes for singlet oxygen." *Angew. Chem. Int. Ed.* **1999**, *38*, 2899–2901.

59. Tanaka, K., Miura, T., Umezawa, N., Urano, Y., Kikuchi, K., Higuchi, T., Nagano, T., "Rational design of fluorescein-based fluorescence probes. Mechanism-based design of a maximum fluorescence probe for singlet oxygen." *J. Am. Chem. Soc.* **2001**, *123*, 2530–2536.

60. Ueno, T., Urano, Y., Kojima, H., Nagano, T., "Mechanism-based molecular design of highly selective fluorescence probes for nitrative stress." *J. Am. Chem. Soc.* **2006**, *128*, 10640–10641.

61. Wu, Q., Anslyn, E. V., "Catalytic signal amplification using a Heck reaction. An example in the fluorescence sensing of Cu(II)." *J. Am. Chem. Soc.* **2004**, *126*, 14682–14683.

62. Zhu, L., Lynch, V. M., Anslyn, E. V., "FRET induced by an 'allosteric' cycloaddition reaction regulated with exogenous inhibitor and effectors." *Tetrahedron* **2004**, *60*, 7267–7275.

63. Houk, R. J. T., Anslyn, E. V., "Luminescent assays for ketones and aldehydes employing catalytic signal amplification." *New. J. Chem.* **2007**, *31*, 729–735.

64. Graf, N., Göritz, M., Krämer, R., "A metal-ion-releasing probe for DNA detection by catalytic signal amplification." *Angew. Chem. Int. Ed.* **2006**, *45*, 4013–4015.

65. Graf, N., Krämer, R., "Enzymatic amplification in a bioinspired, autonomous signal cascade." *Chem. Commun.* **2006**, 4375–4376.

2.0 DESIGN AND SYNTHESIS OF DICHLOROFLUORESCEIN DERIVATIVES

2.1 RESEARCH DESIGN

The Koide lab has been interested in developing a new series of 2',7'-dichlorofluorescein (DCF)-based fluorescence sensors. DCF was chosen as the fluorophore for several reasons: (1) cell-permeable DCF derivatives are known including Zinpyr-1[1] and Fluo-3[2], (2) the fluorescence is nearly pH-independent under physiological conditions (explanation below) and (3) the fluorescein chromophore exhibits appropriate λ_{ex} and λ_{em}.[3]

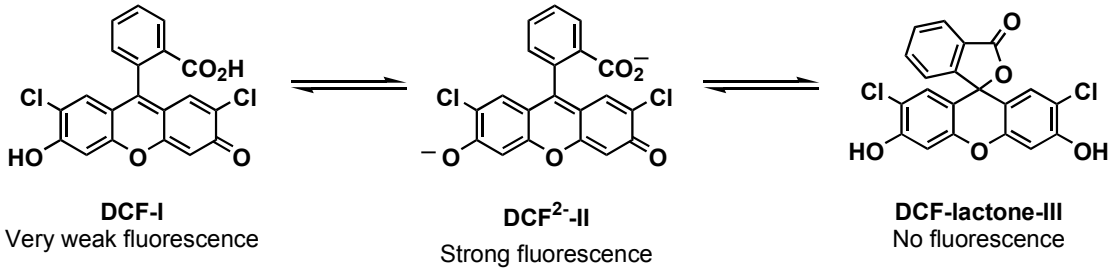

Figure 21. Structures of DCF

DCF, and fluorescein in general, is known to exist in three major forms, shown in Figure 21.[4] At physiological pH, the phenolic OH is largely deprotonated and DCF^{2-}-II predominates because of the pKa lowering effect due to the presence of the chloride substituents (phenol pK_a (fluorescein) = 6.7; phenol pK_a (DCF) = 5.0).[5] Only in acidic aqueous solution and organic solvent does DCF exist as the non-fluorescent DCF-lactone-III. As a result, the fluorescence

intensity of DCF is greatest under physiological conditions and should exhibit a large signal-to-background ratio necessary for a useful sensor. A similar fluorophore containing 2'- and 7'-fluoride substituents (Oregon Green) has also been developed with similar physical properties (phenol pK_a = 4.8).[6]

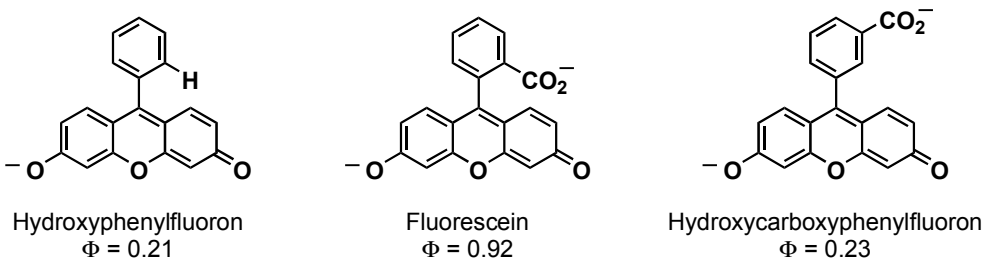

Figure 22. Importance of the carboxyl group presence and position

While DCF and Oregon Green are valuable fluorophore scaffolds, the negatively charged carboxyl group that each contains may cause nonspecific interactions with positively charged moieties of biomolecules. Additionally, the carboxyl group may be responsible when inherently cell-permeable molecules become impermeable following conjugation to fluorescein.[7] However, the Lindqvist group reported that this carboxyl group is indispensable for fluorescence emission because removal of this group caused a reduction in fluorescence quantum yield (Figure 22).[8] Furthermore, an additional study showed that movement of the carboxyl group to the 3-position of the phenyl ring caused a similar reduction in fluorescence emission.[9]

The necessity for the carboxyl group was speculated to be primarily due to structural rigidity, which is a common feature used to explain the high fluorescence emission of conjugated aromatic dyes.[8,9] Radiationless transfer from the excited state to the ground state via internal conversion is less likely for rigid structures because they experience less vibrational dissipation. More specifically to fluorescein, it was speculated that an ordered structure of water molecules

surrounds the negatively charged carboxyl group in alkaline pH, which increases the rigidity of the molecular structure.[8] In addition, only fluorescein is capable of the electronic overlap necessary to form the nonfluorescent lactone (DCF-lactone-III in Figure 21), further demonstrating its potential rigidity. These hypotheses were further corroborated by the fact that all three molecules exhibit the same fluorescence emission in acidic pH.

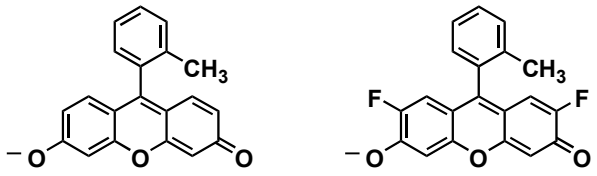

Tokyo Green Pennsylvania Green

Figure 23. Examples of fluorescein-based derivatives

The Nagano group recently demonstrated that the carboxyl group can be replaced with a methyl group with no decrease in fluorescence intensity, and gave the compound the name Tokyo Green (Figure 23).[10] Based on these results, it was hypothesized that the substituent in this position simply keeps the benzene moiety and the fluorophore orthogonal to each other and restricts rotation. A similar methyl substitution was carried out by the Peterson group to produce Pennsylvania Green (Figure 23).[11] In live human cells, Pennsylvania Green was more fluorescent than Tokyo Green due to its lower pK_a value. Despite these successes, the addition of a methyl group may cause nonspecific hydrophobic interactions and poor water solubility.[12]

To overcome the potential fallbacks with the above fluorophores, it was hypothesized that the replacement of the carboxyl group of DCF with a hydroxymethyl group would prove to be superior is those instances in which nonspecific hydrophobic interactions and poor water solubility are detrimental. Moreover, such compounds could be synthetically more accessible

than Tokyo Green or Pennsylvania Green, and conjugation ready via the primary hydroxy group. The synthetic plan for these new sensors is shown in Figure 24.

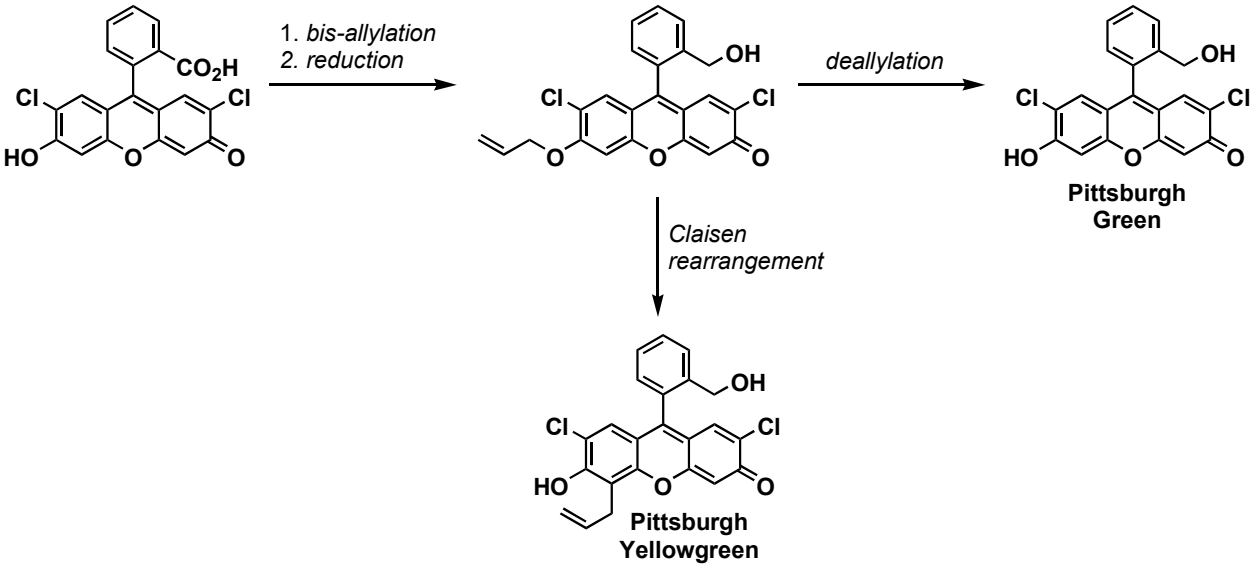

Figure 24. Synthetic plan for Pittsburgh Green and Pittsburgh Yellowgreen

The synthesis of Pittsburgh Green was envisioned to begin with the bis-allylation of DCF, which was previously reported by Drs. Sparano and Shahi in the Koide group.[13] Reduction of the resulting allyl ester would give the allyl-hydroxymethyl DCF intermediate, which following deallylation would yield Pittsburgh Green. This allyl-hydroxymethyl DCF intermediate could also be subjected to Claisen rearrangement conditions to obtain allyl-DCF fluorophore, Pittsburgh Yellowgreen, which is also conjugation-ready via its terminal alkene (olefin cross-metathesis and oxidative cleavage/coupling for example). The Koide group previously reported a similar Claisen rearrangement of DCF for the synthesis of DCF derivatives containing one quenching group.[13] Thus, the proposed scheme provides scalable access to two conjugation-ready DCF-derivatives with a valuable hydroxymethyl substituent in place of the carboxyl or methyl group on the benzene moiety of DCF.

2.2 RESULTS AND DISCUSSION

2.2.1 Synthesis of Pittsburgh Green and Pittsburgh Yellowgreen

The synthesis of the Pittsburgh Green began with the bis-allylation of DCF. Although this transformation was previously reported[13], the purification method for this compound has been improved; this deserves comment here. Commercially available DCF was treated with allyl bromide and K_2CO_3 in DMF (Figure 26). Upon reaction completion, excess water was added to the reaction mixture to precipitate the bis-allyl DCF derivative **29** in excellent purity. Because of the ease of purification, this transformation is routinely performed in multiple gram scale (>25 g).

With successful preparation of compound **29**, attention was next turned to the reduction step. Lithium borohydride[14] was examined as a mild reducing agent, but these conditions consistently yielded a product with incorrect NMR and MS data. From these data, it was speculated that this hydride reagent, in fact, does not reduce the allyl ester, but reduces the xanthene ring either directly (**30**) or through initial reduction of the ketone followed by aromatization (**30→31**) (Figure 25). This side reaction provided insight into reactivity of the xanthene moiety in the presence of reducing agents.

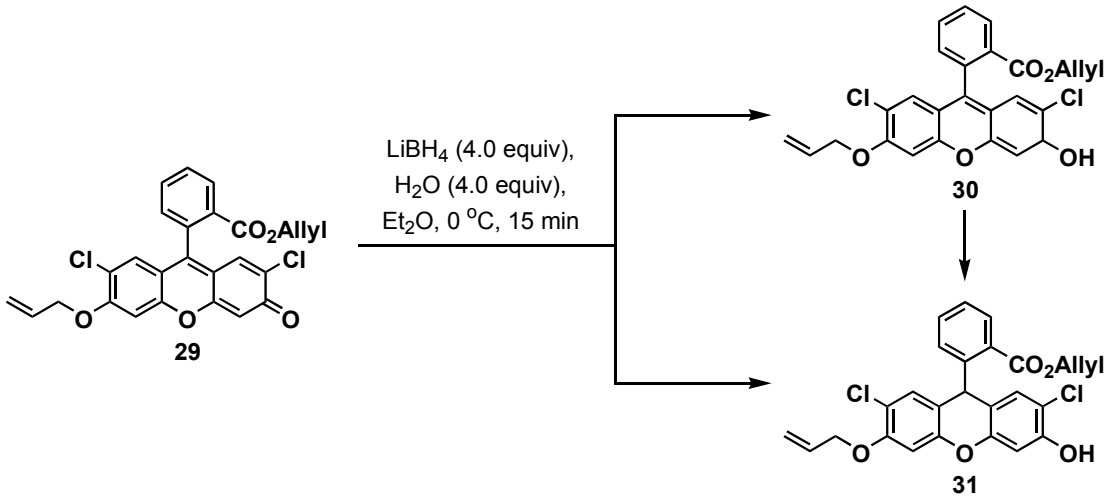

Figure 25. Results of unsuccessful lithium borohydride reduction

With the unsuccessful results with lithium borohydride, diisobutylaluminum hydride (DIBALH)[15] was next examined as a reducing agent. Although treatment of the **29** with DIBALH was successful in reducing the ester, a similar reduction of the xanthene chromophore as with lithium borohydride was noticed. It was speculated that **29** is initially reduced to form putative intermediate **32**, which then presumably isomerizes to the more stable intermediate **33**. To oxidize the chromophore, the excess DIBAL-H was first quenched with aqueous NH_4Cl and the putative intermediate **33** was oxidized with DDQ[16] in one pot to afford compound **34** in 80% yield as crystalline (Figure 26).[17]

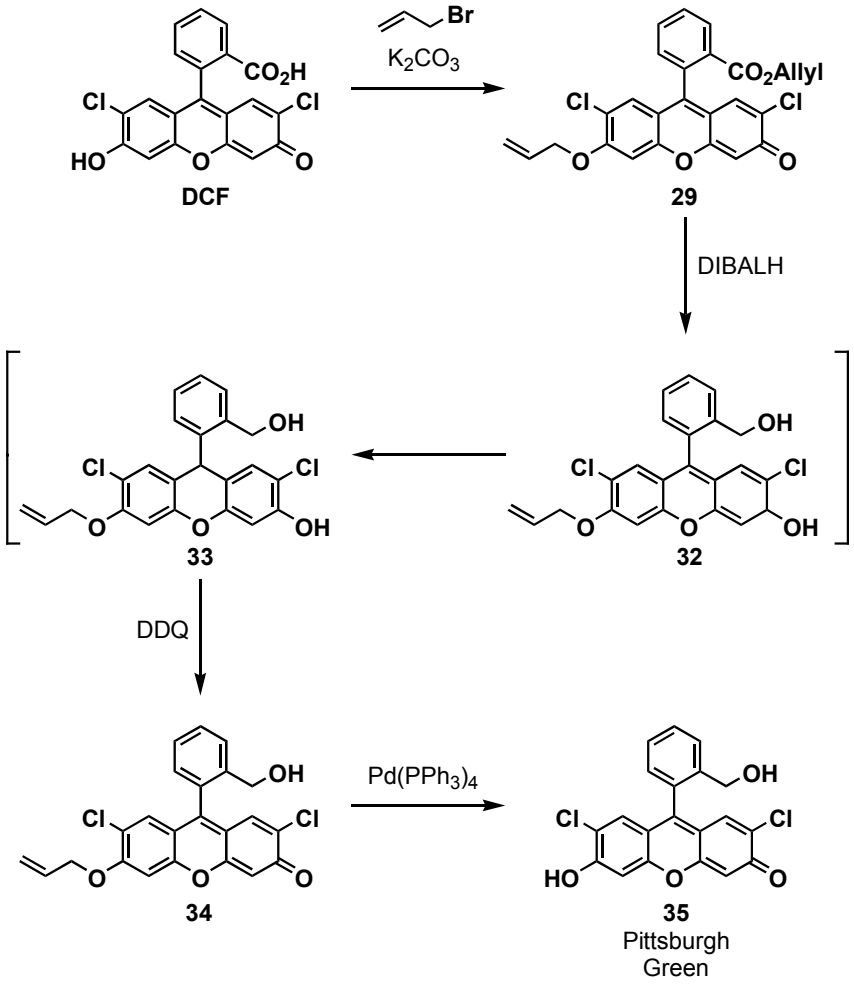

Figure 26. Synthetic scheme for the synthesis of Pittsburgh Green

The final step in the synthesis of Pittsburgh Green is the deallylation of the phenolic ether. A common approach in the deprotection of such allyl aryl ethers is to use a variant of the Pd-catalyzed allylic alkylation, or Tsuji-Trost reaction.[18,19] This reaction will be discussed in detail in the following chapter. As such, Pd^0-catalyzed deallylation was employed with the use of catalytic $Pd(PPh_3)_4$, sodium borohydride[20] and morpholine.[21] The reaction proceeded efficiently to yield Pittsburgh Green (**35**) in 80% as a crystalline solid.[17] In addition to Pd^0 species, the same efficient conversion could also be achieved with Pd^{II} reagents.[17]

The overall synthetic scheme for Pittsburgh Green is shown above in Figure 26. Thus, this new DCF derivative is efficiently synthesized in two steps from commercially available compounds. Since all steps yield crystalline solids, this synthesis is highly scalable and multiple gram to kilogram quantities can be easily prepared.

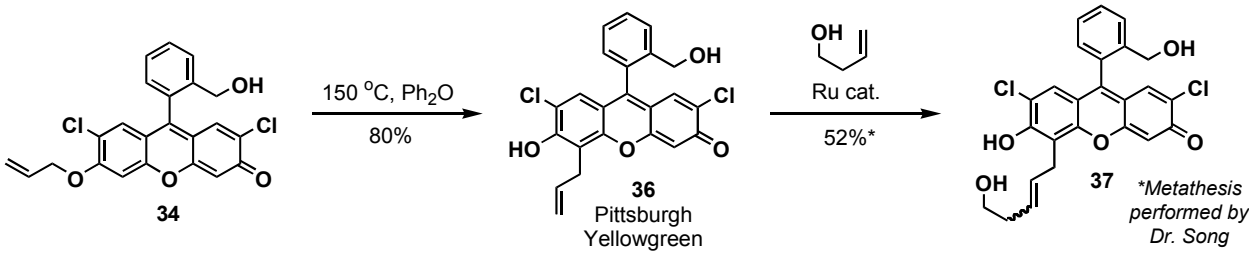

Figure 27. Synthetic scheme for the synthesis of Pittsburgh Yellowgreen

The above synthetic scheme also provides efficient access to a second DCF derivative, Pittsburgh Yellowgreen **36** (Figure 27).[22] This compound was synthesized via Claisen rearrangement of compound **34**. Dr. Shahi in the Koide group previously reported a similar rearrangement of DCF.[13] The terminal alkene of Pittsburgh Yellowgreen provides a useful handle for coupling via the ruthenium-catalyzed olefin cross-metathesis reaction.[22] Despite numerous attempts on my part to couple this olefin to other alkenes, such as alkenyl maleimides, the only successful example was with but-3-en-1-ol to form compound **37**, which was performed by Dr. Song.

2.2.2 Spectroscopic Properties of Pittsburgh Green and Pittsburgh Yellowgreen

To compare the fluorescence emission of these new fluorophores to the parent fluorescein scaffold, Dr. Song measured the quantum yield of each compound in pH 10 buffer.[22] The

quantum yields of **35** and **36** were 0.89 and 0.82, respectively. Thus, these compounds exhibit similar fluorescence emission properties to other fluorescein derivatives ($\Phi_{fluorescein}$ = 0.85 in pH 13 buffer; $\Phi_{TokyoGreen}$ = 0.85 in pH 13 buffer). The emission maxima for **35** and **36** were determined as 523 and 535 nm, respectively. Thus, the two sensors are easily distinguishable by this red shift in the fluorescence emission.

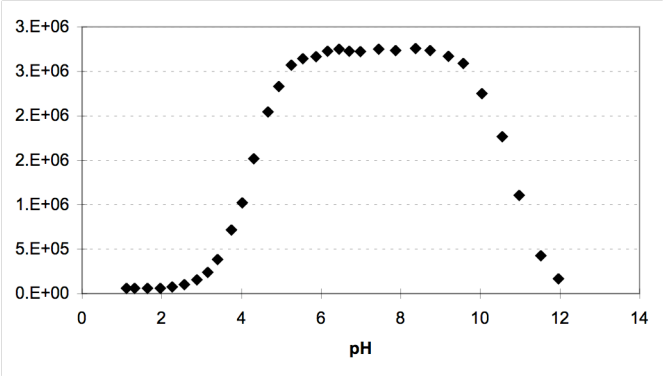

Figure 28. Fluorescence intensity of Pittsburgh Green at 523 nm as a function of pH

For usefulness in biological applications, pH sensitivity under physiological conditions (pH 4–7.4) is a major concern. To address this, Dr. Song measured the fluorescence intensity of **35** at 523 nm from pH 1–12.[22] As Figure 28 shows, the fluorescence intensity is relatively constant from pH 5.5–9.5, indicating its robustness around physiological pH. However, above and below this pH range, the intensity significantly drops.

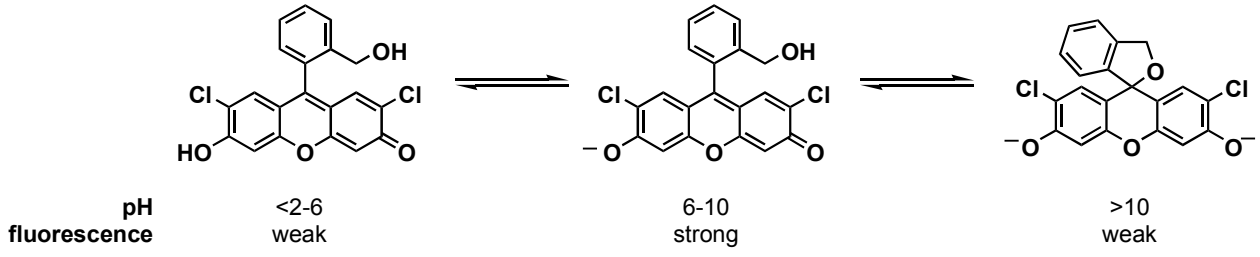

Figure 29. Structure of Pittsburgh Green as a function of pH

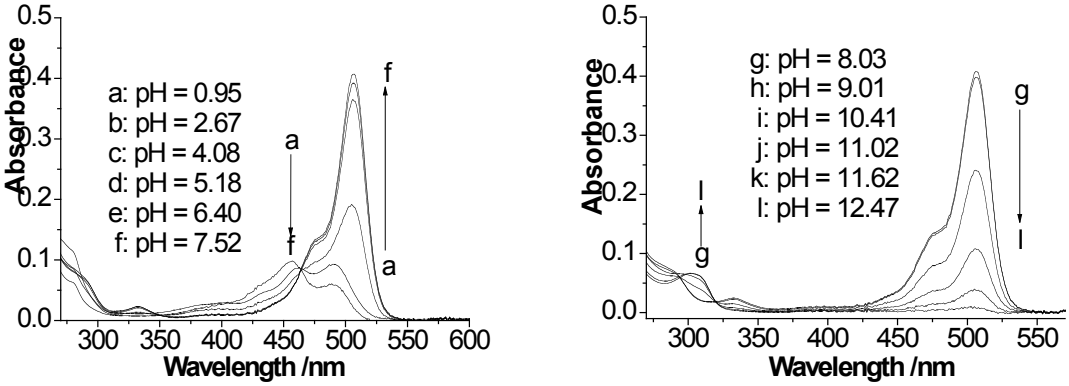

Figure 30. UV absorption spectra of Pittsburgh Green as a function of pH

The weaker fluorescence above pH 10 could be due to deprotonation of the hydroxymethyl group followed by subsequent cyclization to form a cyclic ether, which is analogous to the nonfluorescent, cyclic lactone structure of DCF (Figure 29).[4] To confirm this hypothesis, Dr. Song measured the UV absorption spectrum as a function of pH.[22] As Figure 30 shows, as the pH is raised, the peak at 506 nm decreases and a new peak at 302 nm emerges, which could be an indication of such a cyclic structure. As the pH is decreased, the peak at 506 nm also decreases with a subsequent increase in a new peak at 457 nm. This new peak could be indicative of a fully protonated, non-cyclic form of **35**. In fact, a similar peak is also known for DCF at 440–450 nm. Dr. Song also measured the pK_a of the phenolic hydroxy group and found it to be nearly identical to that of DCF (pK_a (**35**) = 4.27).[22]

2.2.3 Biological Applications of Pittsburgh Green and Pittsburgh Yellowgreen

Zebrafish are becoming increasing popular as a model animal in drug screenings and as a research tool.[23–25] This is partly because they exhibit high fecundity, small embryo size and are

transparent in their early developmental stages, enabling visual inspection in detail. However, a drawback of using zebrafish in bioimaging is that zebrafish are not permissive to many fluorescent probes, and neither rhodamine nor DCF can penetrate zebrafish embryos.

In collaboration with the Hukriede group at the University of Pittsburgh Department of Microbiology and Molecular Genetics, we set out to determine the permeability of **35** and **36** in zebrafish embryos.[22] Dechorionated zebrafish embryos were incubated with either compound (25 μM) for 1 hour and visualized using confocal microscopy to determine compound distribution. To our delight, both derivatives were permeable and distributed throughout the embryos compared to BODIPY TR Methyl Ester, which was used as a control (Figure 31A-C).[26] In fact, **35**, **36** and BODIPY TR Methyl Ester each penetrate the embryos to similar extents (Figure 32D-L). A further description of this figure follows below.

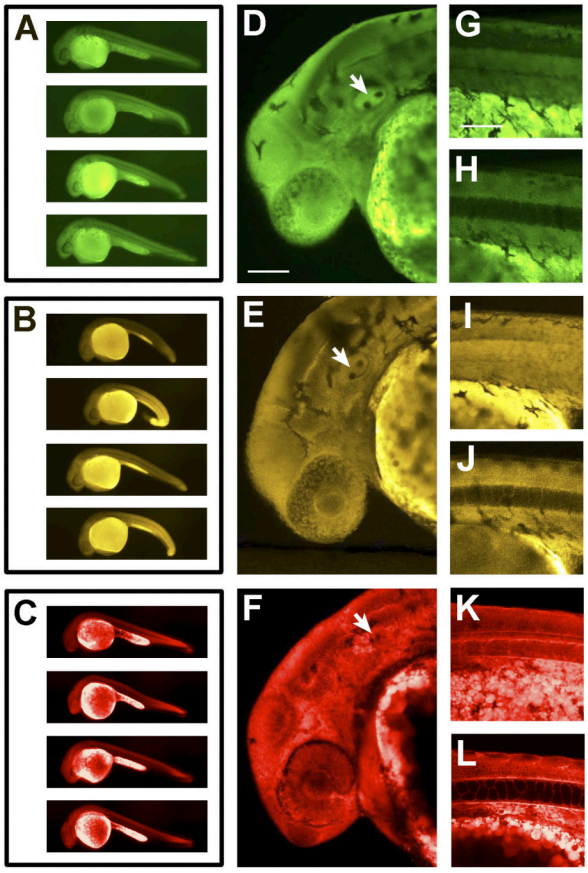

Figure 31. Pseudocolored images of stained zebrafish embryos

35 = green panels (A, D, G, H), **36** = yellow panels (B, E, I, J) or BODIPY TR Methyl Ester = red panels (C, F, K, L). Scale bars = 100 mm. K. Koide, F. Song, E. D. de Groh, A. L. Garner, V. D. Mitchell, L. A. Davidson, N. A. Hukriede: Scalable and Concise Synthesis of Dichlorofluorescein Derivatives Displaying Tissue Permeation in Live Zebrafish Embryos. *ChemBioChem*. **2008**, *9*, Pages 214–218. Copyright Wiley-VCH Verlag GmbH & Co. KGaA. Reproduced with permission.

Figure 31A-C shows representative examples from a group of 20 stained embryos showing the labeling consistency of the compounds. In all cases, the compounds are more highly concentrated in the yolk sac and yolk extension than in the embryo itself, which is likely the result of compound accumulation within the lipidic yolk platelets that comprise almost the entire volume of the yolk.[27] Figure 31D-F shows 80 mm confocal Z projections of the head region

demonstrating that compound penetration extends to the embryonic interior. Structures containing little organic material, such as the calcified otoliths (indicated by arrows) are not labeled. Figure 31G, I, K shows 80 mm Z projections of the tail region taken just above the posterior end of the yolk sac (anterior to the left). Figure 31H, J, L shows 1 mm slices from the tail projections illustrating that the compounds label the notochord sheath and surrounding tissue, but are not found in notochord vacuoles.

The toxicity of the fluorophores was next examined because possible signs of toxicity were detected at 25 μM, including narrowing of the yolk extension and ventral curling of the tail. [22] Embryos were exposed to either compound (25−0.25 μM) from 3.5 h post fertilization (hpf) to 48 hpf. While **35** showed limited toxicity at 8 μM, **36** showed limited toxicity only at 2.5 μM indicating that it could potentially impact zebrafish development to a greater extent. These data are consistent with observations from the staining experiments. Nonetheless, these results strongly indicate the potential for these compounds as useful tools in bioimaging.

2.3 CONCLUSION

In collaboration with Dr. Song, two new DCF derivatives, Pittsburgh Green (**35**) and Pittsburgh Yellowgreen (**36**), have been developed each of which contain a hydroxymethyl group in place of the carboxyl group of the fluorescein scaffold. These compounds possess desirable properties for bioimaging in terms of fluorescence emission and pH insensitivity, and also provide access to further functionalization. The synthesis of these new fluorophores requires only three steps, all of which are scalable. Furthermore, these compounds exhibited desirable staining and permeation

in zebrafish embryos. Thus, these fluorophores should find many applications as new fluorescent sensors.

2.4 EXPERIMENTAL

2.4.1 General Information

All reactions were carried out under a nitrogen atmosphere with freshly distilled solvents under anhydrous conditions, unless otherwise noted. Tetrahydrofuran (THF) was distilled from sodium-benzophenone, and methylene chloride (CH_2Cl_2) was distilled from calcium hydride. Yields refer to chromatographically and spectroscopically (^{1}H NMR) homogenous materials, unless otherwise stated.

All reactions were monitored by thin-layer chromatography (TLC) carried out on 0.25-mm EMD silica gel plates (60F-254) using UV light (254 nm). TSI silica gel (230–400 mesh) was used for flash column chromatography.

NMR spectra were recorded on AM300 (Bruker) instruments and calibrated using a solvent peak or tetramethylsilane as an internal reference. The following abbreviations are used to indicate the multiplicities: s, singlet; d, doublet; t, triplet; q, quartet; m, multiplet; br, broad. Mass spectra were obtained from a Micromass Autospec double focusing instrument.

2.4.2 Synthesis

Compound 29. A 1.0-L round bottom flask was charged with 2',7'-dichlorofluorescein (20.7 g, 51.9 mmol), DMF (175 mL), K_2CO_3 (21.5 g, 155 mmol) and allyl bromide (13.5 mL, 155 mmol) at 24 °C. The reaction mixture was stirred at 24 °C for 16 h under laboratory atmosphere and then poured into 2.0 L water. The resulting precipitate was collected via vacuum filtration, washed with water and dried *in vacuo* to yield **29** as a red-orange solid (24.8 g; quantitative yield).

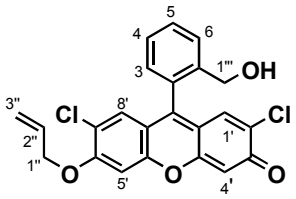

Compound 34. A solution of compound **29** (4.80 g, 10.0 mmol) in CH_2Cl_2 (40 mL) was treated with DIBALH (48 mL, 1.0 M in hexanes, 48.0 mmol) dropwise over 15 min at -78 °C under a nitrogen atmosphere. The mixture was stirred for 5 min at the same temperature and then was warmed to 24 °C. After 2 h, Et_2O (90 mL) was added and the reaction mixture was quenched with saturated aqueous NH_4Cl (15 mL) at 0 °C. This mixture was warmed to 24 °C again and stirred for 1 h. A second portion of Et_2O (180 mL) was added to the mixture followed by DDQ (2.50 g, 11.0 mmol) at 0 °C. After stirring 1 h at 24 °C, the mixture was filtered through Celite® and washed with EtOAc. The filtrate was dried over Na_2SO_4 and the solvents were evaporated under reduced pressure. Silica gel flash chromatography of the residue (5 → 10 % EtOAc in hexanes) afforded compound **34** as a pink solid (3.43 g, 80%).

Data for **34**: mp = 167–168 °C; R_f = 0.69 (50% EtOAc in hexanes); IR (in CH_2Cl_2): 3385 (br, OH), 3077, 2923, 2855, 1608, 1486, 1410, 1266, 1191, 1032, 875, 725 cm^{-1}; ^1H NMR (300 MHz, $CDCl_3$, 293K): δ 7.37–7.40 (m, 2H, Ar), 7.26–7.30 (m, 1H, Ar), 6.89 (s, 1H, Ar), 6.87 (s,

1H, Ar), 6.84 (m, 1H, Ar), 6.83 (s, 1H, Ar), 6.73 (s, 1H, Ar), 6.05 (ddt, J = 17.4, 10.2, 5.1 Hz, 1H, 2′′-H), 5.47 (ddt, J = 17.4 , 3.0, 1.5 Hz, 1H, 3′′-H_{trans}), 5.32 (ddt, J = 10.2, 3.0, 1.5 Hz, 1H, 3′′-H_{cis}), 5.28 (s, 2H, 1′′′-H), 4.63 (ddt, J = 5.1, 1.5, 1.5 Hz, 2H, 1′′-H); ^{13}C NMR (75 MHz, $CDCl_3$, 293K): δ 154.6, 152.1, 150.1, 149.5, 143.6, 138.6, 132.1, 129.6, 128.7 (two carbons), 128.6, 123.7, 121.0, 118.2, 118.1, 118.0, 117.2, 115.6, 103.7, 101.5, 83.1, 72.3, 69.8; HRMS (ESI) *m/z* calcd. for $C_{23}H_{17}Cl_2O_4$ $[M+H]^+$ 427.0504, found 427.0519.

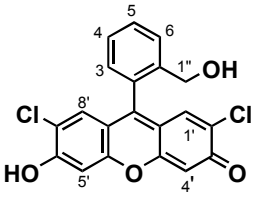

Compound 35. A solution of compound **34** (214 mg, 0.50 mmol) in THF (6 mL) was treated morpholine (48 μL, 0.55 mmol), sodium borohydride (22.7 mg, 0.60 mmol) and $Pd(PPh_3)_4$ (2.9 mg, 0.0025 mmol) at 24 °C. After 3 h, 3 N HCl (1 mL) was added to quench the reaction. The mixture was extracted with EtOAc, dried over Na_2SO_4, filtered, and concentrated under reduced pressure. The residue was purified by silica gel flash chromatography (3% MeOH in CH_2Cl_2) to afford compound **35** as an orange solid (180 mg, 93%).

Data for **35**: mp > 270 °C; R_f = 0.18 (50% EtOAc in hexanes); IR (in CH_2Cl_2): 3174 (br, OH), 2930, 1634, 1593, 1584, 1521, 1347, 1273, 1043, 839 cm^{-1}; ^{1}H NMR (300 MHz, CD_3OD, 293K): δ 7.42–7.47 (m, 2H, Ar), 7.32–7.37 (dd, J = 7.5, 7.5 Hz, 1H, Ar), 6.85 (d, J = 7.5 Hz, 1H, Ar), 6.78 (s, 2H, Ar), 6.74 (s, 2H, Ar), 5.28 (s, 2H, 1′′-H). ^{13}C NMR (75 MHz, CD_3OD, 293K): δ 155.5, 151.3, 145.5, 140.3, 130.7, 129.9, 124.7, 122.4, 118.2, 117.6, 104.5, 84.8, 73.2 (Although 20 peaks expected, only 13 peaks detected); HRMS (EI) *m/z* calcd. for $C_{20}H_{12}Cl_2O_4$ $M^{+\cdot}$ 386.0113, found 386.0108.

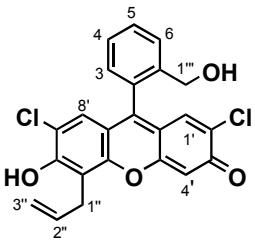

Compound 36. A solution of compound **34** (1.43 g, 3.35 mmol) in Ph_2O (5 mL) was stirred at 150 °C for 12 h. After cooled to 24 °C, the reaction mixture was transferred directly to a silica gel column. The column chromatography was performed with 10 % isopropyl alcohol in hexanes to afford compound **36** as a red-orange solid (1.15 g, 80%).

Data for **36**: mp = 186–188 °C; R_f = 0.59 (50% EtOAc in hexanes); IR (in CH_2Cl_2): 3305 (br, OH), 3074, 2923, 2855, 1635, 1598, 1482, 1446, 1356, 1278, 1213, 737 cm^{-1}; ^1H NMR (300 MHz, $CDCl_3$, 293K): δ 7.42–7.35 (m, 2H, Ar), 7.30–7.28 (m, 1H, Ar), 6.89–6.87 (m, 3H, Ar; overlap of two singlets and one doublet), 6.77 (s, 1H, Ar), 6.01 (ddt, *J* = 17.4, 9.9, 6.3 Hz, 1H, 2′′-H), 5.29 (br s, 2H, 1′′-H), 5.14 (dd, *J* = 17.4, 1.7 Hz, 1H, 3′′-H_{trans}), 5.05 (dd, *J* = 9.9, 1.5 Hz, 1H, 3′′-H_{cis}), 3.63 (br d, *J* = 6.3 Hz, 2H, 1′′-H); ^{13}C NMR (75 MHz, CD_3OD, 293K): δ 155.3, 152.5, 151.2, 149.2, 145.3, 140.1, 138.7, 130.4, 129.8 (two carbons), 127.6, 124.6, 122.2, 118.6, 118.1, 117.5, 117.3, 117.1, 115.6, 104.4, 85.0, 73.0, 29.0; HRMS (EI) *m/z* calcd. for $C_{23}H_{16}Cl_2O_4$ $M^{+\cdot}$ 426.0426, found 426.0419.

2.4.3 UV and Fluorescence Spectroscopy

UV-visible spectroscopy. Absorption spectra were acquired on a Pekin Elmer Lambda 19 UV-Visible spectrometer under the control of a Windows-based PC running the manufacturers' supplied software.

Fluorescence spectroscopy. Fluorescence spectra were recorded in a 1 × 1-cm quartz cuvette on a Jobin Yvon FluoroMax-3 spectrometer under the control of a Windows-based PC running FluorEssence software. The samples were excited at 497 nm and the emission intensities were

collected at 523 or 535 nm. All spectra were corrected for emission intensity using the manufacturer supplied photomultiplier curves.

Relative Quantum Yields. To determine quantum yields relative to fluorescein, stock solutions of **35** and **36** were prepared in DMSO (1 mM) and diluted in borate buffer (pH = 10) to OD_{490} = 0.12. The samples were excited at 490 nm and the integrated emission spectra were compared. The quantum yields of all compounds were referenced to fluorescein in 0.1 N NaOH (Φ = 0.95).[28]

2.5 BIBLIOGRAPHY

1. Walkup, G. K., Burdette, S. C., Lippard, S. J., Tsien, R. Y., "A new cell-permeable fluorescent probe for Zn^{2+}." *J. Am. Chem. Soc.* **2000**, *122*, 5644–5645.

2. Minta, A., Kao, J. P. Y., Tsien, R. Y., "Fluorescent indicators for cytosolic calcium based on rhodamine and fluorescein chromophores." *J. Biol. Chem.* **1989**, *264*, 8171–8178.

3. Czarnik, A. W., "Desperately seeking sensors." *Chem. Biol.* **1995**, *2*, 423–428.

4. Martin, M. M., Lindqvist, L., "The pH dependence of fluorescein fluorescence." *J. Lumin.* **1975**, *10*, 381–390.

5. Leonhardt, H., Gordon, L., Livingston, R., "Acid-base equilibria of fluorescein and 2',7'-dichlorofluorescein in their ground and fluorescent states." *J. Phys. Chem.* **1971**, *75*, 245–249.

6. Sun, W-C., Gee, K. R., Klaubert, D. H., Haugland, R. P., "Synthesis of fluorinated fluoresceins." *J. Org. Chem.* **1997**, *62*, 6469–6475.

7. Wu, M. M., Llopis, J., Adams, S., McCaffery, J. M., Kulomaa, M. S., Machen, T. E., Moore, H-P. H., Tsien, R. Y., "Organelle pH studies using targeted avidin and fluorescein-biotin." *Chem. Biol.* **2000**, *7*, 197–209.

8. Lindqvist, L., Lundeen, G. W., "Radiationless transitions in xanthene dyes." *J. Chem. Phys.* **1966**, *44*, 1711–1712.

9. Fink, D. W., Willis, C. R., "Structure and internal mixing in xanthene dyes." *J. Chem. Phys.* **1970**, *53*, 4720–4722.

10. Urano, Y., Kamiya, M., Kanda, K., Ueno, T., Hirose, K., Nagano, T., "Evolution of fluorescein as a platform for finely tunable fluorescence probes." *J. Am. Chem. Soc.* **2005**, *127*, 4888–4894.

11. Mottram, L. F., Boonyarattanakalin, S., Kovel, R. E., Peterson, B. R., "The Pennsylvania Green fluorophore: a hybrid of Oregon Green and Tokyo Green for the construction of hydrophobic and pH-insensitive molecular probes." *Org. Lett.* **2006**, *8*, 581–584.

12. Dowlut, M., Hall, D. G., Hindsgaul, O., "Investigation of nonspecific effects of different dyes in the screening of labeled carbohydrates against immobilized proteins." *J. Org. Chem.* **2005**, *70*, 9809–9813.

13. Sparano, B. A., Shahi, S. P., Koide, K., "Effect of binding and conformation on fluorescence quenching in new 2',7'-dichlorofluorescein derivatives." *Org. Lett.* **2004**, *6*, 1947–1949.

14. Brown, H. C., Narasimhan, S., Choi, Y. M., "Selective reductions. 30. Effect of cation and solvent on the reactivity of saline borohydrides for reduction of carboxylic esters. Improved procedures for the conversion of esters to alcohols by metal borohydrides." *J. Org. Chem.* **1982**, *47*, 4702–4708.

15. Winterfeldt, E., "Applications of diisobutylaluminum hydride (DIBAH) and triisobutylaluminum (TIBA) as reducing agents in organic synthesis." *Synthesis* **1975**, 617–630.

16. Burn, D., Petrow, V., Weston, G. O., "A new reagent for the selective oxidation of steroidal allylic alcohols to α,β-unsaturated ketones." *Tetrahedron Lett.* **1960**, *1*, 14–15.

17. Song, F., Garner, A. L., Koide, K., "A highly sensitive fluorescent sensor for palladium based on the allylic oxidative insertion mechanism." *J. Am. Chem. Soc.* **2007**, *129*, 12354–12355.

18. Guibé, F., "Allylic protecting groups and their use in complex environment part II: allylic protecting groups and their removal through catalytic palladium π-allyl methodology." *Tetrahedron* **1998**, *54*, 2967–3042.

19. Kürti, L., Czakó, B., "Strategic applications of named reactions in organic synthesis." Elsevier Academic Press, London, 2005.

20. Hutchins, R. O., Learn, K., Fulton, R. P., "Reductive displacement of allylic acetates by hydride transfer via catalytic activation by palladium(0) complexes." *Tetrahedron Lett.* **1980**, *21*, 27–30.

21. Kunz, H., Waldmann, H., "The allyl group as mildly and selectively removable carboxy-protecting group for the synthesis of labile *O*-glycopeptides." *Angew. Chem. Int. Ed.* **1984**, *23*, 71–72.

22. Koide, K., Song, F., de Groh, E. D., Garner, A. L., Mitchell, V. D., Davidson, L. A., Hukriede, N. A., "Scalable and concise synthesis of dichlorofluorescein derivatives displaying tissue permeation in live zebrafish embryos." *ChemBioChem* **2008**, *9*, 214–218.

23. Peterson, R. T., Link, B. A., Dowling, J. E., Schreiber, S. L., "Small molecule developmental screens reveal the logic and timing of vertebrate development." *Proc. Natl. Acad. Sci.* **2000**, *97*, 12965–12969.

24. Nasevicius, A., Ekker, S. C., "The zebrafish as a novel system for functional genomics and therapeutic development applications." *Curr. Opin. Mol. Ther.* **2001**, *3*, 224–228.

25. Patton, E. E., Zon, L. I., "The art and design of genetic screens: zebrafish." *Nat. Rev. Genet.* **2001**, *2*, 956–966.

26. Cooper, M. S., Szeto, D. P., Sommers-Herivel, G., Topczewski, J., Solnica-Krezel, L., Kang, H-C., Johnson, I., Kimelman, D., "Visualizing morphogenesis in transgenic zebrafish embryos using BODIPY TR methyl ester dye as a vital counterstain for GFP." *Dev. Dyn.* **2005**, *232*, 359–368.

27. Cooper, M. S., D'Amico, L. A., Henry, C. A., "Methods in Cell Biology." Vol. 59, Academic Press, New York, 1999.

28. Brannon, J. H., Magde, D., "Absolute quantum yield determination by thermal blooming. Fluorescein." *J. Phys. Chem.* **1978**, *82*, 705–709.

3.0 FLUOROMETRIC DETECTION OF PALLADIUM

3.1 RESEARCH DESIGN

In the synthesis of Pittsburgh Green (**35**), the final step involves a Pd-catalyzed deprotection of the allyl ether (Figure 26).[1] Since it is known that such protection of the phenolic moiety prohibits fluorescence emission,[2] it was envisioned that this transformation could serve as a novel detection method for palladium. More specifically, by deprotecting the allyl ether of compound **34**, a nonfluorescent compound is coverted to a fluorescent compound **35** (Pittsburgh Green) (Figure 32). The proposed approach is conceptually new for metal detection because the metal analyte amplifies fluorescence signal directly through a catalytic process, which is analogous to the fluorometric enzyme assays previously described.

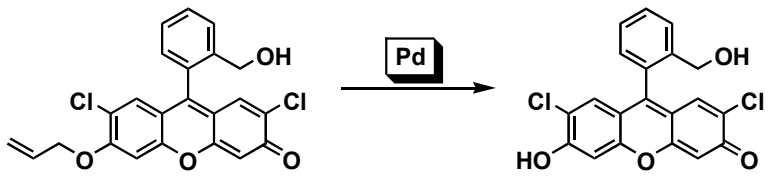

34
nonfluorescent

35
fluorescent

Figure 32. Pd-catalyzed transformation from a nonfluorescent to a fluorescent molecule

3.1.1 Tsuji-Trost Reaction

The chemical principle in which this palladium sensing method is based is a variant of the Pd-catalyzed allylic alkylation chemistry independently reported by Tsuji and Trost in the late 1960's–early 1970's.[3–9] The mechanism of this transformation is shown below in Figure 33.[6,10–12]

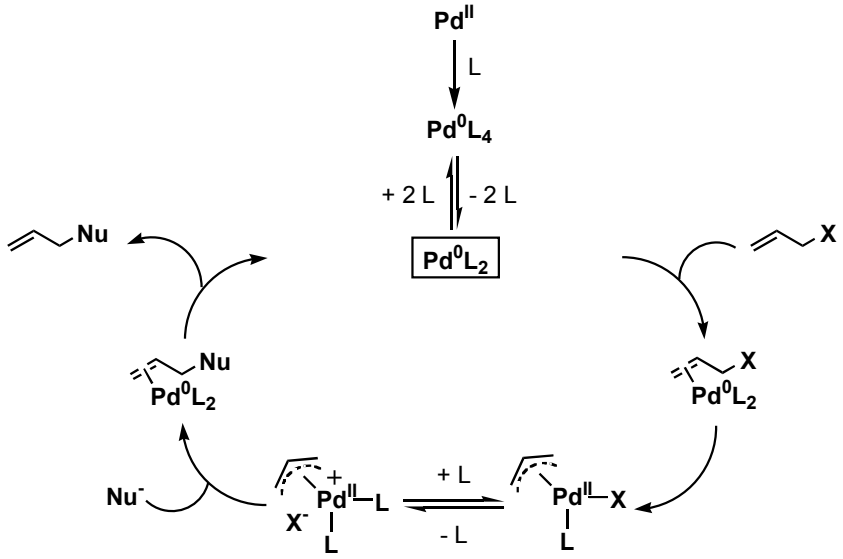

Figure 33. Mechanism of Tsuji-Trost reaction

The reaction mechanism begins with the reduction of Pd^{II} by a ligand to form Pd^0L_4. If a Pd^0 catalyst, such as $Pd(PPh_3)_4$, is used, then this reduction step will be eliminated. Since this species is a stable 18-electron species, it must first dissociate from the ligand to form reactive Pd^0L_2 with available d-orbitals (14-electrons on palladium). It is important to note that the potential for formation of this 18-electron species is highly dependent upon the electron density of the ligand; electron-rich phosphines such as Ph_3P are more likely to promote formation of this unreactive complex than electron-poor ligands.[6] This active Pd^0 catalyst will then oxidatively

insert into the C–X bond to form a π-allyl palladium intermediate. Typical leaving groups (X) include acetate, halides, sulfones, carbonates, epoxides and phenoxides.[9] The reaction is then speculated to take place through a cationic π-allyl palladium species.[4,6,13–15] Formation of this intermediate was initially proposed by Trost because of the requirement of excess Ph_3P and the finding that only soft nucleophiles were successful.[4,5] In one case it has been shown that such a cationic species was 100 times more reactive than a neutral π-allyl palladium species towards nucleophilic substitution.[12] Nucleophilic addition to the cationic complex then occurs and substitution is favored at one of the allylic termini in the presence of an appropriate nucleophile. Typical nucleophiles include malonate anion, nitrogen nucleophiles, sulfur nucleophiles, oxygen nucleophiles and organometallics (dialkylzincs, Grignards, organoaluminum reagents, etc.).[9] Dissociation from the product regenerates the active Pd^0 species to turnover another substrate molecule.

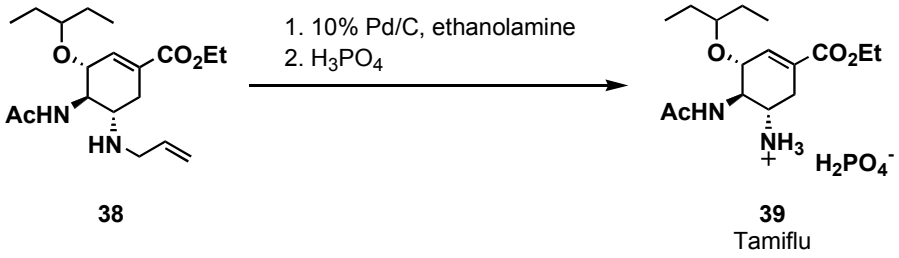

Figure 34. Pd-catalyzed deallylation in the Roche synthesis of Tamiflu

Although this reaction was initially developed as a method of carbon-carbon or carbon-heteroatom bond formation, it quickly found application in the deprotection of allyl carboxylates and allyl ether moieties.[16] For example, the synthesis of the influenza drug, Tamiflu, includes a Pd-catalyzed deallylation as a final synthetic step where allylamine **38** is converted to the free amine salt in **39** (Figure 34).[17] In the case of deprotection, the nucleophilic moiety is used as a

scavenger to release the leaving group, which in this case is the product. Common scavengers include nitrogen nucleophiles such as morpholine,[18] hydride sources (formic acid, tributyltin hydride and sodium borohydride)[19] and sulfur nucleophiles such as 2-thiobenzoic acid.[20]

This same mechanistic principle can be applied to fluorometric palladium detection (Figure 35). In this case, Pd^0 catalyzes the oxidative insertion to cleave the allylic C–O bond of the nonfluorescent allylic ether **34** to form the palladium complex **40**. This complex then reacts with a nucleophile to form the fluorescent compound **35** and an allylated nucleophile. Since this process is catalytic with respect to Pd^0, the analyte (palladium) amplifies fluorescence signal. This is the first example of a system where the metal analyte amplifies fluorescence signal directly through a catalytic process.

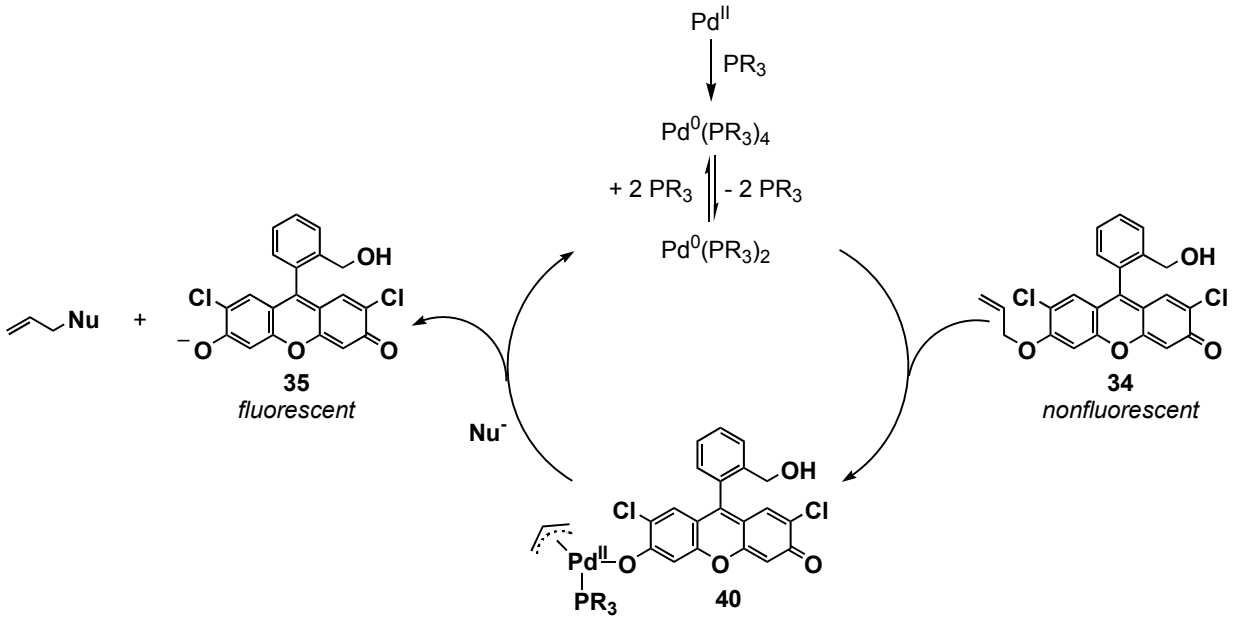

Figure 35. Mechanism of fluorometric palladium detection method

A similar ruthenium-catalyzed allylcarbamate cleavage to yield fluorescent rhodamine was previously reported by the Meggers group although not for ruthenium detection (Figure 36).[21]

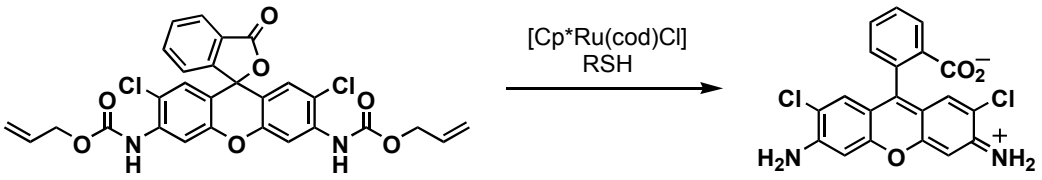

Figure 36. Ruthenium-catalyzed allylcarbamate cleavage to yield rhodamine

3.1.2 Importance of Palladium Detection

Palladium is a widely used precious metal in materials and chemistry. With respect to materials, palladium is found in electronics, dental amalgams, catalytic converters, fuel cells and jewelry. However, despite the importance of palladium in such materials, a major downfall is the subsequent pollution of the environment that comes with the frequent use of this metal.[22] One of the major sources of palladium pollution is the particulate palladium that is emitted due to automobile catalytic converter attrition.[23–27] While the palladium concentration in the earth's crust is estimated as 0.4 μg/kg, palladium contamination found in the environment is estimated as 2–400 times this amount.[22] For example, studies have shown the following amounts of palladium in environmental samples: road dust = 20–146 μg/kg; soil = <0.7–47 μg/kg; sewage sludge = 18–260 μg/kg; and fresh water = 0.5–22 ng/L.[22] These sources of palladium are often attributed to the presence of this metal in human bodies.[28,29]

With respect to chemistry, the benefits of palladium are quite expansive and numerous compounds, including active pharmaceutical ingredients (API), can be synthesized using Pd-catalyzed cross-coupling reactions such as the Buchwald-Hartwig, Heck, Sonogashira and Suzuki-Miyaura reactions.[30,31] Some examples of APIs synthesized using Pd-catalyzed cross-coupling chemistry are shown in Figure 37.[31] The carbon-carbon bond formed using a Pd-catalyzed reaction is indicated in red.

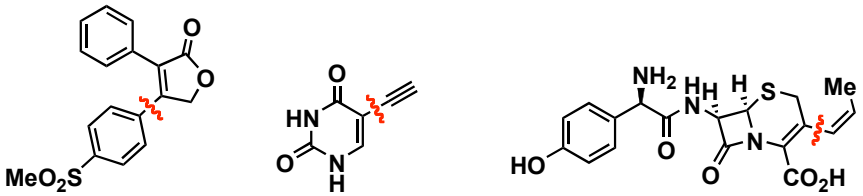

Figure 37. Examples of APIs synthesized using Pd-catalyzed cross-coupling chemistry

Refecoxib is a COX-II inhibitor, which was prepared using a Suzuki-Miyaura cross-coupling reaction as a key step. Eniluracil is a widely used anticancer agent, which was synthesized using Sonogashira chemistry. Cefprozil, an orally active antibiotic, was synthesized via a tin-mediated Stille cross-coupling reaction.

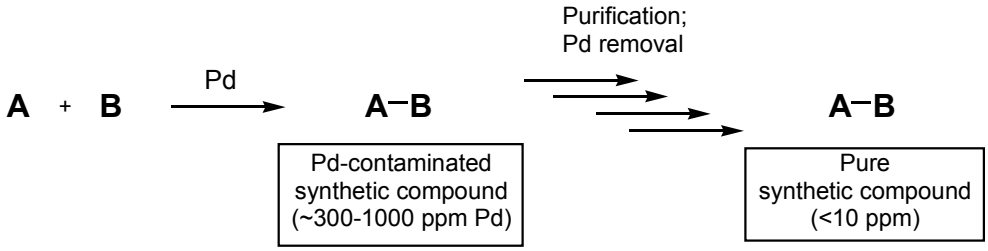

Figure 38. Pd contamination problem in the pharmaceutical and synthetic communities

Despite the frequent and fruitful use of such reactions in the synthetic community, one major setback to these reactions is the high level of palladium that is often found in the resultant synthetic compounds.[32–34] Although there is little known about the specific biological effects of palladium, the metal, particularly in its cationic forms, has potential to bind proteins, DNA or other biomolecules, and thus may be a health hazard.[22,33] As a result, the proposed dietary intake is <1.5–15 μg/day per person and the threshold for palladium in APIs is 5–10 ppm.[33] Because compounds synthesized via Pd-catalyzed reactions often contain much more palladium than this

threshold limit (typically 300–1000 ppm), extensive purifications are required to remove these impurities (Figure 38).[34–38] This quality control process can be quite time-consuming and the streamlining of such methods could greatly aid in getting new drugs to market.

3.1.3 Current Detection Methods for Palladium

Current techniques of quantifying palladium typically rely on spectroscopic methods such as atomic absorption spectroscopy, x-ray fluorescence and inductively-coupled plasma emission spectroscopy. Further descriptions of each of these methods follow below including their detection limit for palladium.

Atomic absorption spectroscopy (AAS) is a method in which a small volume of a sample (~20 μL) or a small amount of solid (0.1–1.0 mg) is atomized at very high temperature, typically by a graphite furnace, and the element is detected by its unique absorption spectrum.[39] The samples are then analyzed by measuring the amount of light emitted, which directly correlates to the amount of the metal in the sample. Although this method is sensitive (detection limit for Pd = 1–3 ng/mL),[40] there are a number of drawbacks with this spectroscopic technique.[39] Most importantly, AAS is extremely sensitive to the matrix of the sample, which makes analysis of field samples difficult. For example, many heavy metals (Pb, Co, Ni, Zn, Cu, Fe, K, Mn) cause spectral interference in palladium detection. In addition, many reagents used in sample preparation and the presence of chloride can also negatively impact signal through non-spectral interference.

X-ray fluorescence (XRF) is a method in which samples are bombarded with high energy x-rays and emission of fluorescence radiation from elemental ions is detected.[39] Although this method requires less sample preparation and preconcentration and is typically faster, it is less

sensitive than other spectroscopic techniques for quantifying palladium. The detection limit using energy-dispersive XRF is 2 ppm for palladium.[41]

The most sensitive method for detecting trace quantities of palladium is inductively-coupled plasma emission spectroscopy (ICP-MS). In ICP-MS, a sample (solid, liquid or gaseous) is ionized by a high temperature (~6000 °C) ICP torch and directed to a quadrupole mass spectrometer for detection.[39] Using this method, as low as 1–10 ppt of Pd can be detected, but more typically quantities between 30–200 ppb.[40] Similar to AAS, ICP-MS also suffers from spectral and non-spectral interferences.[39,40,42] Known spectral interferences (overlapping *m/z*) for palladium are Cu, Zn, Ge, Se, Mo, Zr and Cd among others. Non-spectral interferences are typically due to sample preparation or the sample matrix. Such interferences can also be due to the instrument itself (transport into the plasma source, problems in the ionization or ion transport into the quadrupole). Despite these drawbacks, ICP-MS is the most commonly employed spectroscopic technique for quantifying palladium in environmental, biological and chemical samples.

In general, each of these methods require large and expensive instruments and highly skilled individuals to operate. In addition, such operations require great caution because the electrode can be cross-contaminated.[43] Due to the linear nature of these analyses, such techniques are not amenable to high throughput analysis. A fluorescent method would be more desirable because the measurement requires a far less expensive bench-top or hand-held fluorometer or even a simple laser pen. Moreover, the samples in fluorescent methods are not cross-contaminated because disposable cuvettes (~10 cents/cuvette; 340–800 nm) and multi-well plates are readily available, facilitating high throughput analysis. Therefore, a more desirable approach would rely on high-throughput fluorescent detection.

3.1.4 Fluorescent Sensors for Palladium

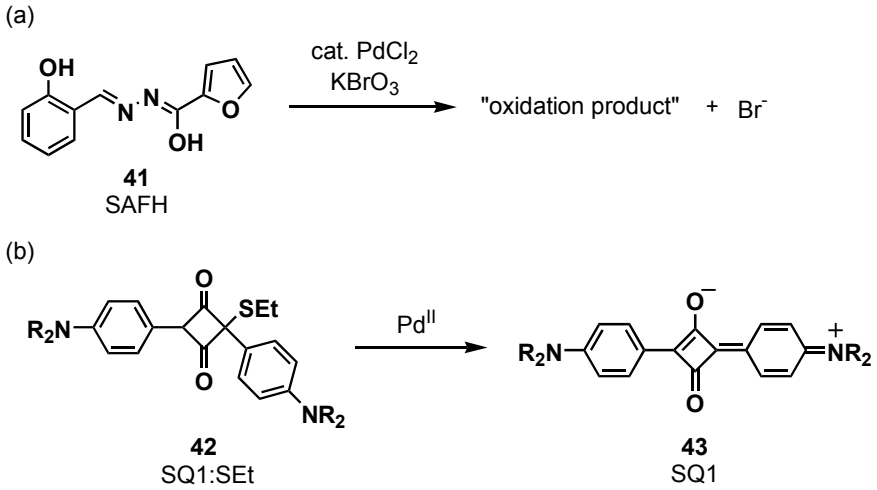

Figure 39. Other fluorescent detection methods for palladium

In addition to our fluorescent sensor for palladium based on the Tsuji-Trost allylic oxidative insertion mechanism[1], two other palladium sensors have been developed and are depicted in Figure 34. In 2004, the Tang group developed sensor **41** based on the salicyladehyde furfuralhydrazone scaffold (SAFH) (Figure 39a).[44] In this method, Pd^{II} catalyzes the oxidation of **41** to an unknown compound, which emits fluorescence at 460 nm. The sensitivity of this method is in the 0–120 ng/mL range with a detection limit of 0.060 ng/mL, and proved to be specific for palladium even in the presence of various metal ions and anions. As applications of this technique, they demonstrated detection in synthetic and mineral samples; however, one potential drawback is the requirement of aqua regia in sample preparation prior to analysis.

More recently, the Anslyn group developed colorimetric chemodosimeter **42** for Pd^{II} detection (Figure 39b).[45] In this system, Pd^{II} scavenges the thiol of colorless **42** to form a color "turn-on" signal from the parent squaraine **43**. The detection limit for this method was estimated as 0.5 ppm using "naked-eye" detection and 0.1 ppm using instrument-based detection. This

technique was then applied to the detection of Pd^{II} in samples synthesized via Suzuki-Miyaura cross-coupling reactions; however, these samples are must be treated with nitric acid in order to convert all Pd species (Pd^0 and Pd^{II}) to a uniform $Pd(NO_3)_2$ species.

3.2 RESULTS AND DISCUSSION

3.2.1 First Generation Palladium Sensing Method: Initial Report

Our first generation palladium sensing method was published in the *Journal of the American Chemical Society* in 2007.[1] The key experiments from this publication are discussed below.

In order to develop a fluorescent method for palladium, it was desirable to perform the conversion of **34** to **35** in aqueous media. More specifically, pH 10 buffer was chosen because a 442-fold fluorescence enhancement is observed in this solvent. As an initial method, the conversion of **34** (10 μM) to **35** was attempted using Ph_3P (250 μM) as a reducing agent and ligand. As Figure 40a shows, this method was successful and selective for palladium, regardless of the metal oxidation state (Figure 40b). It is important to note that this method also exhibited modest specificity for platinum (~40%) (see Chapter 4 for a follow-up on this observation). Interestingly, other π-electrophilic metals such as Ag, Ni, Au, Rh, Co, Hg and Ru did not afford this transformation.

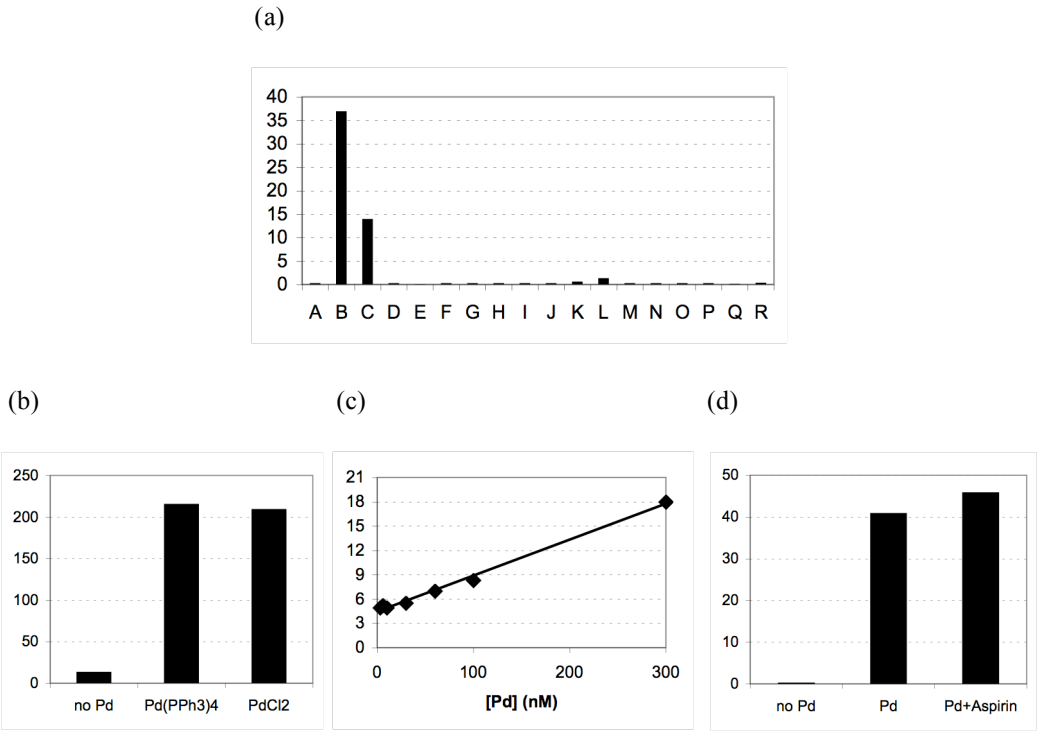

Figure 40. Fluorescence analysis of Pd

In these graphs, the y-axis is fluorescence intensity (a. u. × 10^5) at 523 nm. In all cases, [**34**] = 10 μM and [Ph_3P] = 100 μM, and the assays were performed for 1 h at 24 °C. (a) Metal specificity of Pd sensing method. A = no metal, B = $PdCl_2$, C = $PtCl_2$, D = $FeCl_3$, E = $AgNO_3$, F = $NiCl_2$, G = $Pb(NO_3)_2$, H = $MnCl_2$, I = $CdCl_2$, J = $AuCl_3$, K = $Rh(Ph_3P)_3Cl$, L = $CuCl_2$, M = $MgSO_4$, N = KCl, O = $CrCl_3$, P = $CoCl_2$, Q = $HgCl_2$, R = $RuCl_3$. (b) Fluorescence induction with various Pd oxidation states. (c) Correlation between fluorescence intensity and [$Pd(PPh_3)_4$] (y = 0.0443x + 4.46; R^2 = 0.994); (d) Proof of concept for Pd detection in drugs.

With this successful palladium detection method, the detection limit of this method was determined. As Figure 40c shows, after 1 h incubation at 24 °C the fluorescence intensity is correlated to the concentration of palladium in the 3–300 nM (300 ppt–30 ppb) range. Thus, this method should prove amenable for detecting palladium in various samples.

The applicability of this sensor system for palladium analyses in APIs was next examined. As a proof of concept, Dr. Song spiked a solution containing a commercially available

aspirin tablet (1.0 mg) with palladium (10 ppm final concentration). As Figure 40d shows, the fluorescence signal for the palladium in the aspirin tablet was nearly that of the positive control, which supports the use of this fluorescent method in determining palladium contamination in APIs.

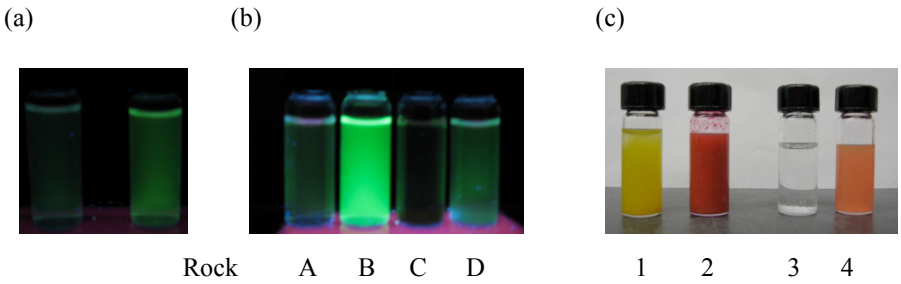

Figure 41. Applications of Pd sensing method

(a) Detection of Pd contamination in a reaction flask. (b) Detection of Pd in rock samples (A = no metals; B = Pd/Pt, 120 ppm; C = Au/Ag; Rock D = Pd/Pt, 35 ppm). (c) Detection of Pd with the naked eyes (1 = $PdCl_2$ (9.4 μmol), dimethylglyoxime; 2 = $PdCl_2$ (9.4 μmol), Sensor, $NaBH_4$; 3 = $PdCl_2$ (30 nmol), dimethylglyoxime; 4 = $PdCl_2$ (30 nmol), Sensor, $NaBH_4$).

An additional concern with Pd-catalyzed cross-coupling reactions is the potential contamination of the reaction vessels in which the reaction was performed. This is especially controversial since in recent years many "Pd-free" cross-coupling reactions have been reported, which have since come into question.[46,47] To test whether this method could detect residual palladium in a reaction flask, a THF solution of a Pd^0 catalyst, $Pd_2(dba)_3$, was stirred in a flask for 1 h at 24 °C. After standard washing procedures (brushing with detergent, washing with water and acetone), fluorescent detection was attempted in the flask. As Figure 41a shows, after 1 h at 24 °C Dr. Song was successful at detecting palladium contamination in the flask, which provides an application for this sensing method in the quality control of reactors.

Current methods of discovering Pd/Pt-containing rock samples typically involve the spectroscopic methods previously described, which cannot be performed at the mining site. As a result, this method may find application in such processes, which can be employed on site with the use of a hand-held fluorometer. Rock samples were obtained from Stillwater Mining Company, each containing either no metal, Pd/Pt or Au/Ag. As Figure 41b shows, only rocks containing Pd/Pt exhibited fluorescence signal demonstrating the viability of our sensor in Pd/Pt detection at mining sites.

As a final application, palladium detection with the naked eyes was attempted. This potential was noted with the first Pd-catalyzed deallylation reaction performed because the THF solution goes from colorless to red/pink nearly instantaneously to signal reaction progress. Dr. Song then compared this method with the well-known spot test for palladium using dimethylglyoxime. The results are shown in Figure 41c where vials 1 and 3 are the spot test results and vials 2 and 4 are the results with our sensor. As Figure 41c indicates, only those solutions containing sensor **34** exhibited a color change detectable with the naked eyes even at 30 nmol further the demonstrating the utility of this sensing method.

3.2.2 First Generation Palladium Sensing Method: Further Studies

Following the initial report describing the palladium sensing method, I wished to further study this transformation. Described below are more in-depth studies concerning **34**.

While the initial experiments were performed in 100% pH 10 buffer, DMSO was added as a co-solvent to aid in the solubility of organic compounds that may be tested using this method. As Figure 42a shows, the addition of DMSO has some effect on the fluorescence intensity of **35**; however, this effect is minor. With respect to **34**, the fluorescence intensity

appears to slightly increase as a function of DMSO content. As a result of these experiments, it was concluded that 5–20% DMSO would be ideal for testing synthetic compounds, and all remaining experiments were conducted using 20% DMSO/buffer as a solvent.

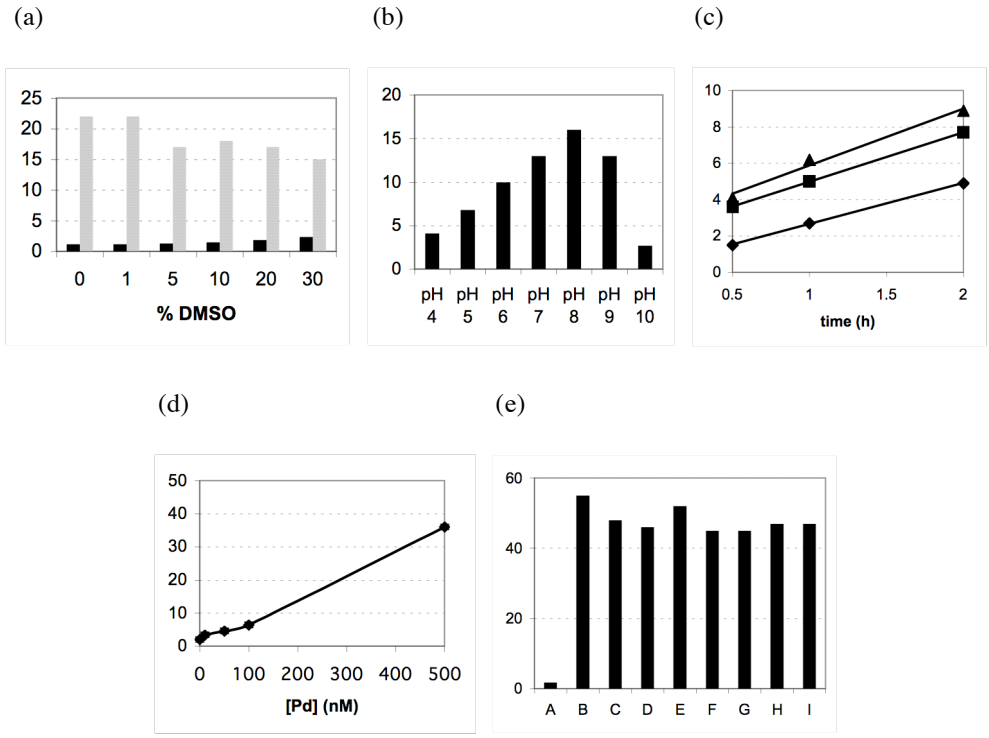

Figure 42. Fluorescence analysis of Pd

In these graphs, the y-axis is fluorescence intensity (a. u. × 10^5) at 525 nm. In all cases, [**34**] = 12.5 μM and [Ph_3P] = 250 μM, and the assays were performed for 1 h at 24 °C. (a) Effect of % DMSO on fluorescence intensity of sensors, black = **34**, gray = **35**. (b) pH-dependent deallylation of **34** in the presence of $PdCl_2$ (625 nM) in 1:4 DMSO/buffer. (c) Initial rate analysis for deallylation of **34** in the presence of $PdCl_2$ (1 mol %) in 1:1 DMSO/buffer. ♦ = pH 4; y = 2.26x + 0.400; R^2 = 0.999. ■ = pH 7; y = 2.73x + 2.25; R^2 = 0.999. ▲ = pH 10; y = 3.13x + 2.75; R^2 = 0.986. (d) Correlation between fluorescence intensity and [$PdCl_2$] in 1:4 DMSO/pH 7 buffer. (e) Fluorescence induction by various Pd species and oxidation states. In all cases, [Pd] = 5.0 μM. A = no Pd, B = $Pd(PPh_3)_4$, C = $PdCl_2$, D = $Pd(OAc)_2$, E = $Pd(acac)_2$, F = $Pd(PPh_3)_2Cl_2$, G = $Pd(MeCN)_2Cl_2$, H = $Pd_2(dba)_3$, I = K_2PdCl_6.

To determine the optimal pH of the palladium-catalyzed deallylation reaction pH dependence in the optimal range for **35** (pH = 4–10) was examined.[48] As Figure 42b shows, the ideal pH with respect to fluorescence intensity lies between pH 6–9. The pH dependence results were then followed up with kinetic assessment. The initial rates were measured at pH 4, 7 and 10 (1:1 DMSO/buffer) using $PdCl_2$ as a catalyst (1 mol %). As Figure 42c shows, reaction occurs at all pHs tested and the rate at pH 10 is fastest although the intensity is lower at this pH due to nonfluorescent cyclic ether formation. The rate at pH 7 was only ~10% slower. From these data, it was deduced that pH 7 is best for palladium fluorescence analysis because it allows for optimal fluorescence intensity and rate.

Using these conditions, the catalytic efficiency and sensitivity of this method was next examined. The turnover frequency (TOF) for palladium in pH 7 buffer under the high dilution and salt conditions ([**34**] = 12.5 μM; [Pd] = 50 nM; $[PO_4^{3-}]$ = 50 mM) was determined as 3.1 h^{-1}. In terms of the quantitative nature of this method for palladium, the fluorescence intensity correlated to the concentration of palladium in the 10 nM–500 nM (1–50 ppb) range after 4 h at 24 °C (Figure 42d).

Although excess Ph_3P is used to fully reduce the palladium species present, other ligands may initially be coordinated to the metal. As such, the generality of this method using a variety of palladium reagents with oxidation states of 0, +2 and +4 was tested. As Figure 42e shows, this method is general for many different palladium species, and thus is successful at effectively converting all palladium to reactive $Pd(PPh_3)_n$ species regardless of other ligands present in the solution. A similar experiment involving various ligands surrounding palladium would be difficult with ICP-MS because it is extremely sensitive to the chemistry within the coordination sphere of the metal.[40] As such, all samples are required to undergo rigorous pre-treatment with

concentrated acid, typically hydrochloric acid, which is necessary to stabilize the chloro-complexes of the metal to obtain a uniform signal. Additionally, the presence of other non-halide ligands may cause undesired spectral interferences.

(a) (b)

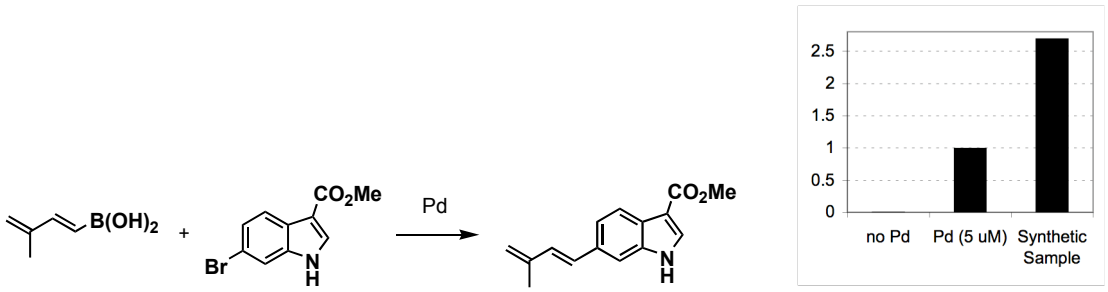

Figure 43. Pd detection in a synthetic sample

(a) Synthetic transformation of Pd-contaminated sample. (b) In this graph, the y-axis is fluorescence intensity (a. u. $\times 10^5$) at 525 nm. The Pd assay was performed in the presence of **34** (12.5 μM) and Ph_3P (250 μM) for 1 h at 24 °C. Left = no Pd; Middle = standard ($PdCl_2$; 5 μM); Right = synthetic sample.

The palladium sensing method was next used to detect palladium content in an actual sample. This method was tested on a purified, indole derivative prepared by a $Pd(PPh_3)_4$-catalyzed Suzuki cross-coupling reaction by Sami Osman. A solution of the purified synthetic sample (5.0 mg) in 1:4 DMSO/pH 7 buffer was treated with **34** and Ph_3P to promote the Pd^0-catalyzed deallylation (Figure 43). The content of Pd was estimated as 14 μM (1200 ppm; 1200 ng/mg) based on relative fluorescent intensities compared to the standard ($PdCl_2$, 5.0 μM). Thus, this method is successful even in the presence of a potentially chelating nitrogen ligand and should find broad application for palladium analysis in pharmaceuticals. From the strong signal with the 5-mg sample, we propose that 0.1–1.0 mg of samples should be sufficient.

3.2.3 Second Generation Palladium Sensing Method

Despite the successes of the first generation palladium sensing method, this method has limitations with respect to sensitivity and catalytic turnover. To enhance these features, a number of different phosphine and phosphite ligands were screened. In addition, the combination of each reagent with $NaBH_4$ was also examined in attempt to further enhance each ligand's reducing capacity.

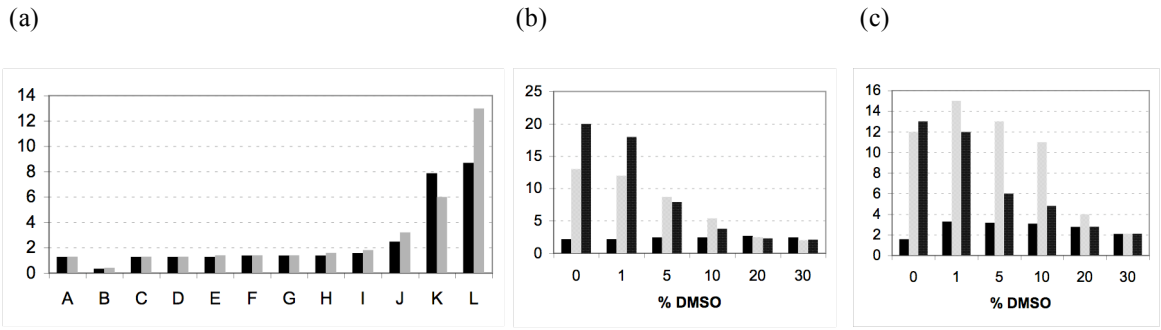

Figure 44. Examination of alternative phosphine ligands

In these graphs, the y-axis is fluorescence intensity (a. u. × 10^5) at 525 nm. In all cases, [**34**] = 12.5 μM, [phosphine] = 250 μM, [$NaBH_4$] = 1.25 mM and [Pd] = 100 nM, and the assays were performed for 1 h at 24 °C. (a) Phosphine screening. Black = phosphine only, gray = phosphine and $NaBH_4$. A = no Pd, B = (1R, 2R)-(+)-1,2-diaminocyclohexane-*N*,*N*'-bis(2'-diphenylphosphinobenzoyl), C = tris(2-carboxyethyl)-phosphine, D = bis(2-diphenylphosphinophenyl)ether, E = 1,1'-bis(diphenylphosphino)ferrocene, F = tris(2,4-di-^{t}butylphenyl)phosphite, G = tri-*o*-tolylphosphine, H = 1,3-bis(diphenylphosphino)propane, I = 1,2-bis(diphenylphosphino)ethane, J = PPh_3, K = JohnPhos, L = TFP. (b) Effect of % DMSO on phosphines. Black = Ph_3P, gray = TFP, dark gray = JohnPhos. (c) Effect of % DMSO on phosphines and $NaBH_4$. Black = Ph_3P, gray = TFP, dark gray = JohnPhos.

From the phosphine ligand screening, two phosphines in addition to Ph_3P were identified that promoted the deallylation reaction, tri-2-furylphosphine (TFP) and 2-(di-

^{t}butylphosphino)biphenyl (JohnPhos). In the absence of $NaBH_4$ (black in Figure 44a), TFP was ~3.5 times more efficient than Ph_3P and JohnPhos was ~3.2 times more efficient than Ph_3P. However, in the presence of $NaBH_4$ (gray in Figure 44a), TFP was ~4.1 times more efficient than Ph_3P and JohnPhos was ~1.9 times more efficient than Ph_3P.

The effect of DMSO on the reaction with these new phosphine ligands was also examined in the absence and presence of $NaBH_4$. As is shown in Figure 44b and 44c, overall the reaction is less efficient as the DMSO content is increased; however, TFP with $NaBH_4$ showed relatively constant fluorescence intensity from 0–10% DMSO.

Interestingly, in organic solvent DMSO is known to take the place of phosphine in its role of reducing agent and ligand to ensure formation of the reactive cationic π-allyl palladium species.[49–51] In this system, the negative impact of DMSO could be the product of a few possibilities. Firstly, aqueous solutions of DMSO are known to exist as highly ordered structures, particularly upon increasing the mole fraction of DMSO, which is primarily due to hydrophobic and hydrophilic hydration of the DMSO molecule.[52] This rigidity in the water molecules could decrease their likelihood of participating as a nucleophile to turnover palladium in the catalytic cycle, which would significantly damper the reaction efficiency. Secondly, there is the potential for increased formation of the cyclic ether form of **35**, which may be less reactive than the open form, and is a common phenomenon for the fluorescein scaffold (see Figure 21).[53] From these results, it was concluded that TFP with $NaBH_4$ was the optmal reducing agent/ligand combination and 5% DMSO was ideal for maximizing reaction efficiency and fluorescence intensity (see Figure 42a).

TFP is a well-studied ligand in the organometallics field, and an article in *Chemical Reviews* is dedicated wholly to this ligand and its utility in organic synthesis.[54] While this ligand

was first discovered to enhance the Stille reaction,[55] it has since been applied to a wide variety of Pd-, Ni-, Rh- and Ru-catalyzed cross-coupling reactions. For the Stille reaction, the key property of TFP is its low electron donating ability, which is proposed to enhance the rate of transmetallation into the C–Sn bond. Interestingly, TFP was found to be a poor ligand in allylic alkylation chemistry unless a substrate capable of undergoing fast oxidative addition was used;[56] however, in another study, TFP was found to enhance the rate of oxidative addition into aryl-halide bonds in comparison to Ph_3P when DMF was employed as a solvent.[57] Although the exact mechanism with which TFP enhances the Pd-catalyzed Tsuji-Trost type reaction in aqueous solution is not known, it may be speculated that TFP helps to promote the formation of the reactive cationic π-allyl palladium intermediate by serving as a weak electron donor, which activates it toward nucleophilic attack by either water or phosphate in the buffer. Additionally, because it is a weaker ligand, it is less likely to form the stable and unreactive $Pd(TFP)_4$ species.

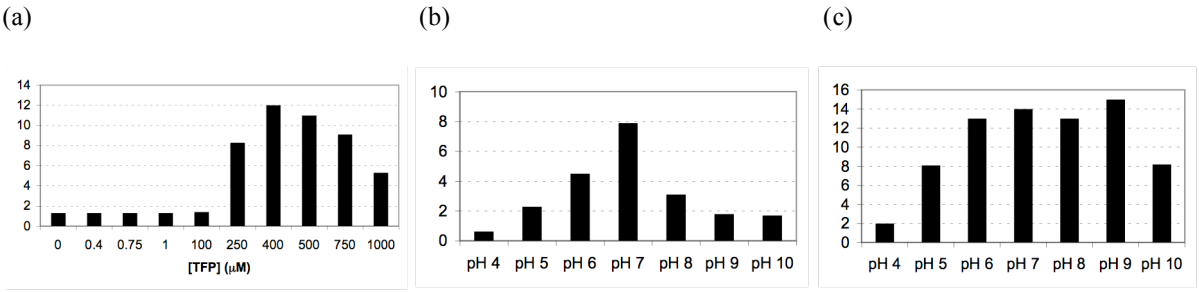

Figure 45. Optimization studies with TFP

In these graphs, the y-axis is fluorescence intensity (a. u. × 10^5) at 525 nm. In all cases, [**34**] = 12.5 μM, [$NaBH_4$] = 1.25 mM and [Pd] = 100 nM, and the assays were performed for 1 h at 24 °C. (a) Correlation between fluorescence intensity and [TFP]. (b) pH-dependent deallylation of **34** in the presence TFP (500 μM) in 5:95 DMSO/buffer. (c) pH-dependent deallylation of **34** in the presence of TFP (500 μM) and $NaBH_4$ in 5:95 DMSO/buffer.

The reaction was first screened to determine the optimal TFP concentration, and as Figure 45a shows 400–500 μM is the ideal TFP concentration range. The optimal pH of the Pd-catalyzed deallylation reaction with TFP in the presence and absence of $NaBH_4$ was next examined. Similar to the results with Ph_3P (see Figure 42b), the ideal pH in the absence of $NaBH_4$ was pH 7 (Figure 45b). In fact, the fluorescence intensity dropped at ± 1 pH unit indicating that reaction with this ligand seems to be more sensitive to changes in pH. This is mostly likely due to the fact that it is a less electron donating ligand. In the presence of $NaBH_4$, however, the ideal pH ranges from pH 6–9 (Figure 45c). From these results, the optimal conditions are TFP (500 μM) and $NaBH_4$ (1.25 mM) in 5:95 DMSO/pH 7 buffer.

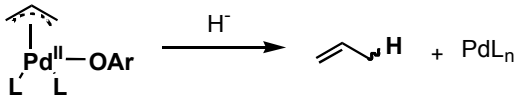

Figure 46. Role of $NaBH_4$ as a nucleophile

The role of hydride reagents is three-fold: first to reduce Pd^{II} to Pd^0 to reinitiate the catalytic cycle, second to act as a nucleophile to directly attack the allyl group (Figure 46) and third to form a highly reactive Pd–H species.[58] In addition to $NaBH_4$, formic acid, tributyltin hydride and silicon hydrides are known to act in the same capacity.[19]

The sensitivity and catalytic efficiency of the Pd-catalyzed deallylation reaction with the new TFP/$NaBH_4$ conditions was next determined. The fluorescence intensity correlated to the concentration of palladium in the 1.0 nM–1.0 μM (0.1–100 ppb) range with signal-to-background (S/B) of 1.1–14 after 4 h at 24 °C (Figure 47a). The detection limit with S/B of 3 is 42 nM (4.5 ppb) after 1 h and 24 nM (2.6 ppb) after 4 h, which is a 8-fold enhancement compared to our previous method (Figure 47c). As this Figure shows, this new method is far

superior to the originally reported method with respect to sensitivity (see Figures 40c and 42d). The initial rate using these conditions ([Pd] = 100 nM; Figure 47b) was measured and the reaction is ~4.8 times greater than that with the previous conditions (see Figure 42c). The TOF for Pd using the TFP/$NaBH_4$ method was determined as 14.1 h^{-1}, which is also ~4.5 times greater than the previous method. To further demonstrate the robustness of this sensing method, Pd-catalyzed deallylation of **34** was attempted in coffee (Figure 47d).

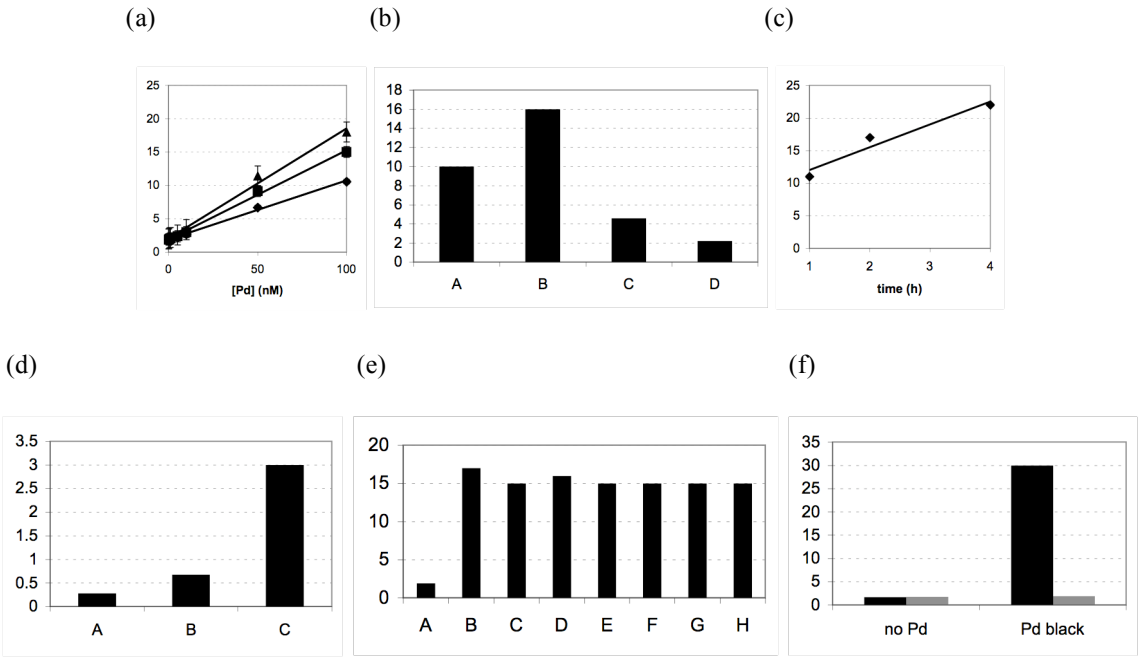

Figure 47. Fluorescence analysis of Pd

In these graphs, the y-axis is fluorescence intensity (a. u. × 10^5) at 525 nm. In all cases, [**34**] = 12.5 μM, [TFP] = 500 μM and [$NaBH_4$] = 1.25 mM, and the assays were performed for 1 h at 24 °C. (a) Correlation between fluorescence intensity and [Pd] in 5:95 DMSO/pH 7 buffer. ♦ = 1 h; y = 0.0888x + 1.87; R^2 = 0.997. ■ = 2 h; y = 0.134x + 1.88; R^2 = 0.997. ▲ = 4 h; y = 0.165x + 2.01; R^2 = 0.993. (b) Comparison of Pd detection methods after 4 h. [Pd] = 100 nM. A = TFP in 5:95 DMSO/pH 7 buffer, B = TFP/$NaBH_4$ in 5:95 DMSO/pH 7 buffer, C = Ph_3P in 1:4 DMSO/pH 7 buffer, D = Ph_3P/$NaBH_4$ in 5:95 DMSO/pH 7 buffer. (c) Initial rate analysis for deallylation of **34** in the presence of Pd (100 nM) in 5:95 DMSO/pH 7 buffer. y = 3.50x + 8.5; R^2 = 0.942. (d) Pd detection in coffee. A = no Pd, B =

100 nM Pd, C = 1.0 μM Pd. (e) Fluorescence induction by various Pd species and oxidation states. In all cases, [Pd] = 100 nM. A = no Pd, B = $PdCl_2$, C = $Pd(OAc)_2$, D = $Pd(acac)_2$, E = $Pd(PPh_3)_2Cl_2$, F = $Pd(MeCN)_2Cl_2$, G = $Pd_2(dba)_3$, H = Pd standard. (f) Fluorescence induction by Pd black (<1.0 mg). Black = with TFP/$NaBH_4$, gray = no reducing agents.

The generality of this method was examined, and it is general for many palladium sources (Figure 47e). In addition to soluble palladium species, detection of Pd black was also examined (Figure 47f). In the presence of reducing agents (TFP with $NaBH_4$; black in Figure 47f), detection of the metal is successful; however, in the absence of reducing agents (gray in Figure 47f), no detection was observed. Thus, sensor **34** is capable of detecting both soluble and insoluble Pd^0 species.

3.2.4 Palladium Detection in Synthetic Samples

While the previous method was successful in detecting palladium contamination in synthetic samples with limited functionality (see Figures 40d and 43), it could not detect palladium in compounds containing potentially chelating functional groups such as sulfides. This task is extremely difficult for two reasons: (1) there is a very large excess of synthetic compound relative to palladium (~100000-fold excess in a 10-ppm Pd contaminated sample), and thus, there is greater chance for palladium to remain bound to the synthetic compound rather than participate in catalysis; and (2) because palladium is bound to these compounds, each palladium species is ligated differently and may react differently. As such, it is important to find a method that will not only break the palladium-synthetic compound complexes but will also effectively convert all palladium contamination to a uniform species that will react in a predictable manner.

In ICP-MS, these requirements are achieved via sample preparation with concentrated nitric acid, typically 1 mg/mL, and in some cases microwave digestion.[59–61] This often time-consuming step is necessary because ICP-MS is extremely sensitive to the chemistry within the coordination sphere of the metal. In addition, because of its linearity and time per sample (15–30 min per sample including instrument washing), analytical laboratories are often overloaded with samples and the analyses are significantly delayed (Dr. Christopher Welch, Merck; personal communication). Thus, although this method is sensitive (detection limit: 10–100 ppb), a high throughput method is greatly needed.

Described below are the best conditions to date to accomplish this challenging feat.

(a)

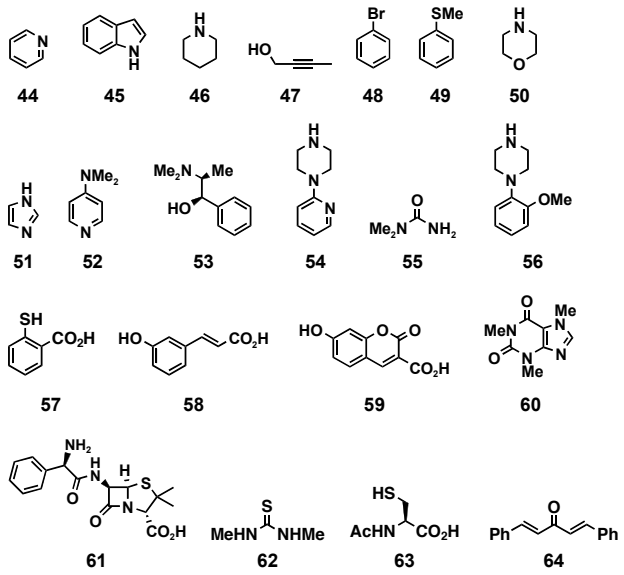

(b)

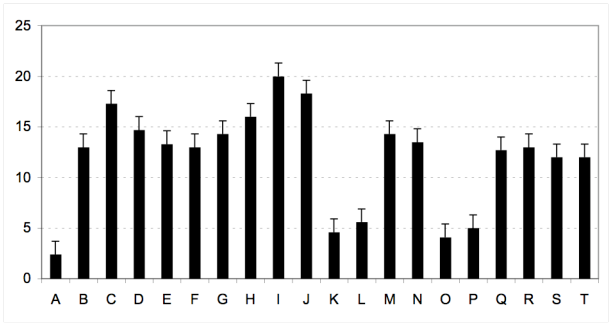

(c)

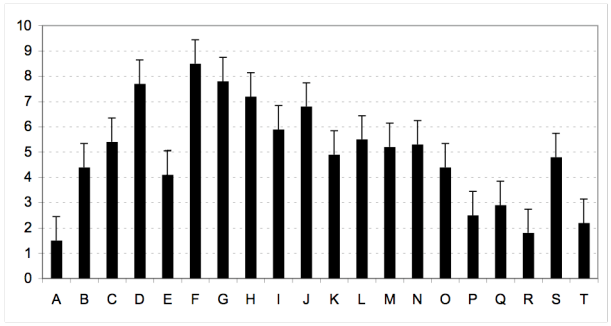

(d) (e)

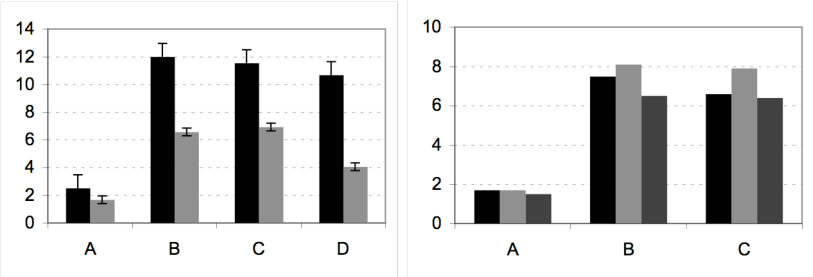

Figure 48. Pd detection in spiked synthetic compounds

In these graphs, the y-axis is fluorescence intensity (a. u. × 10^5) at 525 nm. In all cases, [**34**] = 12.5 μM, [TFP] = 500 μM, [$NaBH_4$] = 1.25 mM and [Pd] = 8.5 ppm with respect to the synthetic compound, and the assays were performed for 1 h at 24 °C. The error bars in (b)–(d) represent the average standard deviation of the compounds from triplicate experiments. (a) Structures of synthetic compounds that were spiked with Pd. (b) Detection of Pd contamination in 5:95 DMSO/pH 10 buffer after pretreatment with concentrated HCl (60 mM). A = no Pd, B = positive control, C = **44**, D = **45**, E = **46**, F = **47**, G = **48**, H = **49**, I = **50**, J = **51**, K = **52**, L = **53**, M = **54**, N = **55**, O = **56**, P = **57**, Q = **58**, R = **59**, S = **60**, T = **61**. (c) Detection of Pd contamination in 5:95 DMSO/pH 7 buffer (150 mM) after pretreatment with concentrated HCl (60 mM). A = no Pd, B = positive control, C = **44**, D = **45**, E = **46**, F = **47**, G = **48**, H = **49**, I = **50**, J = **51**, K = **52**, L = **53**, M = **54**, N = **55**, O = **56**, P = **57**, Q = **58**, R = **59**, S = **60**, T = **61**. (d) Pd detection in the presence of **62** or **63** ([Pd] = 100 nM; [**62**/**63**] = 500 nm). A = no Pd, B = positive control, C = Pd + **62**, D = Pd + **63**. Black = pH 10 method, gray = pH 7 method. (e) Pd detection in the presence of equimolar Ph_3P or dba (**64**) ([Pd] = 100 nM; [Ph_3P/**64**] = 100 nM). Black = no **54**, gray = Pd + **54**, dark gray = Pd + **54** + Ph_3P/**64**. A = no Pd, B = Ph_3P, C = **64**.

Toward this goal, a pretreatment method was developed that met both of the criteria described above. Using ampicillin (**55**; Figure 48a) as a model compound since it is an example of a highly functionalized, drug-like compound, many different pretreatment methods (not shown) were examined, and it was found that treatment of 5 mg of compound in DMSO (200 μL) with 12N HCl (20 μL) was successful in consistently recovering fluorescence signal. This method was then used to examine palladium detection in a variety of functionalized organic

compounds (Figure 48a). To my delight, treatment of solutions of Pd-spiked samples ([Pd] = 8.5 ppm in the compound) in DMSO with 12N HCl followed by dilution with pH 10 buffer and addition of TFP, $NaBH_4$ and **34** led to successful recovery of fluorescent signal (31–153%) for a variety of molecular structures (Figure 48b) after 1 h incubation at 24 °C. These molecules include potentially chelating atoms found in many privileged structures and drug-like compounds (nitrogen, sulfur), potentially reactive groups (bromobenzene, 2-butyn-1-ol, 2-hydroxycinnamic acid) and other fluorophores (carboxyumbelliferone). The fact that quantitative recovery can be obtained even in the presence of such a large excess of compound implies limited interferences from differences in sample matrix, which is a known problem in ICP-MS.

One potential problem with this method, however, became apparent after examination of the unsuccessful compounds. Amines are largely unprotonated at pH 9–10, and this should enhance their ability to chelate to palladium. In order to mask amines, the Pd-spiked samples in DMSO were treated with 12N HCl followed by dilution with pH 7 buffer ($[PO_4^{3-}]$ = 150 mM) to ensure overall pH 7 in the final solution. TFP, $NaBH_4$ and **34** were then added and the samples were incubated for 1 h at 24 °C. As Figure 48c shows, this method was successful in recovering fluorescence signal in the presence of amines. However, signal was lost with sulfur and carboxylic acid-containing compounds. Thus, through the choice of the two pHs, palladium contamination can be determined in a variety of functionalized small molecules.

In order to remove palladium from synthetic samples, many methods utilize sulfur-based reagents such as thiourea and *N*-acetylcysteine.[33,34,36] Residual amounts of these reagents can also be found in samples after removal operation. Thus, it is important for this method to be able to detect palladium even in the presence of these reagents. Although the method failed to detect palladium in the presence of 85000 equivalents of **62** and **63**, as Figure 48d shows palladium can

successfully be detected in the presence of 5 equivalents of each of these reagents, which is a more realistic content. In addition to S-based ligands, other potentially chelating ligands (not the actual synthetic compound) may also be present; and as Figure 48e shows, ligands such as Ph_3P and dba (**64**) (1 equivalent) do not interfere.

3.3 CONCLUSION

In collaboration with Dr. Song, a highly sensitive and robust fluorescent sensor (**34**) has been developed for palladium based upon the Tsuji-Trost allylic oxidative insertion mechanism. This method allows for the detection of total quantities of palladium at sub-ppb levels. Importantly, fluorescent detection of palladium in synthetic samples has been demonstrated. This sensor technology should change the paradigm of palladium analyses and find broad applications in materials, energy and human health.

3.4 EXPERIMENTAL

3.4.1 General Information

$PdCl_2$, $PdCl_2(PPh_3)_4$, $Pt(PPh_3)_4$, $PtCl_2$ and $H_2PtCl_6 \bullet 6H_2O$ were purchased from Alfa Aesar and used as received. $Pd(PPh_3)_4$, $Pd(acac)_2$, $PdCl_2(MeCN)_2$ and K_2PdCl_6 were purchased from Strem and used as received. $Pd(OAc)_2$ was purchased from TCI and used as received. Aspirin is a product of BAYER Co. Buffers were purchased and used as received (pH 4, potassium

biphthalate ([biphthalate] = 49.8–50.2 mM), J. T. Baker, Catalog Number 5606-01; pH 7, phosphate ($[PO_4^{3-}]$ = 46–50 mM, $[K^+]$ = 23–25 mM, $[Na^+]$ = 50–56 mM), J. T. Baker, Catalog Number 5608-01; pH 10, borate ($[K^+]$ = 94–114 mM), J. T. Baker, Catalog Number 5609-01).

3.4.2 First Generation Palladium Sensing Method: Initial Report

Preparation of parent stock solutions used for this study.

Entry	Reagent	Quantity	Solvent (10 mL)	Conc. of stock solution
A	compound **34**	42.7 mg (0.10 mmol)	DMSO	10.0 mM
B	PPh_3	262.3 mg (1.00 mmol)	DMSO	100 mM
C	$PdCl_2$	9.0 mg (50 µmol)	3:1 Brine/MeOH	5.0 mM
D	$Pd(PPh_3)_4$	57.7 mg (50 µmol)	DMSO	5.0 mM
E	Aspirin	500 mg	pH 10 buffer	10 mg/mL

Notes:

(1) All the solutions were stored at 24 °C.

(2) Solution **A** was stored in the dark as a precautionary measure.

(3) Solution **B** was freshly prepared every 2 weeks. We found that 2 month-old solution of PPh_3 was not effective presumably due to air-oxidation.

(4) Each of these stocks with the respective solvent was further diluted to prepare 1.0 mM–1.0 µM stock solutions.

Fluorescence spectroscopy. Fluorescence spectra were recorded in a 1 × 1-cm quartz cuvette on a Jobin Yvon FluoroMax-3 spectrometer under the control of a Windows-based PC running FluorEssence software. The samples were excited at 497 nm and the emission intensities were collected at 523 nm. All spectra were corrected for emission intensity using the manufacturer supplied photomultiplier curves.

First generation Pd sensing method. Varying amounts of Pd solution and solution **B** (5 μL, $[PPh_3]_{final}$ = 100 μM) were added to pH 10 buffer solution (4.0 mL). Solution **A** (5 μL, $[\mathbf{34}]_{final}$ = 10 μM) was then added to the mixture, and the samples were incubated for 1 h at 24 °C before fluorescence measurement.

3.4.3 First Generation Palladium Sensing Method: Further Studies

Preparation of parent stock solutions used for this study.

Entry	Reagent	Quantity	Solvent (10 mL)	Conc. of stock solution
A	compound **34**	42.7 mg (0.10 mmol)	DMSO	10.0 mM
B	PPh_3	262.3 mg (1.00 mmol)	DMSO	100 mM
C	$PdCl_2$	9.0 mg (50 μmol)	3:1 Brine/MeOH	5.0 mM
D	$Pd(OAc)_2$	2.2 mg (10 μmol)	3:1 Brine/MeOH	1.0 mM
E	$Pd(acac)_2$	3.0 mg (10 μmol)	DMSO	1.0 mM
F	$PdCl_2(PPh_3)_4$	7.0 mg (10 μmol)	DMSO	1.0 mM
G	$PdCl_2(MeCN)_2$	2.6 mg (10 μmol)	3:1 Brine/MeOH	1.0 mM
H	K_2PdCl_6	19.9 mg (50 μmol)	3:1 Brine/MeOH	5.0 mM
I	$Pd(PPh_3)_4$	57.7 mg (50 μmol)	DMSO	5.0 mM

Notes: See previous experimental

Fluorescence spectroscopy. Fluorescence spectra were recorded in a 1 × 1-cm disposable cuvette (VWR; catalog number 58017-880) on a Jobin Yvon FluoroMax-3 spectrometer under the control of a Windows-based PC running FluorEssence software. The samples were excited at 497 nm and the emission intensities were collected at 525 nm. All spectra were corrected for emission intensity using the manufacturer supplied photomultiplier curves.

Palladium: buffer screening. $PdCl_2$ solution (25.0 μL of 100.0 μM stock, 625 nM final concentration) and solution **B** (10.0 μL, $[PPh_3]_{final}$ = 250 μM) were added to DMSO/pH X buffer (1:4) solution (X = 4.0–10.0) (4.0 mL). Solution **A** (5.0 μL, $[\mathbf{34}]_{final}$ = 12.5 μM) was then added

to the mixture, and the samples were incubated for 1 h at 24 °C before fluorescence measurement.

Palladium: initial rate analysis. $PdCl_2$ stock solution **C** (50.0 μL, 250 nmol), PPh_3 (4.8 mg, 2.34 μmol) and **34** (10.0 mg, 23.4 μmol) were added to DMSO/pH X buffer (1:1) solution (X = 4.0, 7.0, 10.0) (20 mL) at 24 °C. The experiment was performed in triplicate. At t = 0.5, 1 and 2 h, 100 μL aliquots were taken from each reaction mixture and diluted to 4.0 mL with DMSO/pH 7.0 buffer (1:4) for fluorescence measurement.

Palladium: TOF. To determine the turnover frequency, a solution containing $PdCl_2$ solution ($[PdCl_2]_{final}$ = 50 nM), solution **B** (10.0 μL, $[PPh_3]_{final}$ = 250 μM) and solution **A** (5.0 μL, $[\mathbf{34}]_{final}$ = 12.5 μM) was prepared in DMSO/pH 7.0 buffer (1:4). The intensity of this sample was compared to a standard solution containing Pittsburgh Green **35** ($[\mathbf{35}]_{final}$ = 50 nM) in DMSO/pH 7.0 buffer (1:4). The intensity of the Pd^{2+}-containing sample was 1.9×10^6 after 7 h at 24 °C and the intensity of the standard solution of **35** was 8.8×10^4. The turnover frequency is $1.9 \times 10^6 / 8.8 \times 10^4 = 21.6/7$ h = 3.1 h^{-1}.

Palladium: concentration dependence. Varying amounts of Pd solution and solution **B** (10.0 μL, $[PPh_3]_{final}$ = 250 μM) were added to DMSO/pH 7.0 buffer solution (1:4; $[PO_4^{3-}]$ = 5 mM) (4.0 mL). Solution **A** (5.0 μL, $[\mathbf{34}]_{final}$ = 12.5 μM) was then added to the mixture, and the samples were incubated for 4 h at 24 °C before fluorescence measurement.

Dependence on palladium reagents. Pd solutions (20.0 μL of 1.0 mM stock, $[Pd]_{final}$ = 5.0 μM) and solution **B** (10.0 μL, $[PPh_3]_{final}$ = 250 μM) were added to DMSO/pH 7.0 buffer (1:4) solution (4.0 mL). Solution **A** (5.0 μL, $[\mathbf{34}]_{final}$ = 12.5 μM) was then added to the mixture, and the samples were incubated for 1 h at 24 °C before fluorescence measurement.

Palladium detection in synthetic sample. The synthetic sample (5.0 mg) was dissolved in 800 μL of DMSO and pH 7.0 buffer was added (3.2 mL; total volume = 4.0 mL). Solution **B** (10.0 μL, $[PPh_3]_{final}$ = 250 μM) and solution **A** (5.0 μL, $[\mathbf{34}]_{final}$ = 12.5 μM) were then added to the mixture. A positive control was also prepared ($PdCl_2$; $[Pd]_{final}$ = 5.0 μM) and the samples were incubated for 1 h at 24 °C before fluorescence measurement.

3.4.4 Second Generation Palladium Sensing Method

Preparation of parent stock solutions used for this study.

Entry	Reagent	Quantity	Solvent (10 mL)	Conc. of stock solution
A	compound **34**	42.7 mg (0.10 mmol)	DMSO	10.0 mM
B	TFP	232.17 mg (1.00 mmol)	DMSO	100 mM
C	$NaBH_4$	943 mg (25 mmol)	10 M NaOH	2.5 M
D	Pd standard	10.6 mL (100 μmol)	1% HNO_3	1.0 mM
E	$PdCl_2$	9.0 mg (50 μmol)	3:1 Brine/MeOH	5.0 mM
F	$Pd(OAc)_2$	2.2 mg (10 μmol)	3:1 Brine/MeOH	1.0 mM
G	$Pd(acac)_2$	3.0 mg (10 μmol)	DMSO	1.0 mM
H	$PdCl_2(PPh_3)_4$	7.0 mg (10 μmol)	DMSO	1.0 mM
I	$PdCl_2(MeCN)_2$	2.6 mg (10 μmol)	3:1 Brine/MeOH	1.0 mM

Notes:

(1) Solution A – see previous experimentals

(2) Solution **B** was freshly prepared every 2 weeks.

(3) Solution C – Further dilution with pH 9 buffer was done to prepare a 100 mM solution.

(4) Solution D - This Pd stock was prepared from a commercial Pd standard (1000 ± 3 μg/mL in 10% HNO_3 (product of High-Purity Standards (Cat. # 100038-1, Lot # 632601).

Fluorescence spectroscopy. Fluorescence spectra were recorded in a 1 × 1-cm disposable cuvette (VWR; catalog number 58017-880) on a Jobin Yvon FluoroMax-3 spectrometer under the control of a Windows-based PC running FluorEssence software. The samples were excited at 497 nm and the emission intensities were collected at 525 nm. All spectra were corrected for emission intensity using the manufacturer supplied photomultiplier curves.

Palladium: buffer screening. Pd standard (40.0 μL of 10.0 μM stock, $[Pd]_{final}$ = 100 nM), solution **B** (20.0 μL, $[TFP]_{final}$ = 500 μM), and solution **C** (50.0 μL, $[NaBH_4]_{final}$ = 1.25 mM) were added to DMSO/pH X buffer (5:95) solution (X = 4.0–10.0) (4.0 mL). After shaking, solution **A** (5.0 μL, $[\mathbf{34}]_{final}$ = 12.5 μM) was added, and the samples were incubated for 1 h at 24 °C before fluorescence measurement.

Palladium: Turnover frequency. To determine the turnover frequency, a solution containing Pd standard ($[Pd]_{final}$ = 100 nM), solution **B** (20.0 μL, $[TFP]_{final}$ = 500 μM), solution **C** (50.0 μL, $[NaBH_4]_{final}$ = 1.25 mM) and solution **A** (5.0 μL, $[\mathbf{34}]_{final}$ = 12.5 μM) was prepared in DMSO/pH 7.0 buffer (5:95). The intensity of this sample was compared to a standard solution containing Pittsburgh Green **35** ($[\mathbf{35}]_{final}$ = 100 nM) in DMSO/pH 7.0 buffer (5:95). The intensity of the Pd^{2+}-containing sample was 1.2×10^6 after 1 h at 24 °C and the intensity of the standard solution of **35** was 8.2×10^4. The turnover frequency is $(1.2 \times 10^6 / 8.2 \times 10^4)/1\ h = 14.1\ h^{-1}$.

Palladium: concentration dependence. Varying amounts of Pd solution, solution **B** (20.0 μL, $[TFP]_{final}$ = 500 μM) and solution **C** (50.0 μL, $[NaBH_4]_{final}$ = 1.25 mM) were added to DMSO/pH 7.0 buffer solution (5:95) (4.0 mL). After shaking, solution **A** (5.0 μL, $[\mathbf{34}]_{final}$ = 12.5 μM) was added, and the samples were incubated for 4 h at 24 °C before fluorescence measurement.

Dependence on palladium reagents. Pd solutions (40.0 μL of 10 μM stock, $[Pd]_{final}$ = 100 nM), solution **B** (20.0 μL, $[TFP]_{final}$ = 250 μM) and solution **C** (50.0 μL, $[NaBH_4]_{final}$ = 1.25 mM) were added to DMSO/pH 7.0 buffer (5:95) solution (4.0 mL). After shaking, solution **A** (5.0 μL, $[\mathbf{34}]_{final}$ = 12.5 μM) was added, and the samples were incubated for 1 h at 24 °C before fluorescence measurement.

Palladium detection in compounds: pH 10 method. A solution of compound (5.0 mg) was prepared in DMSO (200 μL) and spiked with Pd standard solution (40 μL of 10 μM solution in 1% HNO_3; $[Pd]_{sample}$ = 8.5 ppm) and the sample was allowed to sit on a bench for 30 min. Following incubation, the sample was treated with 12N HCl (20 μL, $[HCl]_{final}$ = 60 mM) and allowed to incubate at 24 °C for 10 min. The sample solution was then diluted with pH 10 buffer ($[K^+]$ = 114 mM; 3.8 mL) and treated with solution **B** (20.0 μL, $[TFP]_{final}$ = 250 μM) and solution **C** (50.0 μL, $[NaBH_4]_{final}$ = 1.25 mM). After shaking and 5 min incubation at 24 °C, solution **A** (5.0 μL, $[\mathbf{34}]_{final}$ = 12.5 μM) was added, and the samples were incubated for 1 h at 24 °C before fluorescence measurement.

Palladium detection in compounds: pH 7 method. A solution compound (5.0 mg) was prepared in DMSO (200 μL) and spiked with Pd standard solution (40 μL of 10 μM solution in

1% HNO_3; $[Pd]_{sample}$ = 8.5 ppm) and the sample was allowed to sit on a bench for 30 min. Following incubation, the sample was treated with 12N HCl (20 μL, $[HCl]_{final}$ = 60 mM) and allowed to incubate at 24 °C for 10 min. The sample solution was then diluted with pH 7 buffer ($[PO_4^{3-}]$ = 150 mM; prepared by diluting pH 7 buffer concentrate ($[PO_4^{3-}]$ = 1.25 M; Fisher Scientific, Cat. # SB109-500, Lot # 065758) with Aristar® ULTRA Water; 3.8 mL) and treated with solution **B** (20.0 μL, $[TFP]_{final}$ = 250 μM) and solution **C** (50.0 μL, $[NaBH_4]_{final}$ = 1.25 mM). After shaking and 5 min incubation at 24 °C, solution **A** (5.0 μL, $[\mathbf{34}]_{final}$ = 12.5 μM) was added, and the samples were incubated for 1 h at 24 °C before fluorescence measurement.

3.5 BIBLIOGRAPHY

1. Song, F., Garner, A. L., Koide, K., "A highly sensitive fluorescent sensor for palladium based on the allylic oxidative insertion mechanism." *J. Am. Chem. Soc.* **2007**, *129*, 12354–12355.

2. Rotman, B., "Measurement of activity of single molecules of β-D-galactosidase." *Proc. Natl. Acad. Sci. U. S. A.* **1961**, *47*, 1981–1991.

3. Tsuji, J., Takahashi, H., Morikawa, M., "Organic syntheses by means of nobel metal compounds XVII. Reaction of π-allylpalladium chloride with nucleophiles." *Tetrahedron Lett.* **1965**, *49*, 4387–4388.

4. Trost, B. M., Fullerton, T. J., "New synthetic reactions. Allylic alkylation." *J. Am. Chem. Soc.* **1973**, *95*, 292–294.

5. Trost, B. M., Strege, P. E., Weber, L., Fullerton, T. J., Dietsche, T. J., "Allylic alkylation: preparation of π-allylpalladium complexes from olefins." *J. Am. Chem. Soc.* **1978**, *100*, 3407–3415.

6. Trost, B. M., Weber, L., Strege, P. E., Fullerton, T. J., Dietsche, T. J., "Allylic alkylation: nucleophilic attack on π-allylpalladium complexes." *J. Am. Chem. Soc.* **1978**, *100*, 3416–3426.

7. Trost, B. M., Weber, L., Strege, P. E., Fullerton, T. J., Dietsche, T. J., "Allylic alkylation: nature of the nucleophile and application to prenylation." *J. Am. Chem. Soc.* **1978**, *100*, 3426–3435.

8. Trost, B. M., "Organopalladium intermediates in organic synthesis." *Tetrahedron* **1977**, *33*, 2615–2649.

9. Frost, C. G., Howarth, J., Williams, J. M. J., "Selectivity in palladium catalyzed allylic substitution." *Tetrahedron: Asymmetry* **1992**, *3*, 1089–1122.

10. Yamamoto, T., Akimoto, M., Saito, O., Yamamoto, A., "Interaction of palladium(0) complexes with allylic acetates, allyl ethers, allyl phenyl chalcogenides, allylic alcohols, and allyl amines. Oxidative addition, condensation, disproportionation, and π-complex formation." *Organometallics* **1986**, *5*, 1559–1567.

11. Kurosawa, H., "Molecular basis of catalytic reactions involving η^3-allyl complexes of group 10 metals as key intermediates." *J. Organomet. Chem.* **1987**, *334*, 243–253.

12. Åkermark, B., Hansson, S., Krakenberger, B., Vitagliano, A., Zetterberg, K., "Alkylation of (π-allyl)palladium systems. Mechanism and regiocontrol." *Organometallics* **1984**, *3*, 679–682.

13. Powell, J., Shaw, B. L., "Transition metal-carbon bonds. Part XVI. Cationic allylic complexes of palladium(II). A cationic complex of platinum(II)." *J. Chem. Soc. A* **1968**, 774–777.

14. Johnson, B. F. G., Lewis, J., White, D. A., "Cationic transition metal-olefin complexes." *J. Am. Chem. Soc.* **1969**, *91*, 5186–5187.

15. Schrock, R. R., Osborn, J. A., "Coordinatively unsaturated cationic complexes of rhodium(I), iridium(I), palladium(II), and platinum(II). Generation, synthetic utility, and some catalytic studies." *J. Am. Chem. Soc.* **1971**, *93*, 3089–3091.

16. Guibé, F., "Allylic protecting groups and their use in a complex environment part II: allylic protecting groups and their removal through catalytic palladium π-allyl methodology." *Tetrahedron* **1998**, *54*, 2967–3042.

17. Karpf, M., Trussardi, R., "New, azide-free transformation of epoxides into 1,2-diamino compounds: synthesis of the anti-influenza neuraminidase inhibitor Oseltamivir phosphate (Tamiflu)." *J. Org. Chem.* **2001**, *66*, 2044–2051.

18. Kunz, H., Waldmann, H., "The allyl group as mildly and selectively removable carboxy-protecting group for the synthesis of labile *O*-glycopeptides." *Angew. Chem. Int. Ed.* **1984**, *23*, 71–72.

19. Tsuji, J., Mandai, T., "Palladium-catalyzed hydrogenolysis of allylic and propargylic compounds with various hydrides." *Synthesis* **1996**, 1–24.

20. Genêt, J. P., Blart, E., Savignac, M., Lemeurie, S., Lemaire-Audoire, S., Bernard, J. M., "A general and simple removal of the allyloxycarbonyl protecting group by palladium-catalyzed reactions using nitrogen and sulfur nucleophiles." *Synlett* **1993**, 680–682.

21. Streu, C., Meggers, E., "Ruthenium-induced allylcarbamate cleavage in living cells." *Angew. Chem. Int. Ed.* **2006**, *45*, 5645–5648.

22. "Environmental Health Criteria 226: Palladium." World Health Organization, Geneva, 2002.

23. Zereini, F., Wiseman, C., Püttmann, W., "Changes in palladium, platinum, and rhodium concentrations, and their spatial distribution in soils along a major highway in Germany form 1994 to 2004." *Environ. Sci. Technol.* **2007**, *41*, 451–456.

24. Rauch, S., Hemond, H. F., Barbante, C., Owari, M., Morrison, G. M., Peucker-Ehrenbrink, B., Wass, U., "Importance of automobile exhaust catalyst emissions for the deposition of platinum, palladium, and rhodium in the northern hemisphere." *Environ. Sci. Technol.* **2005**, *39*, 8156–8162.

25. Rauch, S., Hemond, H. F., Peucker-Ehrenbrink, B., Ek, K. H., Morrison, G. M., "Platinum group element concentration and osmium isotopic composition in urban airborne particles from Boston, Massachusetts." *Environ. Sci. Technol.* **2005**, *39*, 9464–9470.

26. Ely, J. C., Neal, C. R., Kulpa, C. F., Schneegurt, M. A., Seidler, J. A., Jain, J. C., "Implications of platinum-group element accumulation along U. S. road from catalytic-converter attrition." *Environ. Sci. Technol.* **2001**, *35*, 3816–3822.

27. Schäfer, J., Eckhardt, J-D., Berner, Z. A., Stüben, D., "Time-dependent increase of traffic-emitted platinum-group elements (PGE) in different environmental compartments." *Environ. Sci. Technol.* **1999**, *33*, 3166–3170.

28. Bocca, B., Alimonti, A., Cristaudo, A., Cristallini, E., Petrucci, F., Caroli, S., "Monitoring of the exposure to platinum-group elements for two Italian population groups through urine analysis." *Anal. Chim. Acta.* **2004**, *512*, 19–25.

29. Caroli, S., Alimonti, A., Petrucci, F., Bocca, B., Krachler, M., Forastiere, F., Sacerdote, M. T., Mallone, S., "Assessment of exposure to platinum-group metals in urban children." *Spectrochim. Acta, Part B* **2001**, *56*, 1241–1248.

30. Carey, J. S., Laffan, D., Thomson, C., Williams, M. T., "Analysis of the reactions used for the preparation of drug candidate molecules." *Org. Biomol. Chem.* **2006**, *4*, 2337–2347.

31. King, A. O., Yasuda, N., "Palladium-catalyzed cross-coupling reactions in the synthesis of pharmaceuticals." *Topics Organomet. Chem.* **2004** *6*, 205–245.

32. Buchwald, S. L., Mauger, C., Mignani, G., Scholz, U., "Industrial-scale palladium-catalyzed coupling of aryl halides and amines – a personal account." *Adv. Synth. Catal.* **2006**, *348*, 23–39.

33. Garrett, C. E., Prasad, K., "The art of meeting palladium specifications in active pharmaceutical ingredients produced by Pd-catalyzed reactions." *Adv. Synth. Catal.* **2004**, *346*, 889–900.

34. Bien, J. T., Lane, G. C., Oberholzer, M. R., "Removal of metals from process streams: methodologies and applications." *Topics Organomet. Chem.* **2004**, *6*, 263–283.

35. Flahive, E. J., Ewanicki, B. L., Sach, N. W., O'Neill-Slawecki, S. A., Stankovic, N. S., Yu, S., Guinness, S. M., Dunn, J., "Development of an effective palladium removal process for VEGF oncology candidate AG13736 and a simple, efficient screening technique for scavenger reagent identification." *Org. Process Res. Dev.* **2008**, *12*, 637–645.

36. Galaffu, N., Man, S. P., Wilkes, R. D., Wilson, J. R. H., "Highly functionalized sulfur-based silica scavengers for the efficient removal of palladium species from active pharmaceutical ingredients." *Org. Process Res. Dev.* **2007**, *11*, 406–413.

37. Welch, C. J., Albaneze-Walker, J., Leonard, W. R., Biba, M., DaSilva, J., Henderson, D., Laing, B., Mathre, D. J., Spencer, S., Bu, X., Wang, T., "Adsorbent screening for metal impurity removal in pharmaceutical process research." *Org. Process Res. Dev.* **2005**, *9*, 198–205.

38. Larsen, R. D., King, A. O., Chen, C. Y., Corley, E. G., Foster, B. S., Roberts, F. E., Yang, C., Lieberman, D. R., Reamer, R. A., Tschaen, D. M., Verhoeven, T. R., Reider, P. J., "Efficient synthesis of Losartan, a nonpeptide angiotensin II receptor antagonist." *J. Org. Chem.* **1994**, *59*, 6391–6394.

39. Bencs, L., Ravindra, K., Van Grieken, R., "Methods for the determination of platinum group elements originating from the abrasion of automotive catalytic converters." *Spectrochim. Acta, Part B* **2003**, *58*, 1723–1755.

40. Godlewska-Zylkiewicz, B., "Preconcentration and separation procedures for the spectrochemical determination of palladium and platinum." *Microchim. Acta* **2004**, *147*, 189–210.

41. Van Meel, K., Smekens, A., Behets, M., Kazandijan, P., Van Grieken, R., "Determination of platinum, palladium, and rhodium in automotive catalysts using high-energy secondary target X-ray fluorescence spectrometry." *Anal. Chem.* **2007**, *79*, 6383–6389.

42. Evans, E. H., Giglio, J. J., "Interferences in inductively coupled plasma mass spectrometry a review." *J. Anal. At. Spectrom.* **1993**, *8*, 1–18.

43. Jakubowski, N., Feldmann, I., Stuewer, D., "Grimm-type glow discharge ion sources for operation with a high resolution inductively coupled mass spectrometry instrument." *J. Anal. At. Spectrom.* **1997**, *12*, 151–157.

44. Tang, B., Zhang, H., Wang, Y., "Determination of trace palladium with salicylaldehyde furfuralhydrazone (SAFH) by catalytic kinetic spectrofluorimetry." *Anal. Lett.* **2004**, *37*, 1219–1231.

45. Houk, R. J. T., Wallace, K. J., Hewage, H. S., Anslyn, E. V., "A colorimetric for Pd(II): a method for detecting residual palladium in cross-coupling reactions." *Tetrahedron* **2008**, *64*, 8271–8278.

46. Leadbeater, N. E., Marco, M., "Transition-metal-free Suzuki-type coupling reactions." *Angew. Chem. Int. Ed.* **2003**, *42*, 1407–1409.

47. Arvela, R. K., Leadbeater, N. E., Sangi, M. S., Williams, V. A., Granados, P., Singer, R. D., "A reassessment of the transition-metal-free Suzuki-type coupling methodology." *J. Org. Chem.* **2005**, *70*, 161–168.

48. Koide, K., Song, F., de Groh, E. D., Garner, A. L., Mitchell, V. D., Davidson, L. A., Hukriede, N. A., "Scalabe and concise synthesis of dichlorofluorescein derivatives displaying tissue permeation in live zebrafish embryos." *ChemBioChem* **2008**, *9*, 214–218.

49. Jackson, W. R., Strauss, J. U. G., "The γ-functionalization of α,β-unsaturated ketones via π-allylpalladium compounds." *Tetrahedron Lett.* **1975**, *16*, 2591–2592.

50. Collins, D. J., Jackson, W. R., Timms, R. N., "Stereospecific 6β-functionalization of 3-oxo-4-ene steroids via π-allylpalladium complexes." *Tetrahedron Lett.* **1976**, *17*, 495–496.

51. Sokolov, V. N., Khvostik, G. M., Poddubnyl, I. Y., Kondratenkov, G. P., Grebenshikov, G. K., "The nature of the system $(\pi\text{-}C_4H_7PdCl)_2$-electron donor from ^{1}H, ^{13}C and ^{31}P NMR spectroscopic and electrodialysis studies. III. $(\pi\text{-}C_4H_7PdCl)_2$-dimethylsulfoxide." *J. Organomet. Chem.* **1973**, *54*, 375–383.

52. Mancera, R. L., Chalaris, M., Refson, K., Samios, J., "Molecular dynamics simulation of dilute aqueous DMSO solutions. A temperature-dependence study on the hydrophobic and hydrophilic behavior around DMSO." *Phys. Chem. Chem. Phys.* **2004**, *6*, 94–102.

53. Martin, M. M., Lindqvist, L., "The pH dependence of fluorescein fluorescence." *J. Lumin.* **1975**, *10*, 381–390.

54. Anderson, N. G., Keay, B. A., "2-Furyl phosphines as ligands for transition-metal-mediated organic synthesis." *Chem. Rev.* **2001**, *101*, 997–1030.

55. Farina, V., Baker, S. R., Benigni, D. A., Sapino, Jr., C., "Palladium-catalyzed coupling between cephalosporin derivatives and unsaturated stannanes: a new ligand for palladium chemistry." *Tetrahedron Lett.* **1988**, *29*, 5739–5742.

56. Farina, V., Krishnan, B., "Large rate accelerations in the stille reaction with tri-2-furylphophine and triphenylarsine as palladium ligands: mechanistic and synthetic implications." *J. Am. Chem. Soc.* **1991**, *113*, 9585–9595.

57. Amatore, C., Jutand, A., Meyer, G., Atmani, H., Khalil, F., Chahdi, F. O., "Comparative reactivity of palladium(0) complexes generated in situ in mixtures of triphenylphosphine or tri-2-furylphosphine and $Pd(dba)_2$." *Organometallics* **1998**, *17*, 2958–2964.

58. Hutchins, R. O., Learn, K., Fulton, R. P., "Reductive displacement of allylic acetates by hydride transfer via catalytic activation by palladium(0) complexes." *Tetrahedron Lett.* **1980**, *21*, 27–30.

59. Rao, R. N., Talluri, M. V. N. K., "An overview of recent applications of inductively coupled plasma-mass spectrometry (ICP-MS) in determination of inorganic impurities in drugs and pharmaceuticals." *J. Pharm. Biomed. Anal.* **2007**, *43*, 1–13.

60. Lásztity, A., Kelkó-Lévai, A., Varga, I., Zih-Perényi, K., Bertalan, E., "Development of atomic spectrometric methods for trace metal analysis of pharmaceuticals." *Microchem. J.* **2002**, *73*, 59–63.

61. Lewen, N., Schenkenberger, M., Larkin, T., Conder, S., Brittain, H. G., "The determination of palladium in fosinopril sodium (monopril) by ICP-MS." *J. Pharm. Biomed. Anal.* **1995**, *13*, 879–883.

4.0 FLUOROMETRIC DETECTION OF PLATINUM

4.1 RESEARCH DESIGN

During screening of the metal specificity for the conversion of nonfluorescent compound **34** to the brightly green fluorescent compound **35**, platinum was approximately 40% as effective as palladium at pH 10 (see Figure 40a).[1] Because of the importance of analytical techniques for quantifying platinum in various samples, the Pt-catalyzed deallylation chemistry was explored to find optimal conditions for platinum sensing (Figure 49). This provides a second example of a metal ion amplifying fluorescence signal via a catalytic process.

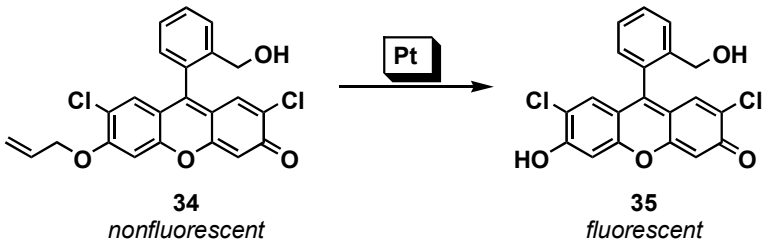

34
nonfluorescent

35
fluorescent

Figure 49. Pt-catalyzed deallylation to produce a fluorescence signal

4.1.1 Importance of Platinum Detection

Platinum, like palladium, is a widely used precious metal in various materials including those involving energy and human health. With respect to energy, platinum is an integral component in

automobile catalytic converters, fuel cells and oil refining. Because of increasing usage and South Africa's production crisis, there has been a marked platinum deficit in recent years.[2] Similar to the palladium problem, platinum pollution in the environment is an emerging problem.[3] Platinum intake occurs frequently because significant amounts of the metal are emitted from automobiles (0.8–1.2 μg/km/car),[4] and such pollution products may account for the metal's presence in human bodies.[5–7] In addition, studies have shown the following amounts of platinum in environmental samples: road dust = 60–250 ng/g; soil = 23–112 ng/g; river water = 155 ng/g; and grasses = 17–96 ng/g.[8]

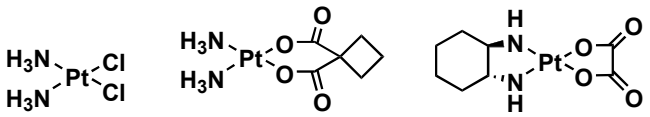

Figure 50. Pt-based anticancer drugs

With respect to human health, platinum-containing drinking water and skin-care products are sold for potential benefits in human health.[9,10] In addition, cisplatin and its analogues are widely used as anticancer drugs, and additional platinum-based compounds are emerging (Figure 50).[11,12] Despite such medical benefits of platinum compounds, other forms of platinum, like palladium, are considered potential health hazards.[3] Moreover, although controversial,[13–15] platinum residue in silicone-based artificial tissues may leach into blood.[16]

4.1.2 Current Detection Methods for Platinum

Similar to palladium, the current techniques for detecting and quantifying platinum are spectroscopic (AAS, XRF, ICP-MS) with similar limitations. The detection limit for platinum using each of these methods is: AAS = 2–10 ppm; XRF = 3 ppm; ICP-MS = 0.01–0.1 ppm.[17,18] For further discussion of each of the methods, please see 3.1.3.

4.2 RESULTS AND DISCUSSION

4.2.1 Platinum Detection

In the palladium method, the oxidative insertion step appeared to be the rate-determining step, resulting in the correlation between the fluorescence intensity of the reaction solution and the palladium concentration. However, it would be premature to expect a similar correlation between the fluorescence signal and platinum concentrations because these metals are different with respect to rate of ligand substitution and affinity for phosphine (size difference), and as such should have different reactivities.[19,20] Additionally, there is no precedence for a generalizable platinum-catalyzed Tsuji-Trost reaction.[21] Thus, these questions warranted independent and rigorous studies on the Pt-catalyzed Tsuji-Trost reaction.

Toward this end, compound **34** was subjected to $Pt(PPh_3)_4$ and $PtCl_2$ (0.5 mol % for each reaction) and morpholine (1.1 equiv) at 24 °C in THF. After 10 min, the reaction with $Pt(PPh_3)_4$ was complete (Figure 49), while that with $PtCl_2$ did not proceed, showing that the conversion of **34** to **35** can be catalyzed by Pt^0 but not by Pt^{II}. The reaction with $PtCl_2$ was driven to completion

by the addition of a reducing agent such as Ph_3P or $NaBH_4$, indicating that this method can be applied to sensing platinum in various oxidation states upon in situ reduction.

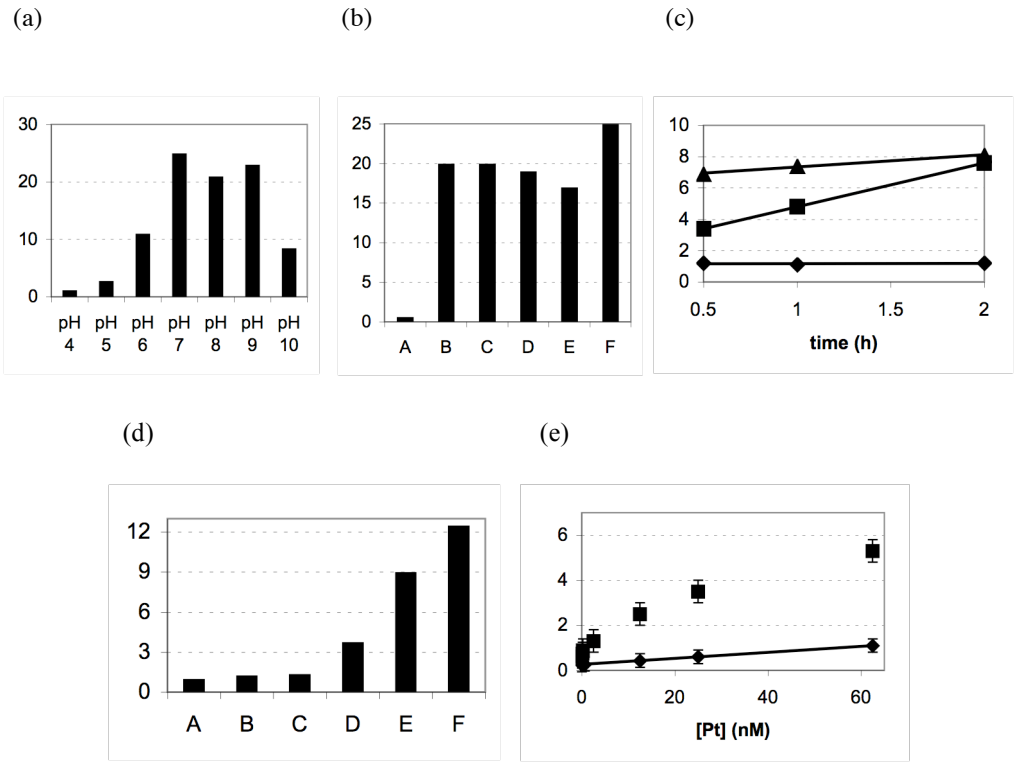

Figure 51. Fluorescence analysis of Pt

In these graphs, the y-axis is fluorescence intensity (a. u. × 10^5) at 525 nm. In all cases, [**34**] = 12.5 μM and [Ph_3P] = 250 μM and the assays were performed for 1 h at 24 °C. (a) The pH-dependent deallylation of **34** in the presence of $PtCl_2$ (625 nM) in 1:4 DMSO/buffer. (b) Fluorescence induction by Pt at various oxidation states and in Pt drink in 1:4 DMSO/pH 7 buffer. In A–E, [Pt] = 625 nM. A = no Pt, B = $Pt(PPh_3)_4$, C = $PtCl_2$, D = H_2PtCl_6, E = cisplatin, F = platinum nanocolloid (50 ppm). (c) Initial rate analysis for deallylation of **34** in the presence of $PdCl_2$ (1 mol %) in 1:1 DMSO/buffer. ♦ = pH 4; y = 0.0143x + 1.15; R^2 = 0.0357. ■ = pH 7; y = 2.80x + 2.00; R^2 = 1.00. ▲ = pH 10; y = 0.786x + 6.55; R^2 = 0.991; (d) Phosphine ligand screening with $PtCl_2$ (625 nM). A = no Pt, B = DPEphos, C = JohnPhos, D = $(o\text{-Tol})_3P$, E = TFP, F = Ph_3P. (e) Correlation between fluorescence intensity and [$PtCl_2$] in 1:4 DMSO/pH 7 buffer. ♦ = 24 °C: y = 0.0136x + 0.255; R^2 = 0.999. The intensity continued to be linear to 625 nM (125 ppb). ■ = 37 °C.

In order to develop a fluorescent method for platinum, **34** was converted to **35** in aqueous media in the presence of $PtCl_2$ (625 nM; 125 ppb) and Ph_3P as a ligand and reducing agent. Buffers were screened in the pH 4–10 range, and the platinum-catalyzed deallylation was most effective in pH 7–9 buffers (Figure 51a) (cf. pH 6–9 for palladium). Excess Ph_3P allowed for generation nearly the same fluorescence signal regardless of the initial oxidation states of platinum (0, +2, and +4) (Figure 51b).

Initial rate studies were performed to verify the pH dependence results. For all Pt species tested ($Pt(PPh_3)_4$, $PtCl_2$, H_2PtCl_6, cisplatin) in the presence of Ph_3P, reaction at pH 7 was approximately 3.5 times faster than that at pH 10 and little reaction occurred at pH 4 (Figure 51c). Similar to palladium, reaction was optimal at pH 7. The TOF for Pt in pH 7 buffer under the high dilution and salt conditions ([**34**] = 12.5 μM; [Pt] = 50 nM; $[PO_4^{3-}]$ = 50 mM) was determined to be 4.5 h^{-1}.

Because platinum has a higher reduction potential than palladium,[22] a number of different phosphines and phosphites were also tested to determine if Ph_3P was the optimal reducing agent. As Figure 51d shows, Ph_3P was the most effective reducing agent. Borohydride reducing agents ($NaBH_4$ and $NaBH(OAc)_3$) were examined, but inconsistent results were observed possibly due to side reduction of the xanthene ring of the sensor (not shown).

The quantitative nature of this method for platinum was next determined. The fluorescence intensity is linear with respect to the concentration of platinum in the 625 pM–625 nM (125 ppt–125 ppb) range at 24 °C (Figure 51e). Further sensitivity in the 125 pM–625 nM (25 ppt–125 ppb) range was obtained by heating to 37 °C (Figure 51e).

With the successful detection method for platinum in hand, attention was next turned toward platinum detection in real samples. As an initial example, the platinum concentration was

confirmed in a commercially available platinum-drink with 50-ppm platinum. As Figure 51b (F) shows, platinum was detected in this drink. It is important to note that the platinum is in nanocolloid form, indicating that this method may be used for the quality control of catalytic converters and fuel cells.

4.2.2 Platinum Detection in Biological Media

Although this platinum sensing method was effective in the presence of various salts in buffers, it was not certain whether it could be applied to platinum monitoring in serum because serum contains many proteins at high concentration (total concentration: 60 mg/mL = 6×10^4 ppm) and sulfur-containing residues (e.g., Cys, Met, glutathione). Approximately 80% of cisplatin in blood is known to be bound to proteins such as albumin, and free cisplatin is of interest for those who need to ensure the effective dose of this drug.[23] Since the pharmacokinetics of drugs varies among individuals, the monitoring of cytotoxic drugs is of paramount importance in medicine. As an initial examination, human serum was spiked with various cisplatin concentrations and the resulting samples were tested with this fluorescent method. As Figure 52a shows, despite the presence of many sulfur-containing proteins and other components in serum, this fluorescent method was robust enough to detect cisplatin easily at 100 nM (20 ppb; free cisplatin: ~20 nM = 4 ppb). With the total concentration of cisplatin at 100 nM in human serum, the fluorescence intensity (2.7×10^5; intensity without cisplatin = 1.0×10^5) corresponded to 20 nM of cisplatin in pH 7 buffer (2.8×10^5), which is consistent with the literature about free vs. protein-bound cisplatin in serum.[23]

(a) (b) (c)

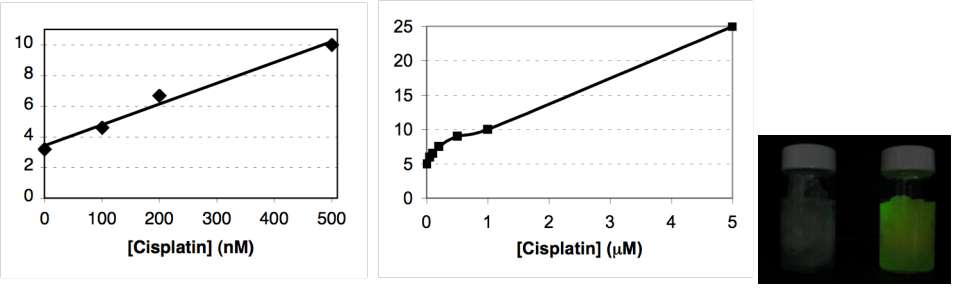

Figure 52. Applications of Pt sensing method

In these graphs, the y-axis is fluorescence intensity (a. u. × 10^5) at 525 nm. In all cases, [**34**] = 300 μM and [Ph_3P] = 6.0 mM and the assays were performed for 1 h at 24 °C. (a) Correlation between the concentration of cisplatin in immunopure human serum and fluorescence intensity. (b) Correlation between the concentration of cisplatin in sheep serum and fluorescence intensity. (c) Kimwipes® in pH 7 buffer solution containing 34 and Ph_3P. Left = clean Kimwipe®. Right = Kimwipe® from cisplatin-doped floor sample.

This method was then tested in sheep serum samples containing immunoglobulins. Sheep serum was used in this case to ensure the purity of the serum samples and human serum samples may contain palladium or platinum impurities depending on the source. Although detection was not observed using the previous method, after initial treatment of serum/cisplatin mixtures with 5% HNO_3, cisplatin was detected to 50 nM (10 ppb) (Figure 52b). Many other additives were tested such as electrophiles (CH_3I, maleimide, epoxides);[24] however, sensitivity was not improved. Further optimizations for sample preparations may be needed, but these results provide a proof of concept that the concentration of free cisplatin can be monitored fluorometrically in serum. Thus far, this method appears to be superior to ICP-MS, whose detection limit in serum is typically 0.1—10 ppm, and our method requires only 50 μL of serum.[25,26]

Next, the utility of this fluorescent platinum sensing method in hospitals and pharmacies, where platinum-based anticancer drugs are handled and contaminations in the working environment are considered to be occupational hazards, was examined.[27,28] A solution of cisplatin was intentionally spilled on a laboratory floor and wiped with a wet paper towel. Subsequently, a piece of Kimwipe® soaked with 1% hydrochloric acid was used to wipe the spill area, and the resulting paper towel was tested for possible residual platinum. As Figure 52c shows, this fluorescent method can detect cisplatin contamination even in such crude samples.

4.2.3 Selective Detection of Palladium in the Presence of Platinum

After examining the kinetic data from both palladium and platinum, it became apparent that the palladium-catalyzed deallylation of **34** is 158 times faster than the platinum-catalyzed reaction at pH 4 (see Figures 42b and 51c). As such, selective detection of palladium in the presence of platinum at pH 4 was attempted. The reaction with a 1:1 mixture of palladium and platinum (100 nM each) in 1:4 DMSO/pH 7 buffer was first performed to confirm that the metals react independently of one another in such a mixture. As Figure 53a shows, in fact this is the case and the fluorescence intensity in the 1:1 mixture is approximately additive with respect to the intensity of each metal alone. The reaction was then performed in 1:4 DMSO/pH 4 buffer. As Figure 53b and 53c show, in this solution palladium was selectively detected in the presence of platinum, even in the presence of excess platinum (10:1 platinum/palladium).

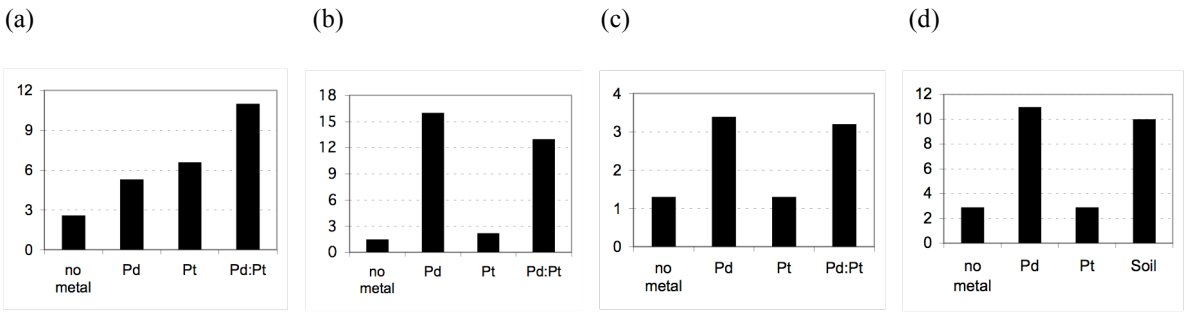

Figure 53. Selective detection of Pd in the presence of Pt

In these graphs, the y-axis is fluorescence intensity (a. u. × 10^5) at 525 nm. In all cases, [34] = 12.5 μM and [PPh_3] = 250 μM, and the assays were performed for 1–4 h at 24 °C. (a) Detection of 1:1 $PdCl_2$/$PtCl_2$ (100 nM each) in 1:4 DMSO/pH 7 buffer compared to positive controls. (b) Detection of 1:1 $PdCl_2$/$PtCl_2$ (5 μM each) in 1:4 DMSO/pH 4 buffer compared to positive controls. (c) Detection of 1:10 $PdCl_2$/$PtCl_2$ (500 nM Pd / 5 μM Pt) in 1:4 DMSO/pH 4 buffer compared to positive controls. (d) Detection of soil spiked with 1:1 $PdCl_2$:$PtCl_2$ (5 μM each) in 1:4 DMSO/pH 4 buffer compared to positive controls.

To demonstrate the potential application of this palladium-specific method, the following proof-of-concept experiment was performed. Soil (heated in an oven at >100 °C for 24 h prior to this experiment; presumably this process can be accelerated by the use of microwave) was suspended in 1:4 DMSO/pH 4 buffer (final: 10 mg/mL). The resulting mixture was spiked with a 1:1 mixture of palladium and platinum and left on a bench for 30 min. After filtering to remove insoluble materials, the solution was then treated with Ph_3P (final concentration = 250 μM) and **34** (final concentration = 12.5 μM) and incubated for 4 h at 24 °C. As Figure 53d shows, even without rigorous sample pretreatment, palladium was specifically detected in this crude sample. Thus, although this experiment is somewhat artificial, this method could have potential application in platinum/palladium manufacturing because these metals are found together in mining sites (ores) and spectroscopic analyses of the individual metals typically require a complex series of purifications to eliminate molecular interferences.[17] Environmental samples,

especially those collected from roadsides, contain both metals and this method will allow the metals to be quantified differentially.

4.3 CONCLUSION

In conclusion, the first experimental evidence for the use of a fluorescent sensor as a quantitative platinum sensor has been provided. This method allows for the detection of total quantities platinum at nanomolar levels, even in heterogenous samples such as human serum. In addition, it was also demonstrated that palladium can be selectively detected in the presence of platinum. This sensor technology should find broad applications in materials, energy and human health.

4.4 EXPERIMENTAL

4.4.1 General Information

All reactions were monitored by thin-layer chromatography (TLC) carried out on 0.25-mm EMD silica gel plates (60F-254) using a hand-held UV lamp (254 nm or 365 nm).

$Pt(PPh_3)_4$, $PtCl_2$ and $H_2PtCl_6 \bullet 6H_2O$ were purchased from Alfa Aesar and used as received. Cisplatin was purchased from Sigma-Aldrich and used as received. WaterOz Platinum is a product of Kornax Superior Nutrition L.L.C. (Houston, Texas). ImmunoPure® normal human serum was purchased from Thermo Scientific and used after restoration with 2.0 mL distilled water. Sheep serum was obtained from Luminos, LLC. Kimwipes® are a product of Kimberly-

Clark. Buffers were purchased (pH 4, potassium biphthalate ([biphthalate] = 49.8–50.2 mM), J. T. Baker, Catalog Number 5606-01; pH 7, phosphate ($[PO_4^{3-}]$ = 46–50 mM, $[K^+]$ = 23–25 mM, $[Na^+]$ = 50–56 mM), J. T. Baker, Catalog Number 5608-01; pH 10, borate ($[K^+]$ = 94–114 mM), J. T. Baker, Catalog Number 5609-01) and used as received.

4.4.2 Platinum Detection in Organic Solvent

Determination of reactive oxidation state for platinum. A solution of compound **34** (5.0 mg, 12 μmol) in THF (150 μL) was treated with morpholine (2 μL, 13 μmol), and $Pt(PPh_3)_4$ (1.0 mg, 0.6 μmol) at 24 °C. The reaction was stirred for 10 min and TLC analysis (50% EtOAc in hexanes) showed formation of **35**.

A solution of compound **34** (5.0 mg, 12 μmol) in THF (150 μL) was treated with morpholine (2 μL, 13 μmol), and $PtCl_2$ (1.0 mg, 0.6 μmol) at 24 °C. The reaction was stirred for 10 min and TLC analysis (50% EtOAc in hexanes) showed no reaction (i.e. only starting material). Following addition of $NaBH_4$ (5 mg, 0.13 mmol), the reaction fully proceeded to form **35**.

4.4.3 Fluorescence Spectroscopy

Preparation of parent stock solutions used for this study.

Entry	Reagent	Quantity	Solvent (10 mL)	Conc. of stock solution
A	compound **34**	42.7 mg (0.10 mmol)	DMSO	10.0 mM
B	PPh_3	262.3 mg (1.00 mmol)	DMSO	100 mM
C	$PtCl_2$	13.3 mg (50 μmol)	DMSO	5.0 mM
D	$Pt(PPh_3)_4$	62.6 mg (50 μmol)	DMSO	5.0 mM
E	$H_2PtCl_6•6H_2O$	25.9 mg (50 μmol)	1% HNO_3 in H_2O	5.0 mM
F	cisplatin	14.5 mg (50 μmol)	pH 7.0 buffer	5.0 mM

Notes: See previous experimentals

Fluorescence spectroscopy. Fluorescence spectra were recorded in a 1 × 1-cm disposable cuvette (VWR; catalog number 58017-880) on a Jobin Yvon FluoroMax-3 spectrometer under the control of a Windows-based PC running FluorEssence software. The samples were excited at 497 nm and the emission intensities were collected at 525 nm. All spectra were corrected for emission intensity using the manufacturer supplied photomultiplier curves.

Platinum: buffer screening. $PtCl_2$ solution (25.0 μL of 100.0 μM stock, $[Pt]_{final}$ = 625 nM) and solution **B** (10.0 μL, $[PPh_3]_{final}$ = 250 μM) were added to DMSO/pH X buffer (1:4) solution (X = 4.0–10.0) (4.0 mL). To the mixture was added solution **A** (5.0 μL, $[\mathbf{34}]_{final}$ = 12.5 μM), and the resulting mixtures were incubated for 1 h at 24 °C before fluorescence measurement.

Platinum: initial rate analysis. $PtCl_2$ stock solution **C** (50.0 μL, 250 nmol), PPh_3 (4.8 mg, 2.34 μmol) and **34** (10.0 mg, 23.4 μmol) were added to DMSO/pH X buffer (1:1) solution (X = 4.0, 7.0, 10.0) (20 mL) at 24 °C. 1:1 DMSO/buffer was used in this case for the solubility of the sensor and PPh_3. The experiment was performed in triplicate. At t = 0.5, 1 and 2 h, 100 μL aliquots were taken from each reaction mixture and diluted to 4.0 mL with DMSO/pH 7.0 buffer (1:4) for fluorescence measurement.

Platinum: Turnover frequency. To determine the turnover frequency, a solution containing $PtCl_2$ ($[PtCl_2]_{final}$ = 50 nM), solution **B** (10.0 μL, $[PPh_3]_{final}$ = 250 μM) and solution **A** (5.0 μL, $[\mathbf{34}]_{final}$ = 12.5 μM) was prepared in DMSO/pH 7.0 buffer (1:4). The intensity of this sample was

compared to a standard solution containing Pittsburgh Green **35** ($[\mathbf{35}]_{final}$ = 50 nM) in DMSO/pH 7.0 buffer (1:4). The intensity of the Pt^{2+}-containing sample was 2.8×10^6 after 7 h at 24 °C and the intensity of the standard solution of **35** was 8.8×10^4. The turnover frequency is $2.8 \times 10^6 / 8.8 \times 10^4 = 31.8/7\ h = 4.5\ h^{-1}$.

Platinum: concentration dependence. Varying amounts of Pt solution and solution **B** (10.0 μL, $[PPh_3]_{final}$ = 250 μM) were added to DMSO/pH 7.0 buffer solution (1:4) (4.0 mL). Solution **A** (5.0 μL, $[\mathbf{34}]_{final}$ = 12.5 μM) was added to the mixture, and the samples were incubated for 20–24 h at 24 °C or 37 °C before fluorescence measurement. Each experiment was performed in triplicate.

Pt detection in WaterOz Platinum. WaterOz Platinum (4.4 mL, 750 nM final concentration) and solution **B** (20.0 μL, $[PPh_3]_{final}$ = 140 μM) were added to DMSO/ pH 7.0 buffer solution (1:4) (10.0 mL). Solution **A** (10.0 μL, $[\mathbf{34}]_{final}$ = 7.0 μM) was added to the mixture, and the samples were incubated for 1 h at 24 °C before fluorescence measurement.

Cisplatin detection in human serum. Varying amounts of cisplatin in pH 7.0 buffer and pH 7 buffer (total volume of pH 7.0 buffer = 100.0 μL) was added to immunopure human serum (50.0 μL). Solution **B** (10.0 μL, $[PPh_3]_{final}$ = 6.0 mM) and solution **A** (5.0 μL, $[\mathbf{34}]_{final}$ = 300.0 μM) were added to the mixture, and the samples were incubated for 24 h at 24 °C before fluorescence measurement. The experiment was performed in triplicate.

Cisplatin detection in sheep serum. Varying amounts of cisplatin in pH 7.0 buffer and 5% HNO_3 (50 μL) were added to sheep serum (50.0 μL). The samples were allowed to sit for 5 min and then heated in a water bath at 100 °C to evaporate the acid. The samples were then diluted with pH 7.0 buffer (total volume of pH 7.0 buffer = 500.0 μL) and treated with solution **B** (10.0 μL, $[PPh_3]_{final}$ = 6.0 mM) and solution **A** (5.0 μL, $[\mathbf{34}]_{final}$ = 300.0 μM). The samples were incubated for 24 h at 24 °C before fluorescence measurement. The experiment was performed in triplicate.

Detection of cisplatin contamination. Cisplatin solution in pH 7.0 buffer (500 μL, 1.0 mM stock solution) was spilled on an uncleaned floor tile. After 5 min, the spilled area was wiped with a wet paper towel (with water) and subsequently with a Kimwipe® containing a 1% HCl solution. The HCl-soaked Kimwipe® was placed into a 20-mL scintillation vial and additional 1% HCl (2.0 mL) was added. After 10 min, the solution was basified to pH 9.0 with 1.0 N NaOH (<1.0 mL) and diluted to 10.0 mL with DMSO/pH 7.0 buffer (1:4). Solution **B** (20.0 μL, $[PPh_3]_{final}$ = 200 μM) and the compound **2** solution **A** (10.0 μL, $[\mathbf{34}]_{final}$ = 10.0 μM) were then added to the mixture, and the samples were incubated for 3 h at 24 °C before visualization under a UV lamp at 365 nm wavelength. The experiment was performed in triplicate.

4.4.4 Detection of Palladium in the Presence of Platinum

Pd/Pt mixtures. $PdCl_2$ solution (10.0 μL of 100.0 μM stock; $[Pd]_{final}$ = 100 nM), $PtCl_2$ solution (10.0 μL of 100.0 μM stock; $[Pt]_{final}$ = 100 nM) or a 1:1 mixture of Pd/Pt ($[Pd/Pt]_{final}$ = 100 nM each) and solution **B** (10.0 μL, $[Pd]_{final}$ = 250 μM) were added to DMSO/pH 7.0 buffer solution

(1:4) (4.0 mL). Solution **A** (5.0 μL, $[\mathbf{34}]_{final}$ = 12.5 μM) was added to the mixture, and the samples were incubated for 1 h at 24 °C before fluorescence measurement.

$PdCl_2$ solution (20.0 μL of 1.0 mM stock; $[Pd]_{final}$ = 5.0 μM), $PtCl_2$ solution (20.0 μL of 1.0 mM stock; $[Pt]_{final}$ = 5.0 μM) or a 1:1 mixture of Pd/Pt ($[Pd/Pt]_{final}$ = 5.0 μM each) and solution **B** (10.0 μL, $[Pd]_{final}$ = 250 μM) were added to DMSO/pH 4.0 buffer solution (1:4) (4.0 mL). Solution **A** (5.0 μL, $[\mathbf{34}]_{final}$ = 12.5 μM) was added to the mixture, and the samples were incubated for 1 h at 24 °C. Concentrated pH 7 buffer ($[PO_4^{3-}]$ = 1.25 M) (1.0 mL) was added before fluorescence measurement to maximize fluorescence signal.

$PdCl_2$ solution (20.0 μL of 1.0 mM stock; $[Pd]_{final}$ = 5.0 μM), $PtCl_2$ solution (20.0 μL of 1.0 mM stock; $[Pt]_{final}$ = 5.0 μM) or a 1:10 mixture of Pd/Pt ($[Pd]_{final}$ = 500 nM; $[Pt]_{final}$ = 5.0 μM) and solution **B** (10.0 μL, $[Pd]_{final}$ = 250 μM) were added to DMSO/pH 4.0 buffer solution (1:4) (4.0 mL). Solution **A** (5.0 μL, $[\mathbf{34}]_{final}$ = 12.5 μM) was added to the mixture, and the samples were incubated for 4 h at 24 °C. Concentrated pH 7 buffer ($[PO_4^{3-}]$ = 1.25 M) (1.0 mL) was added before fluorescence measurement to maximize fluorescence signal.

Soil was heated in an oven at 133 °C for 24 h prior to use. A solution of this soil (10 mg/mL) was prepared in 1:4 DMSO/pH 4.0 buffer solution (1:4) and spiked with $PdCl_2$ solution (20.0 μL of 1.0 mM stock; $[Pd]_{final}$ = 5.0 μM), $PtCl_2$ solution (20.0 μL of 1.0 mM stock; $[Pt]_{final}$ = 5.0 μM) or a 1:1 mixture of Pd/Pt ($[Pd/Pt]_{final}$ = 5.0 μM each), and left on a bench for 30 min at 24 °C. The samples were then filtered through cotton and treated with solution **B** (10.0 μL, $[Pd]_{final}$ = 250 μM) and solution **A** (5.0 μL, $[\mathbf{34}]_{final}$ = 12.5 μM), and the samples were incubated for 4 h at 24 °C. Concentrated pH 7 buffer ($[PO_4^{3-}]$ = 1.25 M) (1.0 mL) was added before fluorescence measurement to maximize fluorescence signal.

4.5 BIBLIOGRAPHY

1. Song, F., Garner, A. L., Koide, K., "A highly sensitive fluorescent sensor for palladium based on the allylic oxidative insertion mechanism." *J. Am. Chem. Soc.* **2007**, *129*, 12354–12355.

2. Johnson Matthey PLC, "Platinum 2008." *Platinum Metals Rev.* **2008**, *52*, 198–199.

3. "Environmental Health Criteria 123: Platinum." World Health Organization, Geneva, 1991.

4. Ely, J. C., Neal, C. R., Kulpa, C. F., Schneegurt, M. A., Seidler, J. A., Jain, J. C., "Implications of platinum-group element accumulation along U. S. roads from catalytic-converter attrition." *Environ. Sci. Technol.* **2001**, *35*, 3816–3822.

5. Rudolph, E., Hann, S., Stingeder, G., Reiter, C., "Ultra-trace analysis of platinum in human tissue samples." *Anal. Bioanal. Chem.* **2005**, *382*, 1500–1506.

6. Bocca, B., Alimonti, A., Cristaudo, A., Cristallini, E., Petrucci, F., Caroli, S., "Monitoring of the exposure to platinum-group elements for two Italian population groups through urine analysis." *Anal. Chim. Acta* **2004**, *512*, 19–25.

7. Caroli, S., Alimonti, A., Petrucci, F., Bocca, B., Krachler, M., Forastiere, F., Sacerdote, M. T., Mallone, S., "Assessment of exposure to platinum-group metals in urban children." *Spectrochim. Acta, Part B* **2001**, *56*, 1241–1248.

8. Pyrzynska, K., "Monitoring of platinum in the environment." *J. Environ. Monit.* **2000**, *2*, 99N–103N.

9. http://www.apt-ca.com

10. Kajita, M., Hikosaka, K., Iitsuka, M., Kanayama, A., Toshima, N., Miyamoto, Y., "Platinum nanoparticle is a useful scavenger of superoxide anion and hydrogen peroxide." *Free Radical Res.* **2007**, *41*, 615–626.

11. Kelland, L., "The resurgence of platinum-based cancer chemotherapy." *Nat. Rev. Cancer* **2007**, *7*, 573–584.

12. Lovejoy, K. S., Todd, R. C., Zhang, S., McCormick, M. S., D'Aquino, J. A., Reardon, J. T., Sancar, A., Giacomini, K. M., Lippard, S. J., "*cis*-Diammine(pyridine)chloroplatinum(II), a monofunctional platinum(II) anticancer agent: uptake, structure, function, and prospects." *Proc. Natl. Acad. Sci. U. S. A.* **2008**, *105*, 8902–8907.

13. Erickson, B. E., "Platinum paper sparks controversy." *Anal. Chem.* **2006**, *78*, 5240–5242.

14. Lane, T. H., "Comments on total platinum concentration and platinum oxidation states in body fluids, tissue, and explants from women exposed to silicone and saline breast implants by IC-ICPMS." *Anal. Chem.* **2006**, *78*, 5607–5608.

15. Brook, M. A., "Comments on total platinum concentration and platinum oxidation states in body fluids, tissue, and explants from women exposed to silicone and saline breast implants by IC-ICPMS." *Anal. Chem.* **2006**, *78*, 5609–5611.

16. Lykissa, E. D., Maharaj, S. V. M., "Total platinum concentration and platinum oxidation states in body fluids, tissue, and explants from women exposed to silicone and saline breast implants by IC-ICPMS." *Anal. Chem.* **2006**, *78*, 2925–2933.

17. Godlewska-Zylkiewicz, B., "Preconcentration and separation procedures for the spectrochemical determination of platinum and palladium." *Microchim. Acta* **2004**, *147*, 189–210.

18. Van Meel, K., Smekens, A., Behets, M., Kazandijian, P., Van Grieken, R., "Determination of platinum, palladium, and rhodium in automotive catalysts using high-energy secondary target X-ray fluorescence spectrometry." *Anal. Chem.* **2007**, *79*, 6383–6389.

19. Peloso, A., "Kinetics of nickel, palladium and platinum complexes." *Coord. Chem. Rev.* **1973**, *10*, 123–181.

20. Chianese, A. R., Lee, S. J., Gagné, M. R., "Electrophilic activation of alkenes by platinum(II): so much more than a slow version of palladium(II)." *Angew. Chem. Int. Ed.* **2007**, *46*, 4042–4059.

21. Pt-catalyzed *O*-deallylation is rare in the literature; see the only example: Moreau, B., Lavielle, S., Marquet, A., "Utilisation du groupe allyle comme groupe protecteur d'amines: application à la synthèse de la biotine." *Tetrahedron Lett.* **1977**, *30*, 2591–2594.

22. Goldberg, R. N., Hepler, L. G., "Thermochemistry and oxidation potentials of the platinum group metals and their compounds." *Chem. Rev.* **1968** *68*, 229–252.

23. Allain, P., Heudi, O., Cailleux, A., Le Bouil, A., Larra, F., Boisdron-Celle, M., Gamelin, E., "Early biotransformations of oxaliplatin after its intravenous administration to cancer patients." *Drug Met. Disp.* **2000**, *28*, 1379–1384.

24. Ivanov, A. I., Christodoulou, J., Parkinson, J. A., Barnham, K. J., Tucker, A., Woodrow, J., Sadler, P. J., "Cisplatin binding sites on human albumin." *J. Biol. Chem.* **1998**, *273*, 14721–14730.

25. Morrison, J. G., White, P., McDougall, S., Firth, J. W., Woolfrey, S. G., Graham, M. A., Greenslade, D., "Validation of a highly sensitive ICP-MS method for the determination of platinum in biofluids: application to clinical pharmacokinetic studies with oxaliplatin." *J. Pharm. Biomed. Anal.* **2000**, *24*, 1–10.

26. Barefoot, R. R., Van Loon, J. C., "Determination of platinum and gold in anticancer and antiarthritic drugs and metabolites." *Anal. Chim. Acta.* **1996**, *334*, 5–14.

27. Brouwers, E. E. M., Huitema, A. D. R., Bakker, E. N., Douman, J. W., Schimmel, K. J. M., van Weringh, E., de Wolf, P. J., Schellens, J. H. M., Beijnen, J. H., "Monitoring of platinum surface contamination in seven Dutch hospital pharmacies using inductively coupled plasma mass spectrometry." *Int. Arch. Occup. Environ. Health* **2007**, *80*, 689–699.

28. Pethran, A., Schierl, R., Hauff, K., Grimm, C-H., Boos, K-S., Nowak, D., "Uptake of antineoplastic agents in pharmacy and hospital personnel. Part I: monitoring of urinary concentrations." *Int. Arch. Occup. Environ. Health* **2003**, *76*, 5–10.

5.0 OXIDATION STATE-SPECIFIC FLUORESCENT METHOD FOR PALLADIUM AND PLATINUM BASED ON THE AROMATIC CLAISEN REARRANGEMENT

5.1 RESEARCH DESIGN

In the synthesis of Pittsburgh Yellowgreen (**36**), the final step is an aromatic Claisen rearrangement, which proceeds under thermal conditions (150 °C).[1] Since it is known that many metal ions, including Pd^{II} and Pt^{IV}, can catalyze this rearrangement,[2,3] it was envisioned that this transformation could serve as a detection method for these metals and would be oxidation state dependent. More specifically, by promoting the Claisen rearrangement of **34**, a nonfluorescent compound is converted to a fluorescent compound **36** (Pittsburgh Yellowgreen) (Figure 54). The proposed approach is novel for detection of oxidation state in a metal.

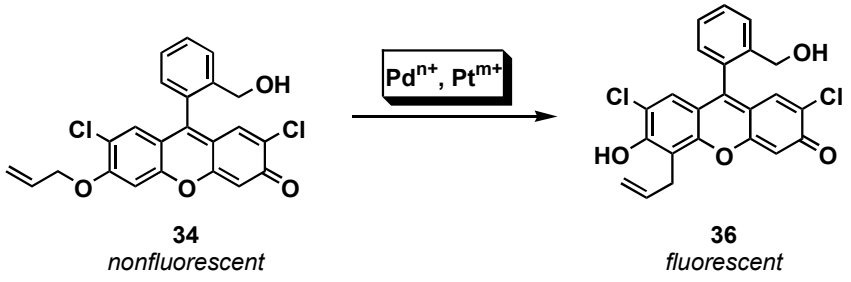

Figure 54. Pd^{n+}/Pt^{m+}-catalyzed aromatic Claisen rearrangement to produce a fluorescent molecule

5.1.1 Palladium- and Platinum-Catalyzed Claisen Rearrangement

One known mechanism of the metal-catalyzed Claisen rearrangement, which proceeds through a cyclization-induced rearrangement pathway, is shown below in Figure 55.[4–7]

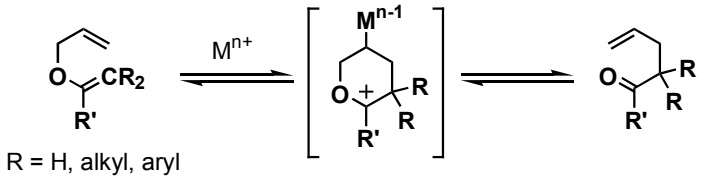

Figure 55. Pathway of the metal-catalyzed Claisen rearrangement

Although many metals are known to promote this transformation (Al, Cr, Mn, Fe, Cu, Ag, Au), typically through a Lewis acid-catalyzed pathway, the examples of Pd- and Pt-catalyzed rearrangement are few. One explanation for this is due to irreversible binding of the electrophilic metal catalyst to the strongly nucleophilic vinyl ether moiety instead of the allyl ether moiety. However, with substrates that contain alkyl-protected vinyl moieties (such as is found in the aromatic Claisen rearrangement), successful rearrangement can occur. As such, several examples have been reported on the Pd^{II}-catalyzed[2] rearrangement and one example with Pt^{IV}.[3]

The same mechanistic principle can be applied to fluorescent detection of the oxidation state of palladium and platinum (Figure 56). In this case, Pd^{n+}/Pt^{n+} induces cyclization of **34** to yield putative intermediate **65**. This complex then rearranges with elimination of Pd^{n+}/Pt^{n+} to form **66**, which rearomatizes to form Pittsburgh Yellowgreen **36**. Since this process is catalytic with respect to Pd^{n+}/Pt^{n+}, similar to the Pd^{0}/Pt^{0} sensor, the fluorescence signal is amplified.

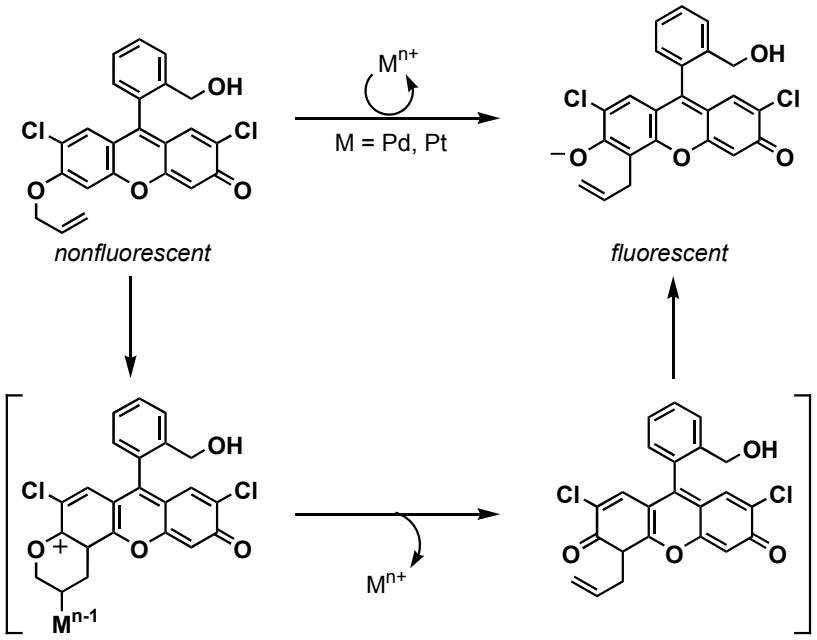

Figure 56. Mechanistic principle of the fluorometric detection of Pd and Pt oxidation state

5.1.2 Importance of Palladium and Platinum Speciation

As previously discussed, Pd- and Pt-catalyzed reactions are very powerful in synthetic organic chemistry.[8–10] Each of these reactions requires a palladium or platinum catalyst at a specific oxidation state, mostly at (0), (II) or (IV). However, since Pd^0 is prone to oxidation to form the more stable Pd^{II}, Pd^0 reagents are often gradually oxidized to Pd^{II} while stored. Because of this oxidation process, many synthetic chemists experience — although not often reported in the literature — that attempts to perform Pd^0-catalyzed reactions fail or result in poor and non-reproducible yields. Thus, identification of catalyst oxidation could greatly aid in understanding failed reactions. Moreover, such techniques would also facilitate studies on palladium materials including polymer-bound catalysts. [11–13]

In addition to identifying the oxidation state of palladium catalysts, determination of the oxidation state of palladium in contaminated active pharmaceutical ingredients (API) is also

important. In fact, it is well known that metal speciation can further complicate the removal of such metal impurities.[14–16] As such, since Pd^0 and Pd^{II} bind to scavengers differently, these synthetic compounds are often purified differently to remove palladium species. For example, a Japanese group developed a method in which polymer-supported trimercaptotriazine was used to effectively scavenge Pd^0, while a polymer-supported ethylenediamine was used to scavenge Pd^{II}.[16] This difference in scavenging may be attributed to the fact that Pd^0 is tetrahedral while Pd^{II} is square planar.

With respect to environmental and biological samples, the mobility, bioavailability and toxicological properties of metals are highly dependent on their oxidation state. For palladium, the World Health Organization's published document from 2002 for palladium explicitly states that there are currently no reliable analytical methods for differentially determining Pd^0 and Pd^{II}.[17] However, much work has been devoted to determination of platinum speciation because of the extensive research on cisplatin-based anticancer drugs.[18–21] In addition, Pt^0 is added to drinking water for health benefits, but Pt^{II} and particularly Pt^{IV} are toxic.[22–24] This commercially available Pt^0 nanocolloid-containing health water is typically made via the reduction of Pt^{IV} species. Once reduced, the Pt^0 species are stable; and thus, monitoring of this reduction process is an important step in making safe platinum water. Therefore, determination of metal oxidation state in biological and environmental samples is important. In addition, metal speciation studies also allow for quality control in industrial processes.

5.1.3 Current Detection Methods for Palladium and Platinum Speciation

Current methods for speciation analysis of metals rely on gas chromatography (GC), high performance liquid chromatography (HPLC) or capillary electrophoresis (CE).[18,25] Each of these

methods requires expensive instrumentation and involves sample injection that can cause cross-contamination. Further descriptions of each of these methods follow below.

GC, HPLC and CE are chromatographic methods, which are based on dynamic partitioning of an analyte carried by a mobile phase through a stationary phase between these two phases, followed by detection using a specific analytical read-out, typically AAS in GC; UV, AAS or ICP-MS in HPLC; and UV, fluorescence or ICP-MS in CE. For GC, one major limitation is the fact that all metal samples must be pre-derivatized to enable the metal to become volatile.[25] Typically derivatization methods include hydride formation and alkylation with alkylborate or Grignard reagents.

Because of these deficiencies with GC, HPLC is becoming more popular in chromatographic metal speciation.[25] In HPLC, metal ion-containing samples can be analyzed without derivatization. In addition, this method is becoming more sensitive because it is often used in conjunction with ICP-MS.

CE is also on the rise as an analytical measurement technique for metal speciation.[18] Separation by CE is based on differential migration of charged analytes along a capillary filled with a suitable conducting analyte. This migration takes place uder the combined effects of electrophoretic and electroosmotic flows generated by applying an electric field across the capillary.

In addition to chromatographic techniques, electrochemical methods, such as ion-selective electrode potentiometry (ISEP) and spectroelectrochemical sensing, have also been utilized but often lack the sensitivity and selectivity needed to analyze trace analytes in complex samples.[26,27] In ISEP, some additional problems include: electrode fouling due to sample matrix components, electrode drift (poor reproducibility), electrode dissolution, electrode carry-over

(cross-contamination), and electrode instability. In spectroelectrochemical sensing, another major drawback is the requirement for preconcentration into a chemically selective film.

With respect to the detection of Pd^{II} contamination in APIs, to date there are no reliable methods with which to accurately detect this oxidation state specifically. For example, electrochemical methods require chromatographic separation, during which Pd^0 is likely oxidized to Pd^{II}. In addition, concentrated acid treatments are required with ICP-MS and a fluorescent method developed by Anslyn, which again can oxidize Pd^0.[28] As a result, it is difficult, if not impossible, to accurately address palladium oxidation states in APIs.

A fluorescent method that does not require acid treatment or chromatographic separation would be more desirable because detection can be observed with an inexpensive fluorometer or UV lamp and sample integrity should be high. Moreover, the samples in fluorescent methods are not cross-contaminated because disposable cuvettes are available, also facilitating high throughput analysis.

5.2 RESULTS AND DISCUSSION

5.2.1 Detection of Palladium Oxidation State in Buffer

Although numerous metal species, including Pd^{II}, catalyze the aromatic Claisen rearrangement in organic solvent, only in rare examples have metal species been shown to perform this transformation in aqueous solvent. As such, various metal ions were screened for the conversion of **34** to **36** in 1:4 DMSO/pH 10 buffer at 50 °C for 4 h. As Figure 57a shows, among the metal reagents tested, only $PdCl_2$ (and later Pt^{IV}) promoted this rearrangement. Although Pd^0 should

afford **35** rather than **36**, this needed to be confirmed.[29] Toward this end, palladium reagents with various oxidation states (0, II, IV) were screened. As Figure 57b shows, the detection method is oxidation state-specific and each Pd^{II} reagent and a Pd^{IV} reagent successfully performed the conversion while Pd^0 and insoluble Pd species did not.

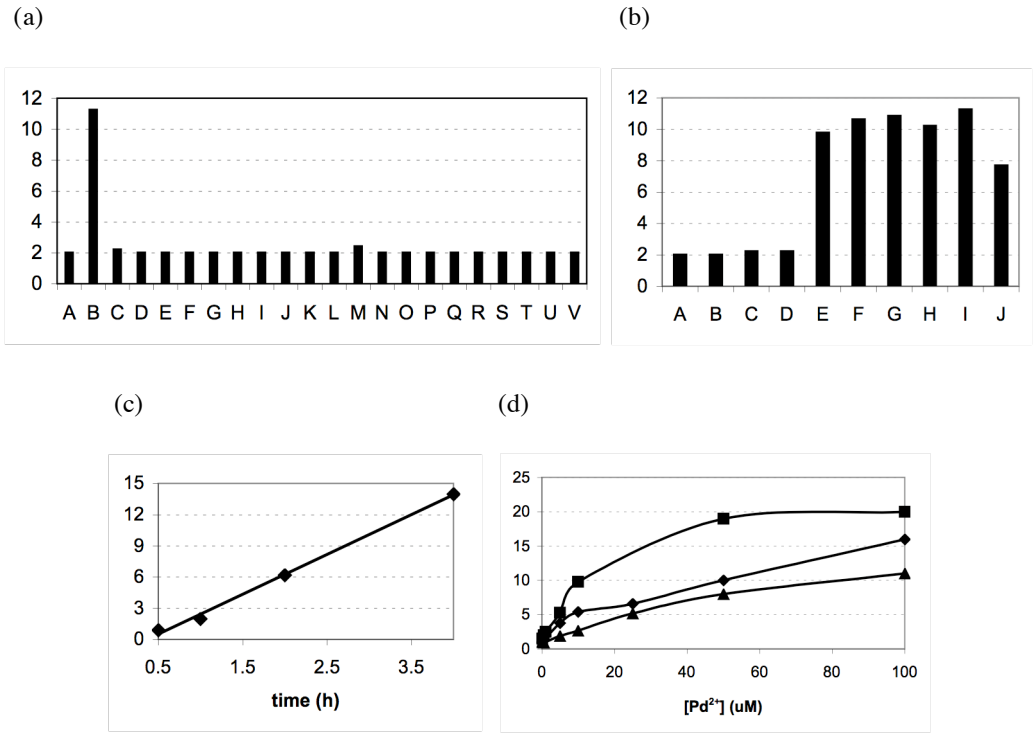

Figure 57. Fluorescence analysis of Pd^{II}

In these graphs, the y-axis is fluorescence intensity (a. u. × 10^5) at 535 nm. In all cases, [**34**] = 12.5 μM and the assays were performed in 1:4 DMSO/pH 10 buffer for 4 h at 50 °C. (a) Metal specificity. [Metal] = 10 μM. A = no metal, B = $PdCl_2$, C = $PtCl_2$, D = LiCl, E = $FeCl_3$, F = $AgNO_3$, G = $NiCl_2$, H = $Pb(NO_3)_2$, I = $MnCl_2$, J = $CdCl_2$, K, L = AuCl and $AuCl_3$, M = $RhCl(PPh_3)_3$, N, O = CuCl and $CuCl_2$, P = $MgSO_4$, Q = KCl, R = $CrCl_3$, S = $CoCl_2$, T = $HgCl_2$, U = $RuCl_3$, V = $ZnCl_2$. (b) Fluorescence induction by various Pd species and oxidation states. In all cases, [Pd] = 5.0 μM. A = no Pd, B = Pd black, C = $Pd_2(dba)_3$, D = $Pd(PPh_3)_4$, E = $PdCl_2$, F = $Pd(PPh_3)_2Cl_2$, G = $Pd(MeCN)_2Cl_2$, H = $Pd(acac)_2$, I = $Pd(OAc)_2$, J = K_2PdCl_6. (c) Initial rate analysis for Claisen rearrangement of **34** in the presence of $PdCl_2$ (20 mol %) in 1:1 DMSO/pH 10 buffer. y = 3.83x – 1.40; R^2 = 0.997. (a) Correlation

between fluorescence intensity and [$Pd^{II/IV}$]. ♦ = Pd^{2+}. ▲ = Pd^{4+}. ■ = Pd^{2+} in 1:4 DMSO/pH 10 buffer (11.4 mM salt).

The initial rate, catalytic efficiency and sensitivity of our $Pd^{II/IV}$ detection method were next examined. The initial rate was measured in 1:1 DMSO/pH 10 buffer using $PdCl_2$ (Figure 57c). The turnover frequency (TOF) was calculated as 0.3 h^{-1} (or 7.2 d^{-1}) in pH 10 buffer under the high dilution and salt conditions. This could be increased to 0.75 h^{-1} by decreasing the buffer salt concentration ten-fold. Using $PdCl_2$ and K_2PdCl_6, it was determined that the fluorescence intensity is correlated to the concentration of $Pd^{II/IV}$ in the 500 nM–100 μM (50 ppb–10 ppm) range for each (Figure 57d). The detection limits for Pd^{II} and Pd^{IV} using these conditions were calculated as 3.9 μM (390 ppb) and 11.1 μM (1.1 ppm), respectively, with S/B of 3. While decreasing the buffer salt concentration ten-fold did not increase the detection limit, the S/B dramatically increased using these dilute buffer conditions (Figure 57d).

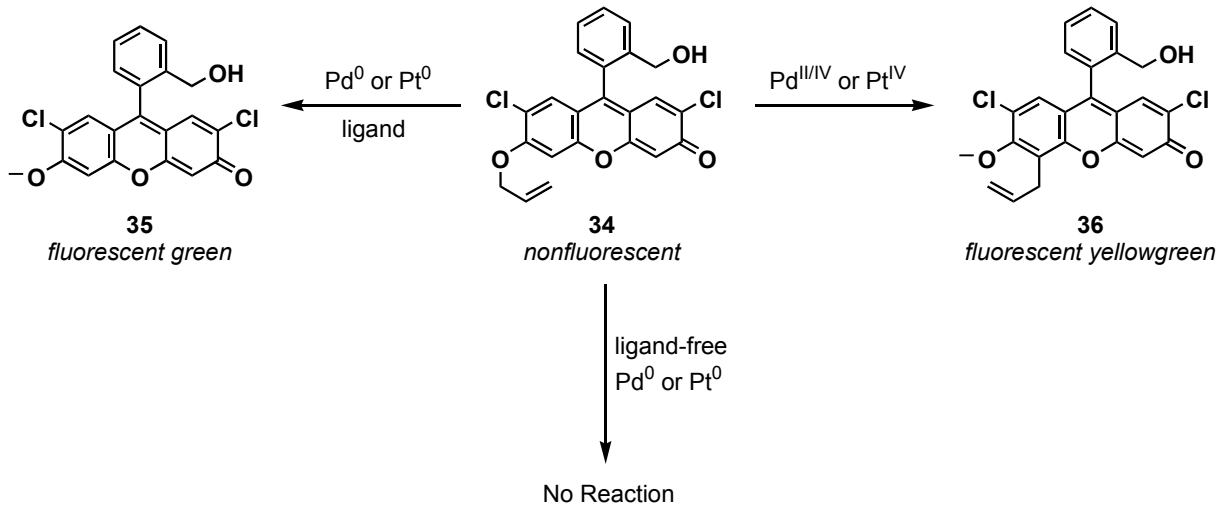

Figure 58. Dual sensor for detecting Pd and Pt in various oxidation states

With these results, it is clear that sensor **34** is a dual probe and can be used in applications of determining both total metal and the amount of oxidized metal in a sample (Figure 58). Thus, using two simple chemical principles, the different states of palladium (Pd black, soluble Pd^0, $Pd^{II/IV}$) can easily be distinguished.

5.2.2 Pd^{II} Detection in Functionalized Compounds

To address the challenging problem of palladium speciation in the pharmaceutical industry, the detection of Pd^{II} contamination in the presence of Pd^0 in synthetic samples was next examined. Since this process requires the detection of Pd^{II} species in the presence of a large excess of synthetic compound (500, 50, 5 ppm = 2000, 20000, 200000 equiv of compound with respect to Pd^{II}), I was skeptical that the metal would effectively bind and promote the Claisen rearrangement of **34**.

Thioanisole, cholesterol, 2-carboxy-7-hydroxycoumarin, morpholine, indole and *N*-methylephedrine were chosen as model structures that represent some of the typical functional groups and pharmacophores in many drugs. Each compound (12.5 mg/mL) was spiked with Pd^0 (<2.25 μmol/mL) and varying amounts of Pd^{II} (5–500 ppm relative to each compound), treated with **34** and heated at 50 °C for 4 h in 1:4 DMSO/pH 10 buffer. Figure 59a shows that, although the absolute fluorescence values are variable to a degree depending on excess organic compounds, the progress of palladium scavenging can be rapidly monitored to prioritize scavenging methods and optimize the protocol in a high throughput manner. Indole quenches the fluorescence signal of **36**, but the relative Pd^{II} concentrations can still be monitored during palladium scavenging because the relative fluorescence signal decreases as the palladium content decreases (Figure 59b). With a substituted indole (see Figure 43a), however, quenching was not

observed and Pd^{II} was successfully detected (Figure 59c). Despite the overall weaker signal presumably due to the competitive binding of *N*-methylephedrine to Pd^{II} (Figure 59b), progress in metal scavenging in such an excellent metal ligand can still be monitored. It should be noted here that this method is less sensitive than the total palladium detection method; however, in terms of monitoring the relative Pd^{II} values throughout the simulated scavenging in this proof-of-concept experiment, this can easily be accomplished for all compounds tested. Lesser amounts of Pd^{II} can be detected by increasing the incubation time due to the method's catalytic nature or by the use of more organic compound (Pd^{II} concentration with respect to the sample will be the same, but the Pd^{II} concentration in solution will increase).

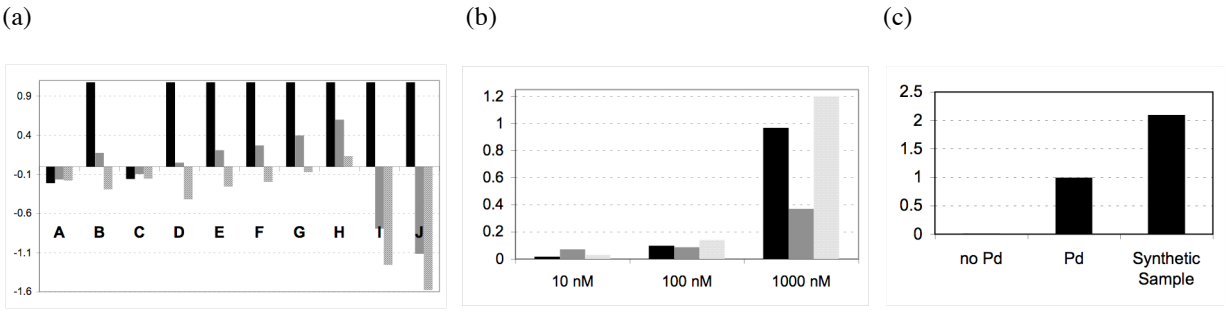

Figure 59. Pd^{II} detection in functionalized organic compounds

Each assay was performed in the presence of **34** (12.5 μM) for 4 h at 50 °C. (a) Pd^{II} detection in compounds. The y-axis is $\log_{10}$(fluorescent intensity (a. u. × 10^5)) at 535 nm The data are normalized so that the fluorescence signal of 500 ppm Pd^{II} is the same for each. Pd^0 in samples is Pd black (<2.25 μmol/mL). The first set of bars for each sample is 60 μM (500 ppm) Pd^{II}; the second set of bars is 6 μM (50 ppm) Pd^{II}; the third set of bars is 600 nM (5 ppm) Pd^{II}. A = no Pd, B = Pd^{II}, C = Pd^0, D = Pd^{II} + Pd^0. All synthetic samples contain both Pd^{II} and Pd^0: E = thioanisole, F = cholesterol, G = 2-carboxy-7-hydroxycoumarin, H = morpholine, I = indole, J = *N*-methylephedrine. In (b) and (c), the y-axis is fluorescent intensity (a. u. × 10^5) at 535 nm. (b) Effect of indole and *N*-methylephedrine on fluorescence intensity of varying concentrations of **36**. The first set of bars is **36** (no compound). The second set of

bars is **36** + indole. The third set of bars is **36** + *N*-methylephedrine. (c) Pd^{II} detection in substituted indole. Left = no Pd; middle = standard ($PdCl_2$; 10 μM); right = synthetic sample.

5.2.3 Detection of Palladium Oxidation State in Organic Solvent

In our laboratory, Sami Osman recently failed to reproduce a previously successful Suzuki coupling using $Pd(PPh_3)_4$ (unpublished results). It was suspected that the Pd reagent was fully oxidized to Pd^{II}, accounting for the failure. In order to test the quality of the reagent, *presumably* $Pd(PPh_3)_4$ (0.2 equiv) was added to a solution of the sensor **34** in CH_2Cl_2 at 24 °C for 24 h, but deallylation did not proceed to give the green fluorescent compound **35**. Instead, the Claisen rearrangement proceeded smoothly to produce the green yellow fluorescent compound **36**, as it was visible with naked eyes and by TLC analysis. This Pd^{II}-catalyzed aromatic Claisen rearrangement was confirmed with a positive control experiment using $PdCl_2$ (0.2 equiv) for the conversion of **34** to **36**. Thus, the lack of **35** and the presence of **36** enabled us to conclude easily, without time-consuming analysis, that the "$Pd(PPh_3)_4$" reagent was indeed oxidized.

To determine the generality of this dual probe in organic solvent, additional sources of Pd at each oxidation state were tested (Table 1). Each Pd reagent (0.2 equiv) was treated with a solution of sensor **1** in CH_2Cl_2 at 24 °C for 24 h. For all Pd^{II} reagents and Pd^{IV} reagent (Table 1, entries 1–5), exclusive formation of the Claisen rearrangement product **36** was observed by TLC analysis. For Pd^0 reagent, $Pd_2(dba)_3$ (Table 1, entry 7), deallylation to **35** was observed.

Table 1. Generality of Fluorogenic Probe **34**

Entry	Pd reagent	Product
1	$PdCl_2$	**36**
2	$PdCl_2(PPh_3)_2$	**36**
3	$PdCl_2(MeCN)_2$	**36**

4	$Pd(acac)_2$	**36**
5	$Pd(OAc)_2$	**36**
6	K_2PdCl_6	**36**
7	$Pd_2(dba)_3$	**35**
8	Pd black	**No reaction**

5.2.4 Determination of Palladium Oxidation State After a Reaction Stalls

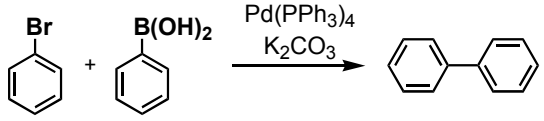

Figure 60. Suzuki-Miyaura cross-coupling reaction

Next, this fluorescent method was applied for the detection of palladium oxidation state after a stalled reaction. The reaction that was examined was the Suzuki cross-coupling (Pd^0-catalyzed) between phenylboronic acid (1.5 equiv) and bromobenzene in the presence $Pd(PPh_3)_4$ (1 mol %) and K_2CO_3 (3.0 equiv) as a base (Figure 60). As is often the case with such a small amount of Pd catalyst, conversion to biphenyl began to stall after approximately 3 h and the reaction did not proceed to completion at 65 °C after 24 h. To determine if the reaction stalled due to catalyst oxidation, the reaction mixture was cooled to 50 °C after 24 h (reaction no longer occurring) and sensor **34** was added. After 2 h, conversion of **34** to **36** was observed by TLC with no detection of **35** indicating that the Pd was indeed oxidized accounting for the halt in reaction.

5.2.5 Determination of Platinum Oxidation State

Based on the similar π-electrophilicity between cationic palladium and platinum species, it was desirable to extend this method to Pt^{n+} detection. Pt^0 has been shown to be beneficial for human

health due to its ability to catalytically quench reactive oxygen species to less toxic materials and is used in many health-related products including commercially bottled-drinking water.[22] Despite such benefits, a major concern in manufacturing these products is the contamination of Pt^{IV} because Pt^0 nanocolloid-containing drinking water is produced through the reduction of the more stable Pt^{IV} species and Pt^{IV} is highly toxic.[23,24] Current analytical methods are instrument intensive requiring highly trained personnel. Thus, for high throughput analysis of the safety of such Pt^0-containing products a better method for Pt^{IV}-specific detection is needed.

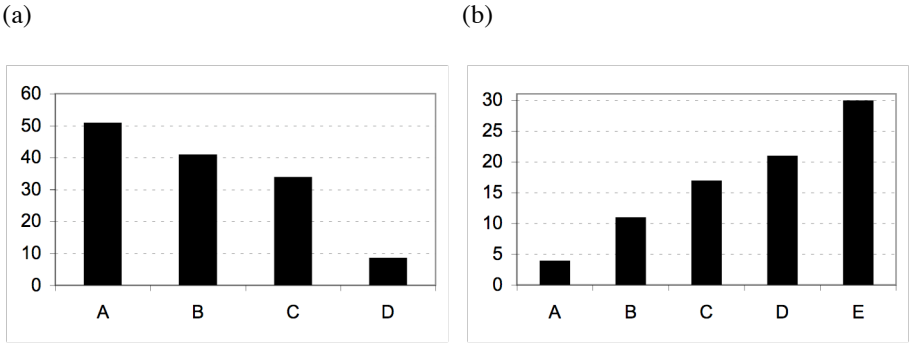

Figure 61. Fluorescence analysis for Pt^{IV}

In these graphs, the y-axis is fluorescence intensity (a. u. × 105) at 535 nm. In all cases, [**34**] = 12.5 μM and the assays were performed in water for 2 h at 80 °C. (a) Monitoring of Pt^{IV} (1 mM) reduction to Pt^0. A = 0 min, B = 10 min, C = 20 min, D = 30 min. (b) Detection of Pt^{IV} in Pt^0-containing drinking water. In all cases, [Pt^0] = 250 μM (50 ppm) and the following amounts of Pt^{IV} were in the samples: A = Pt^0 water, B = 0.5 nM (0.0975 ppb), C = 5 nM (0.975 ppb), D = 50 nM (9.75 ppb), E = 500 nM (97.5 ppb).

Although in the metal screening studies Pt^{II} did not produce fluorescence signal, it was hypothesized that Pt^{IV} would be a more efficient catalyst because it is presumably more π-electrophilic.[30] Indeed, unlike $Pt^{0/II}$, Pt^{IV} catalyzed the Claisen rearrangement in water, which was also confirmed in organic solvent. These conditions were then used to monitor the progress of

the electrochemical reduction of Pt^{IV} to Pt^0 in water. As Figure 61a shows, this detection method was successful for fluorescently monitoring this reduction. This fluorescence method was next used to detect Pt^{IV} contamination in a Pt^0-containing drink. As Figure 61b shows, Pt^{IV} was successfully detected by fluorescence in a concentration-dependent manner with a detection limit of 0.54 nM (0.11 ppb) with S/B of 3 in the presence of Pt^0 at 250 μM. In addition, in the absence of buffer salts, the Pt^{IV}-catalyzed Claisen rearrangement proceeds much more efficiently and low-ppb detection can be achieved easily.

5.3 CONCLUSION

In summary, it has been demonstrated that fluorogenic probe **34** can selectively detect Pd^{II} and Pt^{IV} via Claisen rearrangement to **36**. This method is capable of detecting these metal species in aqueous solvent in the presence of functionalized compounds and Pt^0-water and in organic solvent in reaction mixtures. In combination with the Pd^0/Pt^0 detection method, it is now possible to distinguish Pd^{II} and total Pd contamination. This method should find applications in the pharmaceutical industry, the environment and Pd/Pt quality control.

5.4 EXPERIMENTAL

5.4.1 General Information

All reactions were carried out with dry, freshly distilled solvents under anhydrous conditions, unless otherwise noted. Methylene chloride (CH_2Cl_2) was distilled from calcium hydride. All reactions were monitored by thin-layer chromatography (TLC) carried out on 0.25-mm EMD silica gel plates (60F-254) using UV light (254 nm or 365 nm).

$PdCl_2$, $PdCl_2(PPh_3)_4$, $PtCl_2$, and $H_2PtCl_6 \bullet 6H_2O$ were purchased from Alfa Aesar and used as received. $Pd(PPh_3)_4$, $Pd(acac)_2$, $PdCl_2(MeCN)_2$ and K_2PdCl_6 were purchased from Strem and used as received. $Pd(OAc)_2$ was purchased from TCI and used as received. Platinum water and spiked samples were obtained from APt Co. Buffers were purchased from J. T. Baker (pH 10, borate ($[K^+]$ = 94–114 mM), catalog number 5609-01) and used as received.

5.4.2 Oxidation State Detection in Organic Solvent

$Pd^{II/IV}$-catalyzed Claisen rearrangement. A dry, 10-mL round bottom flask was charged with **34** (10.0 mg, 23.4 μmol) and Pd^{II} or Pd^{IV} catalyst (20 mol %; 4.7 μmol; see table below) at 24 °C. The flask was evacuated and purged with nitrogen, and CH_2Cl_2 (234 μL) was added. The reaction mixture was stirred at 24 °C for 24 h. TLC analysis (50% EtOAc in hexanes; R_f = 0.59) indicated complete conversion to the Claisen-rearranged product **36**.

Pd Reagent	Quantity
$Pd(acac)_2$	1.4 mg
$PdCl_2(PPh_3)_2$	3.3 mg
$PdCl_2(MeCN)_2$	1.2 mg
$PdCl_2$	1.0 mg
$Pd(OAc)_2$	1.0 mg

K_2PdCl_6	1.8 mg

Pt^{IV}-catalyzed Claisen rearrangement. A dry, 10-mL round bottom flask was charged with **34** (10.0 mg, 23.4 μmol) and $H_2PtCl_6 \bullet 6H_2O$ (2.4 mg; 4.7 μmol) at 24 °C. The flask was evacuated and purged with nitrogen and DCE (234 μL) was added. The reaction mixture was stirred at 80 °C for 24 h. TLC analysis (50% EtOAc in hexanes; $R_f = 0.59$) indicated complete conversion to the Claisen-rearranged product **36**.

Detection of Pd oxidation state in a reaction mixture. A dry, 10-mL round bottom flask was charged with bromobenzene (17.0 μL, 162 μmol) and THF (2.43 mL). Subsequently, phenylboronic acid (30.0 mg, 162 μmol), K_2CO_3 (67.2 mg, 486 μmol), and $Pd(PPh_3)_4$ (2.8 mg, 2.4 μmol) were added and the reaction mixture was stirred at 65 °C under nitrogen. After 3 h, the reaction progress began to stall and the reaction was left at 65 °C for 24 h. After this period, the reaction mixture was cooled to 50 °C and treated with compound **34** (10.0 mg, 23.4 μmol). The resulting reaction mixture was stirred at 50 °C for 24 h (initial observation of **36** after 2 h) and TLC analysis (50% EtOAc in hexanes; $R_f = 0.59$) indicated complete conversion of **34** to the Claisen-rearranged product **36**.

5.4.3 Fluorescence Spectroscopy

Preparation of parent stock solutions used for fluorescence study in aqueous solvent.

Solution	Reagent	Quantity	Solvent (10 mL)	Conc. of stock solution
A	compound 1	42.7 mg (0.10 mmol)	DMSO	10.0 mM
B	$PdCl_2$	9.0 mg (50 μmol)	3:1 Brine/MeOH	5.0 mM
C	$Pd(OAc)_2$	2.2 mg (10 μmol)	3:1 Brine/MeOH	1.0 mM
D	$Pd(acac)_2$	3.0 mg (10 μmol)	DMSO	1.0 mM

E	$PdCl_2(PPh_3)_2$	7.0 mg (10 μmol)	DMSO	1.0 mM
F	$PdCl_2(MeCN)_2$	2.6 mg (10 μmol)	3:1 Brine/MeOH	1.0 mM
G	K_2PdCl_6	19.9 mg (50 μmol)	3:1 Brine/MeOH	5.0 mM

Notes: See previous experimentals

Fluorescence spectroscopy. Fluorescence spectra were recorded in a 1 × 1-cm disposable cuvette (VWR; catalog number 58017-880) on a Jobin Yvon FluoroMax-3 spectrometer under the control of a Windows-based PC running FluorEssence software. The samples were excited at 497 nm and the emission intensities were collected at 535 nm. All spectra were corrected for emission intensity using the manufacturer supplied photomultiplier curves.

Initial rate determination. $PdCl_2$ stock solution **B** (200.0 μL, 470 nmol) and **34** (10.0 mg, 23.4 μmol) were added to DMSO/pH 10 buffer (1:1) solution (20 mL) at 24 °C. The experiment was performed in triplicate. At t = 0.5, 1, 2 and 4 h, 200 μL aliquots were taken from each reaction mixture and diluted to 4.0 mL with 1:4 DMSO/pH 10 buffer for fluorescence measurement. **Notes:** No difference was noted between the reaction in 1:1 and 1:4 DMSO/pH 10 buffer. A pH 10 buffer was chosen because a pH study revealed that this was the optimal pH for the rearrangement.

Turnover frequency (TOF). To determine the TOF, a solution containing $PdCl_2$ ($[Pd^{II}]_{final}$ = 500 nM) and solution **A** (5.0 μL, $[\mathbf{34}]_{final}$ = 12.5 μM) was prepared in DMSO/pH 10 buffer (1:4). The intensity of this sample was compared to a standard solution containing **36** ($[\mathbf{36}]_{final}$ = 500 nM) in DMSO/pH 10 buffer (1:4). The intensity of the Pd^{II}-containing sample was 7.3×10^5 after 24 h at 50 °C and the intensity of the standard solution of **36** was 1.0×10^5. The turnover frequency is $7.3 \times 10^5 / 1.0 \times 10^5 = 7.3/24$ h = 0.3 h^{-1}.

Preparation of analytic samples for fluorescence detection. Pd solutions **B–G** (40.0 μL of 1.0 mM stock, $[Pd^{II}]_{final}$ = 10 μM) were added to DMSO/pH 10 buffer solution (1:4) (4.0 mL). To the mixture was added solution **A** (5.0 μL, $[\mathbf{34}]_{final}$ = 12.5 μM), and the samples were incubated for 24 h at 50 °C in a water bath before fluorescence measurement. Each experiment was performed in triplicate.

Concentration dependence of $Pd^{II/IV}$ detection in aqueous solvent. Varying amounts of Pd solution **B/G** were added to DMSO/pH 10 buffer solution (1:4) (4.0 mL). Solution **A** (5.0 μL, $[\mathbf{34}]_{final}$ = 12.5 μM) was added to the mixture, and the samples were incubated for 24 h at 50 °C in a water bath before fluorescence measurement. Each experiment was performed in triplicate.

Determination of Pd^{II} in functionalized organic compounds. A solution of compound (50 mg) in DMSO (800 μL) was treated with Pd black (<2.25 μmol/mL) and varying amounts of $PdCl_2$ (600 nM–60 μM; 5–500 ppm in the compound) and the sample was allowed to sit for 30 min. pH 10 Buffer ([buffer salt] = 1.14 mM; 3.2 mL) and solution **A** (5.0 μL, $[\mathbf{34}]_{final}$ = 12.5 μM) were then added to the mixture, and the samples were heated for 4 h at 50 °C in a water bath before fluorescence measurement.

For comparison, the following control experiments were conducted:

(1) **Negative control** (Background): Solution **A** (5.0 μL, $[\mathbf{1}]_{final}$ = 12.5 μM) was added to DMSO (800 μL) and pH 10 buffer ([buffer salt] = 1.14 mM; 3.2 mL), and the samples were heated for 4 h at 50 °C in a water bath before fluorescence measurement.

(2) **Positive control** (Pd^{II} only): Varying amounts of $PdCl_2$ (0.6–60 μM in solution; 5–500 ppm in the compound) were added to DMSO (800 μL), and the sample was allowed to sit for 30 min.

pH 10 buffer ([buffer salt] = 1.14 mM; 3.2 mL) and solution **A** (5.0 μL, $[\mathbf{1}]_{final}$ = 12.5 μM) were then added to the mixture, and the samples were heated for 4 h at 50 °C in a water bath before fluorescence measurement.

(3) **Negative control** (Pd^0 only): Pd black (<2.25 μmol/mL) was added to DMSO (800 μL), and the sample was allowed to sit for 30 min. pH 10 buffer ([buffer salt] = 1.14 mM; 3.2 mL) and solution **A** (5.0 μL, $[\mathbf{1}]_{final}$ = 12.5 μM) were then added to the mixture, and the samples were heated for 4 h at 50 °C in a water bath before fluorescence measurement.

(4) **Positive control** (Pd^{II} + Pd^0): Pd black (<2.25 μmol/mL) and varying amounts of $PdCl_2$ (600 nM–60 μM in solution; 5–500 ppm in the compound) were added to DMSO (800 μL), and the sample was allowed to sit for 30 min. pH 10 buffer ([buffer salt] = 1.14 mM; 3.2 mL) and solution **A** (5.0 μL, $[\mathbf{1}]_{final}$ = 12.5 μM) were then added to the mixture, and the samples were heated for 4 h at 50 °C in a water bath before fluorescence measurement.

Normalization procedure. The data are normalized for 500 ppm Pd^{II} analogously to ICP-MS analysis, in which a standard curve is generated for Pd in each organic molecule separately.

Monitoring of Pt^{IV} reduction. Pt^{IV} reduction mixture (0.5 mL) was treated with solution **A** (5.0 μL, $[\mathbf{34}]_{final}$ = 12.5 μM) and the samples were heated at 80 °C for 2 h. Prior to fluorescence measurement, each sample was diluted to 1.0 mL with pH 7 buffer.

Pt^{IV} detection in platinum-containing drink. Pt^{IV} containing Pt^0 water (0.5 mL) was treated with solution **A** (5.0 μL, $[\mathbf{34}]_{final}$ = 12.5 μM) and the samples were heated at 80 °C for 2 h. Prior to fluorescence measurement, each sample was diluted to 1.0 mL with pH 7 buffer. In this case, the negative control was the commercially-available Pt^0 nanocolloid-containing water.

5.5 BIBLIOGRAPHY

1. Koide, K., Song, F., de Groh, E. D., Garner, A. L., Mitchell, V. D., Davidson, L. A., Hukriede, N. A., "Scalable and concise synthesis of dichlorofluorescein derivatives displaying tissue permeation in live zebrafish embryos." *ChemBioChem* **2008**, *9*, 214–218.

2. Majumdar, K. C., Alam, S., Chattopadhyay, B., "Catalysis of the Claisen rearrangement." *Tetrahedron* **2008**, *64*, 597–643.

3. Stewart, H. F., Seibert, R. P., "Catalyzed rearrangements of 2-alloxypyridine and 2-crotoxypyridine." *J. Org. Chem.* **1968**, *33*, 4560–4561.

4. Kerrigan, N. J., Bungard, C. J., Nelson, S. G., "Pd(II)-catalyzed aliphatic Claisen rearrangements of acyclic allyl vinyl ethers." *Tetrahedron* **2008**, *64*, 6863–6869.

5. van der Baan, J. L., Bickelhaupt, F., "Palladium(II)-catalyzed Claisen rearrangement of allyl vinyl ethers." *Tetrahedron Lett.* **1986**, *27*, 6267–6270.

6. Schenck, T. G., Bosnich, B., "Homogeneous catalysis. Transition-metal-catalyzed Claisen rearrangements." *J. Am. Chem. Soc.* **1985**, *107*, 2058–2066.

7. A similar mechanism was also proposed for the Pd^{II}-catalyzed Cope rearrangement: Overman, L. E., Knoll, F. M., "Palladium(II) chloride catalyzed Cope rearrangements of acyclic 1,5-dienes." *J. Am. Chem. Soc.* **1980**, *102*, 865–867.

8. Nicolaou, K. C., Bulger, P. G., Sarlah, D., "Palladium-catalyzed cross-coupling reactions in total synthesis." *Angew. Chem. Int. Ed.* **2005**, *44*, 4442–4489.

9. Tietze, L. F., Ila, H., Bell, H. P., "Enantioselective palladium-catalyzed transformations." *Chem. Rev.* **2004**, *104*, 3453–3516.

10. Zeni, G., Larock, R. C., "Synthesis of heterocycles via palladium π-olefin and π-alkyne chemistry." *Chem. Rev.* **2004**, *104*, 2285–2310.

11. MacQuarrie, S., Horton, J. H., Barnes, J., McEleney, K., Loock, H-P., Crudden, C. M., "Visual observation of redistribution and dissolution of palladium during the Suzuki-Miyaura reaction." *Angew. Chem. Int. Ed.* **2008**, *47*, 3279–3282.

12. Köhler, K., Kleist, W., Pröcki, S. S., "Genesis of coordinatively unsaturated palladium complexes dissolved from solid precursors during Heck coupling reactions and their role as catalytically active species." *Inorg. Chem.* **2007**, *46*, 1876–1883.

13. Crudden, C. M., Sateesh, M., Lewis, R., "Mercaptopropyl-modified mesoporous silica: a remarkable support for the preparation of a reusable, heterogeneous palladium catalyst for coupling reactions." *J. Am. Chem. Soc.* **2005**, *127*, 10045–10050.

14. Galaffu, N., Man, S. P., Wilkes, R. D., Wilson, J. R. H., "Highly functionalized sulfur-based scavengers for the efficient removal of palladium species from active pharmaceutical ingredients." *Org. Process Res. Dev.* **2007**, *11*, 406–413.

15. Welch, C. J., Albaneze-Walker, J., Leonard, W. R., Biba, M., DaSilva, J., Henderson, D., Laing, B., Mathre, D. J., Spencer, S., Bu, X., Wang, T., "Adsorbent screening for metal impurity removal in pharmaceutical process research." *Org. Process Res. Dev.* **2005**, *9*, 198–205.

16. Urawa, Y., Miyazawa, M., Ozeki, N., Ogura, K., "A novel methodology for efficient removal of residual palladium from a product of the Suzuki-Miyaura coupling with polymer-supported ethylenediamine derivatives." *Org. Process Res. Dev.* **2003**, *7*, 191–195.

17. "Environmental Health Criteria 226: Palladium." World Health Organization, Geneva, 2002.

18. Dabek-Zlotorzynska, E., Lai, E. P. C., Timerbaev, A. R., "Capillary electrophoresis: the state-of-the-art in metal speciation studies." *Anal. Chim. Acta* **1998**, *359*, 1–26.

19. Timerbaev, A. R., Küng, A., Keppler, B. K., "Capillary electrophoresis of platinum-group elements. Analytical, speciation and biochemical studies." *J. Chromatogr., A* **2002**, *945*, 25–44.

20. Huang, Z., Timerbaev, A. R., Keppler, B. K., Hirokawa, T., "Determination of cisplatin and its hydrolytic metabolite in human serum by capillary electrophoresis techniques." *J. Chromatogr., A* **2006**, *1106*, 75–79.

21. Nischwitz, V., Michalke, B., Kettup, A., "Speciation of Pt(II) and Pt(IV) in spiked extracts from road dust using on-line liquid chromatography-inductively coupled plasma mass spectrometry." *J. Chromatogr., A* **2003**, *1016*, 223–234.

22. http://www.apt-ca.com

23. Kajita, M., Hikosaka, K., Iitsuka, M., Kanayama, A., Toshima, N., Miyamoto, Y., "Platinum nanoparticle is a useful scavenger of superoxide anion and hydrogen peroxide." *Free Radical Res.* **2007**, *41*, 615–626.

24. "Environmental Health Criteria 123: Platinum." World Health Organization, Geneva, 1991.

25. Szpunar-Lobinska, J., Witte, C., Lobinski, R., Adams, F. C., "Separation techniques in speciation analysis for organometallics speices." *Fresenius J. Anal. Chem.* **1995**, *351*, 351–377.

26. Wansapura, C. M., Seliskar, C. J., Heineman, W. R., "Spectroelectrochemical sensing based on multimode selectivity simultaneously achievable in a single device. 20. Detection of metal ions in different oxidation states." *Anal. Chem.* **2007**, *79*, 5594–5600.

27. De Marco, R., Clarke, G., Pejcic, B., "Ion-selective electrode potentiometry in environmental analysis." *Electroanalysis* **2007**, *19*, 1987–2001.

28. Houk, R. J. T., Wallace, K. J., Hewage, H. S., Anslyn, E. V., "A colorimetric for Pd(II): a method for detecting residual palladium in cross-coupling reactions." *Tetrahedron* **2008**, *64*, 8271–8278.

29. Itami, K., Yamazaki, D., Yoshida, J., "Palladium-catalyzed rearrangement/arylation of 2-allyloxypyridine leading to the synthesis of N-substituted 2-pyridones." *Org. Lett.* **2003**, *5*, 2161–2164.

30. Barluenga, J., Diéguez, A., Fernández, A., Rodríguez, F., Fañanás, F. J., "Gold- or platinum-catalyzed tandem cycloisomerization/Prins-type cyclization reactions." *Angew. Chem. Int. Ed.* **2006**, *45*, 2091–2093.

6.0 FLUOROMETRIC DETECTION OF OZONE

6.1 RESEARCH DESIGN

The study of reactive oxygen species (ROS) in biology is quite extensive. Although selective fluorescent sensors exist for many ROS (singlet oxygen, superoxide, hydroxyl radical, nitric oxide, etc.), no such sensor had been previously reported for ozone.[1] As such, it was speculated that a selective, fluorescent "turn-on" probe for ozone could be designed based on ozone's reactivity with alkenes (Figure 62).

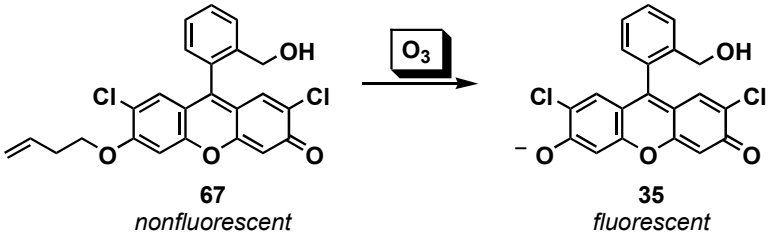

67
nonfluorescent

35
fluorescent

Figure 62. Ozonolysis of homoallyl ether to convert a nonfluorescent molecule to a fluorescent molecule

6.1.1 Importance of Ozone Detection

Ozone exposure is a signficant global health problem, especially in urban areas. While ozone in the stratosphere protects the earth from damaging ultraviolet light, tropospheric or ground level ozone is toxic resulting in damage to the respiratory tract.[2] In fact, the Environmental Protection

Agency recently lowered the allowable ozone level from 84 ppb/8 h to 75 ppb/8 h.[3] Aside from outdoor ozone exposure, indoor exposure to ozone is on the rise, which is largely due to outdoor ozone being trapped indoors and electrical equipment that can produce ozone such as photocopiers (1.3–7.9 mg ozone/h), laser printers (<0.02–6.5 mg ozone/h) and electrostatic air filters.[4,5] In addition to ozone itself as a pollutant, the products of ozone reactions are also toxic. Such ozone-reactive compounds are found in common items such as wood flooring, carpet, paints, cleaning products and perfumes.

In terms of ozone biology, the exact mechanism by which ozone damages the respiratory system is poorly understood.[6–11] It is speculated that ozone is much too reactive to reach and permeate the epithelial cells of the lung. Once ozone is breathed into the respiratory system, it is known to react with many biomolecules including unsaturated fatty acids and antioxidants in the nasal and lung lining fluid. In fact, the antioxidants uric acid, ascorbic acid and glutathione are the first line of defense against ozone.[10,11] While the time for ozone to cross the lung lining was estimated as 2×10^{-6} s, the half-life of ozone was estimated as 7×10^{-7} s. This is due to the fact that the rates of reaction with these antioxidants are 5.83×10^{4} $M^{-1}s^{-1}$ (uric acid), 5.5×10^{4} $M^{-1}s^{-1}$ (ascorbic acid), and 57.5×10^{4} $M^{-0.75}s^{-1}$ (glutathione).[12] Thus, ozone preferentially reacts with antioxidants to prevent damage to the lung tissue.

Although ozone has a negative impact on human health, there are a number of industrial applications for ozone.[13] For example, ozone plays a critical role in wastewater treatment, disinfection and fumigation. In addition, although prohibited in the United States, intravenous ozone therapy is believed to have health benefits. Thus, ozone plays many roles in today's society and selective detection of this toxic, but useful gas is an important challenge.

6.1.2 Endogenous Ozone Controversy

Reactive oxygen species (ROS) have had a rather controversial history.[14] The existence of singlet oxygen and superoxide was first proposed in the late 1960s; however, due to the lack of sensitive and specific probes, these results were met with skepticism and the observations were only confirmed in the late 1980s. Recently, ozone has received its time in the spotlight. It has been proposed that ozone is produced endogenously from singlet oxygen in both neutrophils and atherosclerotic plaque (Figure 63b) implicating ozone in inflammatory responses.[15–17] This conclusion was drawn from the premise that the colorimetric dye, indigo carmine (**68**; Figure 63a),[18] differentially reacted with ozone as opposed to other ROS through incorporation of an ^{18}O label . However, similar to the singlet oxygen/superoxide story, **68** has since been proven to not only react with ozone but also with superoxide in a similar manner, thus, calling into questions these findings of endogenous ozone.[19–21]

Aside from this ozone controversy, chemiluminescent methods, including the use of **68**, are also used to measure ozone in ambient air;[22,23] however, other atmospheric compounds are known to also absorb in this region of the electromagnetic spectrum and false-positive ozone readings are often reported.[24,25] In addition, many of these methods are sensitive to humidity. We reasoned that if a specific probe were available then ozone detection in air and biological systems would be achieved more reliably.

There are several problems associated with the use of **68** as a specific sensor for ozone. First, the dye readily undergoes oxidative cleavage, which is most likely responsible for the lack of specificity.[26] Additionally, the reaction of blue **68** with ROS yields compound **69** (Figure 63), which is colorless and cannot be directly visualized without the use of a spectrometer. In biological samples, HPLC or mass spectrometry are often required in combination with such

spectroscopic techniques because the signal for **69** (UV: λ_{max} = 245 and 298 nm) overlaps with many other bioorganic compounds.

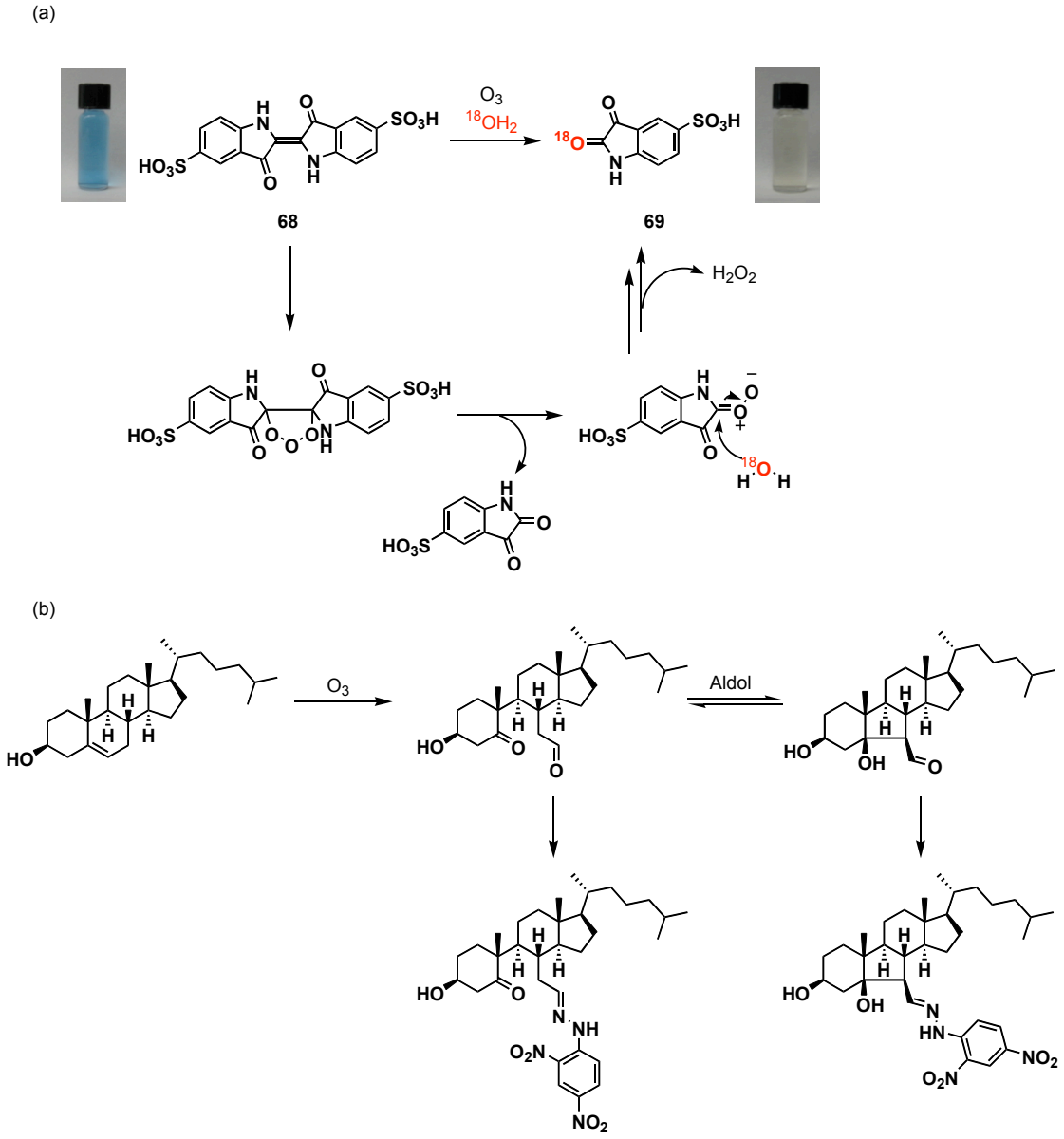

Figure 63. Nonselective indigo carmine sensor for ROS

A similar approach has recently been reported and commercialized for the simultaneous detection of ozone and carbonyls in air.[27] Although this system was shown to be resistant to

humidity, it requires extensive extraction and derivatization prior to HPLC analysis, and its stability in the presence of other oxidizing agents was not reported.

6.1.3 Other Ozone Detection Methods

In addition to colorimetric ozone detection methods, other common ozone detection methods include chemiluminescence (noncolorimetric), UV photometry, electrochemical, differential optical absorption spectrometry (DOAS) and light detection and ranging (LIDAR).[22,28,29] There are two chemiluminescent methods commonly used for ozone: reaction of ozone with ethylene or reaction of ozone with NO. Although this method is sensitive (detection limit = 2–5 ppbv), a known interference is water vapor; and thus, false positive ozone readings are often observed.[28]

The UV photometry method is based on ozone's ability to absorb UV light. Similar to indigo carmine, one major drawback is the fact that other gaseous hydrocarbons such as aromatic hydrocarbons often overlap with ozone's signal (254 nm). The detection limit for this method is 2–5 ppbv.[28]

The most common electrochemical method is based on the reaction of ozone with potassium iodide.[22] In fact, this is one of the oldest methods for ozone detection. Major problems with this method are interferences with other oxidants and insufficient reproducibility, especially at low ozone concentrations.[22,28,29] Nonetheless, this method is still used for calibration.

DOAS and LIDAR are both remote ozone detection methods and the most sensitive to date.[24] Since both of these methods are based on light paths (white light vs. laser), a major interference is any object that interrupts the path of the laser. The detection limit for DOAS and LIDAR are <1.5 ppbv.[28]

6.2 RESULTS AND DISCUSSION

6.2.1 Mechanistic Design and Synthesis of Fluorescent Ozone Sensor

As was previously discussed, fluorescein compounds display fluorescence signal only when the phenolic hydroxy group is deprotonated.[30] Thus, it was proposed that if Pittsburgh Green **35** were functionalized as a nonfluorescent homoallyl ether, after reaction with ozone the resulting aldehyde would undergo β-elimination to yield fluorescent fluorescein and acrolein (Figure 64). This terminal alkene sensor should be specific for ozone because it contains a less electron-rich, isolated (non-conjugated) olefin, which should not react with other ROS to yield a fluorescence signal.[31–33]

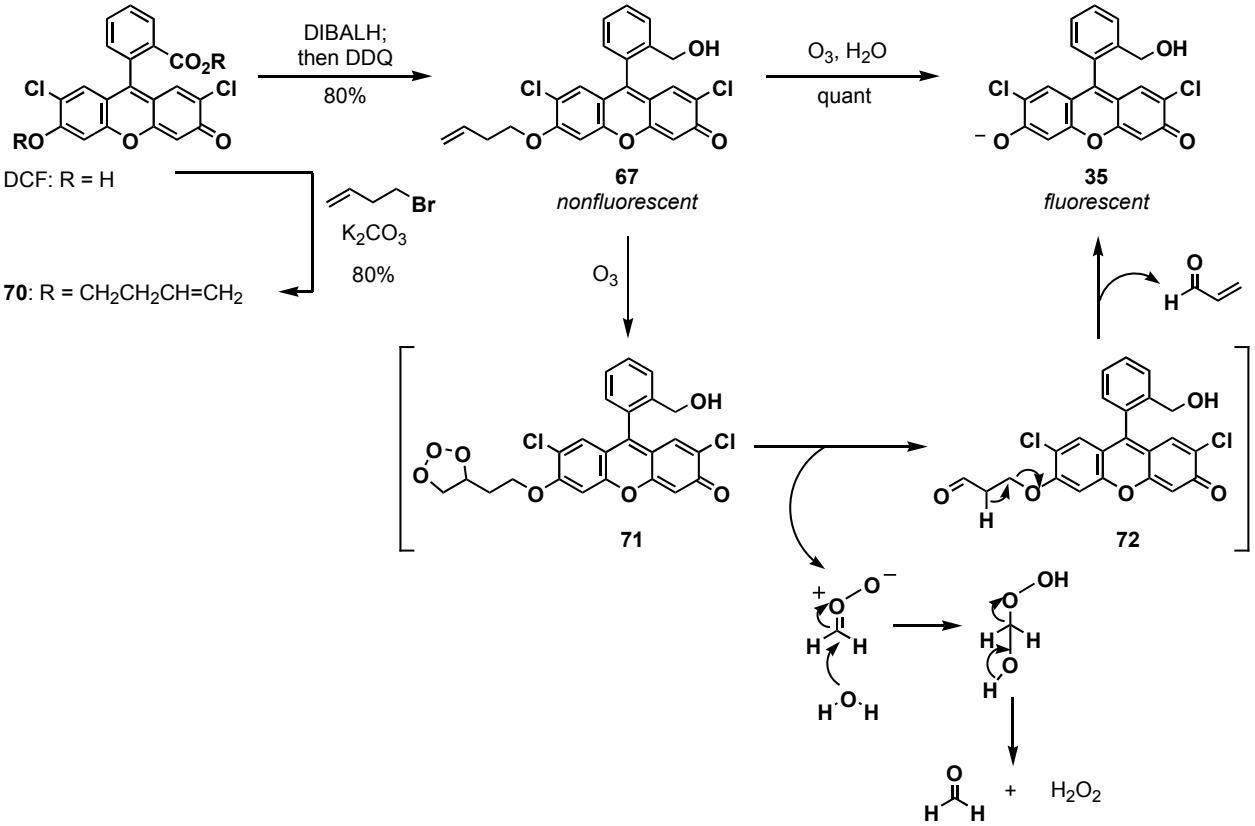

Figure 64. Synthesis and mechanistic design of ozone sensor **67**

Based on this hypothesis, homoallyl ether **67** was designed and synthesized in two steps from commercially available 2',7'-dichlorofluorescein (DCF) in 64% yield (Figure 64). Ozone was bubbled through a solution of **67** in 19:1 acetone/water and fluorescent compound **35** was obtained in quantitative yield presumably through intermediates **71** and **72**, thus, providing positive feedback for the sensor design.

6.2.2 Ozone Detection in Aqueous Media

In order to develop a fluorescent method amenable to both biological and atmospheric detection, pH 7 buffer was chosen to perform the conversion of **67** to **35**. A solution of **67** in 1:19 MeOH/pH 7 buffer at 24 °C was exposed to ozone, and following incubation at 37 °C for 1 h to facilitate β-elimination, formation of **35** was observed (signal-to-background (S/B) = 80) (Figure 65a). A time-dependence study for conversion of **67** to **35** revealed that 1 h is sufficient time for this process to occur (Figure 65b). Presumably, the β-elimination is the rate-determining step because the formation and fragmentation of molozonides are extremely rapid.[34] Because this detection method may be performed in the presence of cells, ozonolysis was also performed in a mixture of pH 7 buffer and RPMI-1640 cell culture media (3:1). Indeed, the method is compatible with components of the cell culture media (S/B = 104; not shown) indicating that this method should be amenable for in vitro and possibly in vivo studies.

With these successful results with ozone in hand, the ROS-specificity of the sensor was next determined. Sensor **67** was tested against singlet oxygen and superoxide; singlet oxygen was generated in situ from sodium molybdate and hydrogen peroxide and potassium superoxide was used as a source of superoxide. To confirm the production of these ROS species, indigo carmine was used as a positive control. No reaction or fluorescence signal was observed with

either of these ROS (Figure 65a). Hydrogen peroxide and hydroxyl radical were also examined because peroxide[35] is a by-product of the aqueous ozonolysis reaction, hydroxyl radical[22] is a product of ozone decomposition in aqueous solution and both are endogenous ROS species. For each, no reaction was observed (Figure 65a). Thus, sensor **67** is specific for ozone and can be used to unambiguously detect ozone even in the presence of other ROS.

The sensitivity of this fluorescent method for ozone detection was next examined. The fluorescence intensity correlated to the concentration of ozone in the 50 nM–12.5 μM (2.4–600 ppbv) range (Figure 65c) with S/B of 2.6–310 after 10-fold dilution of the original samples (0–500 nM shown in Figure 65d). The level of detection is 59 nM (2.9 ppbv; S/B = 3) and the level of quantitation is 340 nM (16 ppbv; S/B = 10), which is comparable to other known ozone measurement techniques.

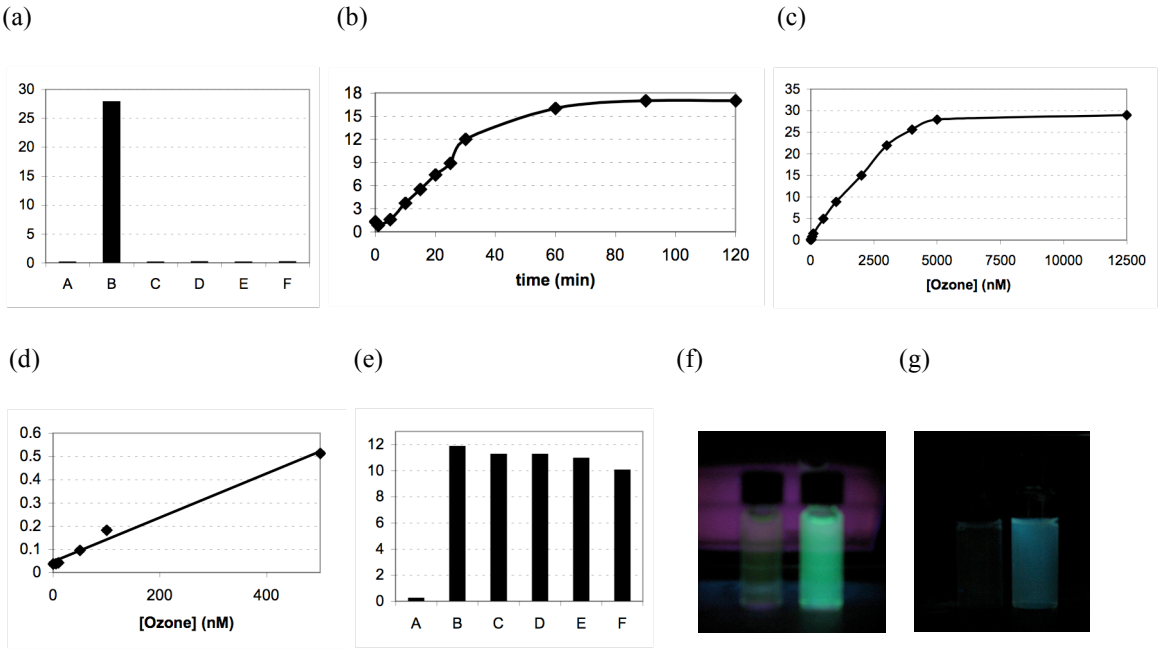

Figure 65. Ozone detection in aqueous and biological media

In (a)–(e), the y-axis is fluorescence intensity (a. u. × 10^5) at 523 nm. In all cases, [**67**] = 12.5 μM and ozone was generated by feeding high purity oxygen into a Welsbach T-series ozone generator. (a) ROS specificity. A = no ROS, B = ozone, C = singlet oxygen, D = superoxide, E = hydrogen peroxide, F = hydroxyl radical. Ozone samples

were incubated in 1:19 MeOH/pH 7 buffer at 37 °C for 1 h after ozone exposure at 24 °C. Singlet oxygen was generated from $NaMoO_4 \bullet 2H_2O$ (1.0 mM) and 30% H_2O_2 (25 mM) in pH 10 borate buffer and samples were incubated at 24 °C for 30 min. Superoxide was generated from KO_2 (250 μM) and samples were incubated in pH 7 phosphate buffer at 37 °C for 30 min. Samples containing only 30% H_2O_2 (25 mM) were incubated in pH 7 phosphate buffer at 37 °C for 30 min. Hydroxyl radical was generated from $FeSO_4 \bullet 7H_2O$ (250 μM) and 30% H_2O_2 (250 μM) and samples were incubated at 37 °C for 30 min. (b) Time-dependence of the conversion from **67** to **35**. (c) Correlation between fluorescence intensity and [ozone] in 1:19 MeOH/pH 7 buffer. (d) Correlation between fluorescence intensity and [ozone] in 1:19 MeOH/pH 7 buffer after ten-fold dilution of original samples. y = 0.000900x + 0.0467; R^2 = 0.987; average standard deviation = 0.00844. (e) Ozone detection in the presence of antioxidants. A = no ozone, B = ozone only, C = ozone with ascorbic acid (50 μM), D = ozone with glutathione (100 μM), E = ozone with uric acid (100 μM), F = ozone with all antioxidants. (f) Ozone detection in human pleural fluid. Left: **67**, no ozone; Right: **67**, + ozone. (g) Ozone detection in human serum. Left: **67**, no ozone; Right: **67**, + ozone.

6.2.3 Ozone Detection: Biological Applications

Because many questions exist in ozone's role in damaging human health, there is necessity for a biomedical probe to better understand the localization of this highly reactive species. Cellular effects of ozone exposure have been observed; however, it is speculated that ozone is much too reactive to reach and permeate the epithelial cells.[10,11] Thus, to examine the utility of this sensing method in such biological samples, ozone detection was attempted first in the presence of antioxidants that are found in the epithelial lining fluid. Ascorbic acid, glutathione, and uric acid are the most predominant antioxidants present,[9,10,12] and as Figure 65e shows, this sensor method is operational even in the presence of physiologically relevant antioxidants. This method was then tested with human pleural fluid to accurately mimic the epithelial lining fluid of the lung.[36]

Indeed, fluorescence signal was produced (S/B = 92; Figure 60f) indicating that sensor **67** should provide a tool to directly visualize this reactive gas in the study of ozone and the respiratory system.

As further demonstration of the robustness of sensor **67**, detection of ozone in human serum was examined. As Figure 65g shows, sensor **67** is capable of detecting ozone even in the presence of other potentially reactive species in serum (S/B = 92). It is interesting to note that although the maximum emission wavelength red-shifted to 531 nm, the observed color was blue. This observation proved to be general for this fluorophore scaffold as both DCF and **35** behaved in a similar manner in serum (not shown). One possible explanation may be due to the small Stokes shift that is found in fluorescein and its derivatives, which makes these fluorophores more prone to influences of scattering and interference.[37]

6.2.4 Ozone Detection: Atmospheric Application

In addition to ozone detection in biological samples, the application of sensor **67** for ozone detection in ambient air was also desired. Solutions of **67** in 5:95 MeOH/pH 7 buffer were prepared and exposed to ambient air in various locations throughout a city on a hot, sunny day (~32 °C) for 8 h. A negative control was prepared in the same manner but incubated at 37 °C in a closed vial for 8 h.

(a) (b)

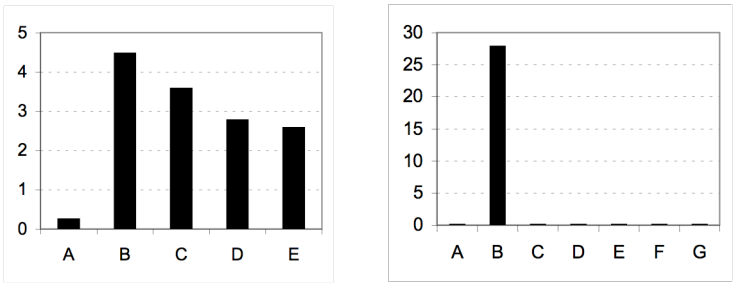

Figure 66. Ozone detection in ambient air

In both graphs, the y-axis is fluorescence intensity (a. u. × 10^5) at 523 nm. In all cases, [**67**] = 12.5 μM and all ozone assays were performed in 1:19 MeOH/pH 7 buffer. (a) Ozone detection in outdoor air for 8 h. A = negative control, B–E = outdoor air samples at various locations. (b) Ozone specificity against other air pollutants. A = no additive, B = ozone, C = HNO_3, D = H_2SO_4, E = Pb, F = Pd, G = Pt. [Acid] = 250 μM. [Metal] = 100 nM. The acid samples were incubated in pure water for 30 min at 37 °C. The metal samples were incubated in pH 7 buffer for 30 min at 37 °C.

Ozone detection was successful with S/B values of 10–17 (Figure 66a), which correlates to 13–22 ppb based on linear regression. To ensure that ozone was selectively detected, a number of other pollutants were screened. Nitrogen dioxide and sulfur dioxide will convert to their corresponding acids in aqueous solution so nitric acid and sulfuric acid were screened. Lead, palladium and platinum, which are known pollutants emitted from automobiles, were also screened.[38] As Figure 66b shows, none of these species produced a fluorescence signal. Aside from the specificity, it is important to note here that my sensing method is performed in aqueous media and will not be impacted by humidity. Thus, sensor **67** may be used as a sensitive probe for ozone in the atmosphere.

6.3 CONCLUSION

A specific and robust fluorescent sensor for ozone has been developed. This method is capable of fluorescently detecting ozone in biological samples, including nasal fluid and serum. In addition, detection of ozone in ambient air has also been demonstrated. The key benefits of this method are resistance to oxidants other than ozone, specificity against other known atmospheric pollutants, water compatibility and ease of measurement. This method should be a valuable tool in better understanding ozone's role in human health and the atmosphere. Additionally, due to the simplicity of the method, it may be possible for the general public to monitor their exposure to ozone at home, especially for those who suffer from respiratory diseases using an inexpensive hand-held fluorometer.

6.4 EXPERIMENTAL

6.4.1 General Information

Ozone was generated by feeding high purity oxygen into a Welsbach T-series ozone generator. RPMI-1640 medium (without L-glutamine and phenol red) is a product of HyClone® and was used as received. Human pleural fluid was purchased from Lee Biosolutions and used as received. Human serum (off-the-clot, type AB) was purchased from PAA Laboratories, Inc. and used as received. Buffers were purchased from J. T. Baker (pH 7, phosphate ($[PO_4^{3-}]$ = 46–50 mM, $[K^+]$ = 23–25 mM, $[Na^+]$ = 50–56 mM), J. T. Baker, Catalog Number 5608-01) and used after dilution with ARISTAR® ULTRA Water.

All reactions were carried out under a nitrogen atmosphere with dry, freshly distilled solvents under anhydrous conditions, unless otherwise noted. Tetrahydrofuran (THF) was distilled from sodium-benzophenone, and methylene chloride (CH_2Cl_2) was distilled from calcium hydride. Yields refer to chromatographically and spectroscopically (^{1}H NMR) homogenous materials, unless otherwise stated.

All reactions were monitored by thin-layer chromatography (TLC) carried out on 0.25-mm EMD silica gel plates (60F-254) using UV light (254 nm). TSI silica gel (230–400 mesh) was used for flash column chromatography.

NMR spectra were recorded on AM300 (Bruker) instruments and calibrated using a solvent peak as an internal reference. The following abbreviations are used to indicate the multiplicities: s, singlet; d, doublet; t, triplet; q, quartet; m, multiplet; br, broad. Mass spectra were obtained from a Micromass Autospec double focusing instrument.

6.4.2 Synthesis

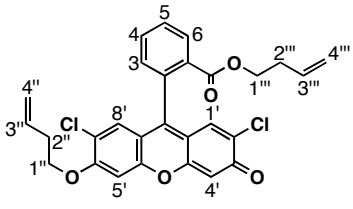

Compound 70. A 100-mL round bottom flask was charged with 2',7'-dichlorofluorescein (2.4 g, 5.89 mmol), DMF (20 mL), K_2CO_3 (2.5 g, 17.7 mmol) and 4-bromobutene (1.8 mL, 17.7 mmol) at 24 °C. The reaction mixture was stirred at 70 °C for 8 h and then poured into 750 mL water. The resulting precipitate was washed with water and dried *in vacuo* to yield **70** as a red-orange solid (2.4 g; 80%).

Data for **70**: mp = 184–185 °C; R_f = 0.34 (70% EtOAc in hexanes); IR (KBr pellet): 1725 (C=O), 1593, 1521, 1278, 997 cm^{-1}; ^{1}H NMR (300 MHz, $CDCl_3$, 293K): δ 8.32 (dd, J = 7.5, 1.2 Hz, 6-H), 7.82–7.68 (m, 2H, 4-H, 5-H), 7.26–7.30 (br d, J = 7.5 Hz, 1H, 3-H), 7.04 (s, 1H, Ar),

7.03 (s, 1H, Ar), 6.95 (m, 1H, Ar), 6.60 (s, 1H, Ar), 5.93 (ddt, J = 16.9, 10.3, 6.6 Hz, 1H, 3‴-H), 5.60 (ddt, J = 16.5, 9.9, 6.6 Hz, 1H, 3″-H), 5.24 (ddt, J = 17.1 , 3.3, 1.5 Hz, 1H, 4‴-H_{trans}), 5.18 (ddt, J = 10.2 , 3.3, 1.5 Hz, 1H, 4‴-H_{cis}), 5.02 (ddt, J = 17.1, 3.3, 1.5 Hz, 1H, 4″-H_{trans}), 4.97 (ddt, J = 10.2, 3.3, 1.5 Hz, 1H, 4″-H_{cis}), 4.20 (t, J = 6.7 Hz, 2H, 1‴-H), 4.13 (t, J = 6.7 Hz, 2H, 1″-H), 2.68 (q, J = 6.6 Hz, 2H, 2‴-H), 2.23 (q, J = 6.6 Hz, 2H, 2″-H); ^{13}C NMR (75 MHz, $CDCl_3$, 293K): δ 177.7, 169.4, 158.6, 157.8, 152.5, 149.8, 135.2, 133.5, 133.3, 133.2, 133.1, 131.6, 130.4, 130.3, 130.2, 128.0, 127.4, 120.5, 118.1, 117.6, 117.4, 114.9, 105.7, 100.7, 69.2, 64.5, 33.0, 32.6; HRMS (ESI) *m/z* calcd. for $C_{28}H_{23}Cl_2O_5$ $[M+H]^+$ 509.0923, found 509.0876.

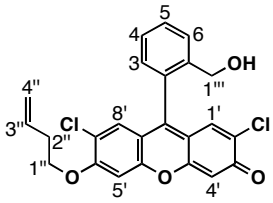

Compound 67. A solution of compound **70** (200 mg, 0.392 mmol) in CH_2Cl_2 (1.32 mL) was treated with DIBALH (1.4 mL, 1.0 M in hexanes, 1.4 mmol) dropwise over 15 min at -78 °C under a nitrogen atmosphere. The mixture was stirred for 5 min at the same temperature and then was warmed to 24 °C. After 2 h, the reaction mixture was quenched with saturated aqueous NH_4Cl (700 μL) and diluted with Et_2O (2.9 mL) at 0 °C. DDQ (2.50 g, 11.0 mmol) was then added to the mixture at 0 °C. After stirring 15 min, the mixture was filtered through Celite® and washed with Et_2O. The filtrate was dried over Na_2SO_4 and the solvents were evaporated under reduced pressure. Silica gel flash chromatography of the residue (5 → 10 % EtOAc in hexanes) afforded compound **67** as a light orange solid (134 mg, 80%).

Data for **67**: mp = 167–168 °C; R_f = 0.69 (50% EtOAc in hexanes); IR (KBr pellet): 3387 (br O-H), 3080, 2925, 2857, 1608, 1480, 1416, 1035 cm^{-1}; ^{1}H NMR (300 MHz, $CDCl_3$, 293K): δ 7.39–7.45 (m, 2H, Ar), 7.28–7.30 (m, 1H, Ar), 6.91 (s, 1H, Ar), 6.90 (s, 1H, Ar), 6.88 (s, 1H, Ar), 6.85 (s, 1H, Ar), 6.76 (s, 1H, Ar), 5.94 (ddt, J = 17.1, 10.5, 6.6 Hz, 1H, 3”-H), 5.26 (ddt, J =

17.1, 3.3, 1.5 Hz, 1H, 4′′-H_{trans}), 5.17 (ddt, *J* = 10.2, 3.3, 1.5 Hz, 1H, 4′′-H_{cis}), 5.34 (s, 2H, 1′′′-H), 4.11 (t, *J* = 6.7 Hz, 2H, 1”-H), 2.63 (ddd, *J* = 6.6, 6.6, 1.5 Hz, 2H, 2”-H); ^{13}C NMR (75 MHz, $CDCl_3$, 293K): δ154.9, 151.9, 150.1, 149.6, 143.9, 138.6, 133.8, 129.5, 128.7, 128.6, 128.3, 123.7, 121.0, 118.2, 118.1, 117.5, 117.1, 115.5, 103.6, 101.1, 83.1, 72.3, 68.6, 33.2; HRMS (ESI) *m/z* calcd. for $C_{24}H_{19}Cl_2O_4$ $[M+H]^+$ 441.0660, found 441.0683.

Compound 35. A solution of **67** (34.2 mg, 0.0775 mmol) was prepared in 95:5 acetone/water[39] (585 μL total, 0.15 mM). The solution was cooled to 0 °C and ozone was bubbled through the sample for 2 min. Following ozonolysis, a small amount of KI (<5 mg) was added and the solution was stirred at 24 °C for 1 min. TLC analysis (50% EtOAc in hexanes) indicated complete conversion to **35**.

6.4.3 Fluorescence Spectroscopy

Preparation of parent stock solutions used for this study.

Entry	Reagent	Quantity	Solvent (10 mL)	Conc. of stock solution
A	compound **67**	44.1 mg (0.10 mmol)	DMSO	10.0 mM
B	$NaMoO_4$•2 H_2O	206.0 mg (1.00 mmol)	pH 10 buffer	100 mM
C	KO_2	71.1 mg (1.00 mmol)	DMSO	100 mM
D	$FeSO_4$•7 H_2O	278.0 mg (1.00 mmol)	pH 7 buffer	100 mM
E	L-Ascorbic acid sodium salt	19.8 mg (0.1 mmol)	pH 7 buffer	10.0 mM
F	Glutathione, reduced	30.7 mg (0.1 mmol)	pH 7 buffer	10.0 mM
G	Uric acid	16.8 mg (0.1 mmol)	pH 7 buffer	10.0 mM
H	$Pb(NO_3)_2$	16.6 mg (50 μmol)	MeOH	5.0 mM
I	$PdCl_2$	9.0 mg (50 μmol)	3:1 Brine/MeOH	5.0 mM
J	$PtCl_2$	13.3 mg (50 μmol)	DMSO	5.0 mM

Notes:

(1) All the solutions were stored at 24 °C.

(2) Solution **A** was stored in the dark as precaution.

(3) All solutions for testing the ROS specificity were prepared and used immediately to prevent decomposition.

(4) All solutions for testing detection in the presence of antioxidants were prepared and used immediately to prevent decomposition.

Fluorescence spectroscopy. Fluorescence spectra were recorded in a 1 × 1-cm disposable cuvette (VWR; catalog number 58017-880) on a Jobin Yvon FluoroMax-3 spectrometer under the control of a Windows-based PC running FluorEssence software. The samples were excited at 497 nm and the emission intensities were collected at 523 nm. All spectra were corrected for emission intensity using the manufacturer supplied photomultiplier curves.

ROS specificity:

Ozone: Solution **A** (5.0 μL, $[\mathbf{67}]_{final}$ = 12.5 μM) was added to 1:19 MeOH/pH 7 buffer ($[PO_4^{3-}]$ = 5 mM) solution (4.0 mL), and the samples were exposed to ozone for 2 min at 24 °C (flow rate = 1 mL/min) followed by 1 h incubation at 37 °C before fluorescence measurement.

Singlet oxygen: Solution **A** (5.0 μL, $[\mathbf{67}]_{final}$ = 12.5 μM), solution **B** (40.0 μL, $[NaMoO_4 \bullet 2H_2O]_{final}$ = 1.0 mM)[40] and 30% H_2O_2 (10 μL, $[H_2O_2]_{final}$ = 25.0 mM) were added to 1:19 MeOH/pH 10 buffer solution (4.0 mL), and the samples were incubated for 30 min at 24 °C.

Superoxide: Solution **A** (5.0 μL, $[\mathbf{67}]_{final}$ = 12.5 μM) and solution **C** (10.0 μL, $[KO_2]_{final}$ = 250 μM) were added to 1:19 MeOH/pH 7 buffer solution (4.0 mL), and the samples were incubated for 30 min at 37 °C.

Hydrogen peroxide: Solution **A** (5.0 μL, $[\mathbf{67}]_{final}$ = 12.5 μM) and 30% H_2O_2 (10 μL, $[H_2O_2]_{final}$ = 25.0 mM) were added to 1:19 MeOH/pH 7 buffer solution (4.0 mL), and the samples were incubated for 30 min at 37 °C.

Hydroxyl radical: Solution **A** (5.0 μL, $[\mathbf{67}]_{final}$ = 12.5 μM), solution **D** (10.0 μL, $[FeSO_4 \bullet 7H_2O]_{final}$ = 250 μM) and 30% H_2O_2 ($[H_2O_2]_{final}$ = 250 μM) were added to 1:19 MeOH/pH 7 buffer solution (4.0 mL),[41] and the samples were incubated for 30 min at 37 °C.

Time dependence of the conversion from 67 to 35. Solution **A** ($[\mathbf{67}]_{final}$ = 12.5 μM) was added to 1:19 MeOH/pH 7 buffer ($[PO_4^{3-}]$ = 5 mM) solution, and the sample was exposed to ozone for 5 min at 24 °C (flow rate = 1 mL/min) followed by incubation at 37 °C. Aliquots of the reaction mixture were taken out at various time for fluorescence measurement.

Concentration dependence. Ozone solutions were prepared in pH 6 buffer and the concentrations were determined by UV absorption (λ_{max} = 258 nm; ε = 2900 l mol^{-1} cm^{-1}.[42,43] To 1:19 MeOH/pH 7 buffer ($[PO_4^{3-}]$ = 5 mM) solution (4.0 mL) was added solution **A** (5.0 μL, $[\mathbf{67}]_{final}$ = 12.5 μM), and the samples were exposed to varying amounts of ozone at 24 °C followed by 1 h incubation at 37 °C. The samples were diluted 10-fold before fluorescence measurement to maintain linearity with respect to fluorescence signal.

Ozone detection in the presence of antioxidants. Solution **A** (5.0 μL, $[\mathbf{67}]_{final}$ = 12.5 μM) and solutions **E–G** (**E**: 20.0 μL, $[\text{Ascorbic acid}]_{final}$ = 50.0 μM; **F, G**: 40.0 μL, $[\text{Glutathione/Uric acid}]_{final}$ = 100.0 μM) were added to 1:19 MeOH/pH 7 buffer ($[PO_4^{3-}]$ = 5 mM) solution (4.0

mL), and the samples were exposed to ozone for 2 min at 24 °C followed by 1 h incubation at 37 °C before fluorescence measurement.

Ozone detection in human pleural fluid. Human pleural fluid (1.0 mL) was diluted in pH 7 buffer ($[PO_4^{3-}]$ = 5 mM) (3.0 mL). Solution **A** (5.0 μL, $[\mathbf{67}]_{final}$ = 12.5 μM) was added to the pleural fluid solution, and the samples were exposed to ozone for 2 min at 24 °C followed by 1 h incubation at 37 °C before fluorescence measurement.

Ozone detection in human serum. Human serum (1.0 mL) was diluted in pH 7 buffer ($[PO_4^{3-}]$ = 5 mM) (3.0 mL). Solution **A** (5.0 μL, $[\mathbf{67}]_{final}$ = 12.5 μM) was added to the serum solution, and the samples were exposed to ozone for 2 min at 24 °C followed by 1 h incubation at 37 °C before fluorescence measurement.

Ozone detection in ambient air. Solution **A** (5.0 μL, $67\mathbf{4}]_{final}$ = 12.5 μM) was added to 1:19 MeOH/pH 7 buffer ($[PO_4^{3-}]$ = 5 mM) solution (4.0 mL), and the samples were placed in 4 outdoor areas throughout University of Pittsburgh campus for 8 h on June 6, 2008 (high temperature = 32.2 °C; AQI = 43; PM2.5 = 64) (data from http://www.airnow.gov. AQI = air quality index. PM2.5 = particulate matter less than 2.5 μm.). Care was taken to ensure the samples were not hit by direct sunlight.

Sample	Location (See the map: http://maps.google.com/?ie=UTF8&ll=40.444612,-79.955739&spn=0.00783,0.009527&t=h&z=17&layer=t)
A	Corner of Forbes Avenue* (3 lane road) and South Bouquet Street (2 lane road) next to a lane of traffic frequently traveled by cars and buses
B	Corner of Fifth Avenue* (4 lane road) and Bigelow Boulevard (4 lane road) next to a lane of traffic frequently traveled by cars and buses
C	In a tree ~200 m from Fifth Avenue (University Drive/Parkman Avenue)

D	Outside a 12th floor window of Chevron Science Center, which is ~200 m from Fifth Avenue (the corner between University Drive and Parkman Avenue)

* Forbes and Fifth Avenues are two of the most heavily traveled streets in Pittsburgh, Pennsylvania

A negative control was prepared in the same manner but incubated at 37 °C in a closed vial for 8 h. Following 8 h incubation, the fluorescence of each sample was measured.

Air pollutant specificity:

Acids: HNO_3 or H_2SO_4 (10 μL of 0.1 M solution; $[Acid]_{final}$ = 250 μM) and solution **A** (5.0 μL, $[\mathbf{67}]_{final}$ = 12.5 μM) were added to 1:19 MeOH/pure water solution (4.0 mL), and the samples were incubated at 37 °C for 30 min before fluorescence measurement.

Metals: Pb, Pd or Pt solution (40 μL of 10 μM solution; $[Metal]_{final}$ = 100 nM) and solution **A** (5.0 μL, $[\mathbf{67}]_{final}$ = 12.5 μM) were added to 1:19 MeOH/pH 7 buffer ($[PO_4^{3-}]$ = 5 mM) solution (4.0 mL), and the samples were incubated at 37 °C for 30 min before fluorescence measurement.

6.5 BIBLIOGRAPHY

1. Soh, N., "Recent advances in fluorescent probes for the detection of reactive oxygen species." *Anal. Bioanal. Chem.* **2006**, *386*, 532–543.

2. "Ozone: good up high, bad nearby." United States Environmental Protection Agency, Washington, DC, June 2003.

3. "Revisions to EPA's ozone air quality index fact sheet." United States Environmental Protection Agency, Washington, DC, March 2008.

4. Weschler, C. J., "Ozone's impact on public health: contributions from indoor exposures to ozone and products of ozone-initiated chemistry." *Environ. Health Perspect.* **2006**, *114*, 1489–1496.

5. Weschler, C. J., "Ozone in indoor environments: concentration and chemistry." *Indoor Air* **2000**, *10*, 269–288.

6. Bocci, V., "Is it true that ozone is always toxic? The end of a dogma." *Tox. Appl. Pharm.* **2006**, *216*, 493–504.

7. Cataldo, F., "Ozone degradation of biological macromolecules: proteins, hemoglobin, RNA, and DNA." *Ozone Sci. Eng.* **2006**, *28*, 317–328.

8. Cvitas, T., Klasinc, L., Kezele, N., Klasine, L., McGlynn, S. P., Pryor, W. A., "New directions: how dangerous is ozone?" *Atm. Environ.* **2005**, *39*, 4607–4608.

9. Mudway, I. S., Kelly, F. J., "Ozone and the lung: a sensitive issue." *Molec. Asp. Med.* **2000**, *21*, 1–48.

10. Pryor, W. A., "Mechanisms of radical formation from reactions of ozone with target molecules in the lung." *Free Radical Biol. Med.* **1994**, *17*, 451–465.

11. Pryor, W. A., "How far does ozone penetrate into the pulmonary air/tissue boundary before it reacts?" *Free Radial Biol. Med.* **1992**, *12*, 83–88.

12. Kermani, S., Ben-Jebria, A., Ultman, J. S., "Kinetics of ozone reaction with uric acid, ascorbic acid, and glutathione at physiologically relevant conditions." *Arch. Biochem. Biophys.* **2006**, *451*, 8–16.

13. Rice, R. G., "Century 21 – pregnant with ozone." *Ozone Sci. Eng.* **2002**, *24*, 1–15.

14. Smith, L. L., "Oxygen, oxysterols, ouabain, and ozone: a cautionary tale." *Free Radical Biol. Med.* **2004**, *37*, 318–324.

15. Wentworth, Jr., P., McDunn, J. E., Wentworth, A. D., Takeuchi, C., Nieva, J., Jones, T., Bautista, C., Ruedi, J. M., Gutierrez, Janda, K. D., Babior, B. M., Eschenmoser, A., Lerner, R. A., "Evidence for antibody-catalyzed ozone formation in bacterial killing and inflammation." *Science* **2002**, *298*, 2195–2199.

16. Babior, B. M., Takeuchi, C., Ruedi, J., Gutierrez, A., Wentworth, Jr., P., "Investigating antibody-catalyzed ozone generation by human neutrophils." *Proc. Natl. Acad. Sci.* **2003**, *100*, 3031–3034.

17. Wentworth, Jr., P., Nieva, J., Takeuchi, C., Galve, R., Wentworth, A. D., Dilley, R. B., DeLaria, G. A., Saven, A., Babior, B. M., Janda, K. D., Eschenmoser, A., Lerner, R. A., "Evidence for ozone formation in human atherosclerotic arteries." *Science* **2003**, *302*, 1053–1056.

18. Takeuchi, K., Ibusuki, T., "Quantitative determination of aqueous-phase ozone by chemiluminescence using indigo-5,5'-disulfonate." *Anal. Chem.* **1989**, *61*, 619–623.

19. Kettle, A. J., Clark, B. M., Winterbourn, C. C., "Superoxide converts indigo carmine to isatin sulfonic acid." *J. Biol. Chem.* **2004**, *279*, 18521–18525.

20. Kettle, A. J., Winterbourn, C. C., "Do neutrophils produce ozone? An appraisal of current evidence." *BioFactors* **2005**, *24*, 41–45.

21. Sies, H., "Ozone in arteriosclerotic plaques: searching for the 'smoking gun'." *Angew. Chem. Int. Ed.* **2004**, *43*, 3514–3515.

22. Horváth, M., Bilitzky, L., Hüttner, J. *"Ozone."* Elsevier, New York, 1985.

23. Jiménez, A. M., Navas, M. J., Galán, G., "Air analysis: determination of ozone by chemiluminescence." *Appl. Spectros. Rev.* **1997**, *32*, 141–149.

24. Williams, E. J., Fehsenfeld, F. C., Jobson, B. T., Kuster, W. C., Goldan, P. D., Stutz, J., McClenny, W. A., "Comparison of ultraviolet, absorbance, chemiluminescence, and DOAS instruments for ambient ozone monitoring." *Environ. Sci. Technol.* **2006**, *40*, 5755–5762.

25. Parrish, D. D., Fehsenfeld, F. C., "Methods for gas-phase measurements of ozone, ozone precursors and aerosol precursors." *Atmos. Environ.* **2000**, *34*, 1921–1957.

26. Kuczkowski, R. L. in "1,3-Dipolar cycloaddition chemistry." Vol. 2., ed. Padwa, A., John Wiley & Sons, New York, 1984.

27. Uchiyama, S., Otsubo, Y., "Simultaneous determination of ozone as carbonyls using *trans*-1,2-bis(4-pyridyl)ethylene as an ozone scrubber for 2,4-dinitrophenylhydrazine-impregnated silica cartridge." *Anal. Chem.* **2008**, *80*, 3285–3290.

28. "NARSTO measurement methods compendium: ozone." http://narsto.ornl.gov/Compendium/methods/o3.shtml.

29. "Ozone in workplace atmospheres." OSHA Salt Lake Technical Center, Salt Lake City, Utah, 1995.

30. Rotman, B., "Measurement of activity of single molecules of β-D-galactosidase." *Proc. Natl. Acad. Sci. U. S. A.* **1961**, *47*, 1981–1991.

31. Clennan, E. L., Pace, A., "Advances in singlet oxygen chemistry." *Tetrahedron* **2005**, *61*, 6665–6691.

32. Sawyer, D. T., Valentine, J. S., "How super is superoxide?" *Acc. Chem. Res.* **1981**, *14*, 393–400.

33. Sawyer, D. T., Gibian, M. J., "The chemistry of superoxide ion." *Tetrahedron* **1979**, *35*, 1471–1481.

34. Greenwood, F. L., Durham, L. J., "Ozonolysis. XI. Kinetic studies on the conversion of the molozonide to ozonolysis products." *J. Org. Chem.* **1969**, *34*, 3363–3366.

35. Bailey, P. S., "Ozonation in organic chemistry Volume I Olefinic Compounds." Academic Press, New York, 1978.

36. Mudway, I. S., Blomberg, A., Frew, A. J., Holgate, S. T., Sandström, Kelly, F. J., "Antioxidant consumption and repletion kinetics in nasal lavage fluid following exposure of healthy human volunteers to ozone." *Eur. Respir. J.* **1999**, *13*, 1429–1438.

37. Soini, E., Hemmilä, I., "Fluoroimmunoassay: present status and key problems." *Clin. Chem.* **1979**, *25*, 353–361.

38. Ely, J. C., Neal, C. R., Kulpa, C. F., Schneegurt, M. A., Seidler, J. A., Jain, J. C., "Implications of platinum-group element accumulation along U. S. road from catalytic-converter attrition." *Environ. Sci. Technol.* **2001**, *35*, 3816–3822.

39. Schiaffo, C. E., Dussault, P. H., "Ozonolysis in solvent/water mixtures: direct conversion of alkenes to aldehydes and ketones." *J. Org. Chem.* **2008**, *73*, 4688–4690.

40. Aubry, J. M., Cazin, B., Duprat, F., "Chemical sources of singlet oxygen. 3. Peroxidation of water-soluble singlet oxygen carriers with the hydrogen peroxide-molybdate system." *J. Org. Chem.* **1989**, *54*, 726–728.

41. Yan, E. B., Unthank, J. K., Castillo-Melendez, M., Miller, S. L., Langford, S. J., Walker, D. W., "Novel method for in vivo hydroxyl radical measurement by microdialysis in fetal sheep brain in utero." *J. Appl. Physiol.* **2005**, *98*, 2304–2310.

42. Ershov, B. G., Panich, N. M., Seliverstov, A. F., Belyaeva, M. P., "Ozone decomposition in concentrated aqueous solutions of salts." *Russ. J. Appl. Chem.* **2008**, *81*, 723–725.

43. Panich, N. M., Ershov, B. G., Seliverstov, A. F., Basiev, A. G., "Ozone solubility in concentrated aqueous solutions of salts." *Russ. J. Appl. Chem.* **2007**, *80*, 1812–1815.

7.0 INTRODUCTION: SMALL MOLECULE LIBRARY SYNTHESIS

Small molecules are powerful tools for the study of biological systems.[1] For instance, such compounds provide rapid and conditional modulation of biological function, can alter an individual function of a multifunctional target and can help to identify new therapeutic targets. As such, processes that generate diverse arrays of small molecules are fundamental to the further understanding of biological pathways.

7.1 DIVERSITY ORIENTED SYNTHESIS

Diversity-oriented synthesis (DOS) has emerged as an important approach in generating vast arrays of compounds for biological screening.[1–5] The key tenet of DOS is the development of divergent synthetic pathways that efficiently lead to collections or libraries of functionally, stereochemically and skeletally diverse small molecules. The methodology is dependent on tandem and complexity generating reactions and driven by advances in solid-phase organic synthesis. Thus, DOS aims to create vast arrays of small molecules in an attempt to occupy all realms of chemical space. By examining some examples of DOS, the power this method of library synthesis has in generating diverse small molecules is quite obvious.

7.1.1 Functional Diversity

The simplest method of generating diversity is based on the principles of combinatorial chemistry, that is, functional group transformations at various reactive sites, such as OH, NH, and SH.[1–5] A major goal in natural product-based library synthesis is to discover molecules that exhibit biological activity beyond that of the natural product in consideration, not to simply improve upon the activity of the parent scaffold. Thus, transformations at these types of reactive sites may provide new avenues to biologically active small molecules compared to the traditional alkyl-substitutions of combinatorial chemistry.

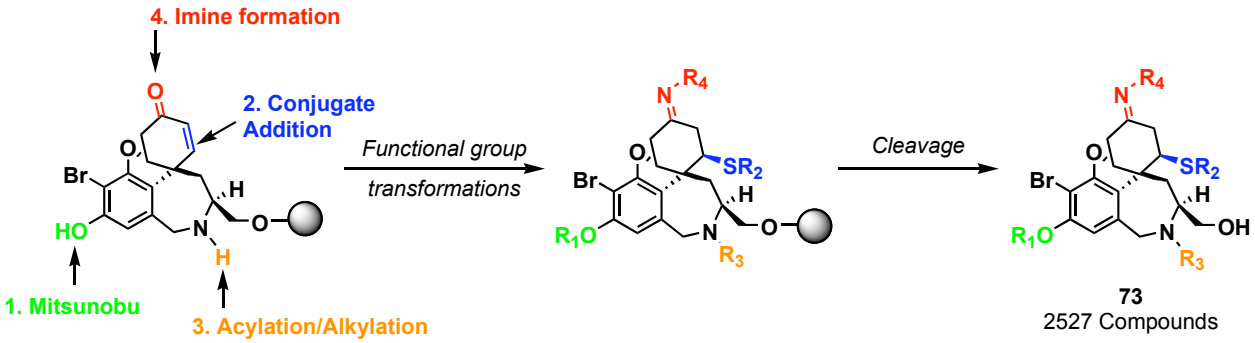

Figure 67. Example of functional diversity

An example of library synthesis demonstrating a functional diversity generating strategy is from the Shair group in the synthesis of galanthamine-like molecules **73** (Figure 67).[6] The synthesis followed a biomimetic approach toward the key skeleton of the galanthamine-like core with four opportunities for functional diversity: (1) Mitsunobu chemistry at the phenol position with various alcohols, (2) conjugate addition into the α,β-unsaturated ketone with sulfur nucleophiles, (3) acylation or alkylation at the secondary amine and (4) formation of imines with hydrazines and hydroxylamines at the newly formed ketone. After the respective functional

group transformations and cleavage with HF•pyridine, 2527 galanthamine-like small molecules were successfully synthesized. One compound was identified as a potent inhibitor of the secratory pathway at 2 μM.

7.1.2 Stereochemical Diversity

In addition to the diversity generated at the appendages of a library of small molecules, the molecular shape of a scaffold is also a variable in DOS. It is known that the complementarity of a small molecule and its target is necessary for biological activity, although not exclusively.[7] Thus, the stereochemical diversity and the spatial arrangement of such appendages must also be a significant factor in a library's bioactivity.

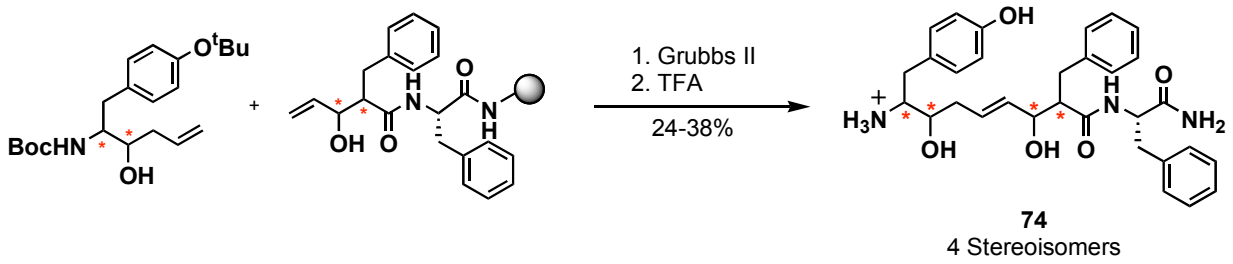

Figure 68. Example of functional diversity

An example of DOS illustrating stereochemical diversity is the synthesis of non-peptidic analogues of endomorphin-2 **74**, a potent agonist of mu-opiod receptor, by the Verdine group.[8,9] The analogues were derived from two stereochemically rich terminal olefins coupled via olefin cross-metathesis (Figure 68). The synthesis generated four stereochemically diverse isomers. Remarkably, each isomer was found to exhibit vastly different binding affinities with the (*S, S, S, R*) isomer having activity closest to that of endomorphin-2.

7.1.3 Skeletal Diversity

Although particularly effective, generating libraries of small molecules containing distinct molecular skeletons remains a difficult task. Two such strategies have been adopted to accomplish this feat. The first relies on pluripotent substrates, which may be treated with an array of reagents to create skeletal diversity.[10] In contrast to the reagent-based approach, a second strategy relies on treating a collection of substrates containing different appendages, or σ-elements, with common reagents to produce distinct molecular skeletons.[11]

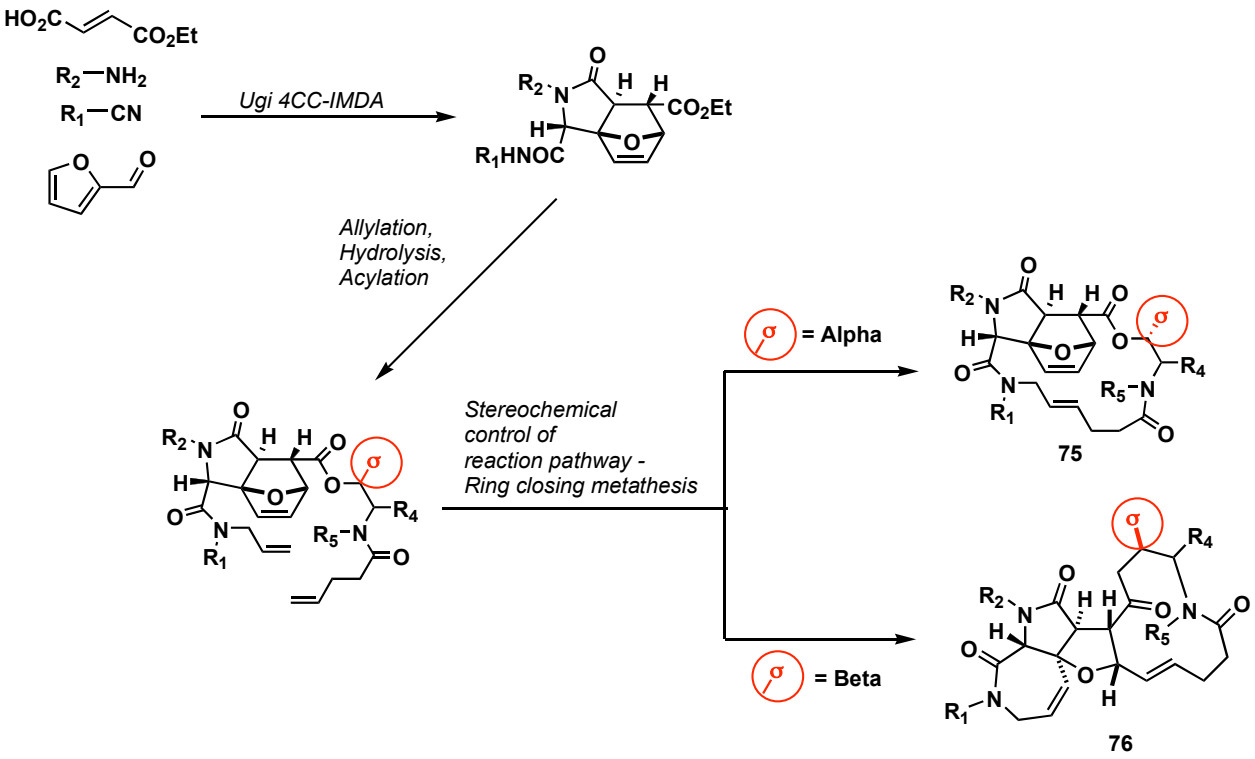

Figure 69. Example of skeletal diversity

An example of a library based upon this σ-element approach to skeletal diversity was completed by the Schreiber group where they examined the idea of appendage stereochemistry to pre-encode skeletal diversity.[11] The pathways began with a tandem, diversity-generating Ugi

four-component reaction followed by an intramolecular Diels-Alder reaction to form various tricyclic compounds (Figure 69). Following allylation, hydrolysis, and acylation, the key σ-element containing intermediates were generated and capable of undergoing the final ring-closing metathesis step. The Schreiber group discovered an interesting phenomenon: if the σ-element was on the α-face, the product contained a bridged molecular skeleton (**75**) following ring-closing metathesis; however, if the σ-element was on the β-face, then the fused product **76** was isolated. Unfortunately, no known biological testing was reported.

7.2 CHEMICAL SPACE

Chemical space, defined as the total number of possible small organic molecules within a molecular weight of less than 500, is often estimated at $\sim 10^{30\text{-}200}$ structures.[1,12,13] One question that remains with respect to drug discovery concerns the known regions of chemical space, more specifically, are the known regions of chemical space the best for discovering biologically-active small molecules. Unfortunately, there is no answer to this question; however, DOS aims at answering this crucial question by synthesizing libraries of small molecules that occupy all regions of chemical space.[1–5]

Besides traditional combinatorial library design, DOS typically relies on two major library design strategies: the design of drug-like or natural product-like libraries.[1,13] These structures are known to more effectively occupy chemical space than their combinatorial counterparts.[14]

Drug-like libraries are traditionally based on nitrogen-containing heteroaromatic scaffolds of appropriate size to effectively occupy the active site binding pocket of its

target.[1,14,15] A good example of such a library is Ellman's benzodiazepine-based library, which is one of the earliest DOS contributions (Figure 70a).[16] Additional examples of these "privileged" structures are shown in Figure 70a.[1] It is important to note that these compounds often have few to no stereogenic centers, which greatly eases their synthesis.

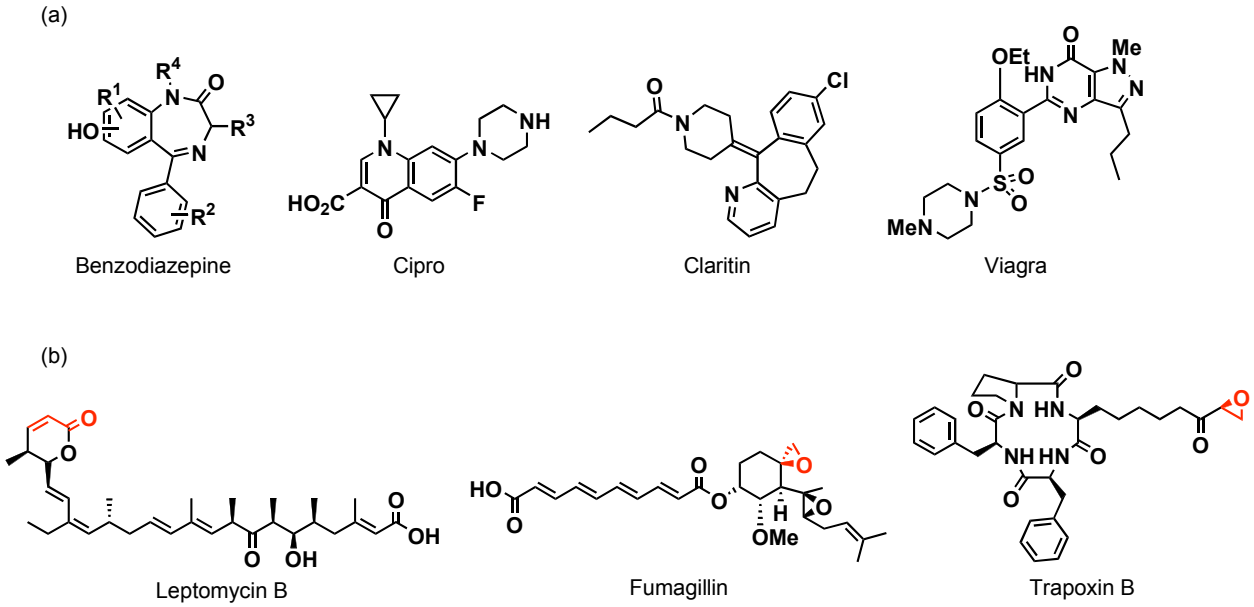

Figure 70. Examples of drugs and natural products

On the other hand, natural product-like libraries can be based on the core scaffold of a natural product, structural motifs found in a class of natural products or generally emulate the structural characteristics of natural products.[1] These molecular types typically have large molecular weight, greater structural complexity, electrophilic sites and a significant number of stereogenic centers.[14,15] Because of this complexity, natural products are known to exhibit high binding specificity for their receptors and highly selective modes of action. As such, libraries based on these scaffolds are highly profitable. Some examples of natural products containing key electrophilic moieties (in red) in addition to molecular recognition sites are shown in Figure 70b.

7.3 CONCLUSION

Diversity-oriented synthesis is a useful approach for generating vast arrays of potentially bioactive small molecules. A survey of the literature reveals three main methods for generating diversity: functional group transformation, diversity at stereochemical centers and the synthesis of diverse molecular skeletons. Through these diversity-generating elements, libraries emulating natural products and drug-like structure are readily attainable. Thus, the development of new methods that can further this approach may be highly profitable toward the goal of examining chemical space through synthesis.

7.4 BIBLIOGRAPHY

1. "Chemical biology: from small molecules to systems biology and drug design." Vol. 2, ed, Schreiber, S. L., Kapoor, T., Wess, G., WILEY-VCH Verlag GmbH & Co. KGaA, Weinhem, 2007.

2. Burke, M. D., Schreiber, S. L., "A planning strategy for diversity-oriented synthesis." *Angew. Chem. Int. Ed.* **2004**, *43*, 46–58.

3. Burke, M. D., Berger, E. M., Schreiber, S. L., "Generating diverse skeletons of small molecules combinatorially." *Science* **2003**, *302*, 613–618.

4. Schreiber, S. L., "The small-molecule approach to biology." *Chem. Eng. News* **2003**, *81*, 51–61.

5. Schreiber, S. L., "Target-oriented and diversity-oriented organic synthesis in drug discovery." *Science* **2000**, *287*, 1964–1969.

6. Pelish, H. E., Westwood, N. J., Feng, Y., Kirchhausen, T., Shair, M. D., "Use of biomimetic diversity-oriented synthesis to discover galanthamine-like molecules with biological properties beyond those of the natural product." *J. Am. Chem. Soc.* **2001**, *123*, 6740–6741.

7. Sauer, W. H. B., Schwarz, M. K., "Molecular shape diversity of combinatorial libraries: a prerequisite for broad bioactivity." *J. Chem. Inf. Comput. Sci.* **2003**, *43*, 987–1003.

8. Harrison, B. A., Gierasch, T. M., Neilan, C., Pasternak, G. W., Verdine, G. L., "High-affinity mu opioid receptor ligands discovered by the screening of an exhaustively stereodiversified library of 1,5-enediols." *J. Am. Chem. Soc.* **2002**, *124*, 13352–13353.

9. Shi, Z., Harrison, B. A., Verdine, G. L., "Unpredictable stereochemical preferences for mu opioid receptor activity in an exhaustively stereodiversified library of 1,4-enediols." *Org. Lett.* **2003**, *5*, 633–636.

10. Taylor, S. J., Taylor, A. M., Schreiber, S. L., "Synthetic strategy toward skeletal diversity via solid-supported, otherwise unstable reactive intermediates." *Angew. Chem. Int. Ed.* **2004**, *43*, 1681–1685.

11. Sello, J. K., Andreana, P. R., Lee, D., Schreiber, S. L., "Stereochemical control of skeletal diversity." *Org. Lett.* **2003**, *5*, 4125–4127.

12. Dobson, C. M., "Chemical space and biology." *Nature* **2004**, *432*, 824–828.

13. Tan, D. S., "Diversity-oriented synthesis: exploring the intersections between chemistry and biology." *Nat. Chem. Biol.* **2005**, *1*, 74–84.

14. Feher, M., Schmidt, J. M., "Property distributions: differences between drugs, natural products, and molecules from combinatorial chemistry." *J. Chem. Inf. Comput. Sci.* **2003**, *43*, 218–227.

15. Clardy, J., Walsh, C., "Lessons from natural products." *Nature* **2004**, *432*, 829–837.

16. Ellman, J. A., "Design, synthesis, and evaluation of small-molecule libraries." *Acc. Chem. Res.* **1996**, *29*, 132–143.

8.0 EFFORTS TOWARD CONVERGENT SOLID-PHASE ORGANIC SYNTHESIS

Solid-phase organic synthesis is an enabling technology and its automation has had profound impact. For example, automated solid-phase oligonucleotide[1] and peptide[2] syntheses have advanced many scientific areas. However, to date, the structural diversity of the molecules derived from this technology is limited[3] because current solid-phase methods are linear. Convergent synthetic approaches are far more versatile and amenable to highly complex molecules due to the ability to functionalize each fragment separately. While solution-phase target- and diversity-oriented syntheses[4] have been greatly aided by such convergency,[5] solid-phase organic synthesis has been limited by its inherent linearity.[6,7] Thus, new technologies for convergency are needed to advance solid-phase organic synthesis for complex molecules.

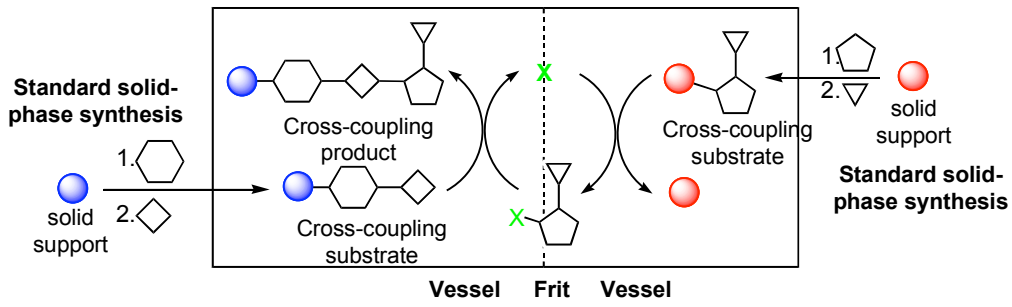

Figure 71. Model for convergent solid-phase organic synthesis

As such, I set out to develop an enabling resin-to-resin transfer technology that unites two spatially separated, functionalized fragments to form highly complex small molecules in a

convergent manner (Figure 71). Such technology should allow for the synthesis of small molecules possessing natural product- and drug-like functionalities that are not readily accessible by conventional linear approaches.

8.1 RESEARCH DESIGN

8.1.1 Convergent Solid-Phase Organic Synthesis

Examples of "convergent" solid-phase organic synthesis in the literature are limited. However, one aspect that all examples have in common is that one of the fragments is coupled with a second fragment on solid support only after synthesis using solution-phase or solid-phase synthesis after cleavage. This cleave-and-couple method is depicted in Figure 72.

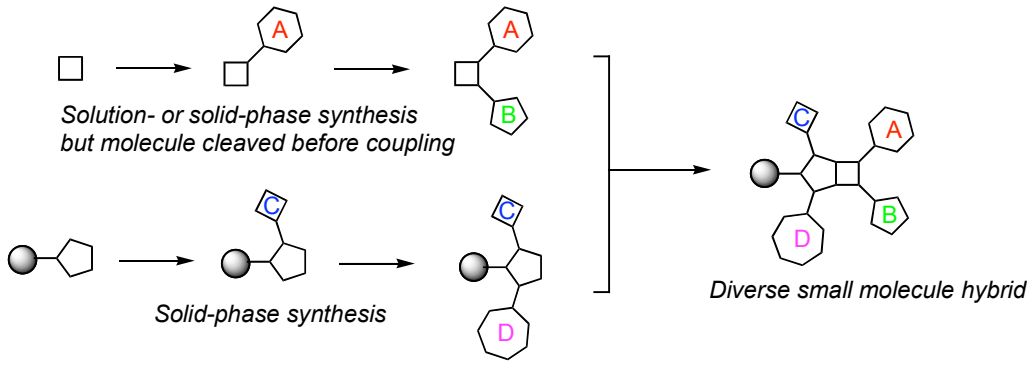

Figure 72. Convergent, cleave-and-couple solid-phase organic synthesis

The first example of convergent solid-phase organic synthesis was demonstrated by Nielsen, who termed the method "double combinatorial chemistry".[8,9] The concept of Nielsen's work was to couple two peptide libraries to a biaryl linker in the synthesis of actinomycin

analogs **77** (Figure 73). Nielsen synthesized a total of 9 library compounds isolated as mixtures, and no biological testing was reported.

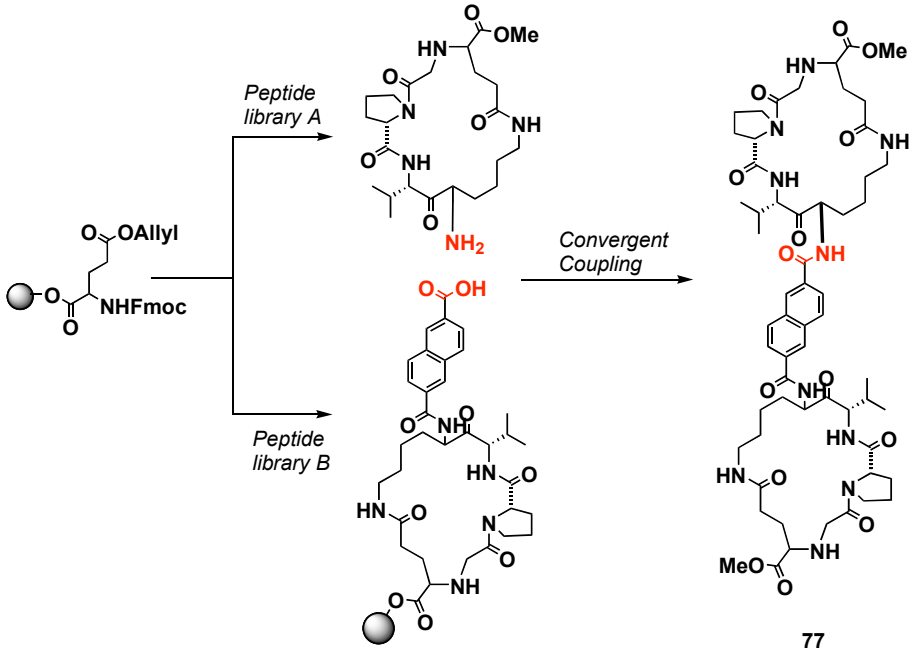

Figure 73. Nielson library

A second example of a convergent solid-phase library strategy was not reported until 2004 by Raveglia in the synthesis of a 48-member benzimidazolone library **78** (Figure 74).[10] The Raveglia group synthesized 3 carboxylic acids on solid support, which were subsequently cleaved, purified, and coupled with 16 amines. Again, no biological testing was reported.

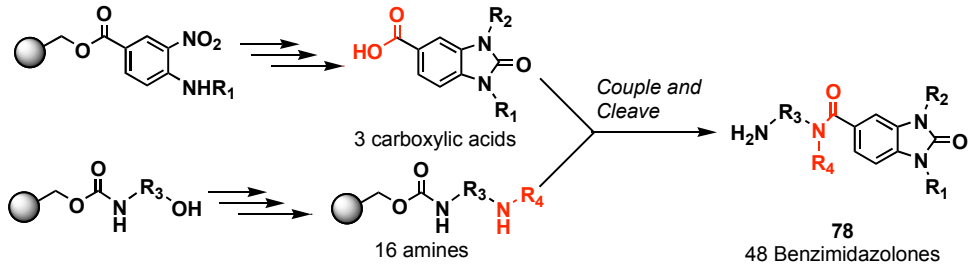

Figure 74. Raveglia library

A final example was demonstrated by Schreiber in the synthesis of small molecule hybrids.[11] The library synthesis makes use of both types of convergent solid-phase synthesis: the coupling of sublibraries I and II demonstrates the reaction of a solid-supported component with a solution-phase component while the coupling of sublibraries II and III demonstrates the cleave-and-couple strategy with both components in solution. The Schreiber group coupled the 3 highly functionalized sublibraries through esterification to generate libraries of 480 (**79**) and 384 (**80**) compounds, respectively, shown in Figure 75. Similar to the previous library syntheses, no biological testing has yet been reported.

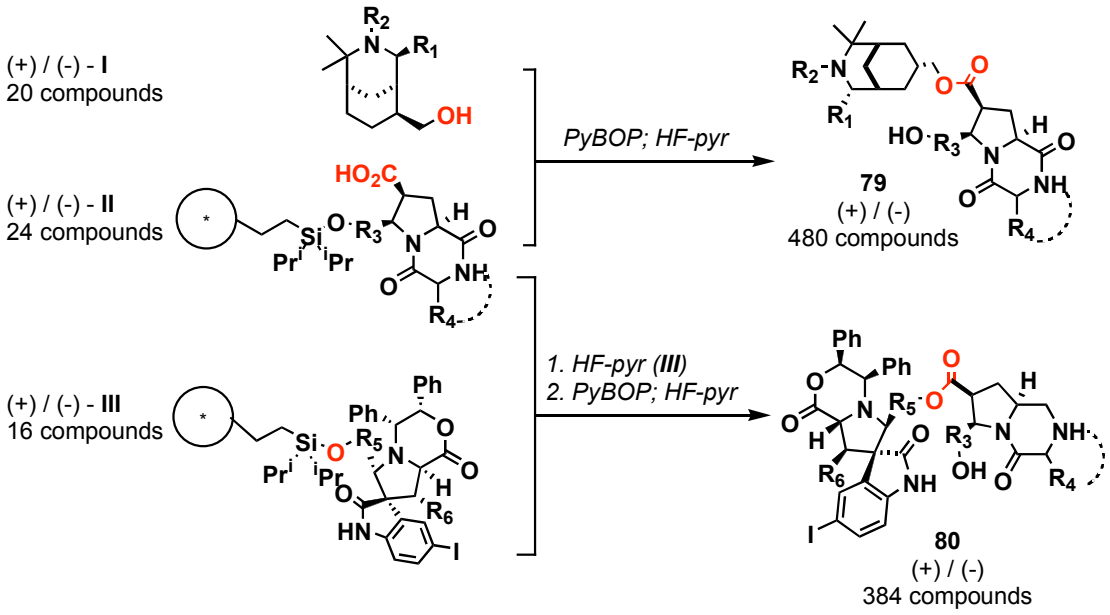

Figure 75. Schreiber library

Although each of these examples validates convergent synthesis partially on the solid support, each coupling requires three steps: (1) initial cleavage from the resin, (2) purification of the intermediate and (3) coupling with an additional fragment. A better and more efficient method of convergent solid-phase library synthesis would be the coupling of both components

on the solid support, thereby eliminating the need for pre-coupling cleavage and purification. This may seem feasible, however, there are some critics. In a recent paper, such an approach was described as, "…conventional convergent synthetic strategy…can only be conveniently conducted using solution-phase, not solid-phase, techniques and avoids the more repetitive independent linear synthesis of each analogue." While this may be the accepted notion, this type of resin-to-resin transfer chemistry has been documented in the literature.

8.1.2 Resin-to-Resin Transfer Chemistry

Resin-to-resin transfer chemistry dates back to the 1970's with Rebek's studies on the "three-phase test" or triphasic reactions.[12–15] The set-up consists of a precursor and trap molecule each on solid support in the same reaction vessel. A cleaving reagent in solution then reacts with the precursor to form an intermediate in solution, which subsequently reacts with the trap to form the adduct or product remaining on the resin (see the following examples in Figures 76 and 77 for more mechanistic detail). Despite the fact that this method could have potential in synthesis, the chemistry was only used to study reaction mechanisms at this time.

Using Rebek's initial studies, two research groups have explored the idea of employing resin-to-resin transfer for synthetic purposes. The first example is acyl- and aminoacyl-transfer reactions using oxime supports from the DeGrado group, which is similar to the reactions examined by Rebek.[16] The mechanistic scheme for acyl-transfer is shown in Figure 76. The mechanism follows a similar pathway to that described by Rebek with the acylated oxime resin serving as the precursor, N-hydroxysuccinimide as the shuttling agent between the precursor and trap, and the amine containing resin serving as a trap.

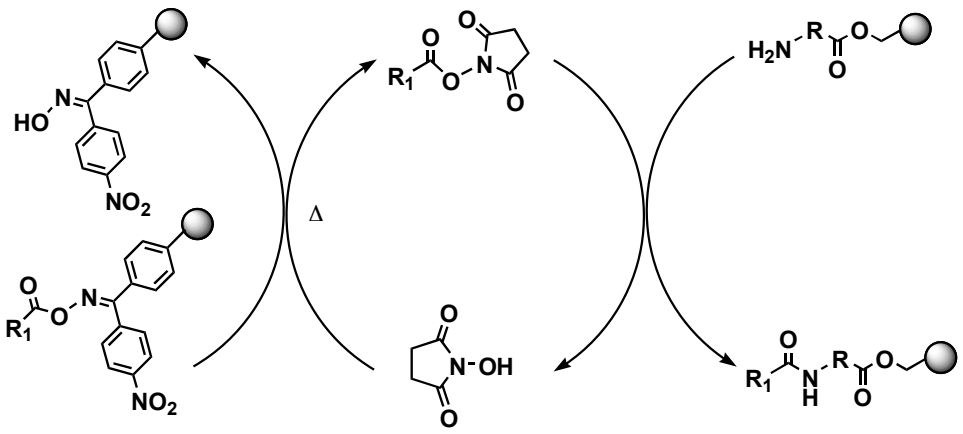

Figure 76. Resin-to-resin acyl transfer reaction

The second example illustrates the first resin-to-resin carbon-carbon bond forming reaction by the Hall group, namely resin-to-resin transfer Suzuki coupling.[17,18] The pathway of the Hall method is shown in Figure 77. The first step involves the release of the boronic acid from the resin in the presence of water. This intermediate is then able to react with the solid-supported aryl iodide in the presence of palladium to complete the Suzuki reaction in 100% yield for the reaction shown. This method has also been more recently applied to Sonogashira chemistry.[19]

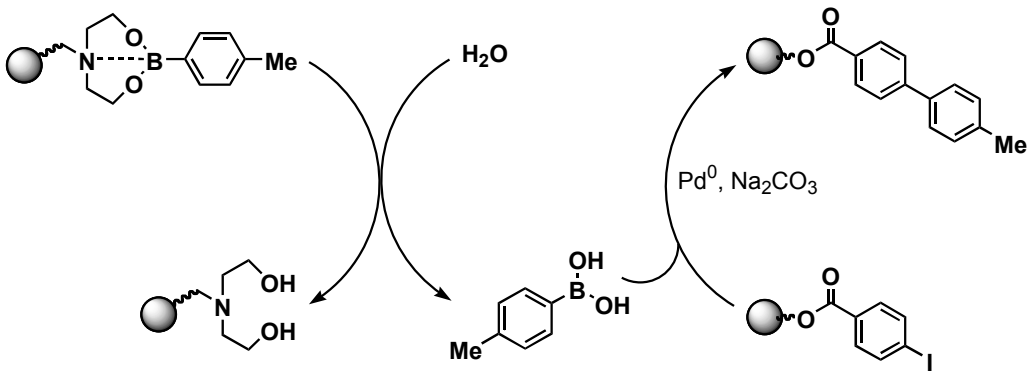

Figure 77. Resin-to-resin Suzuki cross-coupling reaction

By examining each of these resin-to-resin transfer reactions, several benefits are clearly identified. First of all, these reactions allow for convergent fragment coupling with both components on the resin. Secondly, they share a common benefit with typical solid-phase organic synthesis, namely simple purification of intermediates by washing with organic solvents. Finally, resin-to-resin transfer reactions provide vast opportunity for library synthesis whereby many diverse fragments can be coupled to form many small molecules.

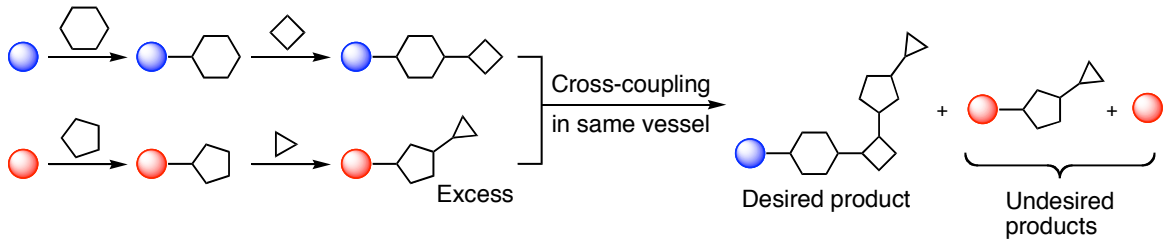

Figure 78. Resin-to-resin transfer approach

Along with these inherent benefits, there are also limitations to the previously described resin-to-resin reactions. Similar to solid-phase organic synthesis, all reactions must be driven to completion to ensure all starting materials are consumed, which is especially important in convergent library synthesis with no intermediate purification steps. Additionally, any by-products formed during the reaction would also be isolated along with the product(s) and remaining starting materials (Figure 78). Each of these limitations can be attributed to one flaw in the reaction set-up – both precursor and trap beads are contained in the same vessel with no separation. Thus, allowing separation of each of these components would provide ease in separating any remaining precursor beads that may not have reacted and any by-products that may have formed on the precursor side of the vessel, thereby greatly simplifying the final purification of library compounds.[20]

8.1.3 Olefin Cross-Metathesis

Carbon-carbon double bond formations are important in organic synthesis. Among these reactions is olefin metathesis, which is a very powerful method for the construction of complex alkenes.[21] Olefin metathesis has been used in the syntheses of a variety of molecules in solution phase.[22] In solid-phase synthesis, although ring-closing olefin metathesis has been widely used,[23–26] olefin cross-metathesis has been rarely used despite its potential for the convergent synthesis of complex alkenes.[27–30] A few notable examples are shown below.

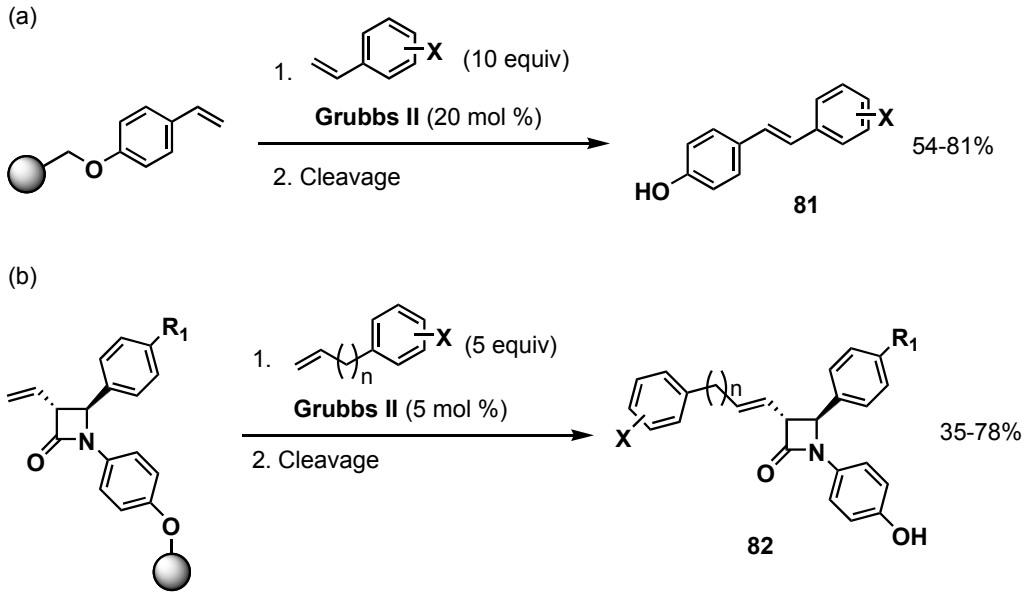

Figure 79. Examples of solid-phase olefin cross-metathesis

A simple example comes from the Chang group, who reported the synthesis of hydroxy (*E*)-stilbenoids **81** using a solid-supported hydroxystyrene (Figure 79a).[29] In a more recent example, Testero and Mata showed that β-lactam analogues **82** could be prepared on solid

support using olefin cross-metathesis between simple alkenes in solution and solid-supported vinyl lactams (Figure 79b).[28]

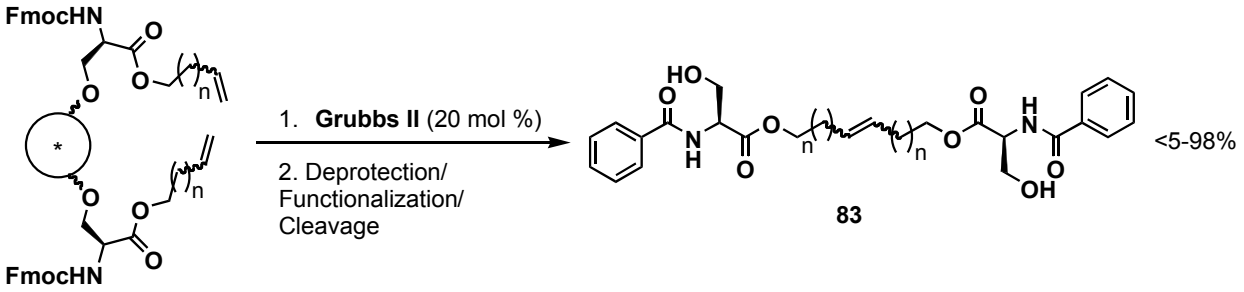

Figure 80. Example of intrabead homodimerization using olefin cross-metathesis

In addition to the synthesis of heterodimers on solid support using olefin cross-metathesis, the synthesis of intrabead homodimers has also been reported.[31–34] The Schreiber group first reported this approach for the synthesis of simple peptidomimetics **83** (Figure 80).[34] This approach has since been used in more complex molecule synthesis and in the synthesis of solid-supported ligands.

In terms of mechanism, olefin cross-metathesis is the combination of two olefins via a ruthenium alkylidene catalyst (**84, 85a-b**)[35–39] (Figure 81a).[21] Ideally, each $\mathbf{R_1}$-containing olefin and each $\mathbf{R_2}$-containing olefin react selectively to give the appropriate $\mathbf{R_1}$-$\mathbf{R_2}$ dimer; however, experimentally, not only is the appropriate dimer isolated but also a mixture of the $\mathbf{R_1}$ and $\mathbf{R_2}$ homodimers and a mixture of regioisomers (Figure 81b). These particular problems are the primary cause of the limited usage of this synthetic method in both solution- and solid-phase synthesis. A generic mechanism for this transformation is shown in Figure 81c. For a more detailed discussion, please see the following section.

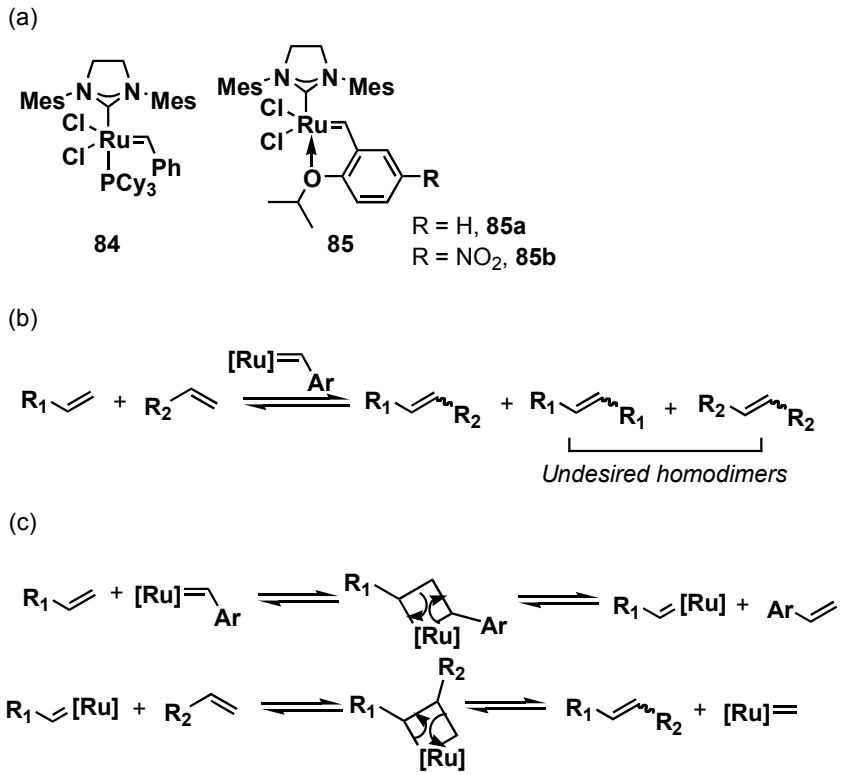

Figure 81. Olefin cross-metathesis catalysts and mechanism

In 2003, Grubbs published a general model for selectivity in olefin cross-metathesis.[40] In this work, several types of olefins were ranked based on their ability to homodimerize. Type I olefins are the most reactive leading to rapid homodimerization; however, the homodimers can additionally participate in a second metathesis reaction. Type II olefins are more electron deficient or sterically bulky, and as a result, undergo slow homodimerization and the homodimers are sparingly consumed. Finally, type III olefins are the least reactive due to extreme steric bulk or electron-deficiency. Examples of each of these types of olefins are shown in Figure 82.

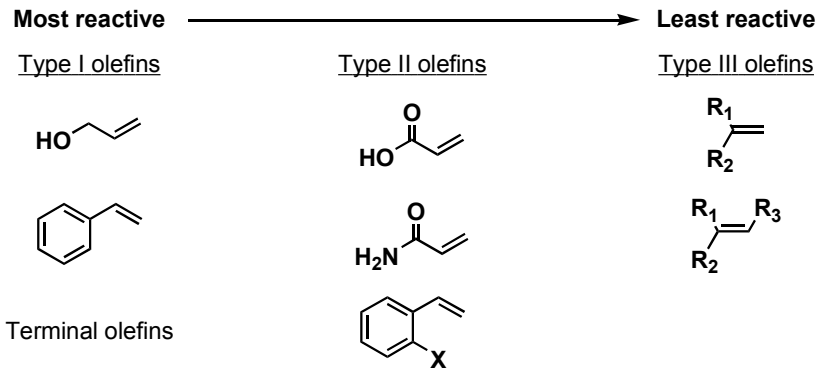

Figure 82. Types of olefins based on reactivity in olefin cross-metathesis reactions

Grubbs found that if two olefins of the same type were coupled, the result is a statistical mixture of hetero- and homodimers (Figure 83a); however, if two olefins of different types were coupled, selective heterodimerization could be obtained (Figure 83b). As a result of Grubbs' study, many selective cross-olefin metathesis reactions have been accomplished and the reaction has seen increased use in synthesis.

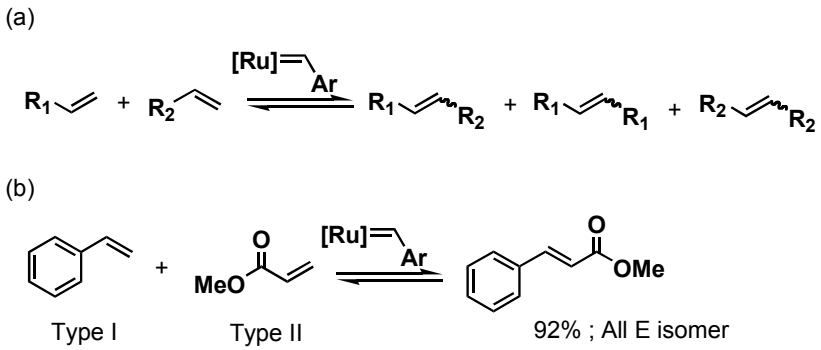

Figure 83. Selective olefin cross-metathesis

8.2 RESULTS AND DISCUSSION

8.2.1 Resin-to-Resin Olefin Cross-Metathesis – First Generation

Thus, the model cross-coupling reaction chosen for this study was olefin cross-metathesis. In addition to its convergency, olefin cross-metathesis is also a mild transformation and well-tolerant of many functional groups.[21,22] Also, olefins themselves are stable for long-term storage and compatible with many synthetic transformations such as carbonyl addition reactions, epoxidation, etc.

In initial experiments, resin-to-resin olefin cross-metathesis was attempted by mixing the two resin-bound substrates **A** and **B** (see Figure 78) as previously described for the three-phase test type reactions. This procedure, however, gave intractable mixtures because desired products were contaminated with starting materials and their derivatives as expected. Furthermore, a large excess of undesired resin after the coupling prohibits the continuation of synthesis (see Figure 84). Alternatively, employing the use of two different linkers further complicates multiple step synthesis on solid support because a method must be developed to easily cleave one resin in the presence of another. After considerable efforts, it was hypothesized that the two solid-supported substrates **A** and **B** did not need to be in the same vessel and could be spatially separated to ease in isolation of the desired cross-coupling product.

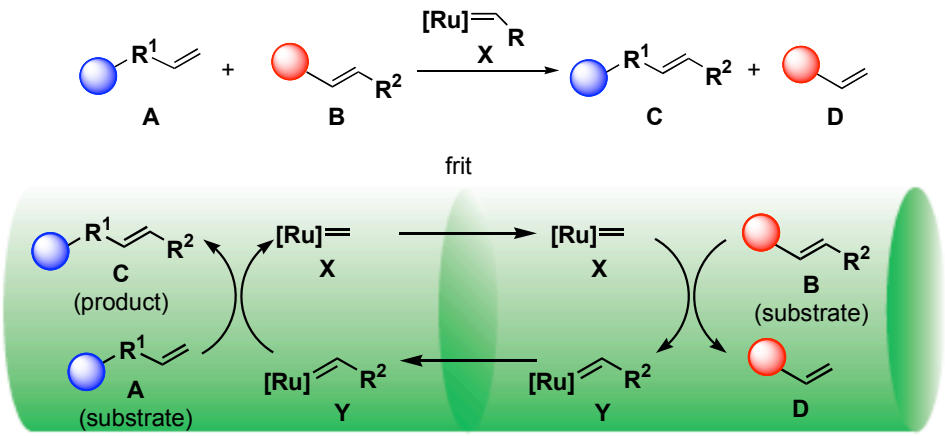

Figure 84. Resin-to-resin olefin cross-metathesis between spatially separated substrates

The strategy for resin-to-resin olefin cross-metathesis is illustrated in Figure 84. First, the polystyrene-bound terminal alkene **A** (acceptor) and the polystyrene-bound internal alkene **B** (donor) are placed in each side of the reaction vessel separated by a frit. This frit keeps the two types of alkene resins separated during reactions, but allows small molecules in solution to traverse between the two vessels. Ruthenium catalyst **X** can react with both alkenes reversibly; however, only when the catalyst reacts with the internal alkene **B**, will the resulting intermediate **Y** form. This ruthenium complex would then react with the terminal alkene **A** to form the coupling product **C**, catalyst **X**, and by-product **D**. Catalyst **X** will then shuttle between the two vessels to transfer the R^2-unit from **A** to **B**, producing predominantly the desired heterodimer **C**. It is envisioned that this process can be automated by placing a frit in the middle of each well of a commercially available 96-well reaction block. Some additional benefits of the above system include: (1) by-products on the donor resin and in solution can easily be removed because the two coupling partners are not mixed; and (2) donor and acceptor compounds are synthesized independently allowing many functional group transformations to be employed with little concern about chemoselectivity.

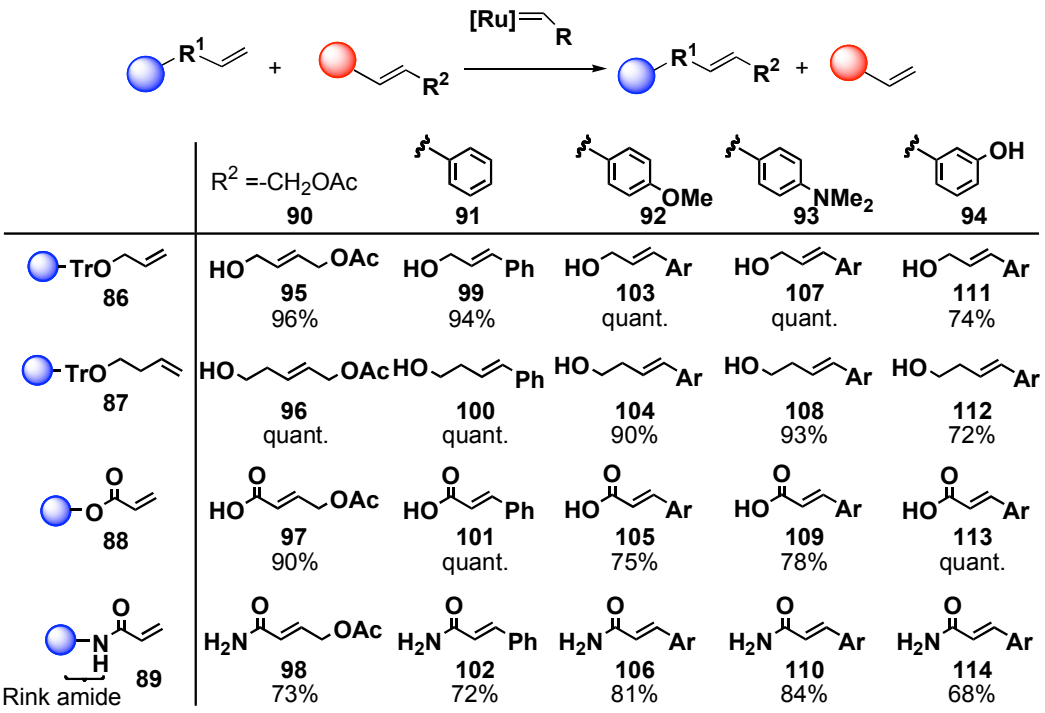

Figure 85. Proof of principle experiments for resin-to-resin olefin cross-metathesis

10 equiv **B** used in each reaction. **A** = **86,87**; catalyst **84**. **A** = **88**; catalyst **85b**. **A** = **89**; catalyst **85a**.

To test the above hypothesis, resin-to-resin olefin cross-metathesis was first investigated with several model substrates of varying electronics (Figure 85). Although 10 equivalents of each internal alkene were used for the initial model study, 3 equivalents were found to be sufficient as demonstrated later. The choice of a ruthenium catalyst was based on the electron-density of each alkene acceptor **86**–**89**; the relatively electron-rich **86** and **87** required mildly active catalyst **84**.[35] The most electron-deficient substrate **88** required the most active catalyst **85b**,[38,39] although catalyst **85a** was also effective in some cases. For the slightly less electron-deficient substrate **89**, catalyst **85a** was used.[36,37]

First, the aliphatic alkene **90** was coupled with each of **86**–**89** in the presence of the respective ruthenium catalyst. At temperatures below 60 °C, little cross-coupling products were observed, indicating that the kinetic ruthenium alkylidene products on each acceptor resin do not

undergo the desired retro [2+2] reaction at these temperatures. After 7 h at 60 °C in 1,2-dichloroethane, all of these cross-couplings were effective and trans selective, affording the expected products **95**–**98** in 73% to quantitative yield upon cleavage of the products from the trityl resin with 2% TFA/5% Et_3SiH in CH_2Cl_2 at 24 °C. Encouraged by this result, each of the four cinnamyl alcohol derivatives **91**–**94** was cross-coupled with each of **86**–**89**. As Figure 85 shows, all of the reactions proceeded smoothly to afford the corresponding coupling products in 68% to quantitative yields in a highly trans-selective manner.[40] Although the trityl ethers of **90**–**94** are not essential, the readily cleavable linker provided a handle for analysis upon cleavage to characterize compounds synthesized on the polymer.

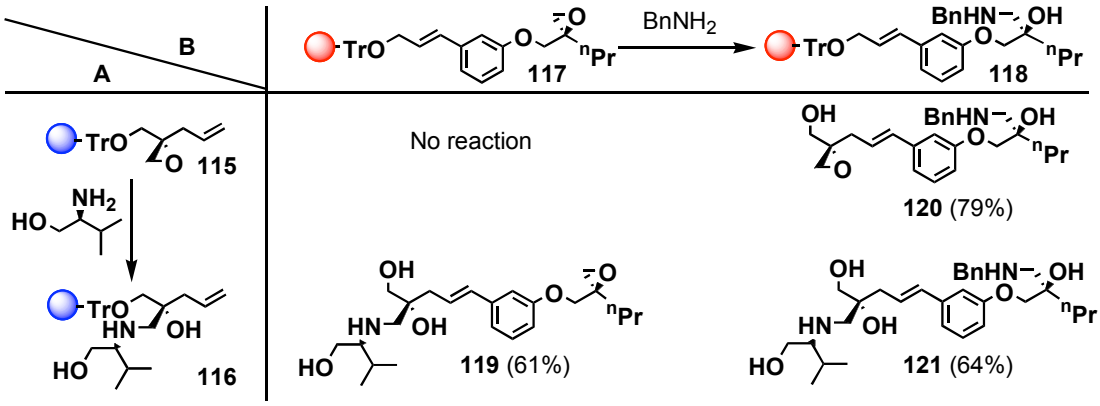

Figure 86. Epoxide openings and couplings between spatially separated resins

With these successes, resin-to-resin transfer technology was then applied in complex molecule synthesis (Figure 86). Epoxides and 1,2-aminoalcohols were used in this study for several reasons: (1) these functional groups are ubiquitous in biologically active compounds, (2) enantiomerically pure epoxides are readily available and (3) epoxide-openings with amines yield 1,2-aminoalcohols with multiple hydrogen-bonding sites. Although the cross-coupling between **115** and **117** did not proceed in these preliminary experiments, products containing more

hydrogen-bonding sites with a possible electrophilic functionality (**119–121**; Figure 86) were more interesting. These highly functionalized compounds with potential electrophiles and hydrogen-bonding sites are not readily accessible by a classical linear approach in the solid phase since one cannot easily distinguish multiple electrophiles, unprotected amines and hydroxy groups. Moreover, compound **121** and its derivatives may mimic positively charged peptides such as lethal factor of *Bacillus anthracis*.[41]

8.2.2 Solid-Phase Olefin Cross-Metathesis Promoted by a Linker[42]

Despite the success with my initial studies, a lack of reproducibility was observed, which is not uncommon in solid-phase organic synthesis. As such the cross coupling of **115** with solution-phase olefin substrates was examined.

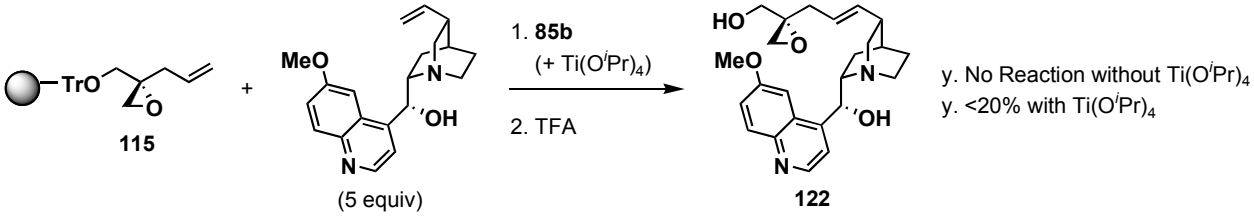

Figure 87. Solid-phase olefin cross-metathesis with epoxide

As a complex olefin in solution, quinine was chosen because it presents high functionality, is commercially available and has been used as an anti-malarial drug.[43] Unexpectedly, treatment of **115** with quinine (5.0 equiv) and **85b** (5 mol %) at 40 °C did not yield the desired alkene **122** as determined by crude ^{1}H NMR analysis (Figure 87). It was speculated that the ruthenium alkylidene complex of **115** might be catalytically inactive due to chelation with the epoxide oxygen atom. Based on this speculation, the above reaction of **115** and quinine was employed in

the presence of $Ti(O^iPr)_4$ (20 mol %),[44] which proceeded but to less than 20%, which was still unsatisfactory. No intrabead homodimerization was observed in either of these experiments.

In light of these poor results and the lack of systematic studies in the literature, cross-metathesis reactions using model systems on solid support were studied in order to further the use of this method in solid-phase organic synthesis. It was noted that the olefin in **115** was much closer to the polymer than those substrates reported in the literature.[28] Although change in linker length has been shown to be non-essential in other solid-phase reactions,[45–47] the proximity of the olefin to the solid support could impact cross-metathesis because the steric bulk of the polymer may block the catalyst's access to the olefin and the steric bulk of the catalyst may prevent it from entering further into the polymer to react with shorter carbon chains. Conversely, too long of a carbon chain would facilitate the formation of undesired homodimers on the same bead as previously shown by others.[31–34]

To study the distance-dependent solid-phase olefin cross-metathesis, compounds **123a–123d** (Table 2) were prepared. For these model studies, alkene **126** was chosen as a symmetrical alkene in solution.[48,49] Metathesis reactions were performed between alkenes **123a–123d** and alkene **126** (5.0 equiv) using pre-catalyst **85b** (5 mol %) in DCE at 24 °C for 22 h. Following cleavage with TFA, alcohols **127a–127d** were isolated (entries 1–4). All reaction yields were quantified based on an external standard method. Indeed, reaction yields were strongly influenced by the carbon chain length; ether **123a** (n = 1) afforded alcohol **127a** in 12% yield (entry 1) while ether **123d** (n = 4) gave alcohol **127d** in quantitative yield. The low yield of **123a** is not due to the steric hindrance imposed by the trityl group because a control cross-coupling between allyl trityl ether and **126** (5 equiv) catalyzed by **85b** (5 mol %) afforded the corresponding metathesis product in 61% yield.[46,50] Also, no intra-bead homodimerization was

observed for each carbon chain length. I found that catalyst **85b** consistently gave higher yields than catalyst **84** (entries 1–4), which is reminiscent of a previous report by the Schreiber group.[51] Thus, it was concluded that **85b** was superior to **84** in solid-phase olefin cross-metathesis.

Table 2. Proximity effect on solid-supported olefin cross-metathesis

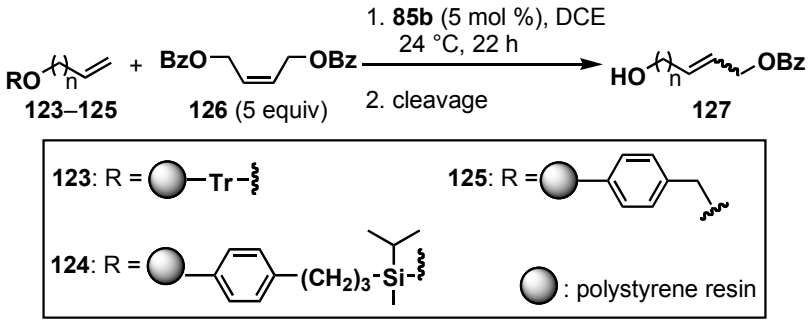

Entry	Substrate	*n*	% yield
1	**123a**	1	12 (<10[a])
2	**123b**	2	62 (48[a])
3	**123c**	3	70[b] (52[a])
4	**123d**	4	>95[c] (60[a])
5	**124a**	1	37
6	**124b**	2	52
7	**124c**	3	80[b]
8	**124d**	4	83[c]
9	**125a**	1	37
10	**125b**	2	42
11	**125c**	3	50[b]
12	**125d**	4	70[c]

[a] Yield using **84** instead of **85b**. [b] Yield, 6:1 *E:Z*. [c] Yield, 5:1 *E:Z*.

To determine the generality of this proximity effect, each alkenyl alcohol was also loaded onto alkylsilyl resin[52] and Merrifield resin to generate compounds **124a–124d** and **125a–125d**, respectively. Metathesis reactions were performed in a similar manner as described above, and products **127a–127d** were isolated after cleavage. These experiments revealed a similar proximity effect; silyl ethers **124a–124d** produced the corresponding alcohols **127a–127d** in 37% (entry 5), 52% (entry 6), 80% (entry 7), and 83% yield (entry 8), respectively. Benzyl ethers

125a–125d produced alcohols **127a–127d** in 37% (entry 9), 42% (entry 10), 50% (entry 11), and 70% (entry 12), respectively. Again, intra-bead homodimerization did not occur. These solid-phase experiments showed that increasing the distance between the reacting olefin and the resin improved the efficiency of olefin cross-metathesis.

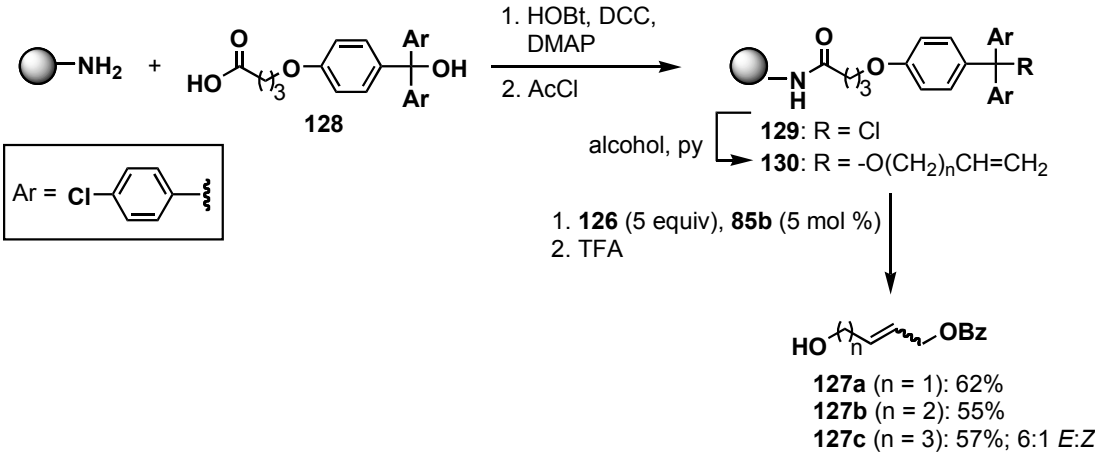

Figure 88. Cross-metathesis with a linker

While these studies provided insight, the addition of unnecessary carbons in the substrate and product is not desirable in organic synthesis. Therefore, on the basis of the proximity effect and the necessity for a traceless linker, attention was turned to the commercially available trityl alcohol **128** (Figure 88). Although **128** contains a chlorotrityl moiety instead of trityl, the chlorine atoms should have no effect on the olefin's reactivity. This alcohol was loaded onto aminomethyl polystyrene resin via a standard amide forming method, and the resulting compound was converted to trityl chloride **129** by the action of acetyl chloride. This trityl chloride was reacted with alkenyl alcohols to form trityl ethers **130a**–**130c** (n = 1–3). To my delight, metathesis of **130a** with **126** (5.0 equiv) using **85b** followed by cleavage (5% TFA in CH_2Cl_2) provided the desired product **127a** in 62% yield. Similar yields were observed with

130b and **130c** with the linker (55 and 57% yield). These data indicate that with an additional linker between the trityl moiety and polymer, more consistent yields can be obtained (cf. Table 2, entries 1–3).

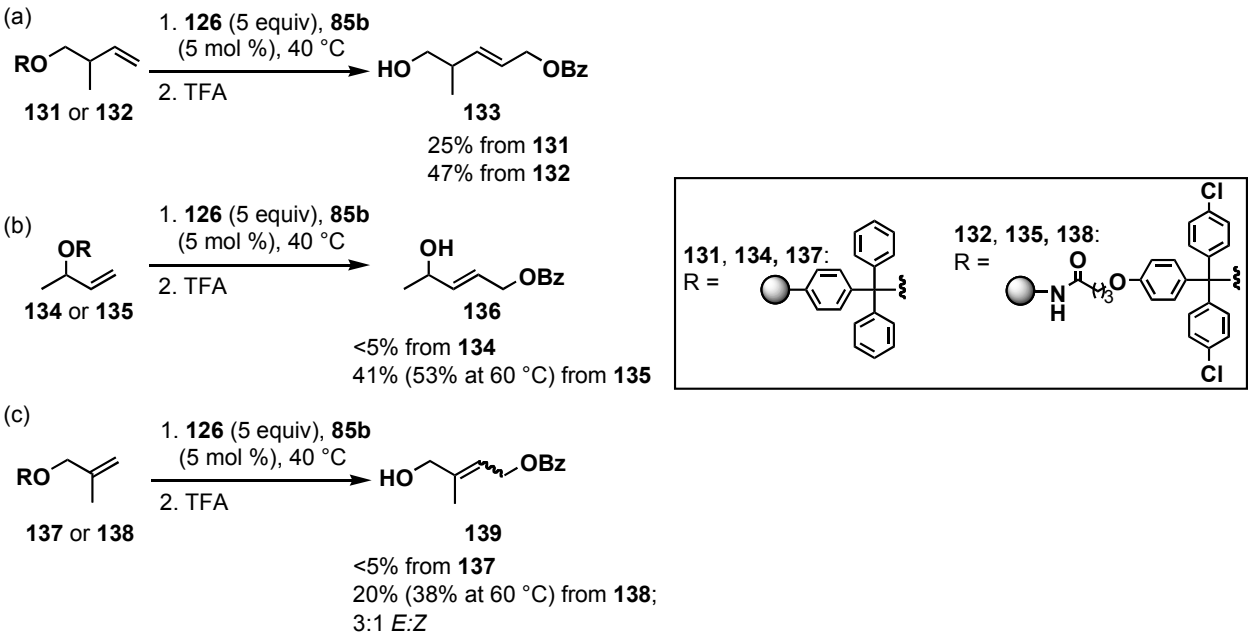

Figure 89. Cross-metathesis with substituted alcohols

More substituted alcohols on solid support were next investigated. With trityl ethers **131**, **134** and **137** without the linker and trityl ethers **132**, **135** and **138** with the linker (Figure 89), metathesis reactions were carried out using **126** (5 equiv) and **85b** (5 mol %). In general, raising the temperature from 24 to 40 °C increased isolated yields by approximately two-fold, thus the yields at 40 °C are shown here. With the substituted homoallylic ethers **131** and **132**, the reaction was again more efficient with the linker (25% vs 47% yield). With the substituted allylic ether **134** without the linker, the reaction essentially did not proceed. In contrast, the allylic ether **135** with the linker underwent olefin metathesis with **126** to form **136** in 41% yield. This coupling could be improved to 53% yield when the reaction mixture was heated to 60 °C. In the case of

type III[40] olefins, **137** and **138**, the reaction was also more efficient with the linker (<5% vs 20% yield). Similar to **135** the coupling was further improved to 38% yield when the reaction mixture was heated to 60 °C. With these more substituted allylic and homoallylic alcohols, the linker effect is prominent.

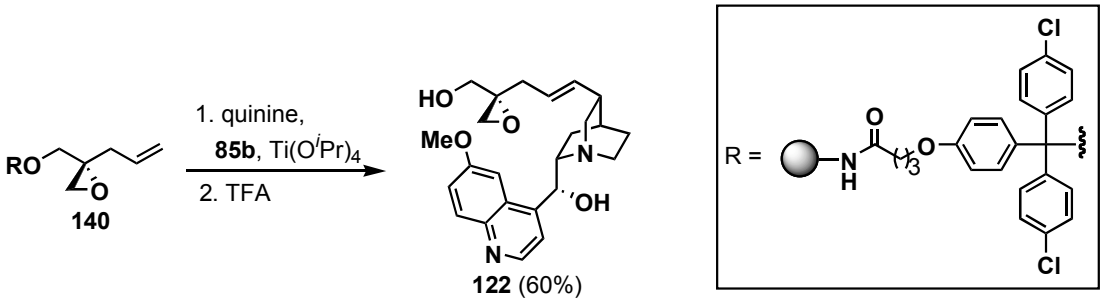

Figure 90. Cross-metathesis with solid-supported epoxide

Having established the olefin cross-metathesis technology on solid support, the initial problem depicted in Figure 87 was revisited. The epoxyalcohol was loaded onto linker resin **129** to generate trityl ether **140**. Metathesis of **140** with quinine (5 equiv) was performed using **85b** and $Ti(O^iPr)_4$ at 40 °C for 24 h. ^1H NMR analysis of the crude material cleaved from the resin revealed that the quinine derivative **122** was formed in 60% yield (Figure 90). In the absence of $Ti(O^iPr)_4$, the reaction again did not proceed validating our initial claim of catalyst inactivation by the epoxide. These results clearly demonstrate the merit of linker **128** in performing metathesis reactions on solid support. Moreover, the quinine example illustrates that the solid-phase olefin cross-metathesis could be applied to the synthesis of morphed drugs/natural products with new properties.

8.2.3 Resin-to-Resin Olefin Cross-Metathesis – Second Generation

The linker technology was next applied to the challenging resin-to-resin olefin cross-metathesis problem. As a model study, the synthesis of the simple and more substituted alkenes synthesized in the linker model studies were examined since authentic samples were in hand. The results for these experiments are shown in Figure 91.

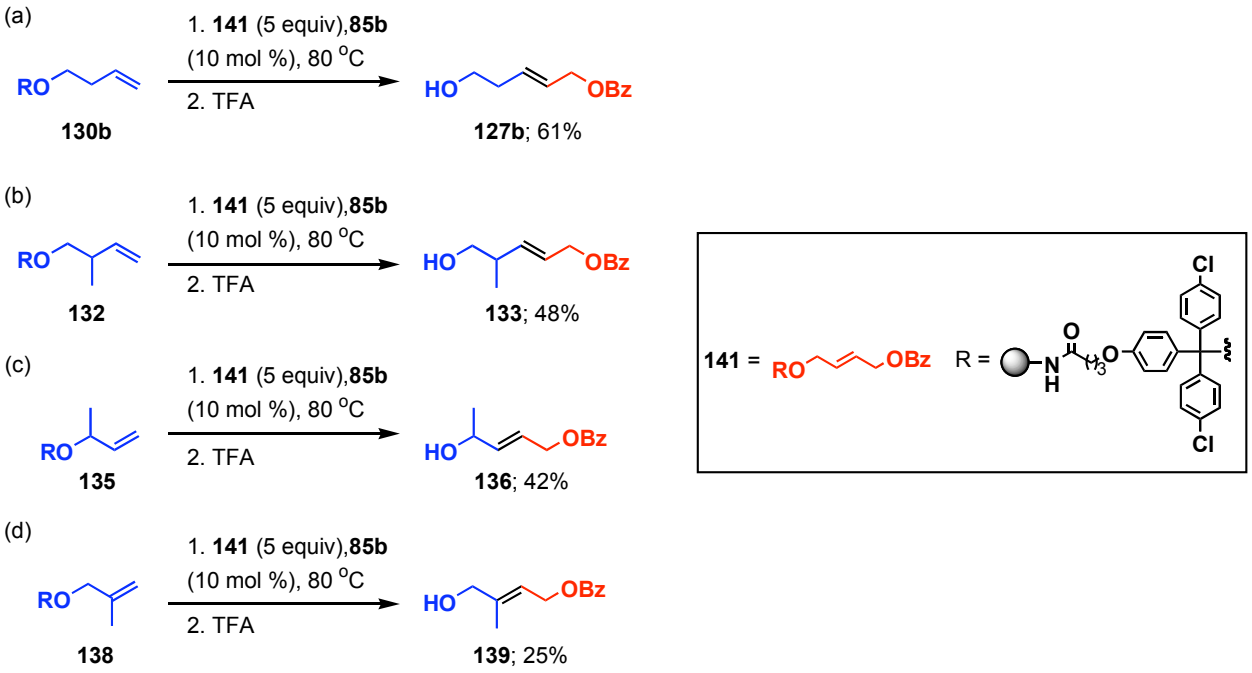

Figure 91. Resin-to-resin olefin cross-metathesis using a linker

Metathesis reactions were performed between acceptor alkenes **130b**, **132**, **135** and **138** and donor alkene **141** (5.0 equiv) using pre-catalyst **86b** (10 mol %) in DCE at 80 °C for 24 h. Following cleavage with TFA, alcohols **127b**, **133**, **136** and **139** were isolated. In general, these reactions were ~25% less efficient than the respective couplings of the solid-phase acceptors

with **126** in solution. This was expected since the reaction is dependent upon the retro [2+2] reaction of the donor olefin.

Despite the success of our model studies described above, all attempts at resin-to-resin olefin cross-metathesis with more functionalized substrates failed (not shown). Although increased equivalency of the donor could have been attempted, it is not practical to require such a large excess of the donor fragment, especially with highly functionalized donor substrates. As a result, it seems that the proximity effect is not the sole culprit in our preliminary failures.

Reproducibility problems are well noted in the literature in solid-phase organic synthesis.[53,50] In fact, most of these problems are linked to inhomogeneities in the cross-linked polystyrene resin, which are likely due to differences in cross-linking reactivities (*meta*- and *para*-divinylbenzenes differ in their reactivity with styrene).[53] Moreover, these differences in reactivity lead to differences in cross-linking topography throughout the resin (variable dense and lightly cross-linked areas). As the swollen polymer matrix is the solvent in the case of solid phase reactions and >99% of the sites of attachment are inside the resin, these parameters are critical for reaction reproducibility.[50,53] As such, resin purification techniques have been developed to improve reproducibility; however, the generality of these methods are not known.[54] More specific to this case, I learned through personal communication (Professor Philip Dawson, The Scripps Research Institute) that aminomethylpolystyrene resin is particularly prone to many differences between batches and vendors because the synthetic process is often different between companies. As such, these potential differences in resin matrix may limit the reproducibility of this reaction.

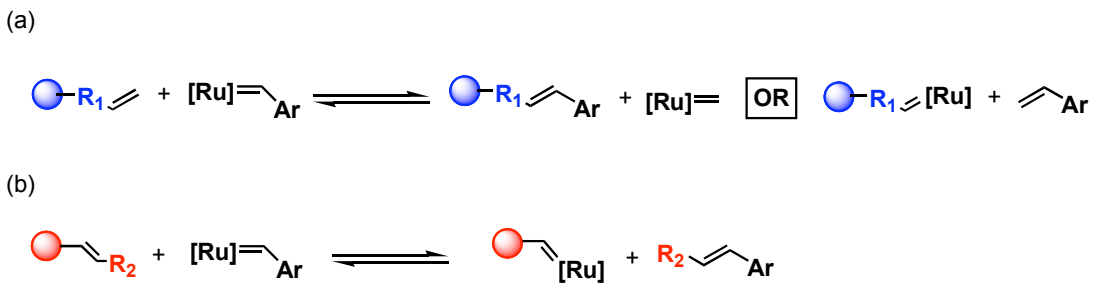

Figure 92. Potential pitfalls in resin-to-resin olefin cross-metathesis

In addition to the distance-dependence issue and potential differences between resin batches, there are a number of more fundamental challenges in performing resin-to-resin olefin cross-metathesis. Firstly, the likelihood for the ruthenium intermediate (**Y** in Figure 84) to escape the polymer matrix, traverse the barrier and react with an acceptor olefin is unclear, especially under thermal conditions and in the presence of many potential olefin substrates within the donor matrix.

Secondly, in terms of reactivity, there are two potential problems. The first potential pitfall is if the ruthenium catalyst preferentially reacts with the terminal olefin, which could result in two outcomes: transfer of the ligand from the catalyst to form an on-bead dimer or transfer of the ruthenium to form a solid-supported alkylidene, each of which kills the catalyst (Figure 92a). The second potential pitfall is if the ruthenium catalyst reacts with the donor resin but with the opposite regiochemistry, which results in a solid-supported ruthenium intermediate again killing the catalyst (Figure 92b). A similar catalyst killing effect was also observed in the case of a resin-to-resin Sonogashira coupling.[19] In this case, Pd^0 initially cleaves the allylic substrates from the resins prior to coupling in solution; however, the most successful examples required equimolar or higher loadings of palladium presumably indicating loss of the catalyst either on the resin or due to oxidation. As such, although I may have solved olefin cross-

metathesis between a solid-supported substrate and a substrate in solution, resin-to-resin olefin cross-metathesis remains an unsolved yet challenging problem.

8.3 CONCLUSION

The challenging resin-to-resin olefin cross-metathesis has been investigated as a convergent approach to library synthesis on solid support. Although unsuccessful, these initial failings led to the development of a general protocol for solid-phase olefin cross-metathesis using a traceless long linker. This model study should enhance the utility of olefin cross-metathesis in solid-phase organic synthesis.

8.4 EXPERIMENTAL

8.4.1 General Information

All reactions were carried out under laboratory atmosphere, unless otherwise noted. Tetrahydrofuran (THF) was distilled from sodium-benzophenone, and methylene chloride (CH_2Cl_2) was distilled from calcium hydride. Yields refer to chromatographically and spectroscopically (^{1}H NMR) homogenous materials, unless otherwise stated.

All reactions were monitored by thin layer chromatography (TLC) carried out on 0.25-mm E. Merck silica gel plates (60F-254) using UV light (254 nm) with 2.4% phosphomolybdic acid/5% sulfuric acid/1.4% phosphoric acid in water, anisaldehyde in ethanol, or 0.2% ninhydrin

in ethanol and heat as developing agents. TSI silica gel (230–400 mesh) was used for flash column chromatography.

NMR spectra were recorded on AM300 (Bruker) instruments and calibrated using a solvent peak or tetramethylsilane (TMS) as an internal reference. The following abbreviations are used to indicate the multiplicities: s, singlet; d, doublet; t, triplet; q, quartet; m, multiplet; br, broad. Mass spectra were obtained from a Micromass Autospec double focusing instrument.

HPLC/MS data was recorded using an Agilent HP 1100 series LC-MSD instrument with purities determined by a UV-Vis detector. HPLC analyses were performed with a reverse-phase Eclipse XDB-C18 (4.6 X 750 mm, 3.5 μm) column using 5→30% MeCN in H_2O/0.1% HCO_2H as a solvent system. The flow rate was 0.4 mL/min. UV detection was performed at 254 and 280 nm.

Bio-Rad Poly-Prep® chromatography columns and Bio-Rad Bio-Spin® chromatography columns are a product of Bio-Rad Laboratories.

The following apparati were used for solid-phase reactions: reaction spinner (Tube Rotator, Scientific Equipment Products, this instrument has only one speed), incubator (Lab-Line® Incubator-Shaker) and reaction shaker (VWR Analog Vortex Mixer).

8.4.2 Resin-to-Resin Olefin Cross-Metathesis – First Generation

Preparation of 86. A 10-mL Bio-Rad Poly-Prep® chromatography column was charged with 500 mg of trityl chloride resin (Advanced ChemTech, 100–200 μm, 1.5 mmol/g) and 5.0 mL of CH_2Cl_2 at 24 °C. The mixture was gently agitated on a reaction spinner for 10 min to swell the resin. The solvent was removed by vacuum filtration and a fresh 5.0 mL portion of CH_2Cl_2 was added at 24 °C followed by allyl alcohol (510 μL, 7.5 mmol), Et_3N (1.78 mL, 13.5 mmol) and

DMAP (45.8 mg, 0.375 mmol). After gentle agitation at 24 °C for 12 h on a reaction spinner, the solution was filtered via vacuum filtration and the yellow resin was washed with CH_2Cl_2 (3×5 mL), THF (3×5 mL), DMF (3×5 mL), and CH_2Cl_2 (3×5 mL). Loading was assumed to be quantitative (1.4 mmol/g) due to the volatility of allyl alcohol.

Preparation of 87. Homoallyl-alcohol acceptor **87** was loaded in a similar fashion as was used in the preparation of **86**. Loading was assumed to be quantitative due to volatility (quant, 1.4 mmol/g, yellow resin).

Preparation of 88. Acrylic acid (329 μL) was loaded onto Wang resin (Nova Biochem, 100–200 μm, 0.96 mmol/g) according to literature precedent[55] to prepare 500 mg of **88** as white beads. Theoretically, the quantitative loading level of **88** is 0.90 mmol/g. Resin **88** (20.0 mg, 0.018 mmol) was swelled in a 1.0-mL Bio-Rad Bio-Spin® chromatography column with CH_2Cl_2, filtered via vacuum filtration, and treated with 0.5 mL of a 1:10:9 Et_3SiH/TFA/CH_2Cl_2 solution for 30 min at 24 °C. The beads were filtered via gravity filtration with CH_2Cl_2 and the resulting liquid was concentrated *in vacuo* yielding 15.3 mg (0.212 mmol, 85%, 0.82 mmol/g) of acrylic acid as a colorless oil. ^{1}H NMR spectrum was consistent with that of the starting material.

Preparation of 89. A 20-mL Bio-Rad chromatography column was charged with 4-methylbenzhydrylamine resin hydrochloride salt (300 mg, 0.18 mmol, Nova Biochem, 0.62 mmol/g, 100–200 μm), and the salt was washed with 5% diisopropylethylamine in CH_2Cl_2 (2×5.0 mL for 2 min at 24 °C followed by washing with CH_2Cl_2) to yield the free amine. Rink amide linker (Nova Biochem) was then coupled to this amine resin according to the literature[56]

followed by Fmoc deprotection with 1:1 piperidine/DMF and additional coupling with acrylic acid to afford **89**. All reactions were monitored by the Kaiser ninhydrin test.[57] Loading was assumed to be quantitative (0.60 mmol/g) based on the negative result in the Kaiser test. ^{1}H NMR spectrum was consistent with that of the starting material.

Preparation of 90. *cis*-But-2-en-1,4-diol was loaded onto trityl chloride resin (500 mg) in a similar manner as that used to prepare acceptor **86**. The resin was then carried on to acetylation using acetic anhydride (3.5 mL, 37.5 mmol) in pyridine (5.0 mL) at 24 °C for 2 h to prepare **90** as pale yellow beads. The resin was washed with CH_2Cl_2 (3×5 mL), THF (3×5 mL), DMF (3×5 mL) and CH_2Cl_2 (3×5 mL) and dried under vacuum overnight. A small portion of **90** was cleaved for analysis. A portion of **90** in a 1.0-mL Bio-Rad Bio-Spin® chromatography column was swelled with CH_2Cl_2, filtered via vacuum filtration, and treated with 0.5 mL of a 1:2.5:46 TFA/Et_3SiH/CH_2Cl_2 solution for 3 min at 24 °C. The beads were filtered via gravity filtration with CH_2Cl_2 and the resulting solution was concentrated *in vacuo* yielding a colorless oil (quant, 1.3 mmol/g). ^{1}H NMR spectrum consistent with that of the known compound: ^{1}H NMR (300 MHz, $CDCl_3$, 20 ºC): δ 5.91–5.64 (m, 2H); 4.69 (d, J = 6.8 Hz, 2H); 4.29 (d, J = 6.8 Hz, 2H); 2.08 (s, 3H).[58]

Preparation of 91. Donor **91** (cinnamyl alcohol) was loaded onto trityl chloride resin in a similar fashion as that used to prepare **86** (quant, 1.3 mmol/g). ^{1}H NMR spectrum was consistent with that of cinnamyl alcohol: ^{1}H NMR (300 MHz, $CDCl_3$, 20 ºC): δ 7.4 (m, 5H); 6.6 (d, J = 16.0 Hz, 1H); 6.40 (dt, J = 16.0, 5.5 Hz, 1H); 4.30 (d, J = 5.5 Hz, 2H).

Preparation of 92. (*E*)-3-(4-Methoxyphenyl)prop-2-en-1-ol was loaded onto trityl chloride resin (Advanced ChemTech, 100–200 μm, 1.5 mmol/g) in an analogous fashion as that used to prepare **86** to produce **92** as yellow beads. A portion of **92** was cleaved by treatment with a 1:2.5:46 TFA/Et_3SiH/CH_2Cl_2 solution to yield a white solid (quant., 1.2 mmol/g). ^{1}H NMR spectrum was consistent with that of the known compound: ^{1}H NMR (300 MHz, $CDCl_3$, 20 ºC): δ 7.32 (d, *J* = 8.7 Hz, 2H); 6.85 (d, *J* = 8.7 Hz, 2H); 6.55 (d, *J* = 15.9 Hz, 1H); 6.23 (dt, *J* = 15.9, 6.0 Hz, 1H); 4.78 (br s, 1H); 4.28 (dd, *J* = 6.0, 1.1 Hz, 2H); 3.80 (s, 3H).[59]

Preparation of 93. (*E*)-3-(4-Dimethylaminophenyl)prop-2-en-1-ol was loaded onto trityl chloride resin (Advanced ChemTech, 100–200 μm, 1.5 mmol/g) in an analogous fashion as that used to prepare **86** to produce **93** as yellow beads (79%, 0.95 mmol/g). ^{1}H NMR spectrum was consistent with that of the known compound: ^{1}H NMR (300 MHz, $CDCl_3$, 20 ºC): δ 7.37 (d, *J* = 8.7 Hz, 2H); 6.77 (d, *J* = 8.7 Hz, 2H); 6.61 (d, *J* = 15.8 Hz, 1H); 6.26 (dt, *J* = 15.8, 5.9 Hz, 1H); 4.35 (d, *J* = 5.9 Hz, 2H); 3.05 (s, 6H).[60]

Preparation of 94. (*E*)-3-(3-Hydroxypropenyl)phenol was loaded onto trityl chloride resin (Advanced ChemTech, 100–200 μm, 1.5 mmol/g) in an analogous fashion as that used to prepare **86** to produce **94** as yellow beads (90%, 1.3 mmol/g). ^{1}H NMR spectrum was consistent with that of the known compound: ^{1}H NMR (300 MHz, CD_3OD, 20 ºC): δ 7.19 (dd, *J* = 7.5, 7.5 Hz, 1H), 6.95 (d, *J* = 7.5 Hz, 1H), 6.87 (d, *J* = 7.5 Hz, 1H), 6.73 (s, 1H), 6.46 (d, *J* = 15.9 Hz, 1H), 6.23 (dt, *J* = 15.9, 5.6 Hz, 1H), 4.25 (d, *J* = 5.6 Hz, 2H).[61]

Reaction Vessel for Resin-to-Resin Metathesis Reactions. Two Bio-Rad Micro Biospin® chromatography columns were cut at the frit. Removal of one frit followed by coupling of the two columns with a Teflon connector (prepared by cutting a piece of Teflon tubing to XX in) provided the reaction vessel for resin-to-resin metathesis reactions (see photo below). Each column was capped with the cap sold together with the chromatography column.

Metathesis of Acceptors (86–89) and Donors (90–94). To one half of the reaction vessel was added **Donor resin** (10.0 equiv), ruthenium catalyst (5–10 mol %) and 1.0 mL DCE at 24 °C. The vessel was capped, and to the other side was added **Acceptor resin** (1.0 equiv) and another 1.0 mL portion of DCE. In a typical experiment, 75 mg of the **Acceptor resin** is coupled with the appropriate amount of the **Donor resin** based on the 1:10 molar ratio using the appropriate amount of the ruthenium catalyst. The vessel was then placed into a shaking incubator and allowed to vigorously shake at 60 °C for 7 h. Following reaction, the resin from the acceptor side of the vessel was transferred to a new column using a disposable plastic pipet and the resin was washed with CH_2Cl_2 (3×2 mL), THF (3×2 mL), DMF (3×2 mL) and CH_2Cl_2 (3×2 mL) and dried under vacuum overnight. The acceptor beads were then swelled with CH_2Cl_2 and treated with the respective cleavage solution. The beads were filtered via gravity filtration with CH_2Cl_2 and the resulting liquid was concentrated *in vacuo.*

Metathesis of Acceptor **86** *and Donors* **(90–94)**: Ruthenium catalyst **84** (5 mol %); Cleavage with 1:2.5:46 TFA/Et_3SiH/CH_2Cl_2 solution for 3 min at 24 °C.

Data for **95**: Colorless oil (96%); ^{1}H NMR spectrum was consistent with that of **90**.

Data for **99**: Colorless oil (94%); ^{1}H NMR spectrum was consistent with that of **91**.

Data for **103**: Yellow oil (quant.); ^{1}H NMR spectrum was consistent with that of **92**.

Data for **107**: Green oil (quant.); ^{1}H NMR spectrum was consistent with that of **93**.

Data for **111**: White solid (74%); ^{1}H NMR spectrum was consistent with that of **94**.

Metathesis of Acceptor **87** *and Donors* **(90–94)**: Ruthenium catalyst **84** (5 mol %); Cleavage with 1:2.5:46 TFA/Et_3SiH/CH_2Cl_2 solution for 3 min at 24 °C.

Data for **96**: Colorless oil (quant.); ^{1}H NMR spectrum was consistent with that of the known compound: ^{1}H NMR (300 MHz, $CDCl_3$, 20 ºC): δ 5.79 (dt, *J* = 15.4, 6.6 Hz, 1H); 5.65 (dt, *J* = 15.4, 5.9 Hz, 1H); 4.52 (d, *J* = 5.9 Hz, 2H); 3.66 (t, *J* = 6.6 Hz, 2H); 3.28 (br s, 1H); 2.32 (q, *J* = 6.5 Hz, 2H); 2.06 (s, 3H).[62]

Data for **100**: (quant.); ^{1}H NMR spectrum was consistent with that of the known compound: ^{1}H NMR (300 MHz, $CDCl_3$, 20 ºC): δ 7.40–7.12 (m, 5H); 6.48 (d, *J* = 15.9 Hz, 1H); 6.19 (dt, *J* = 15.9, 7.2 Hz, 1H); 3.72 (t, *J* = 6.3 Hz, 2H); 2.46 (dt, *J* = 7.2, 6.3 Hz, 2H); 2.01 (br s, 1H).[63]

Data for **104**: Yellow oil (90%); ^{1}H NMR spectrum was consistent with that of the known compound: ^{1}H NMR (300 MHz, $CDCl_3$, 20 ºC): δ 7.19 (d, *J* = 8.5 Hz, 2H); 6.72 (d, *J* = 8.5 Hz, 2H); 6.38 (d, *J* = 16.0 Hz, 1H); 6.18 (dt, *J* = 16.0, 6.5 Hz, 1H); 3.82 (s, 3H); 3.53 (t, *J* = 6.5 Hz, 2H); 2.45 (q, *J* = 6.5 Hz, 2H).[64]

Data for **108**: Yellow oil (93%); ^{1}H NMR spectrum was consistent with that of the known compound: ^{1}H NMR (300 MHz, $CDCl_3$, 20 ºC): δ 7.12 (d, *J* = 8.6 Hz, 2H); 6.54 (d, *J* = 8.6 Hz,

2H); 6.41 (d, J = 15.9 Hz, 1H); 6.06 (dt, J = 15.9, 6.5 Hz, 1H); 3.57 (t, J = 6.5 Hz, 2H); 2.85 (s, 6H); 2.15 (q, J = 6.5 Hz, 2H).[64]

Data for **112**: Colorless oil (72%); ^{1}H NMR spectrum was consistent with that of the known compound: ^{1}H NMR (300 MHz, CD_3OD, 20 ºC): δ 7.04 (t, J = 7.5 Hz, 1H); 6.86 (d, J = 7.5 Hz, 1H); 6.77 (s, 1H); 6.61 (d, J = 7.5 Hz, 1H); 6.46 (d, J = 15.9 Hz, 1H); 6.15 (dt, J = 15.9, 6.4 Hz, 1H); 3.55 (t, J = 6.4 Hz, 2H); 2.27 (q, J = 6.4 Hz, 2H).[64]

Metathesis of Acceptor **88** *and Donors* **(90–94)**: Ruthenium catalyst **85b** (10 mol %) prepared from Grubbs II catalyst; Cleavage with 1:10:9 Et_3SiH/TFA/CH_2Cl_2 solution for 30 min at 24 °C.

Data for **97**: Colorless oil (90%); ^{1}H NMR spectrum was consistent with that of the known compound: ^{1}H NMR (300 MHz, CD_3OD, 20 ºC): δ 7.30 (dt, J = 15.8, 6.3 Hz, 1H); 6.21 (d, J = 15.8 Hz, 1H); 4.75 (d, J = 6.3 Hz, 2H); 2.01 (s, 3H).[65]

Data for **101**: Colorless oil (quant.); ^{1}H NMR spectrum was consistent with that of cinnamic acid: ^{1}H NMR (300 MHz, CD_3OD, 20 ºC): δ 12.1 (s, 1H); 7.73–7.25 (m, 6H); 6.41 (d, J = 16.0 Hz, 1H).[64]

Data for **105**: Colorless oil (75%); ^{1}H NMR spectrum was consistent with that of the known compound: ^{1}H NMR (300 MHz, $CDCl_3$, 20 ºC): δ 10.2 (br s, 1H); 7.67 (d, J = 8.6 Hz, 2H); 7.57 (d, J = 16.0 Hz, 1H); 6.99 (d, J = 8.6 Hz, 2H); 6.41 (d, J = 16.0 Hz, 1H); 3.84 (s, 3H).[66]

Data for **109**: Yellow oil (78%); ^{1}H NMR spectrum was consistent with that of the known compound: ^{1}H NMR (300 MHz, CD_3OD, 20 ºC): δ 7.72 (d, J = 8.7 Hz, 2H); 7.65 (d, J = 16.0 Hz, 1H); 6.91 (d, J = 8.7 Hz, 2H); 6.50 (d, J = 16.0 Hz, 1H); 3.08 (s, 6H).[66]

Data for **113**: Colorless oil (quant.); ^{1}H NMR spectrum was consistent with that of the known compound: ^{1}H NMR (300 MHz, CD_3OD, 20 ºC): δ 7.56 (d, *J* = 16.0 Hz, 1H); 7.21 (dd, *J* = 7.9, 7.9 Hz, 1H); 7.04 (d, *J* = 7.9 Hz, 1H); 6.99 (dd, *J* = 2.3, 1.2 Hz, 1H); 6.82 (ddd, *J* = 7.9, 2.3, 1.2 Hz, 1H); 6.40 (d, *J* = 16.0 Hz, 1H).[67]

Metathesis of Acceptor **89** *and Donors* **(90–94)**: Ruthenium catalyst **85a** (10 mol %); Cleavage with 1:2.5:46 TFA/Et_3SiH/CH_2Cl_2 solution for 3 min at 24 °C.

Data for **98**: Colorless oil (73%); ^{1}H NMR spectrum was consistent with that of the known compound: ^{1}H NMR (300 MHz, $CDCl_3$, 20 ºC): δ 7.30 (dt, *J* = 15.8, 6.3 Hz, 1H); 6.21 (d, *J* = 15.8 Hz, 1H); 4.75 (d, *J* = 6.3 Hz, 2H); 2.01 (s, 3H).[68]

Data for **102**: Colorless oil (72%); ^{1}H NMR spectrum was consistent with that of the known compound: ^{1}H NMR (300 MHz, $CDCl_3$, 20 ºC): δ 7.73–7.25 (m, 6H); 6.41 (d, *J* = 16.0 Hz, 1H).[68]

Data for **106**: Colorless oil (81%); ^{1}H NMR spectrum was consistent with that of the known compound: ^{1}H NMR (300 MHz, $CDCl_3$, 20 ºC): δ 7.50 (d, *J* = 8.7 Hz, 2H); 7.36 (d, *J* = 15.9 Hz, 1H); 6.97 (d, *J* = 8.7 Hz, 2H); 6.46 (d, *J* = 15.9 Hz, 1H); 3.79 (s, 3H).[69]

Data for **110**: Colorless oil (84%); ^{1}H NMR spectrum was consistent with that of the known compound: ^{1}H NMR (300 MHz, $CDCl_3$, 20 ºC): δ 7.72 (d, *J* = 8.7 Hz, 2H); 7.55 (d, *J* = 16.0 Hz, 1H); 6.91 (d, *J* = 8.7 Hz, 2H); 6.50 (d, *J* = 16.0 Hz, 1H); 3.08 (s, 6H).[69]

Data for **114**: Colorless oil (68%); ^{1}H NMR spectrum was consistent with that of the known compound: ^{1}H NMR (300 MHz, $CDCl_3$, 20 ºC): δ 7.56 (d, *J* = 16.0 Hz, 1H); 7.21 (dd, *J* = 7.9, 7.9 Hz, 1H); 7.04 (d, *J* = 7.9 Hz, 1H); 6.99 (dd, *J* = 2.3, 1.2 Hz, 1H); 6.82 (ddd, *J* = 7.9, 2.3, 1.2 Hz, 1H); 6.40 (d, *J* = 16.0 Hz, 1H).[69]

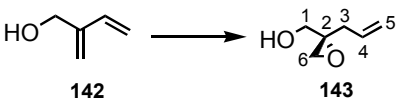

142 143

Preparation of 115 and 140. Diene **142** was prepared according to the literature.[70] A stirred suspension of activated 4Å molecular sieves (19.24 g) in CH_2Cl_2 (200 mL) was treated with (+)-diisopropyl tartrate (1.2 mL, 5.71 mmol) at 24 °C under an argon atmosphere. The reaction mixture was cooled to -20 °C, then titanium isopropoxide (1.4 mL, 4.7 mmol) was added, followed by *tert*-butyl hydroperoxide (5–6 M in isooctane, 22.2 mL, 111.3–133.2 mmol). The mixture was stirred for 1 h at -20 °C to allow the catalyst to form, then **142** (5.9 g, 60.1 mmol) in CH_2Cl_2 (40 mL) was added over 15 min. The reaction was stirred for 12 h at -20 °C, then was quenched with 3 N NaOH (20 mL) and vigorously stirred for 1 h at 24 °C. Celite, solid NaCl and anhydrous Na_2SO_4 was then added to the resulting reaction mixture. The mixture was filtered through a pad of Celite, eluting with 60% EtOAc in hexanes (500 mL), and concentrated under reduced pressure. The residue was purified by flash chromatography (20→40% EtOAc in hexanes) on silica gel to afford **143** (5.1 g, 73%) as a colorless oil.

Data for **143**: colorless oil; R_f = 0.30 (30% EtOAc in hexanes); IR (neat): ν_{max} 3421 (br, O-H), 2926, 1550, 1445, 1048 cm^{-1}; $[\alpha]_D^{22}$ -36.5 (*c* 1.0, $CHCl_3$); ^1H NMR (300 MHz, $CDCl_3$, 293 K): δ 5.87 (dddd, *J* = 16.9, 10.1, 7.4, 7.4 Hz, 1H; C_4-H), 5.19–5.11 (m, 2H; C_5-H), 3.79 (dd, *J* = 12.3, 4.5 Hz, 1H; C_1-H), 3.65 (dd, *J* = 12.3, 8.4 Hz, 1H; C_1-H'), 2.90 (d, *J* = 4.7 Hz, 1H; C_6-H), 2.71 (d, *J* = 4.7 Hz, 1H; C_6-H'), 2.52 (dd, *J* = 14.6, 7.4 Hz, 1H; C_3-H), 2.31 (dd, *J* = 14.6, 7.4 Hz, 1H; C_3-H'), 1.73 (dd, *J* = 8.4, 4.5 Hz, 1H; OH); ^{13}C NMR (75 MHz, $CDCl_3$, 20 °C): δ 133.1, 117.3, 63.3, 60.4, 49.1, 35.9; MS (EI) *m/z* calcd. for C_5H_7O M-43 83.0497, found 83.0505.

Epoxyalcohol **143** was subsequently loaded onto trityl chloride resin (Advanced ChemTech, 100–200 μm, 1.0 mmol/g) or resin **129** to generate resins **115** or **140**, respectively. A

10-mL Bio-Rad Poly-Prep® chromatography column was charged with 500 mg of trityl chloride resin (Advanced ChemTech, 100–200 μm, 1.0 mmol/g) or resin **129** and 8.0 mL of CH_2Cl_2 at 24 °C. The mixture was gently agitated for 10 min on a reaction spinner to swell the resin. The solvent was removed via vacuum filtration and a fresh portion of CH_2Cl_2 (5.0 mL; 1.00 mL/100 mg resin) was added at 24 °C followed by **143** (1.25 mmol, 2.5 equiv) and pyridine (2.5 mmol, 5 equiv). After gentle agitation at 24 °C for 24 h on a reaction spinner, the solution was filtered via vacuum filtration and the resin was washed with CH_2Cl_2 (3×5 mL), DMF (3×5 mL), and CH_2Cl_2 (3×5 mL). The resin was dried under high vacuum for at least 8 h. Loading was quantitative (0.93 mmol/g).

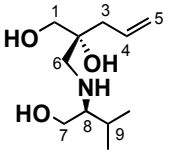

116'

Preparation of 116. A 10-mL Bio-Rad Poly-Prep® chromatography column was charged with **115** (150 mg, 0.19 mmol) and 5.0 mL toluene at 24 °C, and the resulting mixture was gently agitated for 10 min at 24 °C on a reaction spinner. The resin was then filtered via vacuum filtration, and a new 3.0 mL portion of toluene and (*S*)-2-amino-3-methylbutan-1-ol (433 mg, 4.2 mmol) was added. The resulting mixture was heated in a sand bath at 80 ºC for 12 h. The resulting resin was washed with CH_2Cl_2 (3×5 mL), THF (3×5 mL), DMF (3×5 mL), and CH_2Cl_2 (3×5 mL) and dried under vacuum overnight to form **116**. A small portion of **116** was cleaved for analysis. Theoretically, the quantitative loading level of **116** is 1.0 mmol/g. Resin **116** (5.3 mg, 5.3 μmol) was swelled in a 1.0-mL Bio-Rad Bio-Spin® chromatography column with CH_2Cl_2, filtered via vacuum filtration, and treated with 0.5 mL of a 1:2.5:46 TFA/Et_3SiH/CH_2Cl_2 solution for 3 min at 24 °C. The beads were filtered via gravity filtration with CH_2Cl_2 and the resulting liquid concentrated *in vacuo* yielding a single product **116'** (1.1 mg, quant, 1.0 mmol/g) as a colorless oil.

Data for **116'**: R_f = 0.10 (60% EtOAc in hexanes); IR (neat): ν_{max} 3630 (br, O-H), 3321 (N-H), 2926, 1645 (C=C), 1220 cm^{-1}; ^1H NMR (300 MHz, CD_3OD, 20 °C): δ 5.82 (dddd, *J* = 15.6, 11.1, 7.5, 5.8 Hz, 1H; C_4-H), 5.13–5.07 (m, 2H; C_5-2H), 3.86–3.50 (m, 5H; C_1-2H, C_7-2H, C_8-H), 3.25–3.11 (m, 2H; C_6-H), 2.98–2.86 (m, 1H; C_9-H), 2.06 (dd, *J* = 14.2, 7.5 Hz, 1H; C_3-H), 1.93 (dd, *J* = 14.2, 5.8 Hz, 1H; C_3-H'), 1.23 (br s, 6H); ^{13}C NMR (75 MHz, $CDCl_3$, 20 °C): δ 130.6, 117.6, 67.3, 64.4, 58.2, 55.6, 51.0, 39.5, 27.4, 16.9, 16.6; MS (ESI) *m/z* calcd. for $C_{11}H_{24}NO_3$ $[M+H]^+$ 218.1756, found 218.1745.

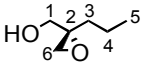

144

Preparation of 144. A 250-mL round-bottom flask was charged with 10% palladium on carbon (20.0 mg, 1.69 mmol) and EtOAc (71 mL) at 24 °C. Subsequently, **143** (1.00 g, 8.76 mmol) in EtOAc (17 mL) was added and the solvent was degassed and put under a hydrogen atmosphere (1 atm) at 24 °C. The mixture was allowed to stir at the same temperature for 12 h then filtered through filter paper and the filter was washed with CH_2Cl_2. The crude residue was purified by flash chromatography (20→40% EtOAc in hexanes) on silica gel to afford **144** (940 mg, 92%) as a colorless liquid.

Data for **144**: R_f = 0.25 (30% EtOAc in hexanes); IR (neat): ν_{max} 3421 (br, O-H), 2926, 1048, 890 cm^{-1}; $[\alpha]_D^{22}$ -36.8 (*c* 1.0, $CHCl_3$); ^1H NMR (300 MHz, $CDCl_3$, 20 °C): δ 3.79 (d, *J* = 12.3 Hz, 1H; C_1-H), 3.65 (d, *J* = 12.3 Hz, 1H; C_1-H'), 2.90 (d, *J* = 4.7 Hz, 1H; C_6-H), 2.68 (d, *J* = 4.7 Hz, 1H; C_6-H'), 1.52–1.33 (m, 2H; C_3-H), 1.33–1.20 (m, 2H; C_4-H), 0.95 (t, *J* = 7.1 Hz, 3H; C_5-H); ^{13}C NMR (75 MHz, $CDCl_3$, 20 °C): δ 63.3, 60.4, 49.8, 33.7, 17.9, 13.5; MS (EI) *m/z* calcd. for C_5H_9O M-31 85.0653, found 85.0651.

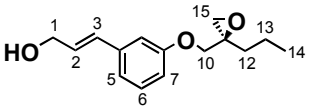

117'

Preparation of 117. A 10-mL Bio-Rad Poly-Prep® chromatography column was charged with 200 mg of **94** (0.266 mmol) and 3.0 mL of THF at 24 °C, and the resulting mixture was gently agitated for 10 min at 24 °C on a reaction spinner. The resin was then filtered via vacuum filtration, and triphenylphosphine (472 mg, 1.8 mmol) in 1.8 mL of THF, **144**, and diisopropyl azodicarboxylate (175 μL) in 430 μL of THF were added. The resulting solution was gently agitated for 1.5 h at 24 °C on a reaction spinner. The resulting resin was washed with CH_2Cl_2 (3×5 ml), THF (3×5 mL), DMF (3×5 mL), and CH_2Cl_2 (3×5 mL) and dried under vacuum overnight. A small portion of **117** was cleaved for analysis. Theoretically, the quantitative loading level of **117** is 1.0 mmol/g. Resin **117** (5.5 mg, 5.7 μmol) was swelled in a 1.0-mL Bio-Rad Bio-Spin® chromatography column with CH_2Cl_2, filtered via vacuum filtration and treated with 0.5 mL of a 1:2.5:46 TFA/Et_3SiH/CH_2Cl_2 for 3 min at 24 °C. The beads were filtered via gravity filtration with CH_2Cl_2 and the resulting liquid was concentrated in *vacuo* yielding a single product **117'** (1.4 mg, quant, 1.05 mmol/g) as a colorless oil.

Data for **117'**: R_f = 0.17 (30% EtOAc in hexanes); IR (neat): ν_{max} 3108 (br, O-H), 3050, 1670 (C=C), 1251, 1224 cm^{-1}; ^1H NMR (300 MHz, CD_3OD, 20 °C): δ 6.91 (dd, *J* = 7.8, 7.8 Hz, 1H; C_6-H), 6.67 (d, *J* = 7.8 Hz, 1H; C_5-H or C_7-H), 6.65 (d, J = 7.8 Hz, 1H; C_5-H or C_7-H), 6.54 (s, 1H; C_9-H), 6.33 (d, *J* = 15.9 Hz, 1H; C_3-H), 6.11 (ddd, *J* = 15.9, 5.6, 5.6 Hz, 1H; C_2-H), 4.16 (apparent dd, *J* = 5.6, 1.5 Hz, 2H; C_1-H), 4.07–3.98 (br m, 2H; C_{10}-H), 3.32 (d, *J* = 4.3 Hz, 1H; C_{15}-H), 3.24 (d, *J* = 4.3 Hz, 1H; C_{15}-H'), 1.13–1.05 (m, 2H; C_{12}-H), 0.96–0.91 (m, 2H; C_{13}-H), 0.57–0.51 (m, 3H; C_{14}-H); ^{13}C NMR (75 MHz, $CDCl_3$, 20 °C): δ 157.5, 130.6, 129.4, 128.7, 123.7, 117.9, 114.0, 112.8, 89.3, 80.2, 62.5, 53.2, 30.1, 22.3, 21.1; MS (ESI) *m/z* calcd. for $C_{15}H_{20}O_3$ $[M+H]^+$ 249.1491, found 249.1518.

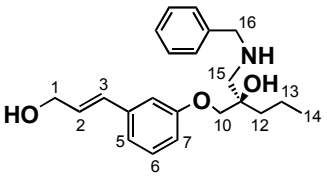

118'

Preparation of 118. 118' was prepared in a similar manner as that used to prepare **116** using benzylamine. (quant., 0.76 mmol/g)

Data for **118'**: R_f = 0.34 (100% EtOAc); IR (neat): ν_{max} 3540 (OH), 3230 (NH), 3110, 3072, 1673 (C=C), 1227 cm^{-1}; ^1H NMR (300 MHz, CD_3OD, 20 °C): δ 7.28 (m, 5H), 6.93 (dd, *J* = 7.8 Hz, 7.8 Hz, 1H; C_6-H), 6.70 (d, *J* = 7.8 Hz, 1H; C_5-H or C_7-H), 6.67 (d, *J* = 7.8 Hz, 1H; C_5-H or C_7-H), 6.51 (s, 1H; C_9-H), 6.36 (d, *J* = 15.9 Hz, 1H; C_3-H), 6.14 (ddd, *J* = 15.9, 5.8, 5.8 Hz, 1H; C_2-H), 4.18 (apparent dd, *J* = 5.8, 1.7 Hz, 2H; C_1-H), 4.07–3.96 (br m, 2H; C_{10}-H), 3.63–3.35 (m, 4H; C_{15}-H, C_{16}-H), 1.21–1.07 (m, 7H); ^{13}C NMR (75 MHz, $CDCl_3$, 20 °C): δ 157.2, 138.1, 133.2, 130.3, 129.1, 128.8, 128.5, 125.5, 123.4, 117.7, 115.1, 114.3, 114.1, 112.5, 70.1, 69.1, 62.2, 48.4, 46.7, 42.9, 20.8, 20.4; MS (ESI) *m/z* calcd. for $C_{22}H_{30}NO_3$ $[M+H]^+$ 356.2226, found 356.2242.

Metathesis of Acceptors (115, 116) and Donors (117, 118). For each donor and acceptor containing an amine (**116** and **118**), these resins were initially treated with *p*-TsOH (1.1 equiv) in THF (0.01 M) at 24 °C for 3 min to afford the solid supported amine salts. The amine salts were subsequently used in metathesis reactions.

To one half of the reaction vessel (described above with the model studies) was added **Donor resin** (3.0 equiv), ruthenium catalyst **85b** (10 mol %), and 1.0 mL DCE at 24 °C. The vessel was capped, and to the other side **Acceptor resin** (1.0 equiv) and another 1.0 mL portion of DCE were added. In a typical experiment, 75 mg of the **Acceptor resin** is coupled with the appropriate amount of the **Donor resin** based on the 1:3 molar ratio using the appropriate

amount of the ruthenium catalyst. The vessel was then placed into a shaking incubator and allowed to shake at 60 ºC for 7 h. Following reaction, the resin from the acceptor side of the vessel was transferred to a new column with a disposable plastic pipet and washed with CH_2Cl_2 (3×2 mL), THF (3×2 mL), DMF (3×2 mL), and CH_2Cl_2 (3×2 mL) and dried under vacuum overnight. The acceptor beads were then swelled with CH_2Cl_2 and treated with 0.5 mL of a 1:2.5:46 TFA/Et_3SiH/CH_2Cl_2 solution for 3 min at 24 °C. The beads were filtered via gravity filtration with CH_2Cl_2 and the resulting liquid was concentrated *in vacuo*. All crude residues were initially analyzed by LC-MS and purified by reverse-phase C18 column (5→50% MeOH in H_2O/0.1% HCO_2H). Following purification, all ^{1}H NMR peaks were greatly obscured resulting in poor spectra. All crude ^{1}H NMR and HPLC data are described.

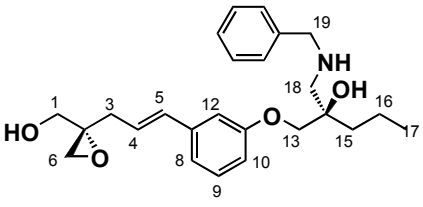

119

Data for **119**: 10.3 mg, 79%: R_f = 0.44 (4:1:1 ^{i}PrOH/H_2O/AcOH); t_R (5→30% MeCN in H_2O/0.1% HCO_2H, 0.4 mL/min, 254 and 280 nm) = 6.549 min; ^{1}H NMR (300 MHz, CD_3OD, 20 °C): δ 7.48-7.33 (m, 5H), 6.91 (dd, J = 7.8, 7.8 Hz, 1H; C_9-H), 6.66 (d, J = 7.8 Hz, 1H; C_8-H or C_{10}-H), 6.59 (d, J = 7.8 Hz, 1H; C_8-H or C_{10}-H), 6.47 (s, 1H; C_{12}-H), 6.34 (d, J = 16.0 Hz, 1H; C_5-H), 6.12 (ddd, J = 16.0, 5.8, 5.8 Hz, 1H; C_4-H), 4.17–4.14 (br m, 2H; C_1-H), 4.04–4.00 (br m, 2H; C_{13}-H), 3.48–3.27 (m, 4H; C_{18}-H, C_{19}-H), 3.06 (d, J = 4.3 Hz, 1H; C_6-H), 2.99 (d, J = 4.3 Hz, 1H; C_6-H'), 2.07 (d, J = 5.8 Hz, 2H; C_3-H), 1.14–1.10 (m, 4H; C_{15}-H, C_{16}-H), 0.73–0.66 (m, 3H; C_{17}-H).

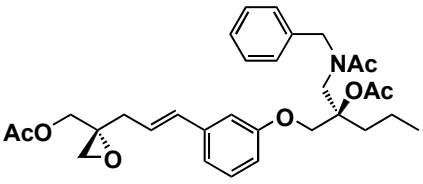

In an attempt to further verify the structure of **119**, the compound was acetylated in a similar manner as **90**. 5.7 mg, 86%: $R_f = 0.47$; t_R (5→30% MeCN in H_2O/0.1% HCO_2H, 0.4 mL/min, 254 and 280 nm) = 7.141 min; LC-MS (ESI) *m/z*: $C_{31}H_{40}NO_7$ $[M+H]^+$ 537.3.

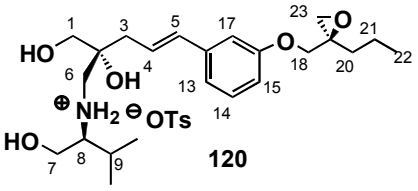

Data for **120**. 8.6 mg, 61%: R_f = 0.53 (4:1:1 ^{i}PrOH/H_2O/AcOH); t_R (5→30% MeCN in H_2O/0.1% HCO_2H), 0.4 mL/min, 254 and 280 nm) = 6.582 min; ^{1}H NMR (300 MHz, CD_3OD, 20 °C): δ 7.54 (d, *J* = 8.0 Hz, 2H; OTs), 7.07 (d, *J* = 8.0 Hz, 2H; OTs), 6.94 (dd, *J* = 7.9, 7.9 Hz, 1H; C_{14}-H), 6.77 (d, *J* = 7.9 Hz, 1H; C_{13}-H or C_{15}-H), 6.69 (d, *J* = 7.9 Hz, 1H; C_{13}-H or C_{15}-H), 6.66 (s, 1H; C_{17}-H), 6.35 (d, *J* = 15.9 Hz, 1H; C_5-H), 6.14 (ddd, *J* = 15.9, 5.5, 5.5 Hz, 1H; C_4-H), 4.11 (d, *J* = 14.0 Hz, 1H; C_1-H), 4.07–3.98 (br m, 2H; C_{18}-H), 3.88 (d, *J* = 14.0 Hz, 1H; C_1-H'), 3.72–3.34 (m, 3H; C_7-2H, C_8-H), 3.29 (d, *J* = 4.7 Hz, 1H; C_{23}-H), 2.92 (d, *J* = 4.7 Hz, 1H; C_{23}-H'), 2.86–2.77 (m, 2H; C_6-H), 2.20–2.10 (m, 2H; C_3-H), 1.99–1.75 (m, 1H; C_9-H), 1.12 (br s, 6H), 0.94–0.79 (m, 4H; C_{20}-H, C_{21}-H), 0.52–0.34 (m, 3H; C_{22}-H); LC-MS (ESI) *m/z*: $C_{30}H_{45}NO_8S$ $[M+H]^+$ 579.2.

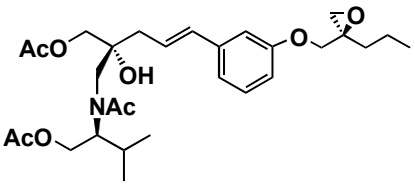

In an attempt to further verify the structure of **120**, the compound was derivatized via acetylation. A solution of **120** (7.3 mg, 0.018 mmol) in CH_2Cl_2 (200 μL) was treated with acetic anhydride (170 μL, 1.8 mmol), dimethylaminopyridine (1.1 mg, 0.009 mmol), and triethylamine (240 μL, 1.8 mmol) at 24 °C. The resulting solution was allowed to stir for 12 h at

room temperature. The crude mixture was purified by preparative TLC (0.25-mm in thickness) using 60% EtOAc in hexanes. 7.0 mg, 73%: R_f = 0.32; t_R (5→30% MeCN in H_2O/0.1% HCO_2H, 0.4 mL/min, 254 and 280 nm) = 5.886 min; ^1H NMR analysis was obscured presumably due to acyl migrations at elevated temperatures; LC-MS (ESI) *m/z*: $C_{29}H_{42}NO_8$ $[M+H]^+$ 532.3.

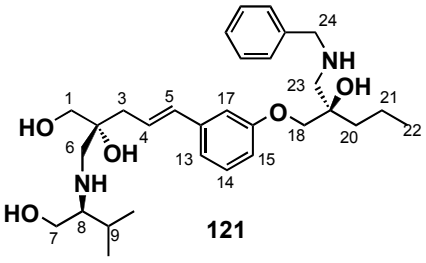

121

Data for **121**. 8.1 mg, 64%: R_f = 0.50 (4:1:1 ^{i}PrOH/H_2O/AcOH); t_R (5→30% MeCN in H_2O/0.1% HCO_2H, 0.4 mL/min, 254 and 280 nm) = 6.400 min; ^1H NMR (300 MHz, CD_3OD, 20 °C): δ 7.48-7.33 (m, 5H), 6.94 (dd, *J* = 7.8, 7.8 Hz, 1H; C_{14}-H), 6.72 (d, *J* = 7.8 Hz, 1H; C_{13}-H or C_{15}-H), 6.67 (d, *J* = 7.8 Hz, 1H; C_{13}-H or C_{15}-H), 6.50 (s, 1H; C_{17}-H), 6.36 (d, *J* = 15.9 Hz, 1H; C_5-H), 6.14 (ddd, *J* = 15.9, 5.6, 5.6 Hz, 1H; C_4-H), 4.13 (d, *J* = 14.9 Hz, 1H; C_1-H), 4.06–4.02 (br m, 2H; C_{18}-H), 3.87 (d, *J* = 14.9 Hz, 1H; C_1-H'), 3.75–3.21 (m, 9H; C_6-H, C_7-H, C_8-H, C_{23}-H, C_{24}-H), 2.17–2.11 (m, 3H; C_3-H, C_9-H), 1.13 (br s, 6H), 0.85–0.77 (m, 4H; C_{20}-H, C_{21}-H), 0.51–0.35 (m, 3H; C_{22}-H); LC-MS (ESI) *m/z*: 481.2 ($C_{29}H_{42}N_2O_4$; $[M–OCH_3+H]^+$; 6%), 437.3 ($C_{24}H_{40}N_2O_5$; $[M–C_6H_5+H]^+$; 14%), 393.2 ($C_{22}H_{36}NO_5$; $[M–CH_2NBn+H]^+$; 30%), 349.1 ($C_{19}H_{29}NO_5$; $[M–C_3H_7+2H]^+$; 49%).

8.4.3 Solid-Phase Olefin Cross-Metathesis Promoted by a Linker

General procedure for the loading of simple and substituted alkenyl alcohols onto trityl chloride resin and 129. A 10-mL Bio-Rad Poly-Prep® chromatography column was charged with 300 mg of trityl chloride resin (Advanced ChemTech, 100–200 μm, 1.0 mmol/g) or **129** and 5.0 mL of CH_2Cl_2 at 24 °C. The mixture was shaken for 10 min at 24 °C on a reaction shaker to

swell the resin. The solvent was removed via vacuum filtration and a fresh portion of CH_2Cl_2 (3.0 mL; 1.00 mL/100 mg resin) was added at 24 °C followed by the respective alcohol (1.5 mmol, 5 equiv) and pyridine (3.0 mmol, 10 equiv). After agitation at 24 °C for 24 h on a reaction shaker, the solution was filtered via vacuum filtration and the resin was washed with CH_2Cl_2 (3×5 mL), DMF (3×5 mL), and CH_2Cl_2 (3×5 mL). The resin was dried under high vacuum for at least 8 h. Loading was assumed to be quantitative (0.98–0.94 mmol/g) due to the volatility of the alkenyl alcohols.

General procedure for the loading of simple alkenyl alcohols onto alkylsilyl resin. Alkenyl alcohols were loaded onto (4-methoxyphenyl)diisopropylsilylpropyl polystyrene resin according to the literature.[52]

General procedure for the loading of simple alkenyl alcohols onto Merrifield resin. A 5.0-mL silanized vial was charged with the respective alcohol (1.275 mmol, 5 equiv) and NaH (1.402 mmol, 5.5 equiv) in DMF (3.0 mL; 1.0 mL/100 mg resin) at 24 °C. 300 mg of Merrifield HL resin (Novabiochem, 100–200 mesh), 0.85 mmol/g) was then added and the mixture was heated to 60 °C in an oil bath. After gently stirring at 60 °C for 16 h, the resin was transferred to a 10-mL Bio-Rad Poly-Prep® chromatography column with a disposable plastic pipet and the solution was filtered via vacuum filtration. The resin was washed with DMF (3×5 mL), 1:1 DMF/CH_2Cl_2 (3×5 mL), DMF (3×5 mL), CH_2Cl_2 (3×5 mL), and MeOH (3×5 mL). The resin was dried under high vacuum for at least 8 h. Loading was assumed to be quantitative (0.83–0.81 mmol/g) due to the volatility of the alkenyl alcohols.

Preparation of resin 129. A 10-mL Bio-Rad Poly-Prep® chromatography column was charged with 300 mg of aminomethylated polystyrene HL resin (Novabiochem, 100–200 mesh, 0.78 mmol/g) and 5.0 mL of DMF at 24 °C. The mixture was shaken for 10 min at 24 °C on a reactio shaker to swell the resin. The solvent was removed via vacuum filtration and a fresh portion of DMF (3.0 mL; 1.00 mL/100 mg resin) was added at 24 °C followed by linker **128** (0.47 mmol, 2 equiv), 1-hydroxybenzotriazole monohydrate (0.47 mmol, 2 equiv), *N,N'*-dicyclohexylcarbodiimide (0.23 mmol, 1 equiv), and DMAP (0.023 mmol, 0.1 equiv). After agitation at 24 °C for 24 h on a reaction shaker, the solution was filtered via vacuum filtration and the resin was washed with CH_2Cl_2 (3×5 mL), DMF (3×5 mL), and CH_2Cl_2 (3×5 mL). Loading was assumed to be quantitative (0.53 mmol/g).

The above resin in the same 10-mL Bio-Rad Poly-Prep® chromatography column at 24 °C was then treated with 10% AcCl in CH_2Cl_2 (3.0 mL). After agitation at 24 °C for 3 h on a reaction shaker, the solution was filtered via vacuum filtration and the resin was washed with CH_2Cl_2 (5×5 mL). The resin was dried under high vacuum for at least 8 h. Loading was assumed to be quantitative (0.52 mmol/g).

General procedure for olefin cross-metathesis reactions with solid-supported simple and substituted alkenyl alcohols. A 2-mL Bio-Rad Micro Bio-Spin® chromatography column was charged with solid-supported alcohol (25–75 mg resin, 0.035–0.049 mmol) and 500 μL of DCE at 24 °C. The mixture was shaken for 10 min at 24 °C on a reaction shaker to swell the resin. The solvent was removed via vacuum filtration and a fresh portion of DCE (500 μL) was added at 24 °C followed by **126** (0.175–0.245 mmol, 5 equiv) and ruthenium catalyst (0.002 mmol, 0.05 equiv). After agitation at 24 °C for 22 h on a reaction shaker, the solution was filtered via

vacuum filtration and the resin was washed with CH_2Cl_2 (3×2 mL), DMF (3×2 mL), and CH_2Cl_2 (3×2 mL). The resin was dried under high vacuum for at least 4 h and cleaved according to resin type.

General procedure for the cleavage of trityl-linked metathesis products. A 2-mL Bio-Rad Micro Bio-Spin® chromatography column containing the solid-supported metathesis product was charged with 1.0 mL of 1:19 TFA/CH_2Cl_2 at 24 °C. After agitation at 24 °C for 1 h on reaction shaker, the liquid was gravity filtered with CH_2Cl_2 and concentrated *in vacuo*. Because of the volatility of the starting alkenyl alcohols, drying under high vacuum yielded pure metathesis products.

General procedure for the cleavage of alkylsilyl-linked metathesis products. Metathesis products were cleaved from alkylsilyl resin according to the literature.[52]

General procedure for the cleavage of Merrifield-linked metathesis products. A 2-mL Bio-Rad Micro Bio-Spin® chromatography column containing the solid-supported metathesis product was charged with 1.0 mL of 4:1:15 TFA/Et_3SiH/CH_2Cl_2 solution at 24 °C. After agitation at 24 °C for 1 h on a reaction shaker, the liquid was gravity filtered with CH_2Cl_2 and concentrated *in vacuo*. Because of the volatility of the starting alkenyl alcohols, drying under high vacuum yielded pure metathesis products.

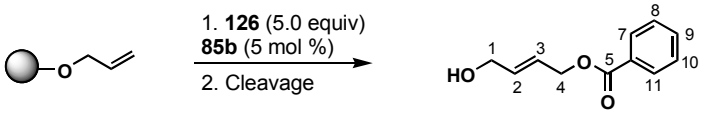

127a

Data for **127a** matches that of the known compound[71]: colorless oil; ^{1}H NMR (300 MHz, 293K, $CDCl_3$) δ 8.05 (d, J = 7.5 Hz, 2H; C_7, C_{11}-H), 7.57 (dd, J = 7.5, 7.5 Hz, 1H; C_9-H), 7.44 (dd, J = 7.5, 7.5 Hz, 2H; C_8, C_{10}-H), 6.03 (ddd, J = 15.7, 4.7, 4.7 Hz, 1H; C_2-H), 5.93 (ddd, J = 15.7, 4.7, 4.7 Hz, 1H; C_3-H), 4.84 (d, J = 4.7 Hz, 2H; C_4-H), 4.20 (d, J = 4.7 Hz, 2H; C_1-H).

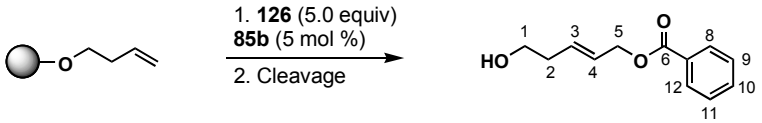

127b

Data for **127b** matches that of the known compound[72]: colorless oil; ^{1}H NMR (300 MHz, 293K, $CDCl_3$) δ 8.05 (d, J = 7.5 Hz, 2H; C_8, C_{12}-H), 7.56 (dd, J = 7.5, 7.5 Hz, 1H; C_{10}-H), 7.44 (dd, J = 7.5, 7.5 Hz, 2H; C_9, C_{11}-H), 5.87 (ddd, J = 15.3, 6.0, 6.0 Hz, 1H; C_3-H), 5.82 (ddd, J = 15.3, 4.8, 4.8 Hz, 1H; C_4-H), 4.80 (d, J = 4.8 Hz, 2H; C_5-H), 3.73 (t, J = 6.0 Hz, 2H; C_1-H), 2.38 (q, J = 6.0 Hz, 2H; C_2-H), 1.60 (br s, 1H; OH).

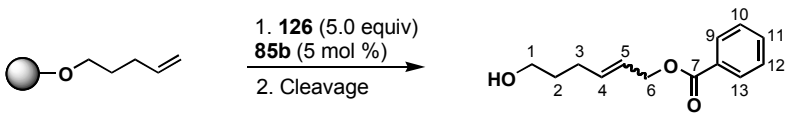

127c

Data for **127c**: colorless oil; R_f = 0.17 (30% EtOAc in hexanes); IR: 3397 (br, O-H), 2924, 2852, 2360, 1716 (C=O), 1272 cm^{-1}; ^{1}H NMR (300 MHz, 293K, $CDCl_3$) δ 8.07 (d, J = 7.5 Hz, 2H; C_9, C_{13}-H), 7.57 (dd, J = 7.5, 7.5 Hz, 1H; C_{11}-H), 7.46 (dd, J = 7.5, 7.5 Hz, 2H; C_{10}, C_{12}-H), 5.90 (ddd, J = 15.6, 6.3, 6.3 Hz, 1H; C_4-H), 5.75 (ddd, J = 15.6, 6.0, 6.0 Hz, 1H; C_5-H), 4.79 (d, J = 6.0 Hz, 2H; C_6-H), 3.69 (t, J = 6.3 Hz, 2H; C_1-H), 2.22 (q, J = 6.3 Hz, 2H; C_3-H), 1.72 (quint, J = 6.3 Hz, 2H; C_2-H), 1.58 (br s, 1H; OH); ^{13}C NMR (75 MHz, 293K, $CDCl_3$) δ 166.6,

135.5, 132.9, 129.6, 129.6, 128.4, 128.4, 124.5, 124.3, 65.5, 62.4, 31.8, 28.6; MS (EI) *m/z* calcd. for $C_{13}H_{16}O_3$ $M^{+\cdot}$ 220.1099, found 220.1103.

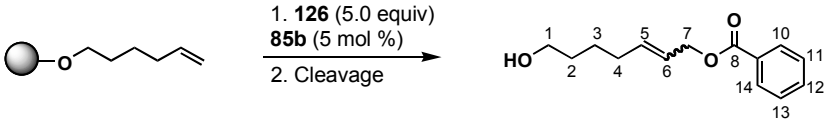

127d

Data for **127d**: colorless oil; R_f = 0.20 (30% EtOAc in hexanes); IR: 3392 (br, O-H), 2932, 2860, 1717 (C=O), 1272 cm^{-1}; ^1H NMR (300 MHz, 293K, $CDCl_3$) δ 8.05 (d, *J* = 7.5 Hz, 2H; C_{10}, C_{14}-H), 7.57 (dd, *J* = 7.5, 7.5 Hz, 1H; C_{12}-H), 7.45 (dd, *J* = 7.5, 7.5 Hz, 2H; C_{11}, C_{13}-H), 5.85 (ddd, *J* = 15.3, 6.3, 6.3 Hz, 1H; C_5-H), 5.71 (ddd, *J* = 15.3, 6.0, 6.0 Hz, 1H; C_6-H), 4.77 (d, *J* = 6.0 Hz, 2H; C_7-H), 4.36 (t, *J* = 6.3 Hz, 2H; C_1-H), 2.13 (q, *J* = 6.3 Hz, 2H; C_2-H), 1.67–1.40 (m, 4H; C_3, C_4-H); ^{13}C NMR (75 MHz, 293K, $CDCl_3$) δ 166.5, 136.0, 135.2, 132.9, 129.6, 129.6, 128.3, 128.3, 124.2, 65.7, 62.7, 32.2, 32.0, 25.6; MS (EI) *m/z* calcd. for $C_{14}H_{17}O_3$ $M^{+\cdot}$ 233.1178, found 233.1179.

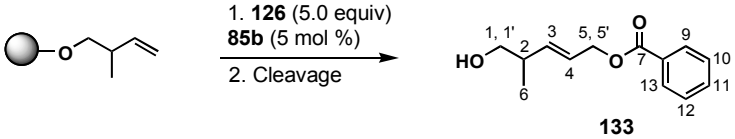

133

Data for **133**: colorless oil; R_f = 0.27 (30% EtOAc in hexanes); IR: 3433 (br, O-H), 2925, 1717 (C=O), 1272 cm^{-1}; ^1H NMR (300 MHz, 293K, $CDCl_3$) δ 8.05 (d, *J* = 7.5 Hz, 2H; C_9, C_{13}-H), 7.56 (dd, *J* = 7.5, 7.5 Hz, 1H; C_{11}-H), 7.44 (dd, *J* = 7.5, 7.5 Hz, 2H; C_{10}, C_{12}-H), 5.80 (dd, *J* = 15.6, 5.8 Hz, 1H; C_3-H), 5.73 (ddd, J = 15.6, 4.8, 4.8 Hz, 1H; C4-H), 4.81 (d, J = 4.8 Hz, 2H; C5-H), 3.52 (dddd, J = 6.9, 6.9, 5.8, 5.8 Hz, 2H; C1-H), 2.45 (septet, J = 6.9 Hz, 1H; C2-H), 1.63 (br s, 1H; OH), 1.05 (d, J = 6.9 Hz, 3H; C6-H); 13C NMR (75 MHz, 293K, CDCl3) δ 166.2,

137.7, 132.9, 130.5, 129.6, 129.6, 128.4, 128.4, 125.3, 67.1, 65.4, 39.4, 16.1; MS (EI) *m/z* calcd. for $C_{13}H_{16}O_3Na$ M+23 243.0997, found 243.0999.

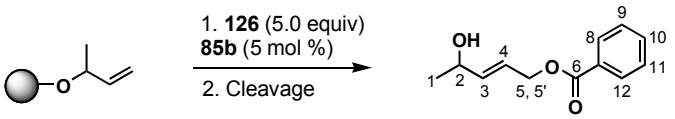

136

Data for **136**: colorless oil; R_f = 0.23 (30% EtOAc in hexanes); IR: 3431 (br, O-H), 2971, 2926, 1718 (C=O), 1272 cm^{-1}; ^1H NMR (300 MHz, 293K, $CDCl_3$) δ 8.06 (d, *J* = 7.2 Hz, 2H; C_8, C_{12}-H), 7.56 (dd, *J* = 7.2, 7.2 Hz, 1H; C_{10}-H), 7.44 (dd, *J* = 7.2, 7.2 Hz, 2H; C_9, C_{11}-H), 6.03 (ddd, *J* = 15.7, 4.9, 4.9 Hz, 1H; C_4-H), 5.93 (dd, *J* = 15.7, 6.3 Hz, 1H; C_3-H), 4.81 (d, *J* = 4.9 Hz, 2H; C_5-H), 4.37 (dq, *J* = 6.3 Hz, 1H; C_2-H), 1.60 (br s, 1H; OH), 1.30 (d, *J* = 6.3 Hz, 3H; C_1-H); ^{13}C NMR (75 MHz, 293K, $CDCl_3$) δ 166.3, 138.4, 133.0, 130.1, 129.7, 129.7, 128.4, 128.4, 123.7, 68.1, 64.7, 23.2; MS (EI) *m/z* calcd. for $C_{12}H_{14}O_3$ $M^{+\cdot}$ 206.0943, found 206.0937.

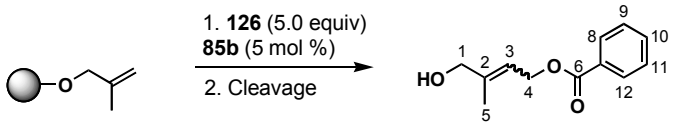

139

Data for **139** match those in the literature[73]: colorless oil; ^1H NMR (300 MHz, 293K, 1% CD_3OD in $CDCl_3$) δ 8.13 (d, *J* = 7.5 Hz, 2H; C_8, C_{12}-H, cis), 8.05 (d, *J* = 7.5 Hz, 2H; C_8, C_{12}-H, trans), 7.73–7.43 (m; C_9, C_{10}, C_{11}-H, cis and trans), 5.77 (t, *J* = 6.3 Hz, 1H; C_3-H, cis), 5.56 (t, *J* = 6.3 Hz, 1H; C_3-H, trans), 4.92 (d, *J* = 6.3 Hz, 2H; C_4-H, cis), 4.90 (d, *J* = 6.3 Hz, 2H; C_4-H, trans), 4.26 (br s, 2H; C_1-H, cis), 4.09 (br s, 2H; C_1-H, trans), 1.89 (br s, 3H; C_5-H), 1.80 (br s, 3H; C_5-H).

Control experiment with trityl ether.

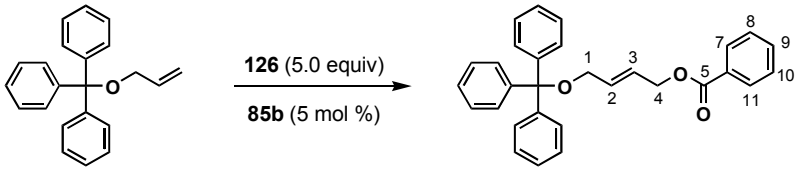

145

A solution of the trityl ether of allyl alcohol (34.6 mg, 0.115 mmol) in DCE (1.15 mL) was treated with **126** (171 mg, 0.576 mmol) and **85b** (3.8 mg, 0.005 mmol) at 24 °C. The resulting solution was stirred at 24 °C for 5 h, then pushed through a plug of silica with 30% EtOAc in hexanes. The crude residue was purified by flash column chromatography (Hexanes→1% EtOAc in hexanes) on silica gel to afford **145** (30.6 mg, 61%) as a colorless oil.

Data for **145**: off-white solid; ^{1}H NMR (300 MHz, 293K, $CDCl_3$) δ 8.06 (d, J = 7.2 Hz, 2H; C_7, C_{11}-H), 7.56 (dd, J = 7.2, 7.2 Hz, 1H; C_9-H), 7.45 (dd, J = 7.2, 7.2 Hz, 2H; C_8, $C_{10\text{-H}}$), 7.36–7.19 (m, 15H; trityl), 6.07 (ddd, J = 16.2, 5.7, 5.7 Hz, 1H; C_2-H), 6.00 (ddd, J = 16.2, 5.7, 5.7 Hz, 1H; C_3-H), 4.83 (d, J = 5.7 Hz, 2H; C_4-H), 3.65 (d, J = 5.7 Hz, 2H; C_1-H).

Further purification of **145** resulted in loss of the trityl group. The ^{1}H NMR spectrum of this compound matched that of known compound **127a** and no further characterization was completed.

Preparation of 122.

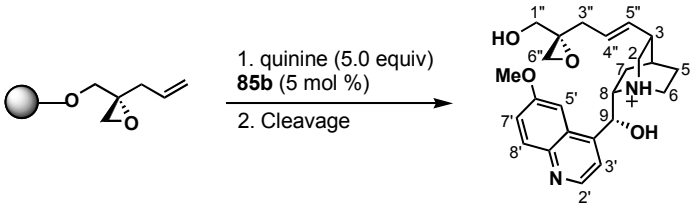

122

A 2-mL Bio-Rad Micro Bio-Spin® chromatography column was charged with **140** (75 mg resin, 0.0375 mmol) and 500 μL of DCE at 24 °C. The mixture was shaken for 10 min at 24 °C on a reaction shaker to swell the resin. The solvent was removed via vacuum filtration and a fresh portion of DCE (500 μL) was added at 24 °C followed by quinine (0.188 mmol, 5 equiv), $Ti(O^iPr)_4$ (0.007 mmol, 0.2 equiv), and ruthenium catalyst (0.002 mmol, 0.05 equiv). After agitation at 24 °C for 22 h on a reaction shaker, the solution was filtered via vacuum filtration and the resin was washed with CH_2Cl_2 (3×2 mL), DMF (3×2 mL), and CH_2Cl_2 (3×2 mL). The resin was dried under high vacuum for 8 h. Cleavage with 1:19 TFA/CH_2Cl_2 afforded **122** as a crude residue which was purified by pushing through a reverse-phase C_{18} silica plug with 1% MeOH in CH_2Cl_2.

Data for **122**: white solid; R_f = 0.11 (7.5% MeOH in CH_2Cl_2); ^{1}H NMR (300 MHz, 293K, d^6-DMSO) δ[74,75] 11.76 (br s, 1H; NH), 8.86 (d, J = 4.5 Hz, 1H; $C_{2'}$-H), 8.07 (d, J = 9.1 Hz, 1H; $C_{8'}$-H), 7.78 (d, J = 4.5 Hz, 1H; $C_{3'}$-H), 7.70 (s, 1H, $C_{5'}$-H), 7.54 (d, J = 9.1 Hz, 1H; $C_{7'}$-H), 6.62 (br s, 1H; C_9 enantiomer), 6.29 (br s, 1H, C_9 enantiomer), 5.82 (ddd, J = 17.2, 7.3, 7.3 Hz, 1H; $C_{4''}$), 5.03 (dd, J = 17.2, 9.6 Hz, 1H; $C_{5''}$), 4.07 (s, 3H; OMe), 3.98 (m, 2H; C_{6en}, C_8), 3.55 (m, 3H; $C_{1''}$, C_{2t}), 3.22 (m, 4H; C_{6ex}, C_{2c}, $C_{6''}$), 2.73 (m, 1H, C_3), 2.05 (m, 3H; $C_{3''}$, C_4), 1.85 (m, 2H; C_5), 1.43 (m, 2H; C_7);^{13}C NMR (75 MHz, 293K, $CDCl_3$ + 0.1% CD_3OD) δ 160.4 ($C_{6'}$), 152.6 ($C_{4'}$), 141.3 ($C_{2'}$), 136.9 ($C_{10'}$), 136.1 ($C_{5''}$), 131.8 ($C_{4''}$), 126.7 ($C_{8'}$), 125.5 ($C_{9'}$), 119.3 ($C_{3'}$), 117.6 ($C_{7'}$), 100.9 ($C_{5'}$), 67.4 (C_9), 66.2 ($C_{1''}$), 59.9 (C_8), 57.8 ($C_{2''}$), 54.8 (OMe), 44.2 (C_3), 36.9 ($C_{3''}$), 29.7 (C_4), 26.7 (C_5), 24.2 (C_7); C_2, C_6, $C_{6''}$ are buried in CD_3OD between 50.3–49.1[76]; MS (EI) *m/z* calcd. for $C_{24}H_{30}N_2O_4$ $M^{+\cdot}$ 410.2205, found 410.2208.

8.4.4 Resin-to-Resin Olefin Cross-Metathesis – Second Generation

Preparation of 141. *cis*-But-2-en-1,4-diol was loaded onto resin **129** according to the general procedure. The resin was then carried on to benzoylation using benzoyl chloride (650 μL, 5.6 mmol) and pyridine (910 μL, 11.2 mmol) in CH_2Cl_2 (20 mL) at 24 °C for 24 h to prepare **141** as pale yellow beads. The resin was washed with CH_2Cl_2 (3×5 mL), THF (3×5 mL), DMF (3×5 mL) and CH_2Cl_2 (3×5 mL) and dried under vacuum overnight. A small portion of **141** was cleaved for analysis as previously described and the loading was found to be quantitative (100%, 0.56 mmol/g). ^{1}H NMR spectrum consistent with that of compound **127a**.

Metathesis of Acceptors (130b, 132, 135, 138) and Donor (141). The **Donor resin** (5.0 equiv) and ruthenium catalyst **85b** (10 mol %) were added to a portion of Kimwipe, which was closed by tying with a string (see photo below). The **Acceptor resin** (1.0 equiv) was then added to a scintillation vial with a stir bar. DCE (3.0 mL) and the Kimwipe bag containing the **Donor resin** were then added and the vial was capped (see below for photo of reaction setup). In a typical experiment, 75 mg of the **Acceptor resin** is coupled with the appropriate amount of the **Donor resin** based on the 1:5 molar ratio using the appropriate amount of the ruthenium catalyst. The vial was then placed into an oil bath and heated at 80 ^{o}C for 24 h. Following reaction, the acceptor resin was transferred to a new column with a disposable plastic pipet and washed with CH_2Cl_2 (3×2 mL), THF (3×2 mL), DMF (3×2 mL) and CH_2Cl_2 (3×2 mL) and dried under vacuum overnight. The acceptor beads were then swelled with CH_2Cl_2 and treated with 1:19 TFA/CH_2Cl_2. The beads were filtered via gravity filtration with CH_2Cl_2 and the resulting liquid

was concentrated *in vacuo*. The formation of products **127b**, **133**, **136** and **139** was verified by comparison to the authentic samples.

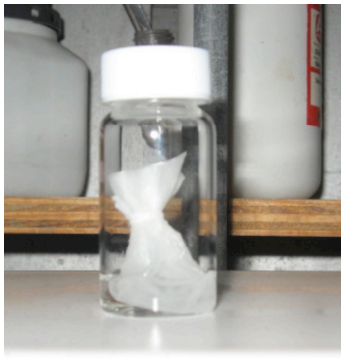

8.5 BIBLIOGRAPHY

1. Matteucci, M. D., Caruthers, M. H., "Synthesis of deoxyoligonucleotides on a polymer support." *J. Am. Chem. Soc.* **1981**, *103*, 3185–3191.

2. Merrifield, R. B., "Solid phase peptide synthesis. I. The synthesis of a tetrapeptide." *J. Am. Chem. Soc.* **1963**, *85*, 2149–2154.

3. Feher, M., Schmidt, J. M., "Property distributions: differences between drugs, natural products, and molecules from combinatorial chemistry." *J. Chem. Inf. Comput. Sci.* **2003**, *43*, 218–227.

4. Schreiber, S. L., "Target-oriented and diversity-oriented organic synthesis in drug discovery." *Science* **2000**, *287*, 1964–1969.

5. Beeler, A. B., Schaus, S. E., Porco, Jr., J. A., "Chemical library synthesis using convergent approaches." *Curr. Opin. Chem. Biol.* **2005**, *9*, 277–284.

6. Chen, Y., Bilban, M., Foster, C. A., Boger, D. L., "Solution-phase parallel synthesis of a pharmacophore library of HUN-7293 analogues: a general chemical mutagenesis approach to defining structure-function properties of naturally occurring cyclic (depsi)peptides." *J. Am. Chem. Soc.* **2002**, *124*, 5431–5440.

7. Boger, D. L., Chai, W., Jin, Q., "Multistep convergent solution-phase combinatorial synthesis and deletion synthesis deconvolution." *J. Am. Chem. Soc.* **1998**, *120*, 7220–7225.

8. Tong, G., Nielsen, J., "A convergent solid-phase synthesis of actinomycin analogues – towards implementation of double-combinatorial chemistry." *Bioorg. Med. Chem.* **1996**, *4*, 693–698.

9. Nielsen, J., Jensen, F. R., "Solid-phase synthesis of small molecule libraries using double combinatorial chemistry." *Tetrahedron Lett.* **1997**, *38*, 2011–2014.

10. Bianchi, I., La Porta, E., Barlocco, D., Raveglia, L. F., "Solid-phase convergent synthesis of benzimidazolone library via the combination of two smaller arrays of carboxylic acids and secondary amines." *J. Comb. Chem.* **2004**, *6*, 835–845.

11. Chen, C., Li, X., Neumann, C. S., Lo, M. M-C., Schreiber, S. L., "Convergent diversity-oriented synthesis of small-molecule hybrids." *Angew. Chem. Int. Ed.* **2005**, *44*, 2–4.

12. Rebek, Jr., J., "Mechanistic studies using solid supports: the three-phase test." *Tetrahedron* **1979**, *35*, 723–731.

13. Rebek, Jr., J., Gaviña, F., Navarro, C., "The three-phase test: intermediates in phosphate transfer reactions." *J. Am. Chem. Soc.* **1978**, *100*, 8113–8117.

14. Rebek, Jr., J., Gaviña, F., "Three-phase test. Detection of free cyclobutadiene." *J. Am. Chem. Soc.* **1975**, *97*, 3453–3456.

15. Rebek, Jr., J., Brown, D., Zimmerman, S., "The three-phase test for reaction intermediates. Nucleophilic catalysis and elimination reactions." *J. Am. Chem. Soc.* **1975**, *97*, 454–455.

16. Hamuro, Y., Scialdone, M. A., DeGrado, W. F., "Resin-to-resin acyl- and aminoacyl-transfer reactions using oxime supports." *J. Am. Chem. Soc.* **1999**, *121*, 1636–1644.

17. Gravel, M., Thompson, K. A., Zak, M., Bérubé, C., Hall, D. G., "Universal solid-phase approach for the immobilization, derivatization, and resin-to-resin transfer reactions of boronic acids." *J. Org. Chem.* **2002**, *67*, 3–15.

18. Gravel, M., Bérubé, C., Hall, D. G., "Resin-to-resin Suzuki coupling of solid supported arylboronic acids." *J. Comb. Chem.* **2000**, *2*, 228–231.

19. Tulla-Puche, J., Barany, G., "Development of resin-to-resin transfer reactions (RRTR) using Sonogashira chemistry." *Tetrahedron* **2005**, *61*, 2195–2201.

20. A similar approach: Hari, A., Miller, B. L., "Segregation of separate steps in chromium-catalyzed reactions for convenience and mechanistic analysis." *Org. Lett.* **2000**, *2*, 691–693.

21. Grubbs, R. H., "Handbook of Metathesis." Wiley-VCH, Weinheim, Germany, 2003.

22. Nicolaou, K. C., Bulger, P. G., Sarlah, D., "Metathesis reactions in total synthesis." *Angew. Chem. Int. Ed.* **2005**, *44*, 4490–4527.

23. Koide, K., Finkelstein, J. M., Ball, Z., Verdine, G. L., "A synthetic library of cell-permeable molecules." *J. Am. Chem. Soc.* **2001**, *123*, 398–408.

24. Nicolaou, K. C., Winssinger, N., Pastor, J., Ninkovic, S., Sarabia, F., He, Y., Vourloumis, D., Yang, Z., Li, T., Giannakakou, P., Hamel, E., "Synthesis of epithilones A and B in solid and solution phase." *Nature* **1997**, *387*, 268–272.

25. van Maarseveen, J. H., den Hartog, J. A. J., Engelen, V., Finner, E., Visser, G., Kruse, C. G., "Solid phase ring-closing metathesis: cyclization/cleavage approach towards a seven membered cycloolefin." *Tetrahedron Lett.* **1996**, *37*, 8249–8252.

26. Miller, S. J., Blackwell, H. E., Grubbs, R. H., "Application of ring-closing metathesis to the synthesis of rigidified amino acids and peptides." *J. Am. Chem. Soc.* **1996**, *118*, 9606–9614.

27. Poeylaut-Palena, A., Testero, S. A., Mata, E. G., "Solid-supported cross metathesis and the role of the homodimerization of the non-immobilized olefin." *J. Org. Chem.* **2008**, *73*, 2024–2027.

28. Testero, S. A., Mata, E. G., "Synthesis of 3-(aryl)alkenyl-*β*-lactams by an efficient application of olefin cross-metathesis on solid support." *Org. Lett.* **2006**, *8*, 4783–4786.

29. Chang, S., Na, Y., Shin, H. J., Choi, E., Jeong, L. S., "A short and efficient synthetic approach to hydroxy (*E*)-stilbenoids via solid-phase cross metathesis." *Tetrahedron Lett.* **2002**, *43*, 7445–7448.

30. Schuster, M., Lucas, N., Blechert, S., "Ruthenium-catalyzed cross metathesis binding of functionalized olefins to polystyrene resin *via* a novel allylsilyl linker suitable for electrophilic cleavage." *Chem. Commun.* **1997**, 823–824.

31. Liao, Y., Fathi, R., Yang, Z., "Convergent solid-phase synthesis of symmetric benzo[*b*]furan's dimerizer." *J. Comb. Chem.* **2003**, *5*, 79–81.

32. Olenyuk, B., Jitianu, C., Dervan, P. B., "Parallel synthesis of H-pin polyamides by alkene metathesis on solid phase." *J. Am. Chem. Soc.* **2003**, *125*, 4741–4751.

33. Tang, Q., Wareing, J. R., "Ring-closing metathesis versus cross metathesis of resin-bound olefins." *Tetrahedron Lett.* **2001**, *42*, 1399–1401.

34. Blackwell, H. E., Clemons, P. A., Schreiber, S. L., "Exploiting site-site interactions on solid support to generate dimeric molecules." *Org. Lett.* **2001**, *3*, 1185–1188.

35. Scholl, M., Ding, S., Lee, C. W., Grubbs, R. H., "Synthesis and activity of a new generation of ruthenium-based olefin metathesis catalysts coordinated with 1,3-dimesityl-4,5-dihydroimidazol-2-ylidene ligands." *Org. Lett.* **1999**, *1*, 953–956.

36. Kingsbury, J. S., Harrity, J. P. A., Bonitatebus, Jr., P. J., Hoveyda, A. H., "A recyclable Ru-based metathesis catalyst." *J. Am. Chem. Soc.* **1999**, *121*, 791–799.

37. Garber, S. B., Kingsbury, J. S., Gray, B. L., Hoveyda, A. H., "Efficient and recyclable monomeric and dendritic Ru-based metathesis catalysts." *J. Am. Chem. Soc.* **2000**, *122*, 8168–8179.

38. Grela, K., Harutyunyan, S., Michrowska, A., "A highly efficient ruthenium catalyst for metathesis reactions." *Angew. Chem. Int. Ed.* **2002**, *41*, 4038–4040.

39. Michrowska, A., Bujok, R., Harutyunyan, S., Sashuk, V., Dolgonos, G., Grela, K., "Nitro-substituted Hoveyda-Grubbs ruthenium carbenes: enhancement of catalyst activity through electronic activation." *J. Am. Chem. Soc.* **2004**, *126*, 9318–9325.

40. Chatterjee, A. K., Choi, T-L., Sanders, D. P., Grubbs, R. H., "A general model for selectivity in olefin cross metathesis." *J. Am. Chem. Soc.* **2003**, *125*, 11360–11370.

41. Pannifer, A. D., Wong, T. Y., Schwarzenbacher, R., Renatus, M., Petosa, C., Bienkowska, J., Lacy, D. B., Collier, R. J., Park. S., Leppla, S. H., Hanna, P., Liddington, R. C., "Crystal structure of the anthrax lethal factor." *Nature* **2001**, *414*, 229–233.

42. Garner, A. L., Koide, K., "Solid-phase olefin cross-metathesis promoted by a linker." *Org. Lett.* **2007**, *9*, 5235–5238.

43. White, N. J., "The treatment of malaria." *New Engl. J. Med.* **1996**, *335*, 800–806.

44. Fürstner, A., Langemann, K., "Total syntheses of (+)-ricinelaidic acid lactone and of (-)-gloeosporone based on transition-metal-catalyzed C-C bond formations." *J. Am. Chem. Soc.* **1997**, *119*, 9130–9136.

45. Yan, B., Sun, Q., "Crucial factors regulating site interactions in resin supports determined by single bead IR." *J. Org. Chem.* **1998**, *63*, 55–58.

46. Li, W., Yan, B., "Effects of polymer supports on the kinetics of solid-phase organic reactions: a comparison of polystyrene- and TentaGel-based resins." *J. Org. Chem.* **1998**, *63*, 4092–4097.

47. Sarin, V. K., Kent, S. B. H., Mitchell, A. R., Merrifield, R. B., "A general approach to the quantification of synthetic efficiency in solid-phase peptide synthesis as a function of chain length." *J. Am. Chem. Soc.* **1984**, *106*, 7845–7850.

48. O'Leary, D. J., Blackwell, H. E., Washenfelder, R. A., Grubbs, R. H., "A new method for cross-metathesis of terminal olefins." *Tetrahedron Lett.* **1998**, *39*, 7427–7430.

49. Blackwell, H. E., O'Leary, D. J., Chatterjee, A. K., Washenfelder, R. A., Bussmann, D. A., Grubbs, R. H., "New approaches to olefin cross-metathesis." *J. Am. Chem. Soc.* **2000**, *122*, 58–71.

50. Czarnik, A. W., "Solid-phase synthesis supports are like solvents." *Biotechnol. Bioeng.* **1998**, *61*, 77–79.

51. Brittain, D. E. A., Gray, B. L., Schreiber, S. L., "From solution-phase to solid-phase enyne metathesis: crossover in the relative performance of two commonly used ruthenium pre-catalysts." *Chem. Eur. J.* **2005**, *11*, 5086–5093.

52. Tallarico, J. A., Depew, K. M., Pelish, H. E., Westwood, N. J., Lindsley, C. W., Shair, M. D., Schreiber, S. L., Foley, M. A., "An alkylsilyl-tethered, high-capacity solid support amenable to diversity-oriented synthesis for one-bead, one-stock solution chemical genetics." *J. Comb. Chem.* **2001**, *3*, 312–318.

53. Vaino, A. R., Janda, K. D., "Solid-phase organic synthesis: a critical understanding of the resin." *J. Comb. Chem.* **2000**, *2*, 579–596.

54. Rentsch, D., Hany, R., Barthélémy, S., Steinauer, R., "Improved reproducibility of chemical reactions on purified polystyrene resins monitored by ^{31}P MAS NMR." *Tetrahedron Lett.* **2003**, *44*, 6987–6990.

55. Nouvet, A., Lamaty, F., Lazaro, R., "Efficient synthesis of bromoacetylated wang resin." *Tetrahedron Lett.* **1998**, *39*, 3469–3470.

56. Rinnová, M., Vidal, A., Nefzi, A., Houghten, R. A., "Solid-phase synthesis of 1,2,5-trisubstituted 4-imidazolidinones." *J. Comb. Chem.* **2002**, *4*, 209–213.

57. Kaiser, E., Colescott, R. L., Bossinger, D., Cook, P. I., "Color test for detection of free terminal amino groups in the solid-phase synthesis of peptides." *Anal. Biochem.* **1970**, *34*, 595–598.

58. Genet, J. P., Balabane, M., Legras, Y., "Alkylation catalysees par 6 palladium des monoacetates du butene-2-diol-1,4 et de l'hexene-3-diols-2,5. Synthese d'hydroxy-6-alkenoates (*E*) ou (*Z*)." *Tetrahedron Lett.* **1982**, *23*, 331–334.

59. Wu, Z., Minhas, G. S., Wen, D., Jiang, H., Chen, K., Zimniak, P., Zheng, J., "Design, synthesis, and structure-activity relationship of haloenol lactones: site-directed and isozyme-selective glutathione *S*-transferase inhibitor." *J. Med. Chem.* **2004**, *47*, 3282–3294.

60. Turnbull, M. D., "Productivity in synthesis: a mixture protocol to raise compound output is demonstrated for asymmetric cyclopronation of allyl alcohols." *J. Chem. Soc., Perkin Trans. 1* **1997**, *8*, 1241–1248.

61. Olafsdottir, E. S., Jorgensen, L. B., Jaroszewski, J. W., "Substrate specificity in the biosynthesis of cyclopentanoid cyanohydrin glucosides." *Phytochem*. **1992**, *31*, 4129–4134.

62. Trost, B. M., Verhoeven, T. R., "Cyclization catalyzed by palladium(0). Initial studies and macrolide formation." *J. Am. Chem. Soc.* **1980**, *102*, 4743–4763.

63. Wang, Z-X., Shi, Y., "A pH study on the chiral ketone catalyzed asymmetric epoxidation of hydroxyalkenes." *J. Org. Chem.* **1998**, *63*, 3099–3104.

64. Breuer, E., Sarel, S., "Homoallylic rearrangement of cyclopropylcarbinyl borates: a stereospecific synthesis of *trans*-4-aryl-3-butenols." *Tetrahedron* **1968**, *24*, 6339–6349.

65. Dardoize, F., Goasdoué, N., Laborit, H. M., Topall, G., "4-Hydroxybutyric acid (and analogues) derivatives of D-glucosamine." *Tetrahedron* **1989**, *45*, 7783–7794.

66. Moore, L. R., Shaughnessy, K. H., "Efficient aqueous-phase Heck and Suzuki couplings of aryl bromide using tri(4,6-dimethyl-3-sulfonatophenyl)phosphine trisodium salt (TXPTS)." *Org. Lett.* **2004**, *6*, 225–228.

67. Kohri, T., Suzuki, M., Nanjo, F., "Identification of metabolites of (-)-epicatechin gallate and their metabolic fate in the rat." *J. Agric. Food Chem.* **2003**, *51*, 5561–5566.

68. Owston, N. A., Parker, A. J., Williams, J. M. J., "Highly efficient ruthenium-catalyzed oxime to amide rearrangement." *Org. Lett.* **2007**, *9*, 3599–3601.

69. Imashiro, R., Seki, M., "A catalytic asymmetric synthesis of chiral glycidic acid derivatives through chiral dioxirane-mediated catalytic asymmetric epoxidation of cinnamic acid derivatives." *J. Org. Chem.* **2004**, *69*, 4216–4226.

70. Frangi, Y., Gaudemar, M., "Addition des organozinciques allyliques aux triples liaisons: syntheses d'alcools et d'ethers-oxydes dieniques." *J. Organomet. Chem.* **1977**, *142*, 9–22.

71. Poulsen, S-A., Bornaghi, L. F., Healy, P. C., "Synthesis and structure-activity relationships of novel benzene sulfonamides with potent binding affinity for bovine carbonic anhydrase II." *Bioorg. Med. Chem. Lett.* **2005**, *15*, 5429–5433.

72. Larock, R. C., Stolz-Dunn, S. K., "Highly stereoselective synthesis of di- and trisubstituted homoallylic alcohols via palladium(0)-catalyzed nucleophilic opening of vinylic oxetanes." *Tetrahedron Lett.* **1989**, *30*, 3487–3490.

73. Rustaiyan, A., Jakupovic, J., Chau-Thi, T. V., Bohlmann, F., Sadjadi, A., "Further sesquiterpene lactones from the genus *Dittrichia*." *Phytochemistry* **1987**, *26*, 2603–2606.

74. Chazin, W. J., Colebrook, L. D., "Use of proton spin-lattice relaxation and nuclear Overhauser effect data in structure analysis of alkaloids." *J. Org. Chem.* **1986**, *51*, 1243–1253.

75. Díaz-Araúzo, H., Cook, J. M., Christie, D. J., "Synthesis of 10,11-dihydroxydihydroquinidine *N*-oxide, a new metabolite of quinidine. Preparation and ^{1}H-NMR spectroscopy of the metabolites of quinine and quinidine and conformation analysis via 2D COSY NMR spectroscopy." *J. Nat. Pdt.* **1990**, *53*, 112–124.

76. Moreland, C. G., Philip, A., Carroll, F. I., “Carbon-13 nuclear magnetic resonance spectra of cinchona alkaloids.” *J. Org. Chem.* **1974**, *39*, 2413–2416.

APPENDIX A

SYNTHESIS OF PITTSBURGH GREEN AND PITTSBURGH YELLOWGREEN

A.1 ^{1}H NMR AND ^{13}C NMR SPECTROSCOPY

^{1}H NMR spectrum of compound **34**: $CDCl_3$, 293K, 300 MHz

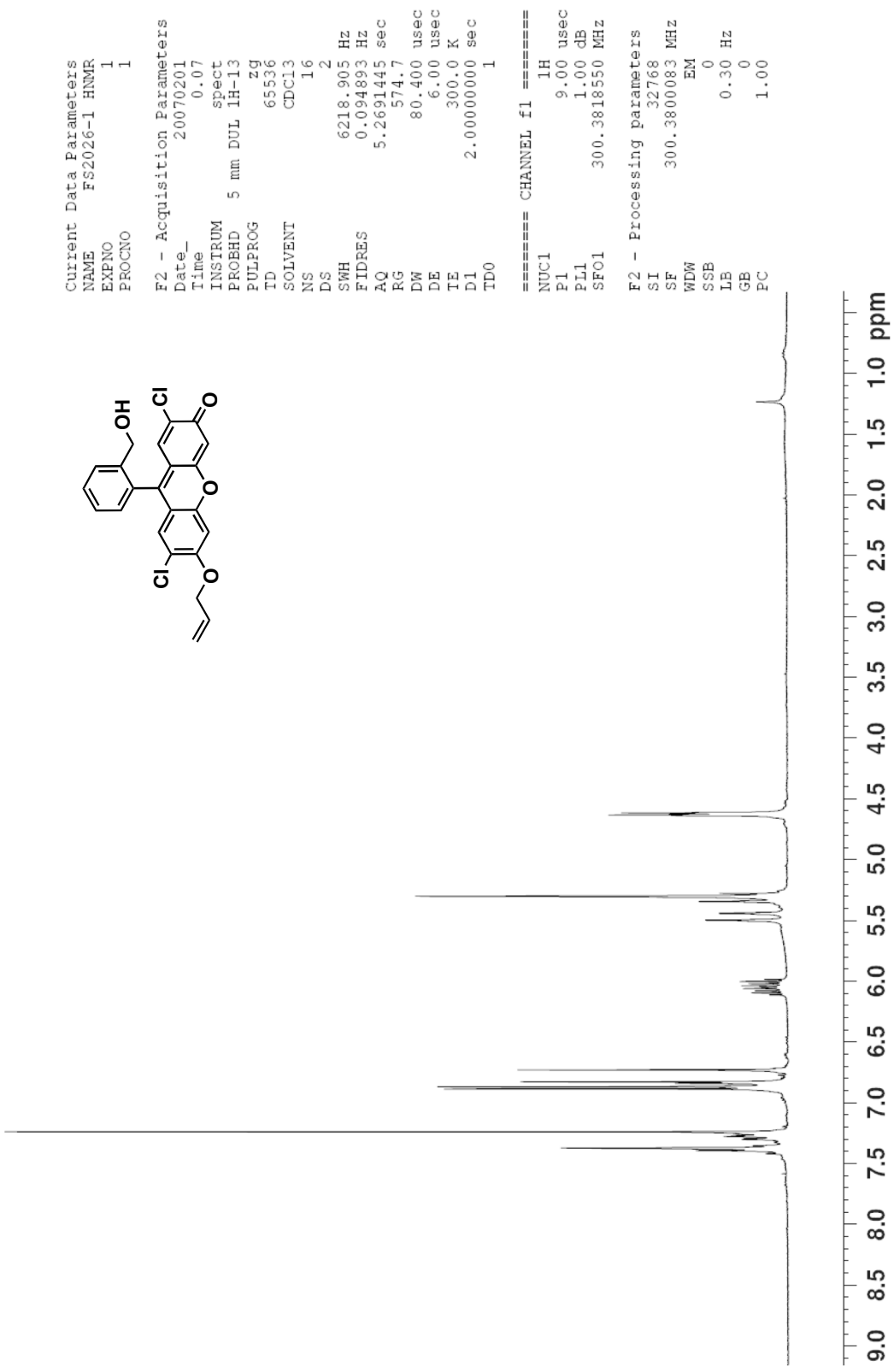

^{13}C NMR spectrum of compound **34**: $CDCl_3$, 293K, 75 MHz

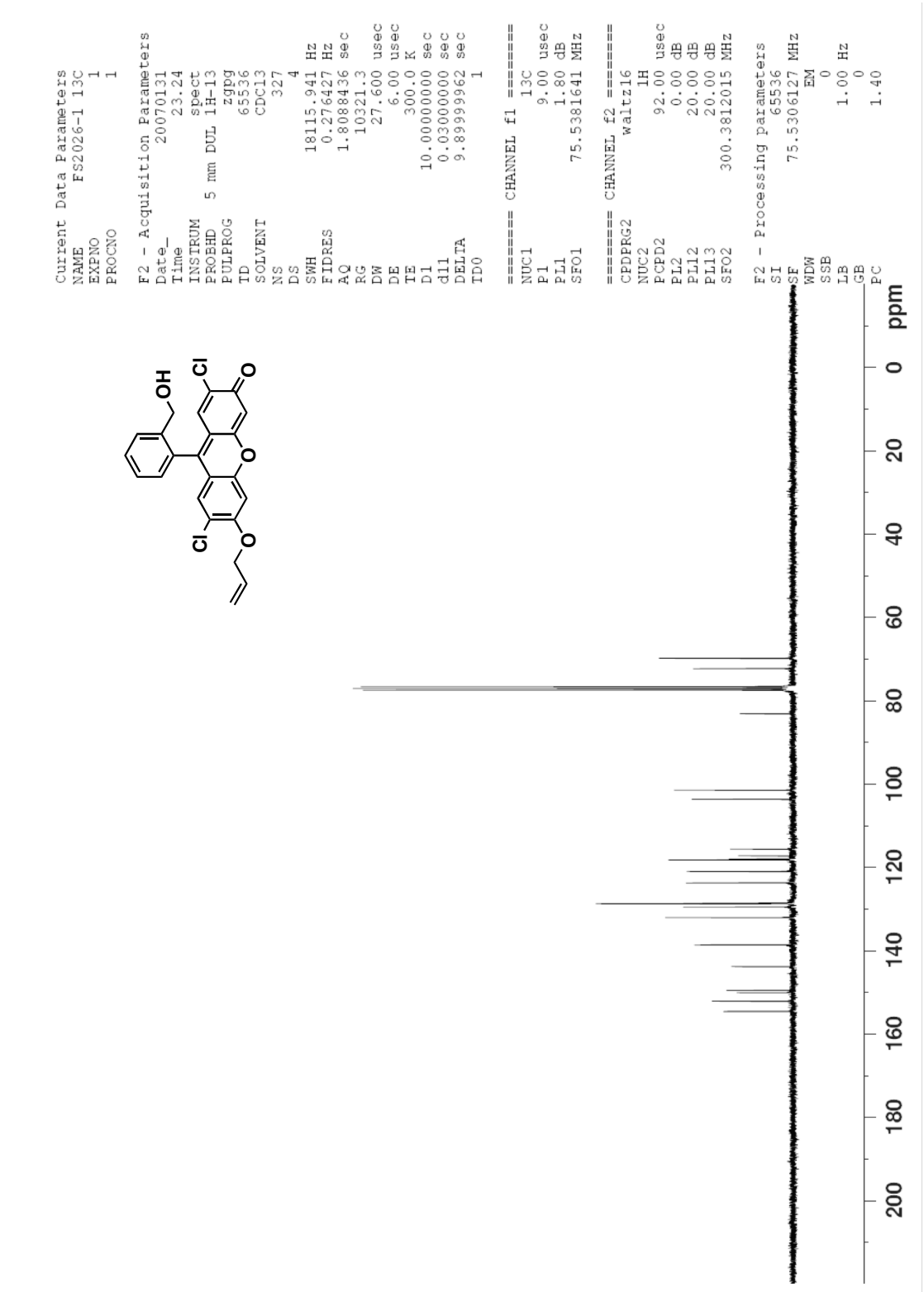

^{1}H NMR spectrum of compound **35**: CD_3OD, 293K, 300 MHz

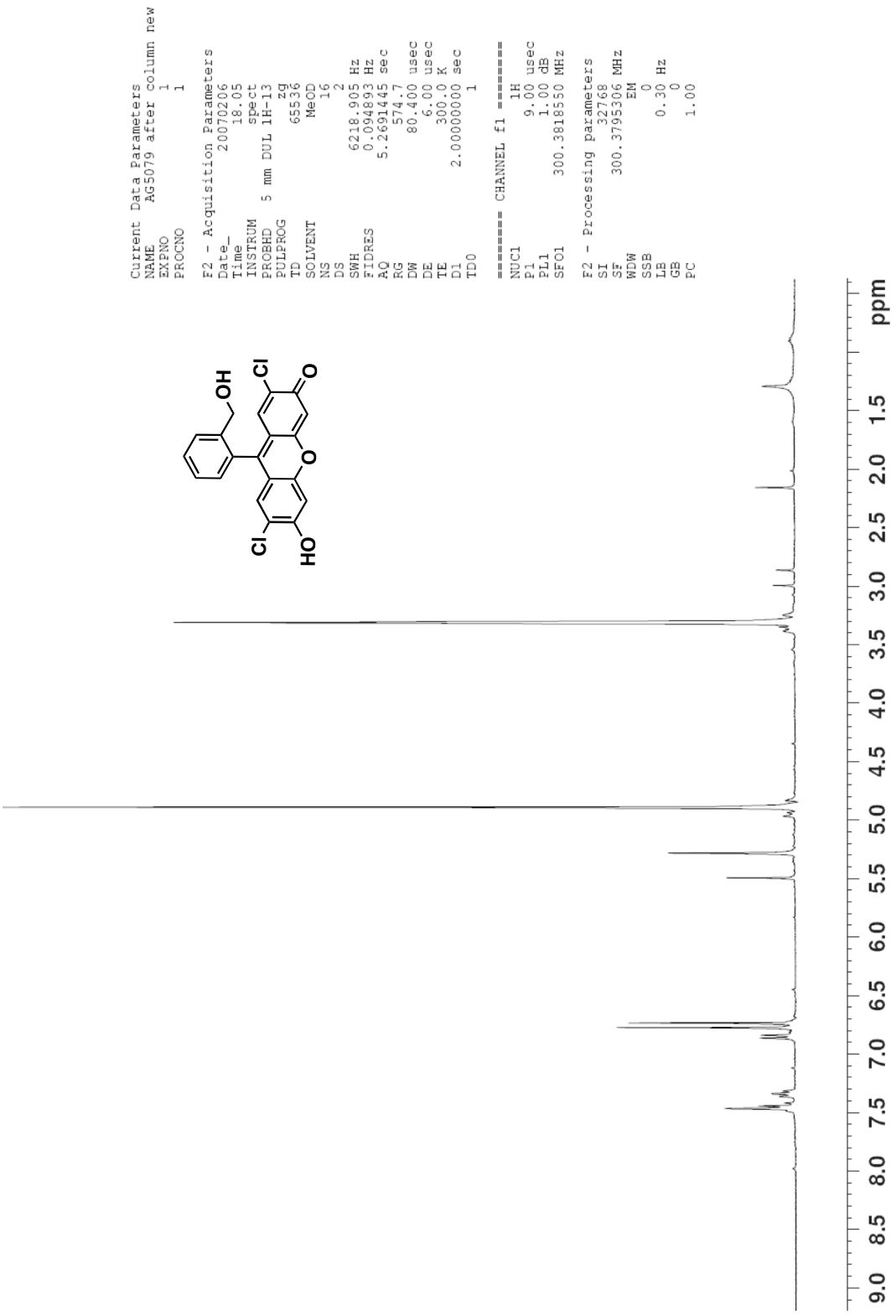

^{13}C NMR spectrum of compound **35**: CD_3OD, 293K, 75 MHz

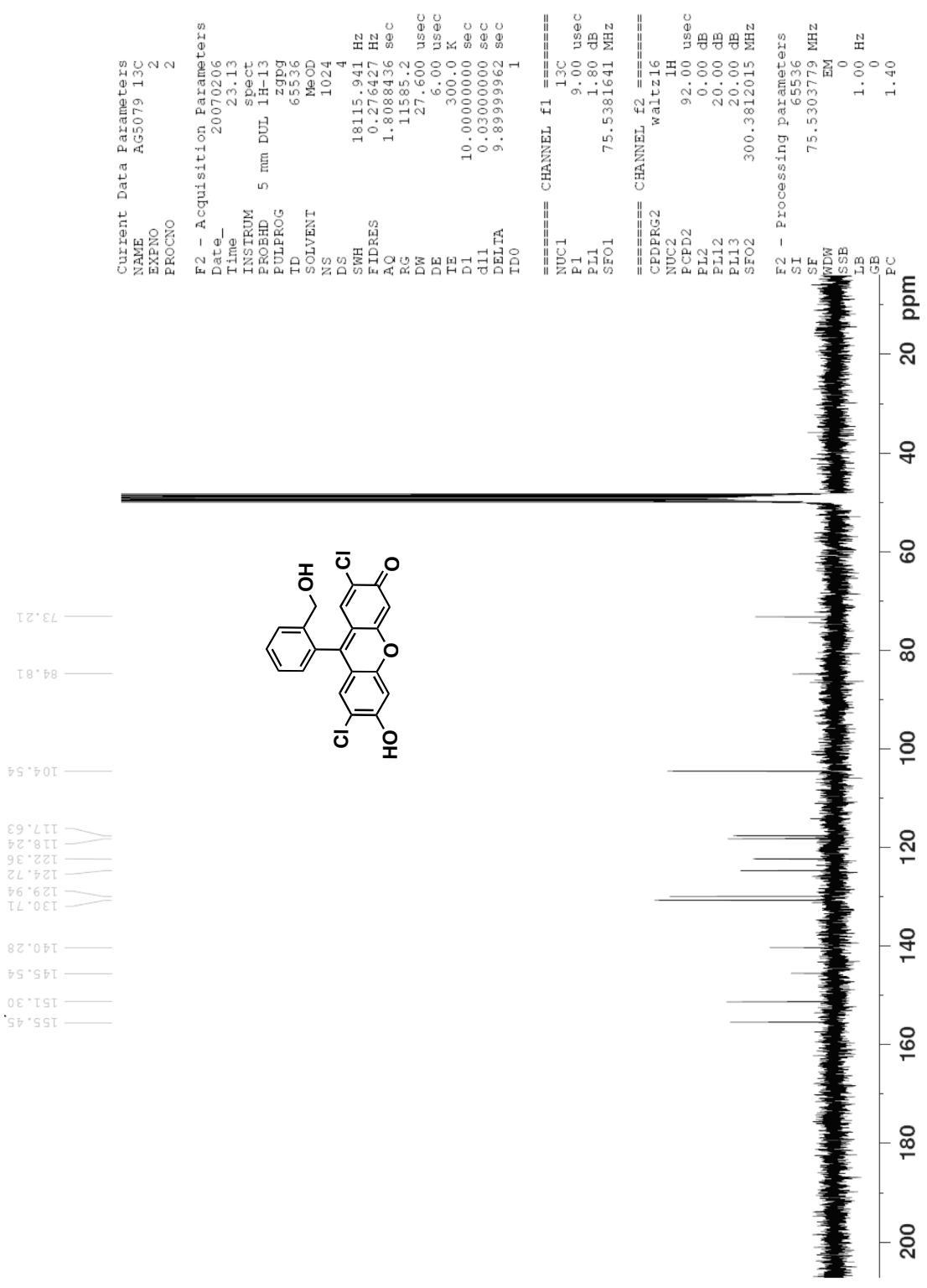

^{1}H NMR spectrum of compound **36**: $CDCl_3$, 293K, 300 MHz

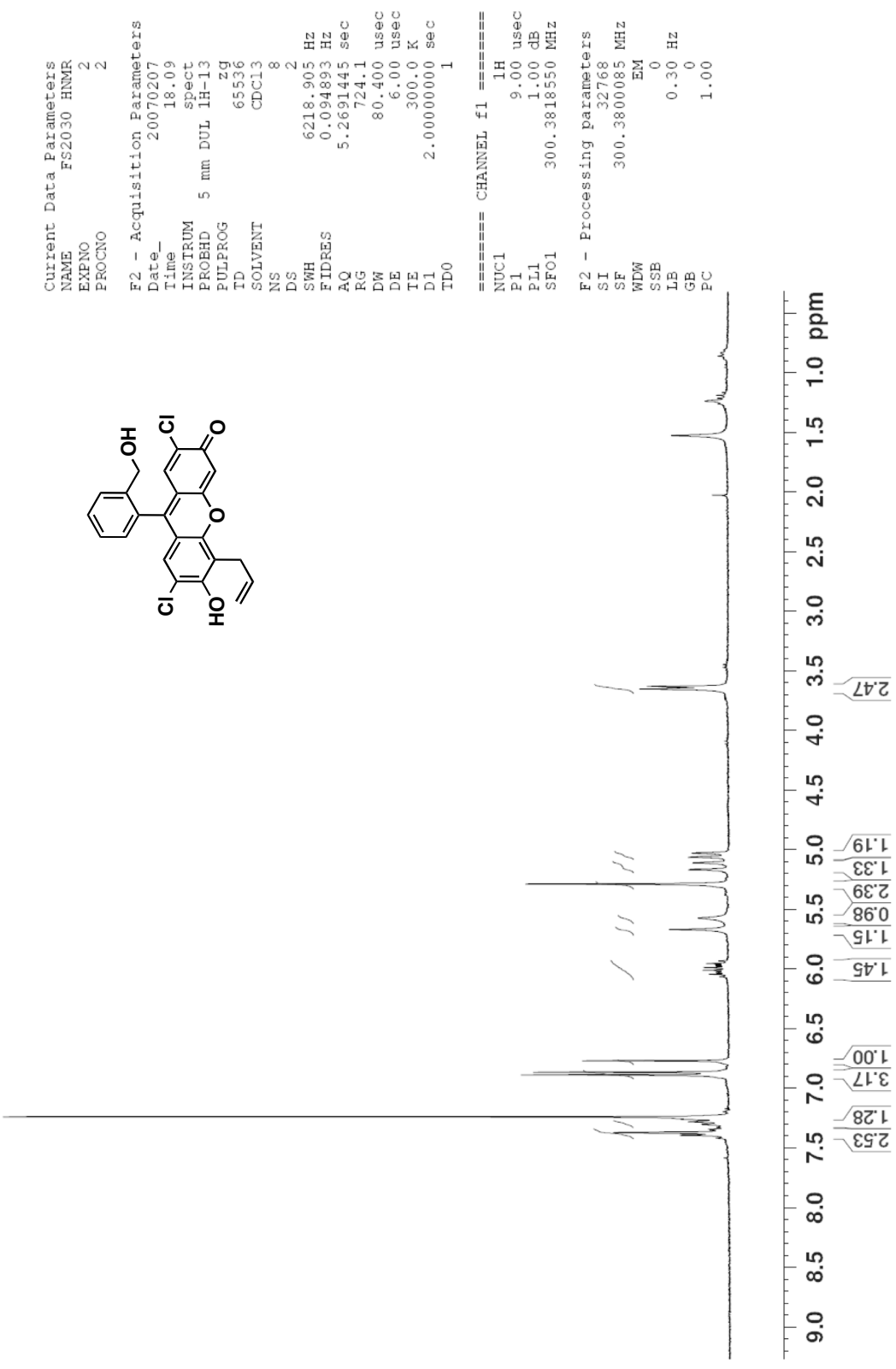

^{13}C NMR spectrum of compound **36**: CD_3OD, 293K, 75 MHz

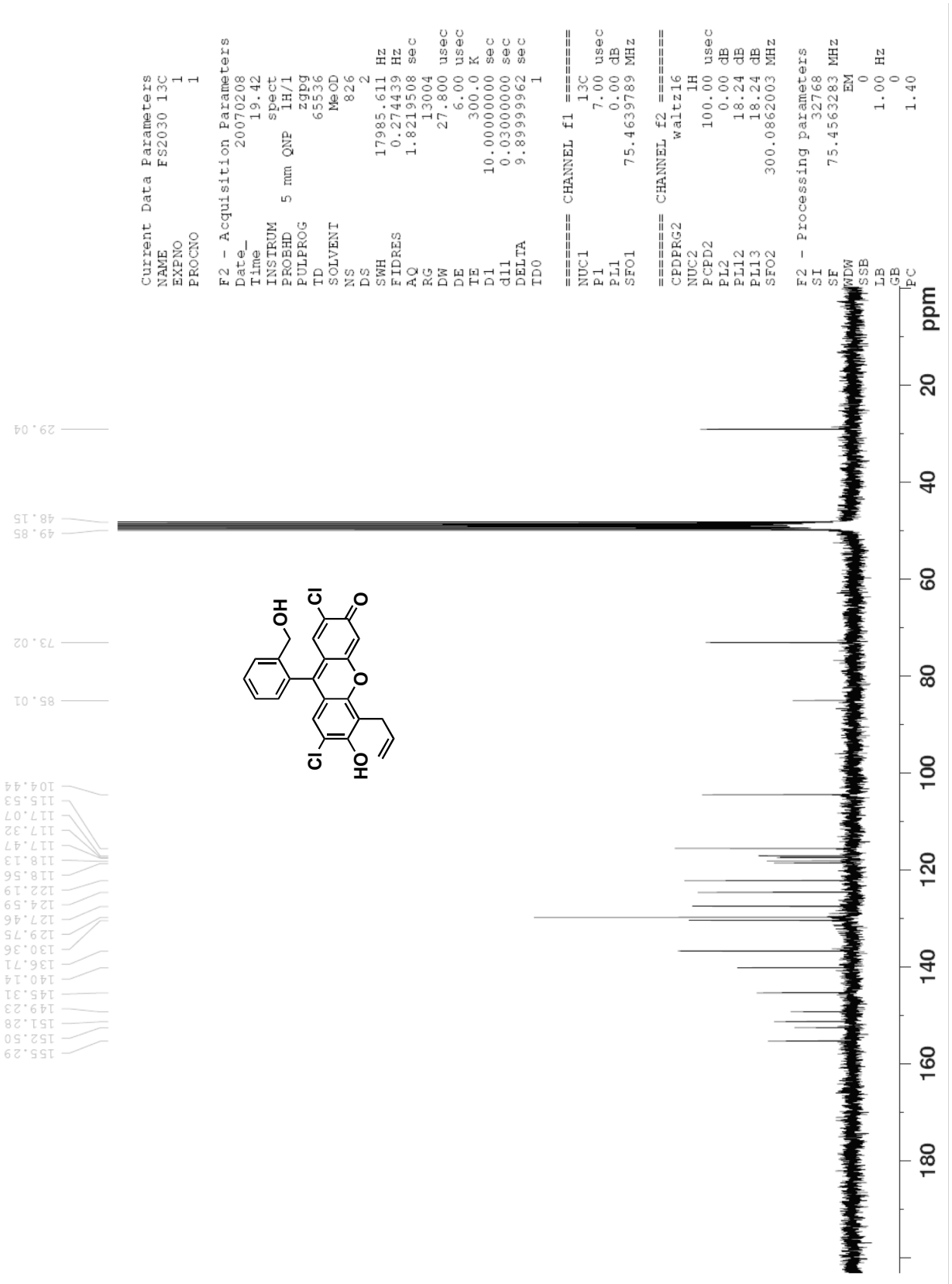

APPENDIX B

SYNTHESIS OF OZONE SENSOR

B.1 ^{1}H NMR AND ^{13}C NMR SPECTRA

^{1}H NMR spectrum of compound **70**: $CDCl_3$, 293K, 300 MHz

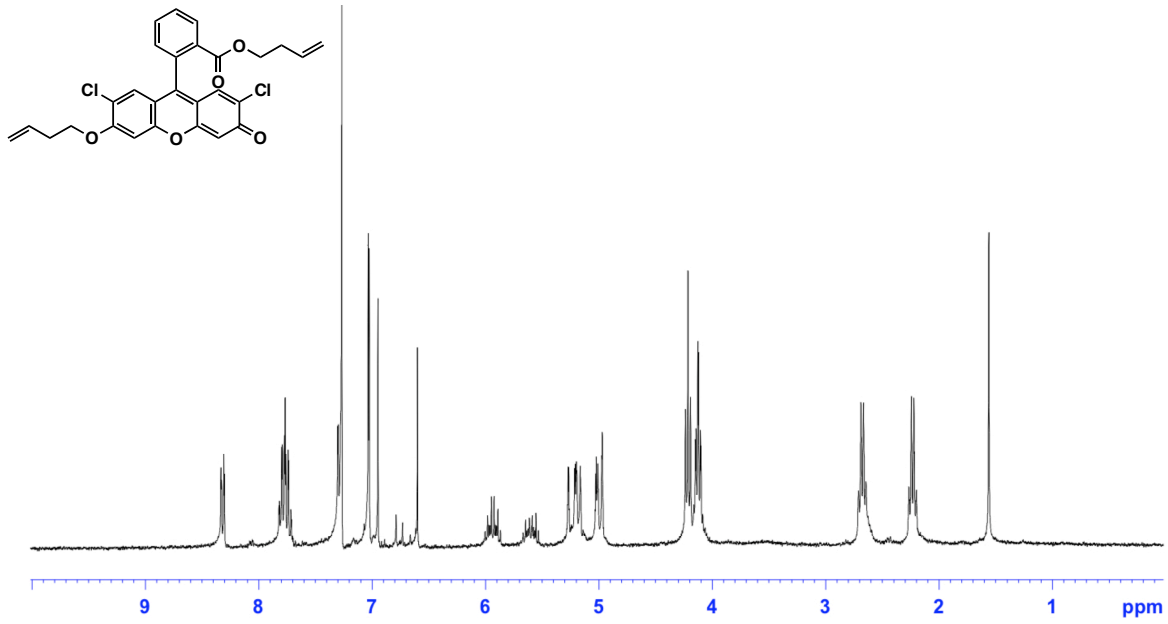

^{13}C NMR spectrum of compound **70**: $CDCl_3$, 293K, 75 MHz

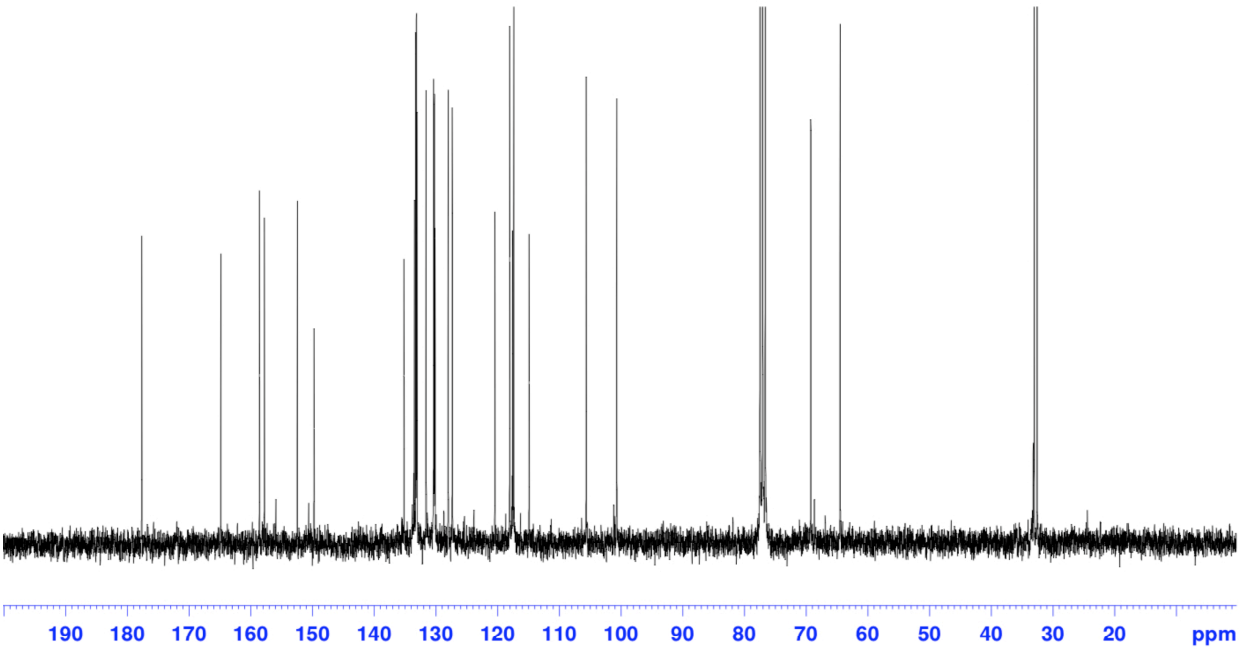

^{1}H NMR spectrum of compound **67**: $CDCl_3$, 293K, 300 MHz

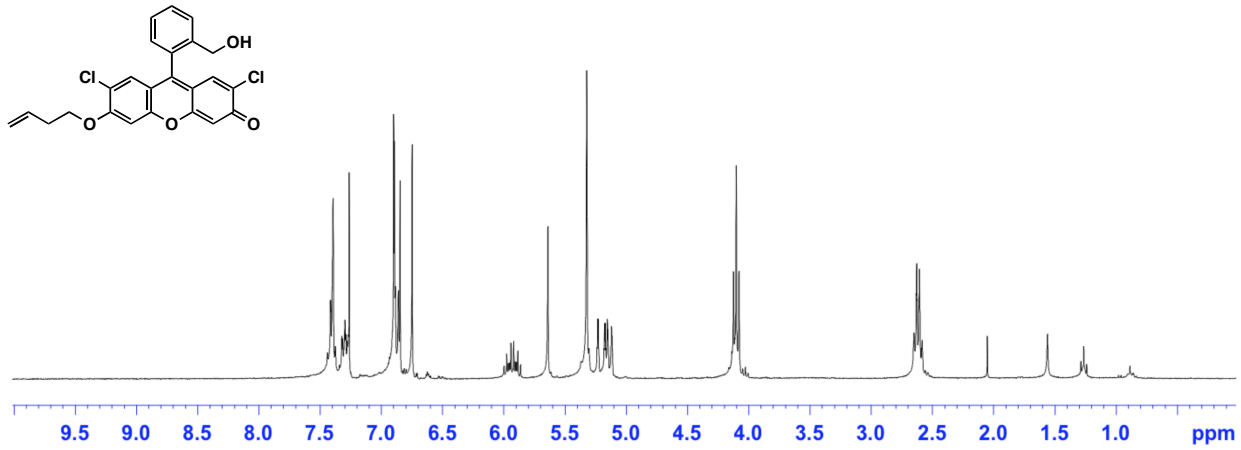

^{13}C NMR spectrum of compound **67**: $CDCl_3$, 293K, 75 MHz

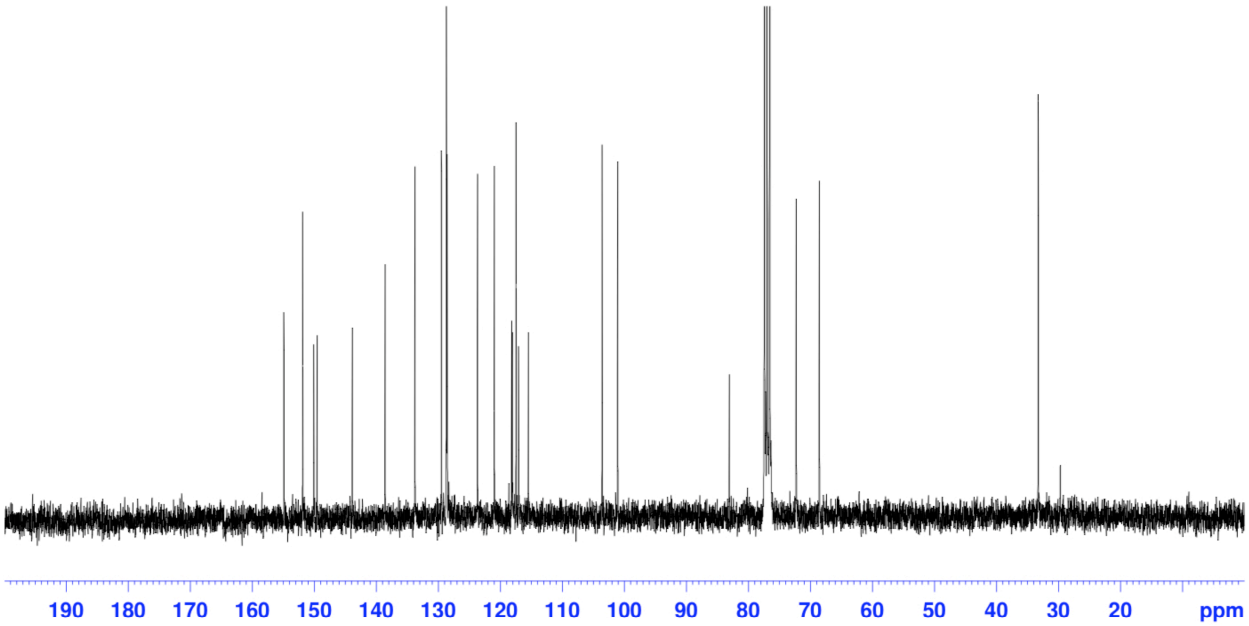

APPENDIX C

RESIN-TO-RESIN OLEFIN CROSS-METATHESIS

C.1 ^{1}H NMR AND ^{13}C NMR SPECTRA AND LC-MS DATA

^{1}H NMR spectrum of compound **143**: 1% CD_3OD in $CDCl_3$, 293K, 300 MHz

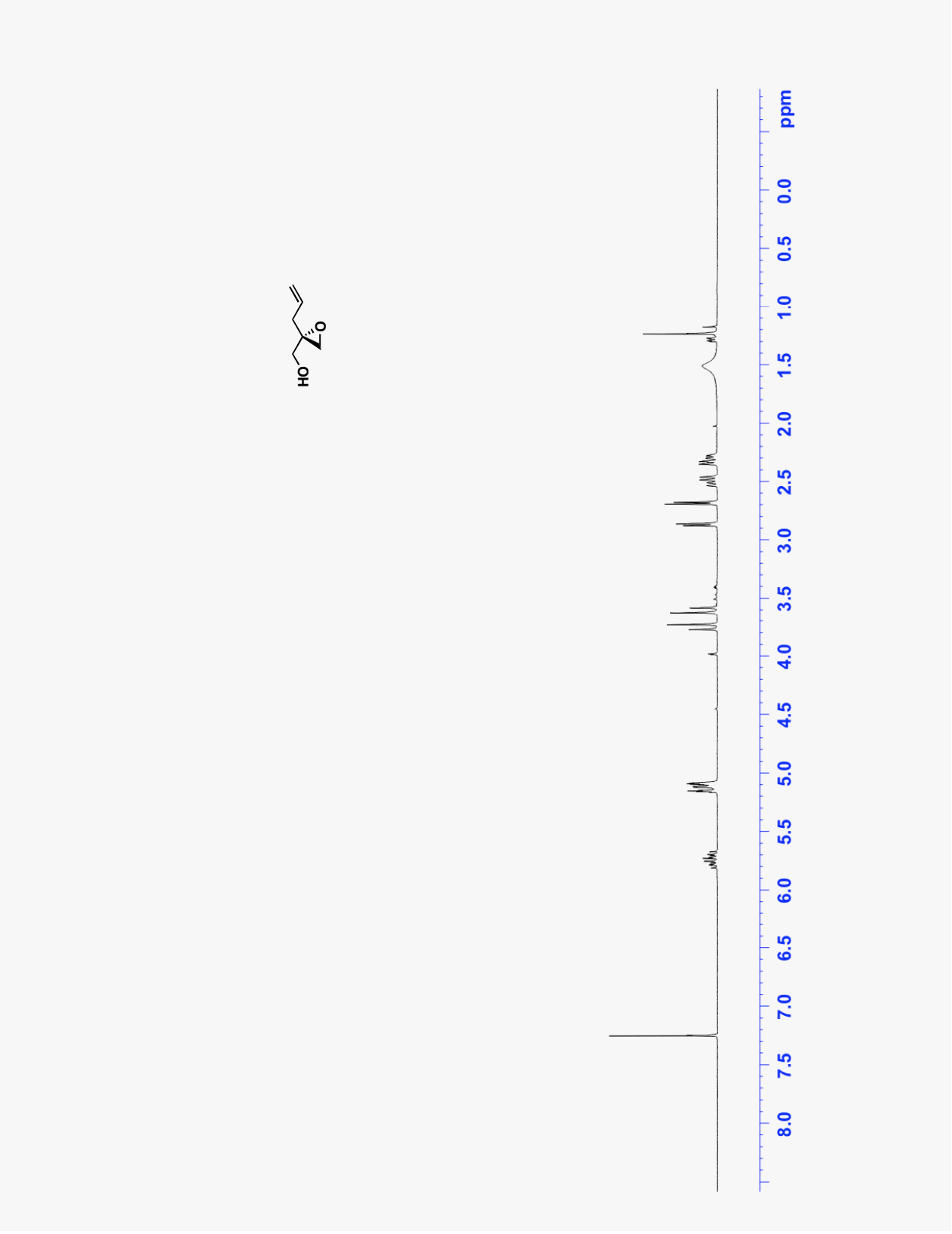

^{13}C NMR spectrum of compound **143**: $CDCl_3$, 293K, 75 MHz

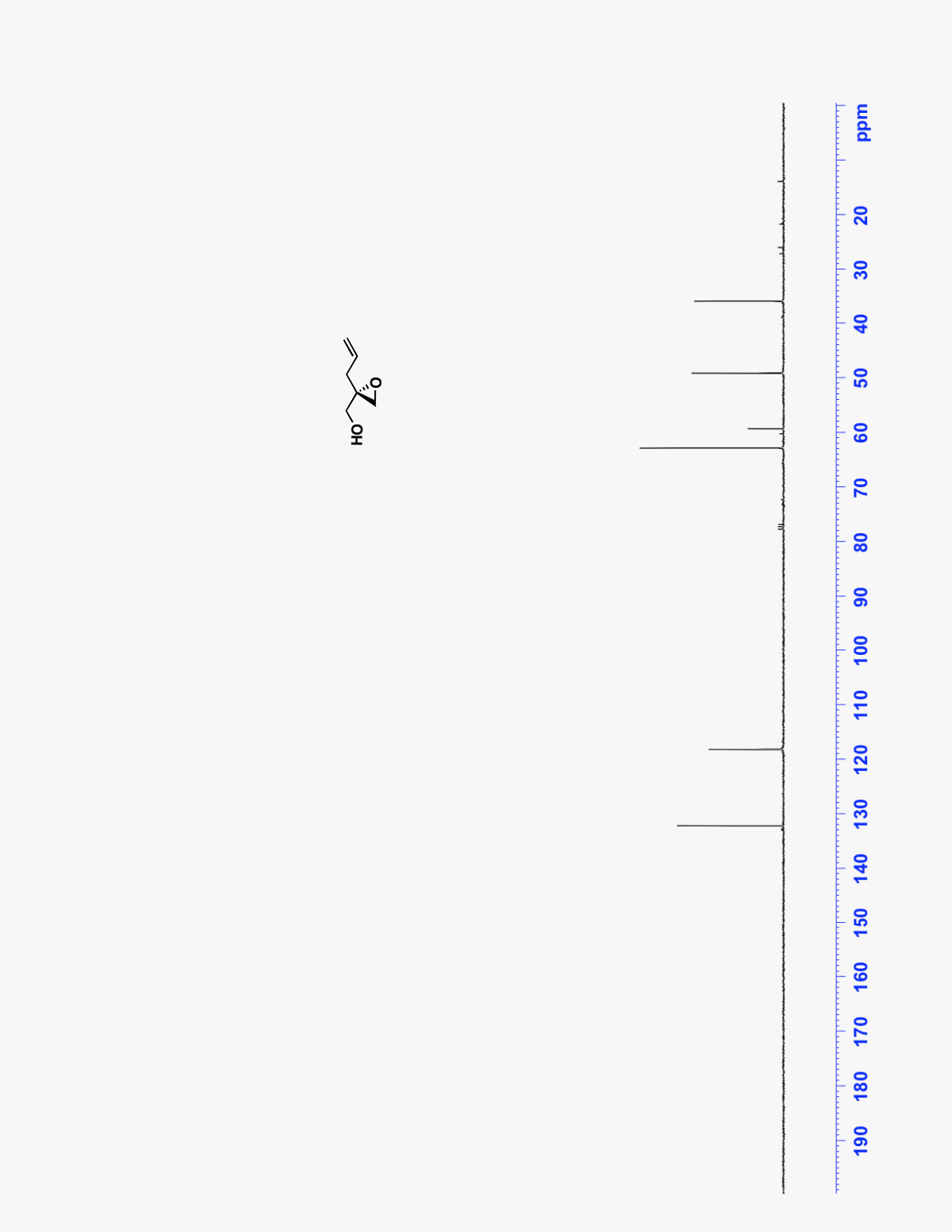

^{1}H NMR spectrum of compound **116'**: CD_3OD, 293K, 300 MHz

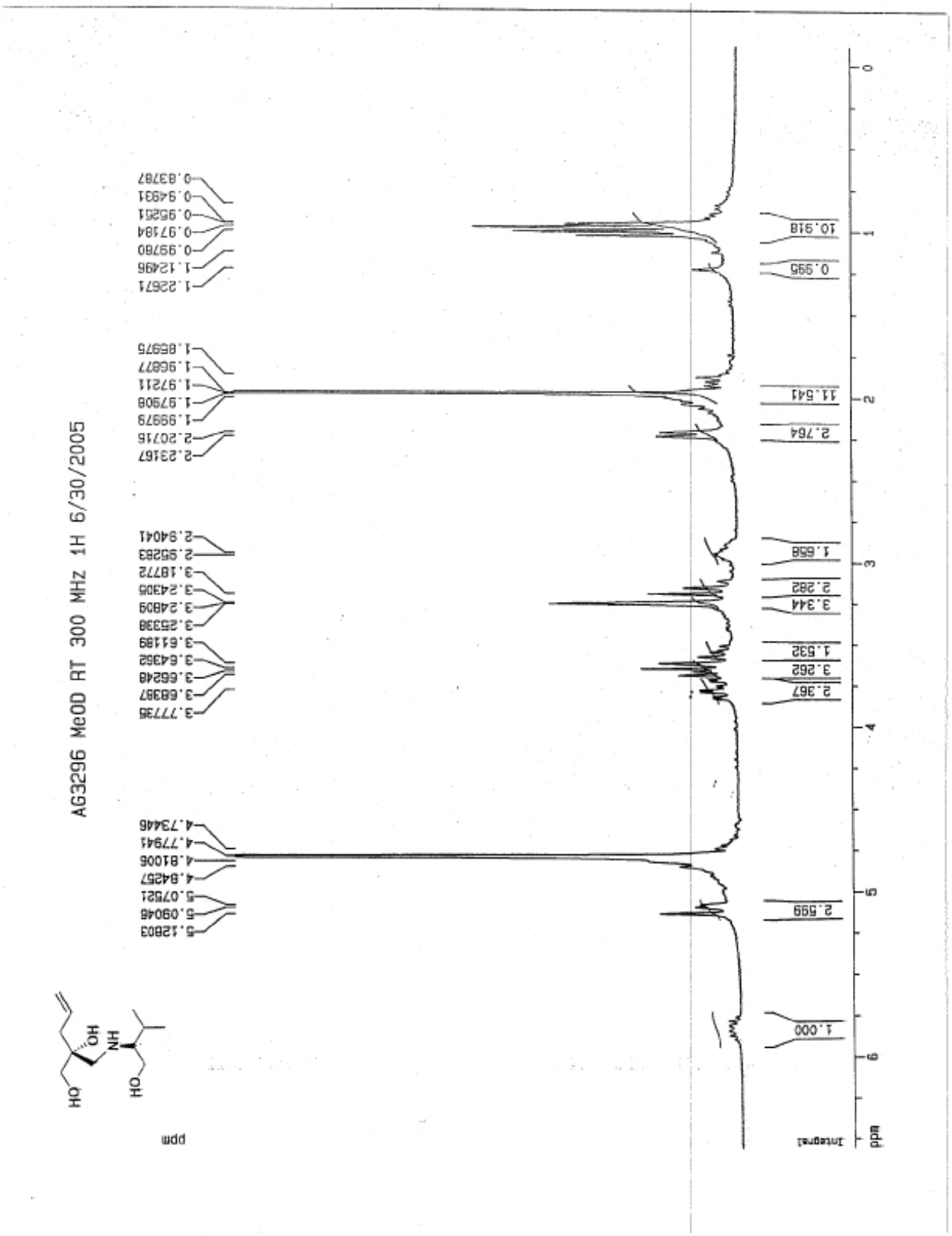

^{13}C NMR spectrum of compound **116'**: CD_3OD, 293K, 75 MHz

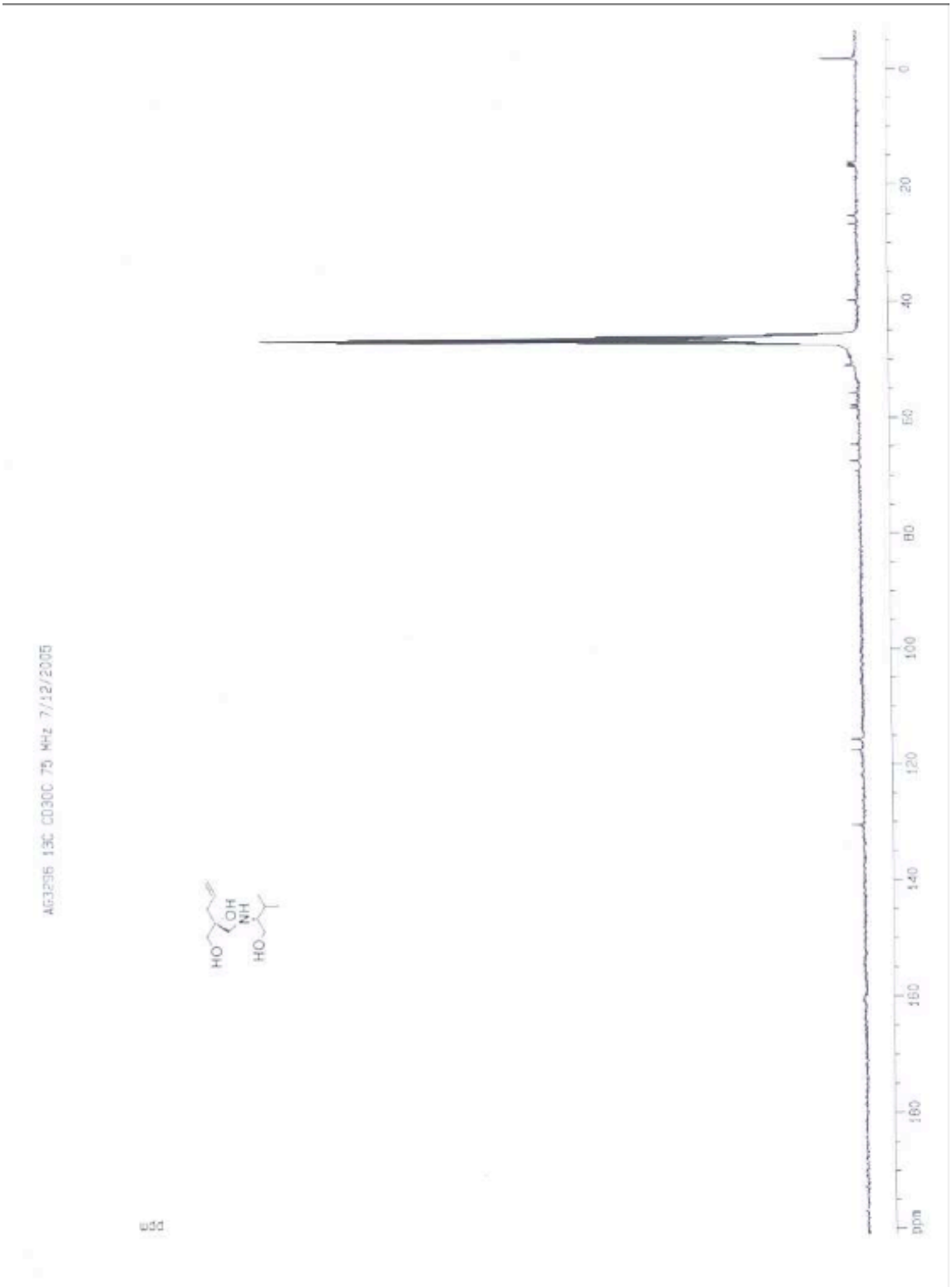

^{1}H NMR spectrum of compound **144**: $CDCl_3$, 293K, 300 MHz

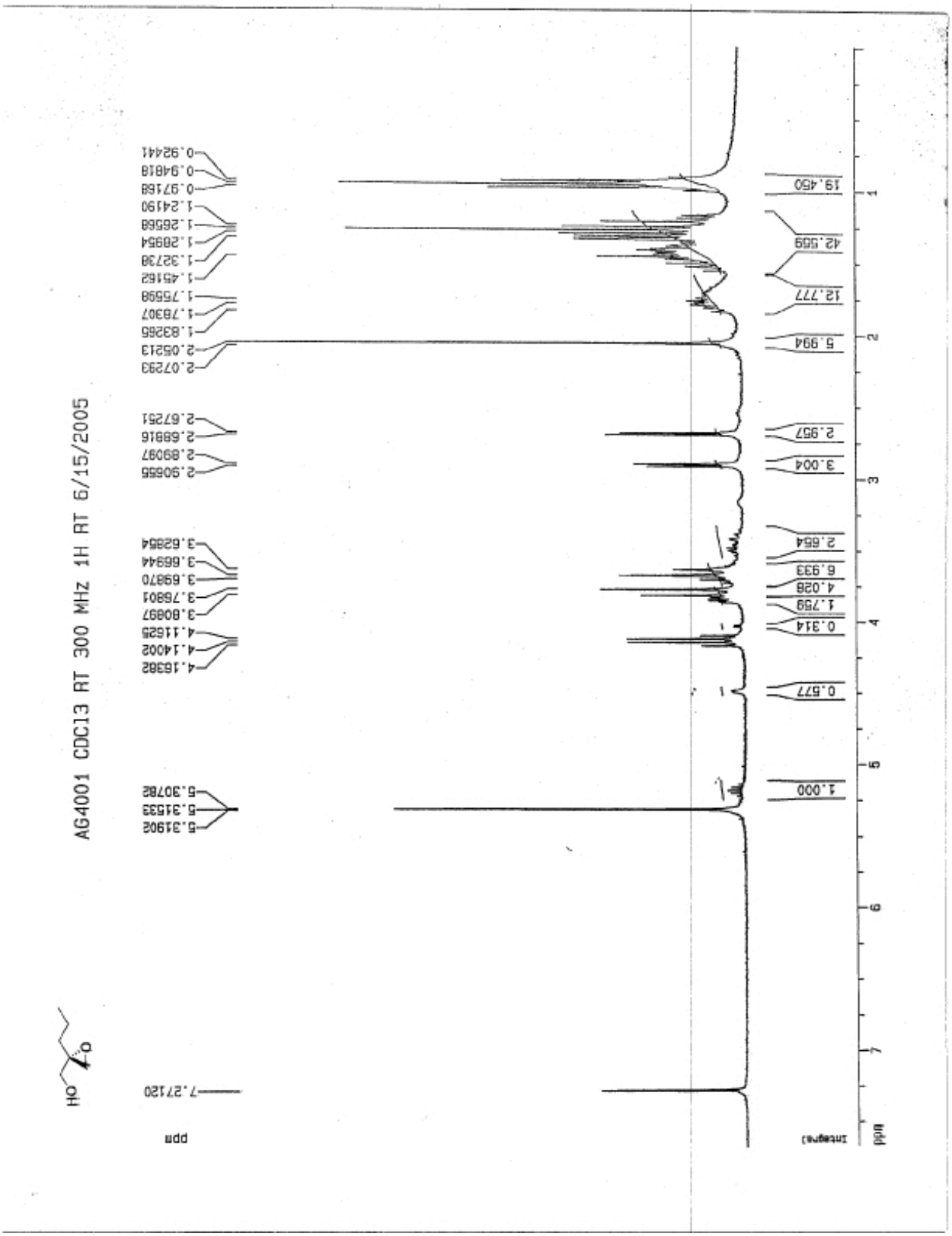

^{13}C NMR spectrum of compound **144**: $CDCl_3$, 293K, 75 MHz

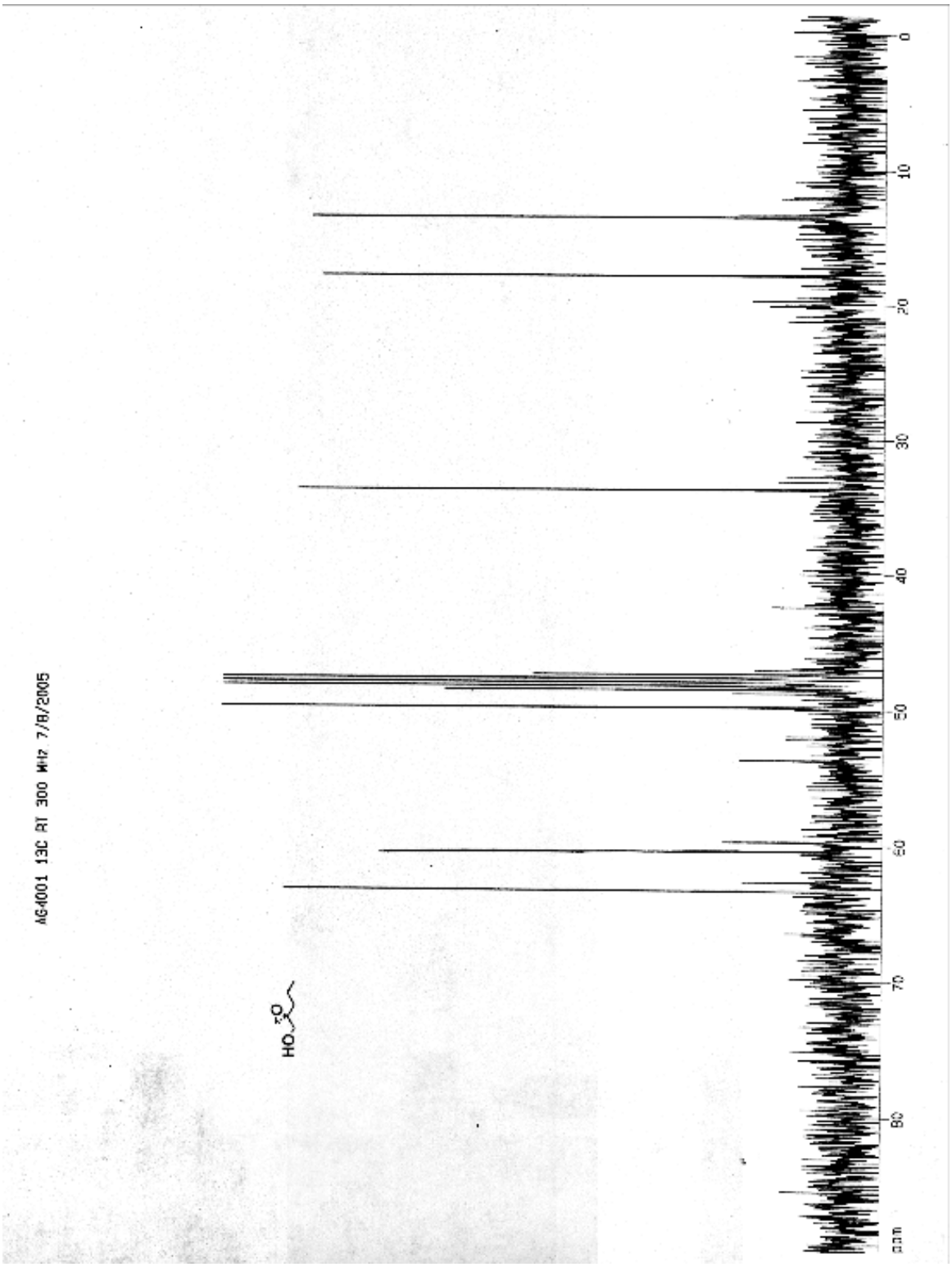

^{1}H NMR spectrum of compound **117'**: CD_3OD, 293K, 300 MHz

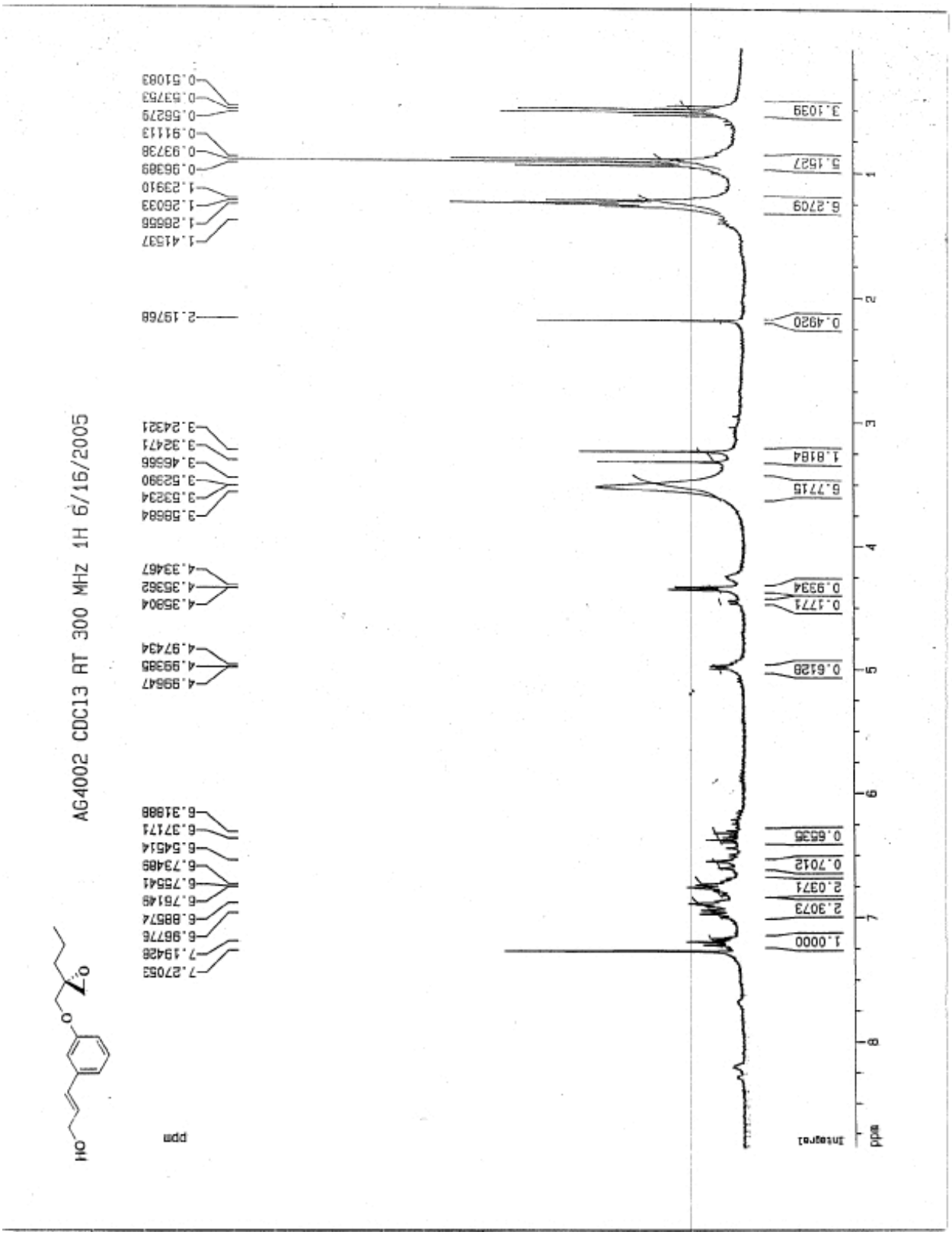

^{13}C NMR spectrum of compound **117'**: CD_3OD, 293K, 75 MHz

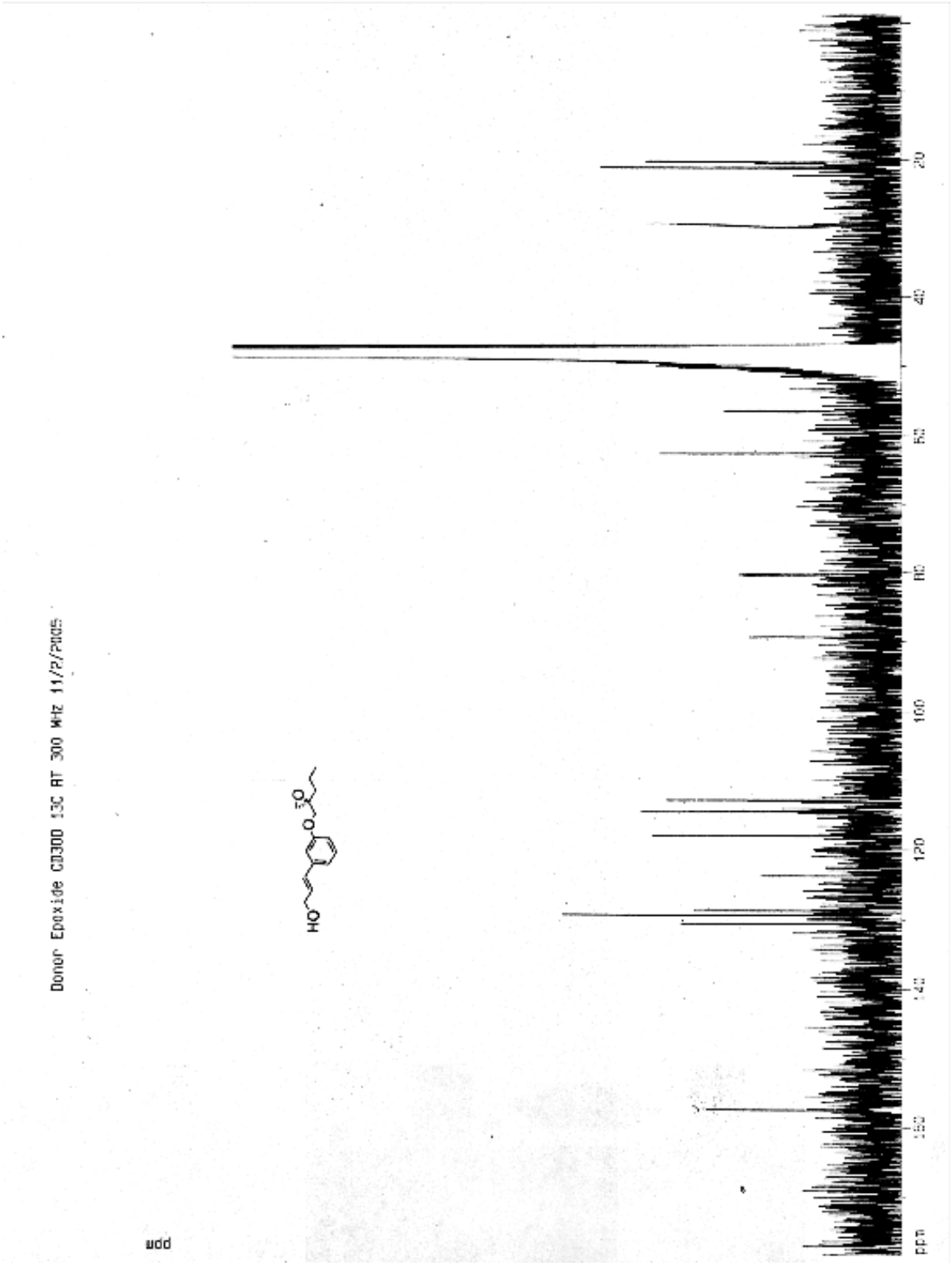

^{1}H NMR spectrum of compound **118'**: CD_3OD, 293K, 300 MHz

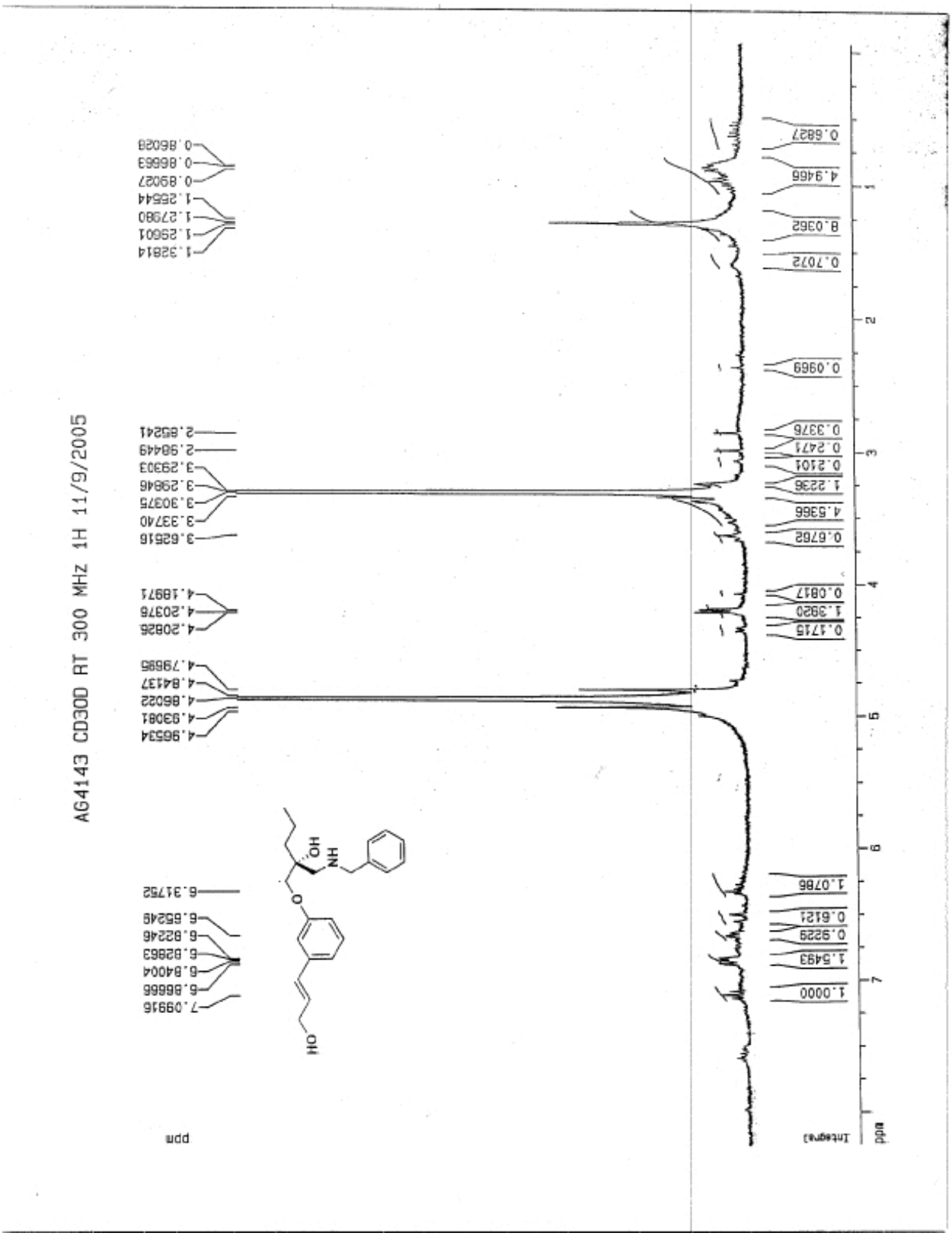

^{13}C NMR spectrum of compound **118'**: CD_3OD, 293K, 75 MHz

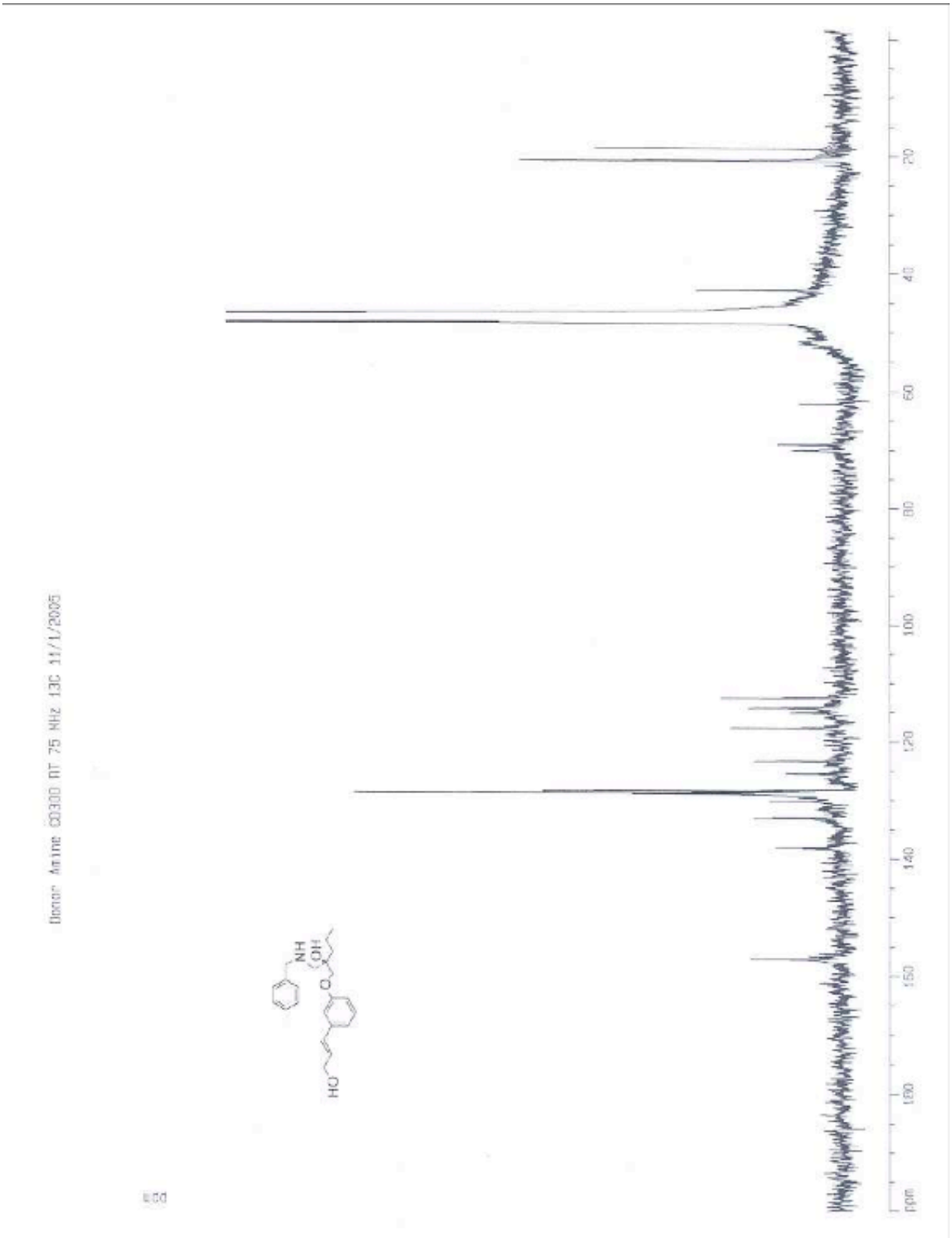

crude ^{1}H NMR spectrum of compound **119**: CD_3OD, 293K, 300 MHz

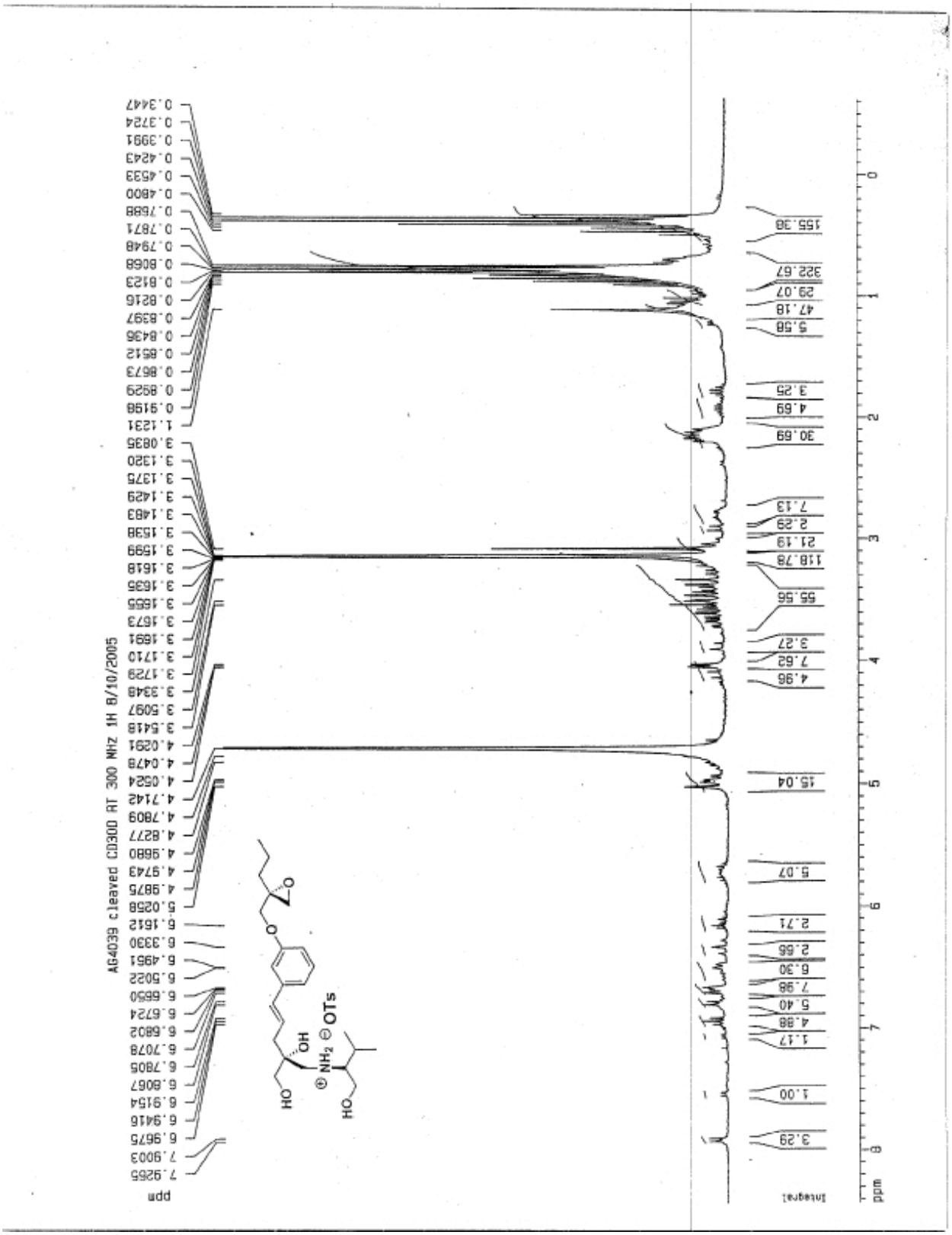

HPLC, MS, UV data for compound **119** (crude)

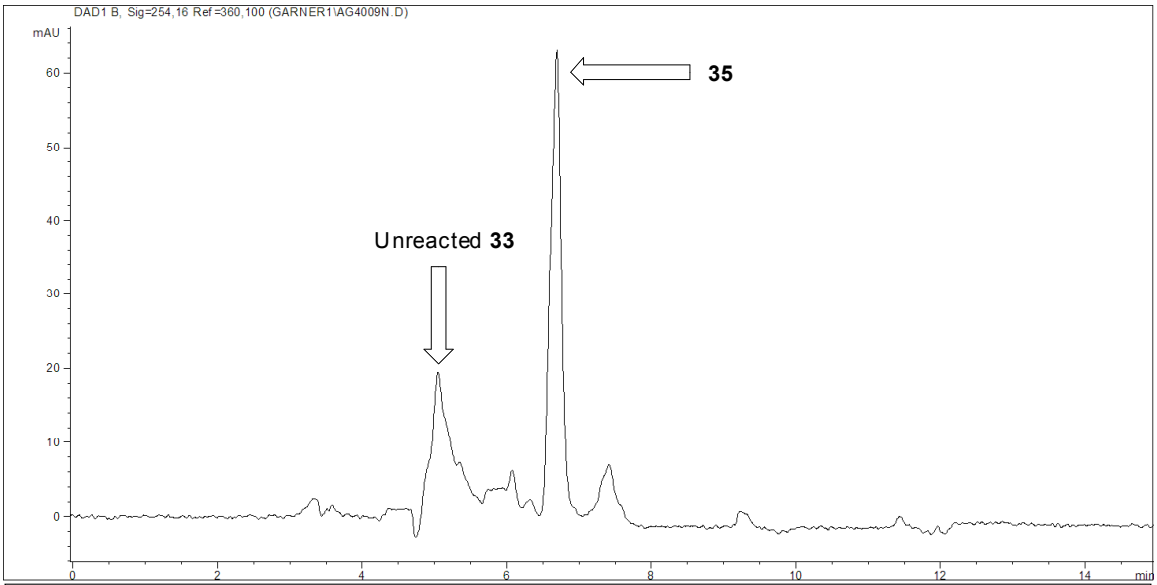

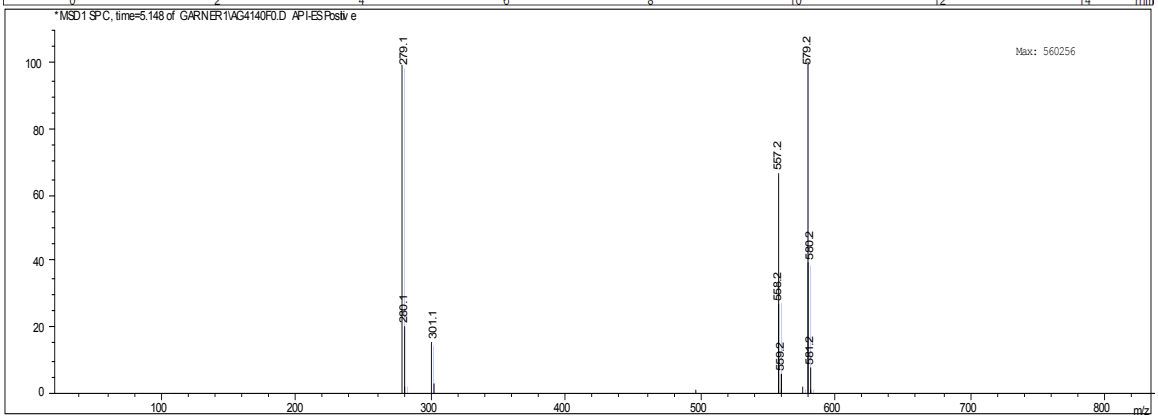

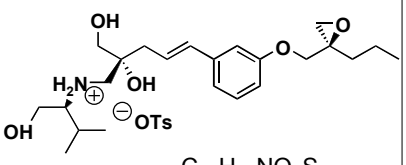

$C_{30}H_{45}NO_8S$

Mol. Wt.: 579.2

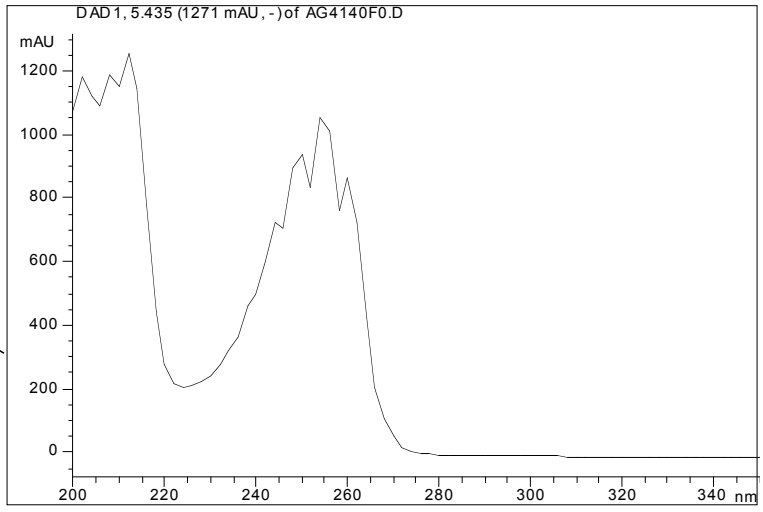

crude ^{1}H NMR spectrum of compound **120**: CD_3OD, 293K, 300 MHz

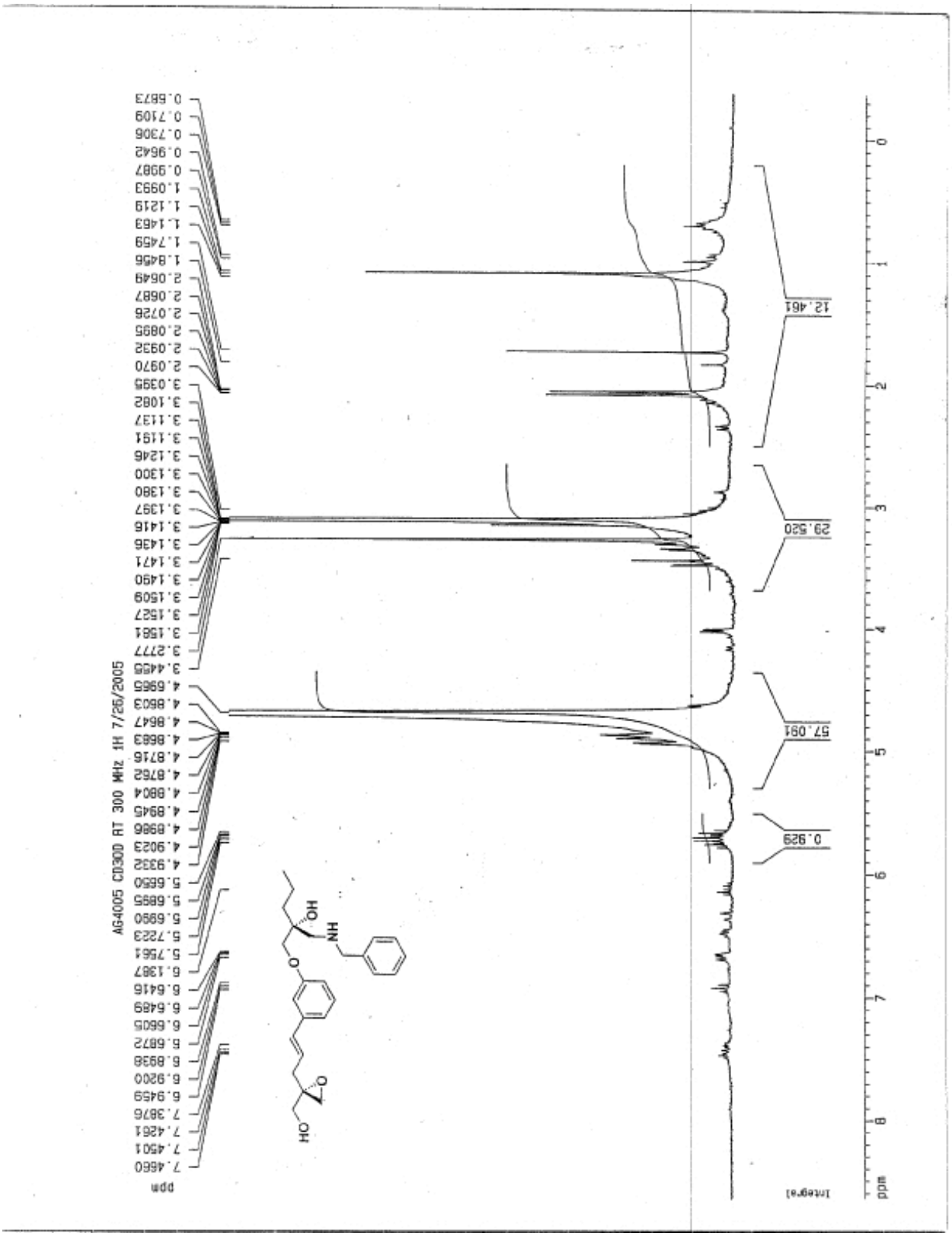

HPLC, MS, UV data for compound **120** (crude)

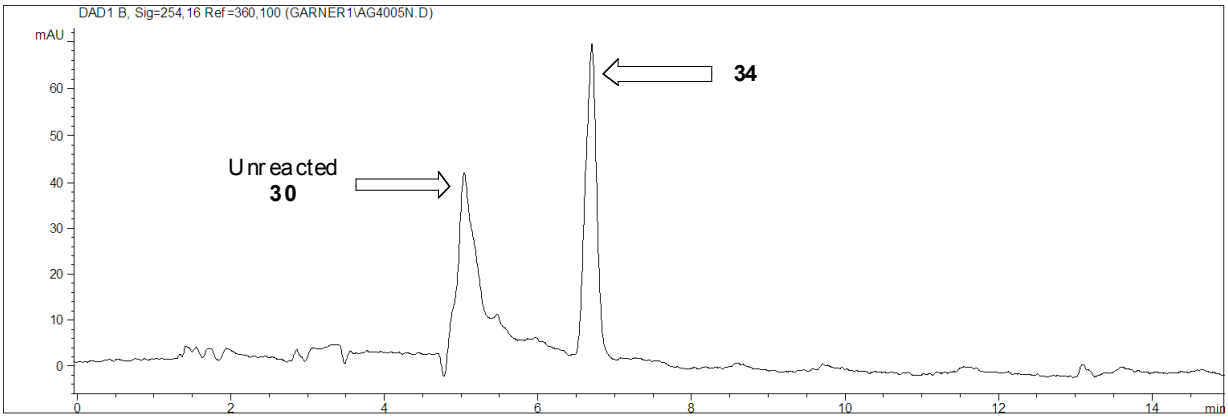

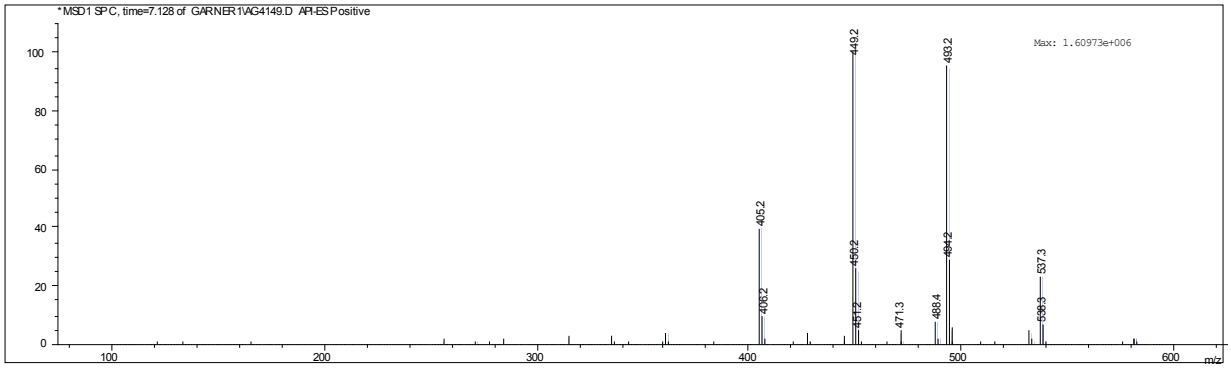

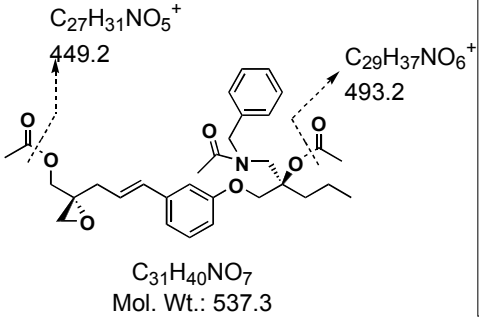

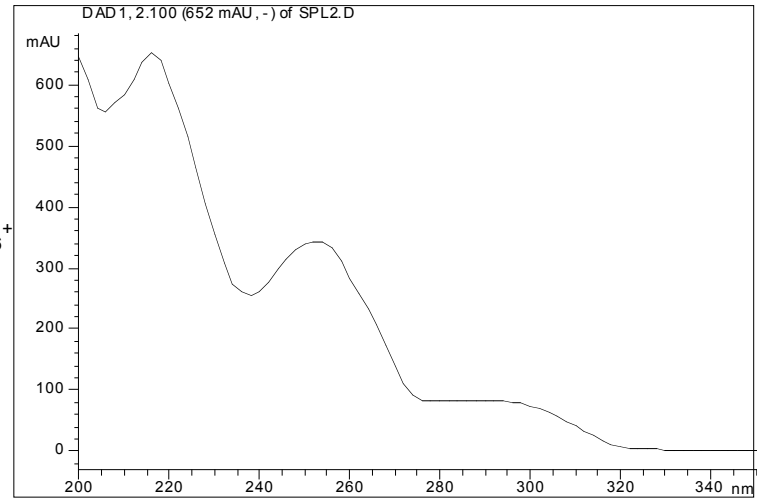

crude ^{1}H NMR spectrum of compound **121**: CD_3OD, 293K, 300 MHz

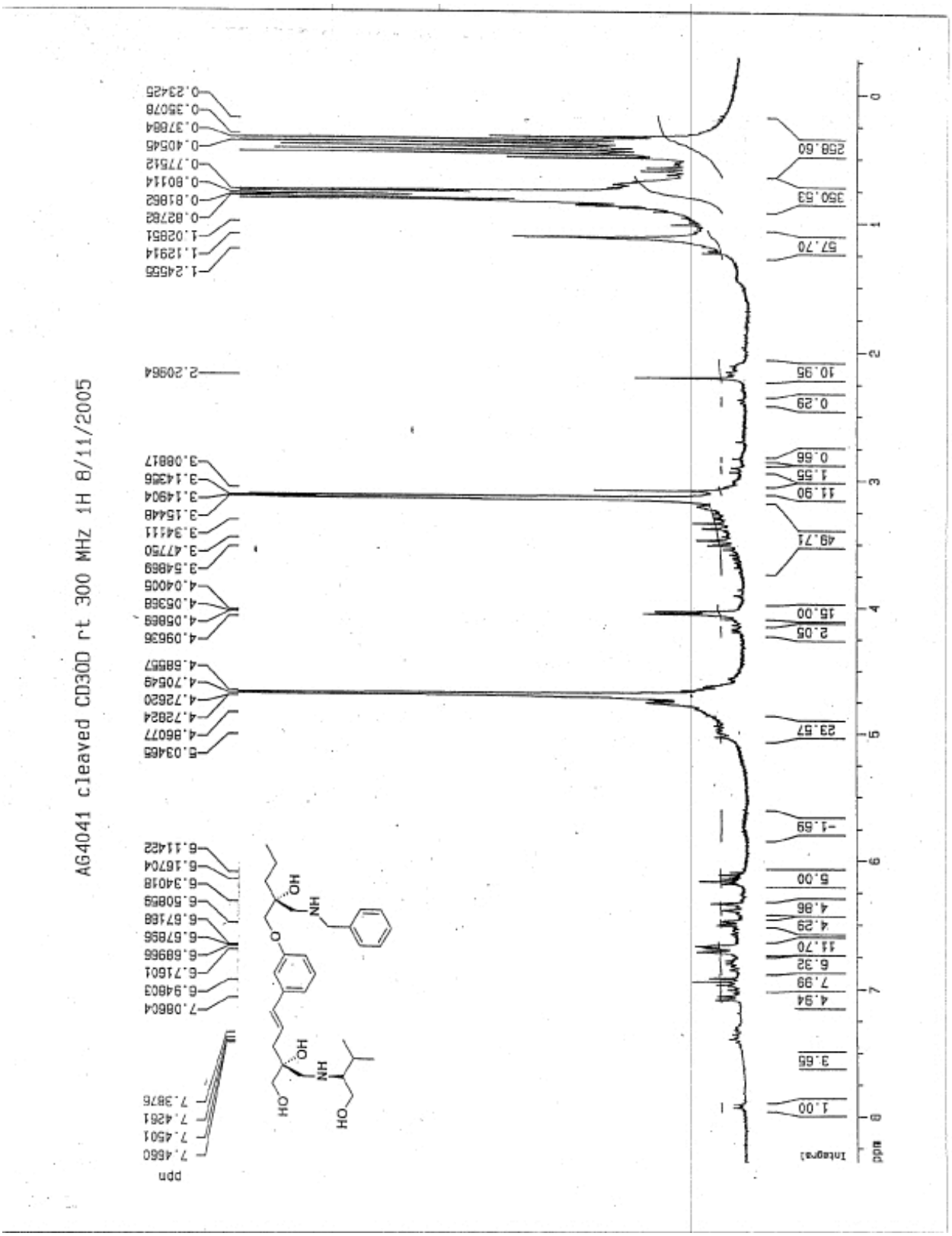

HPLC, MS, UV data for compound **121** (crude)

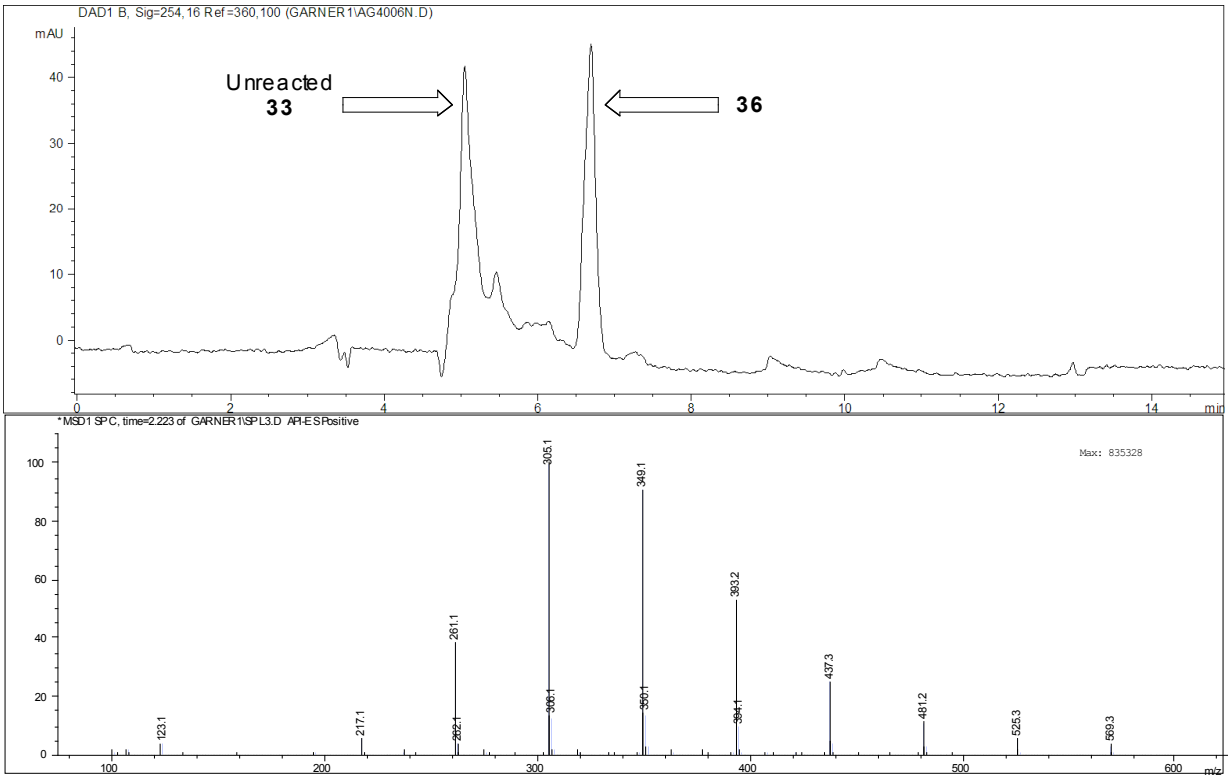

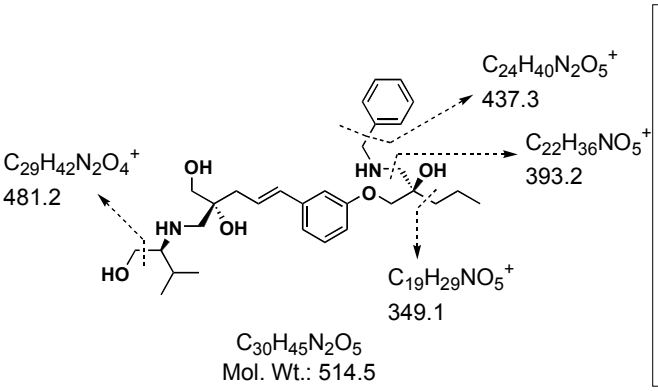

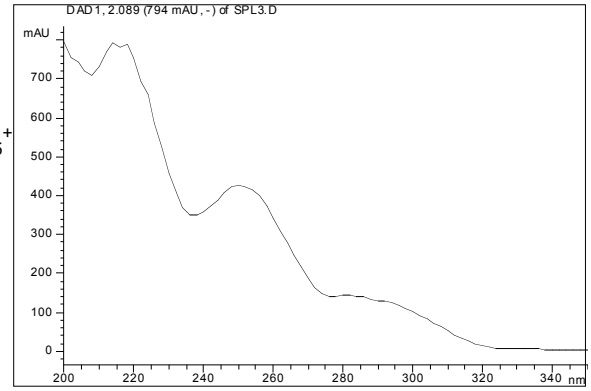

APPENDIX D

SOLID PHASE OLEFIN CROSS-METATHESIS WITH A LINKER

D.1 ^{1}H NMR AND ^{13}C NMR SPECTRA

^{1}H NMR spectrum of compound **127c** (cis and trans): 1% CD_3OD in $CDCl_3$, 293K, 300 MHz

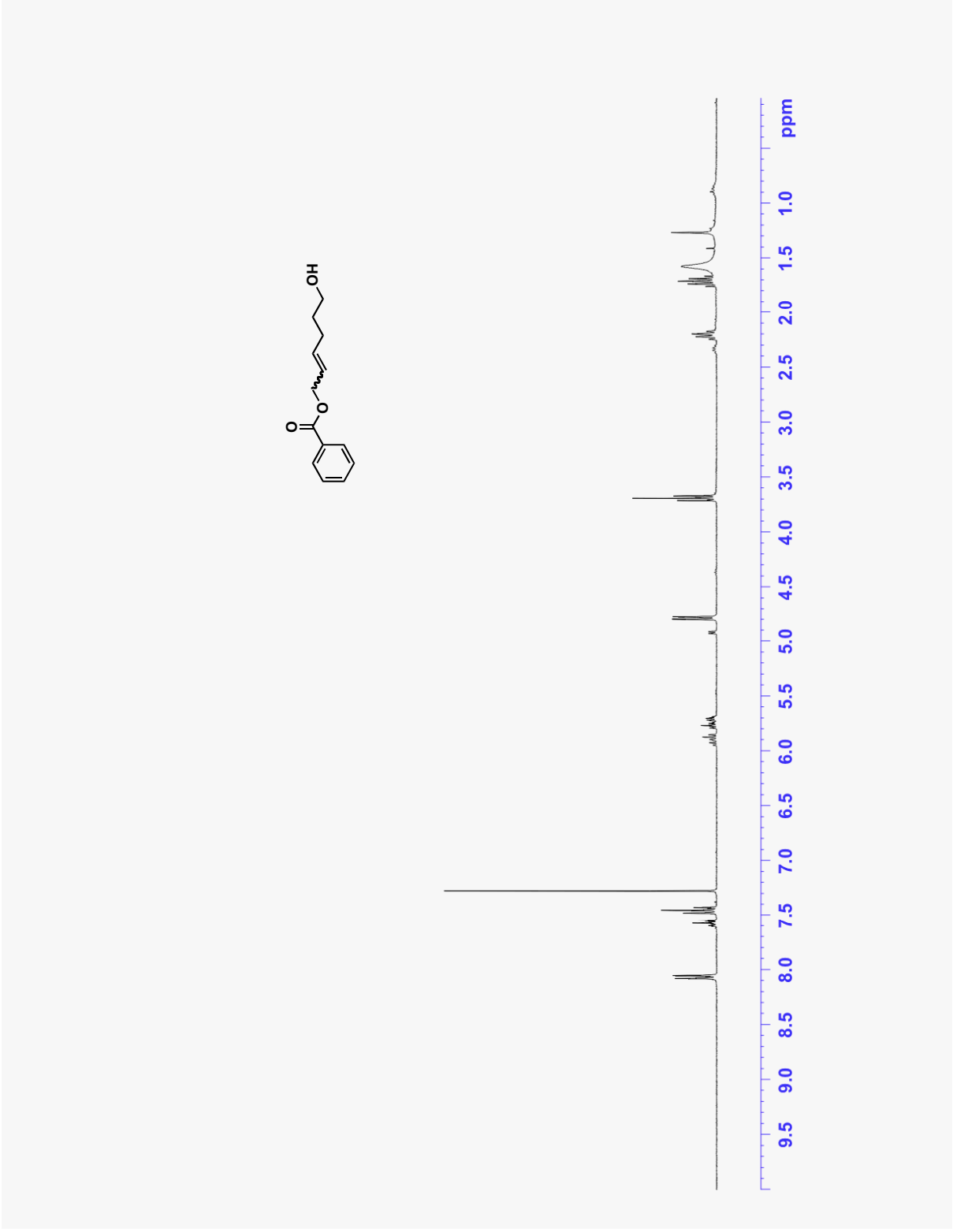

^{13}C NMR spectrum of compound **127c** (cis and trans): $CDCl_3$, 293K, 75 MHz

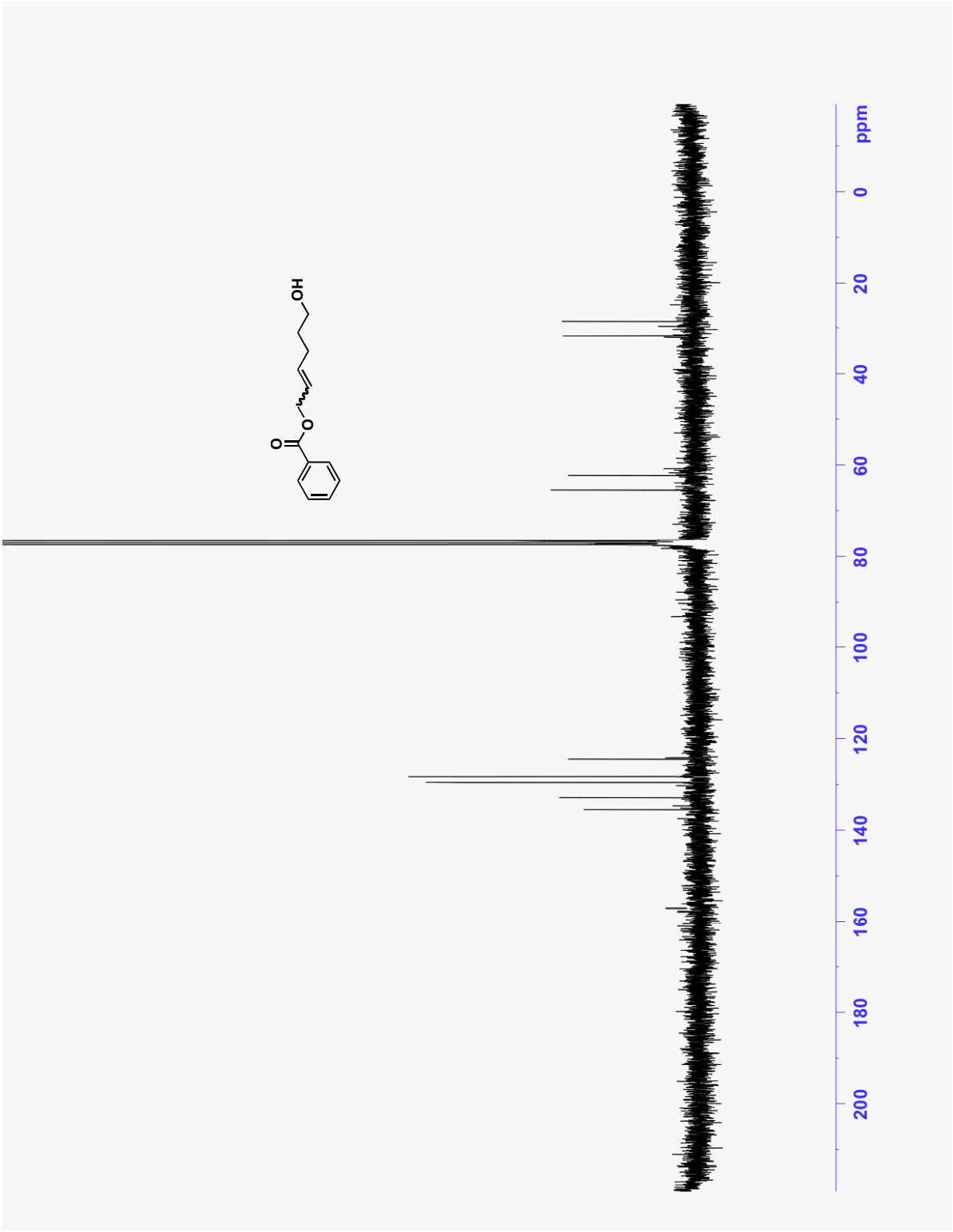

^{1}H NMR spectrum of compound **127d** (cis and trans): 1% CD_3OD in $CDCl_3$, 293K, 300 MHz

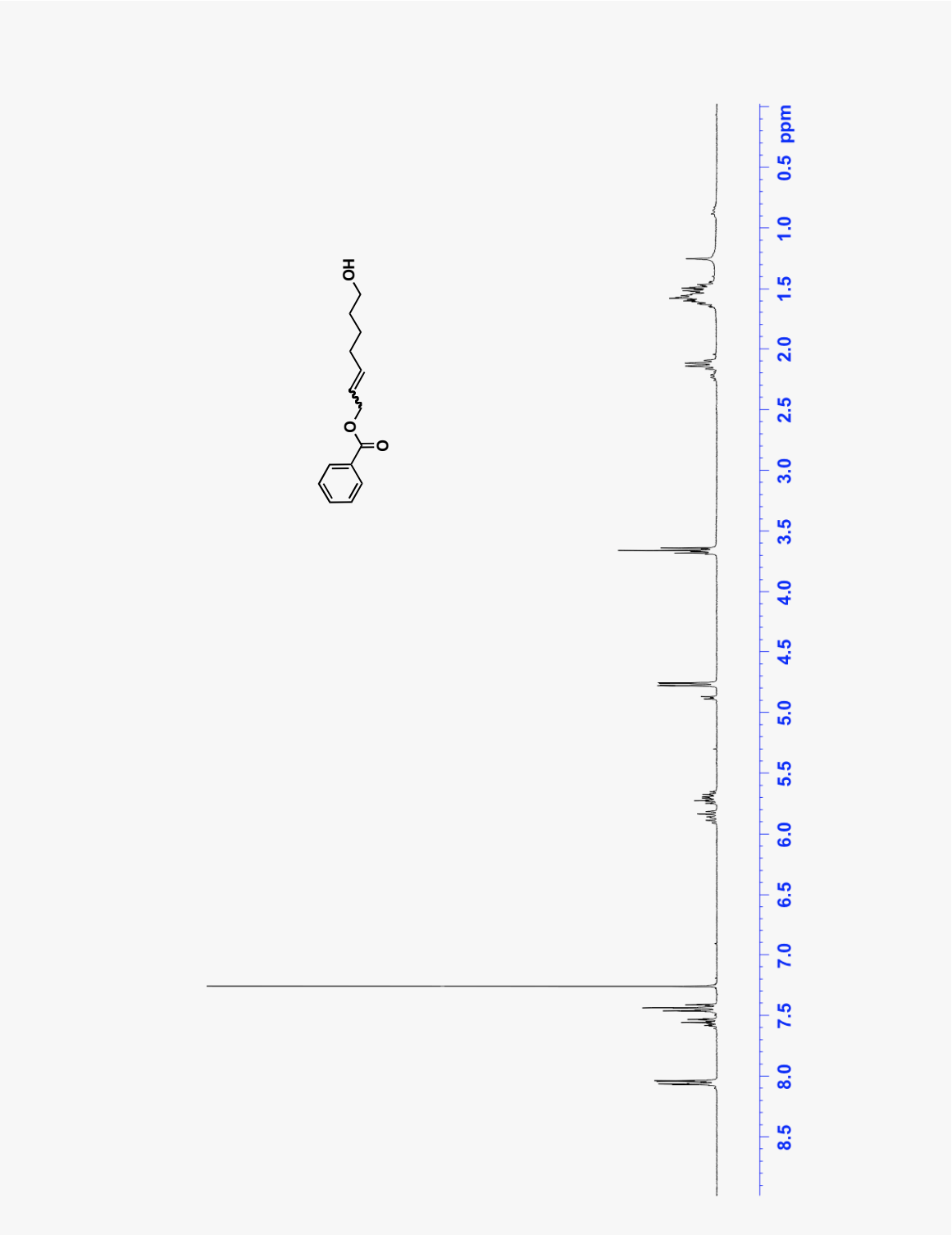

^{13}C NMR spectrum of compound **127d** (cis and trans): $CDCl_3$, 293K, 75 MHz

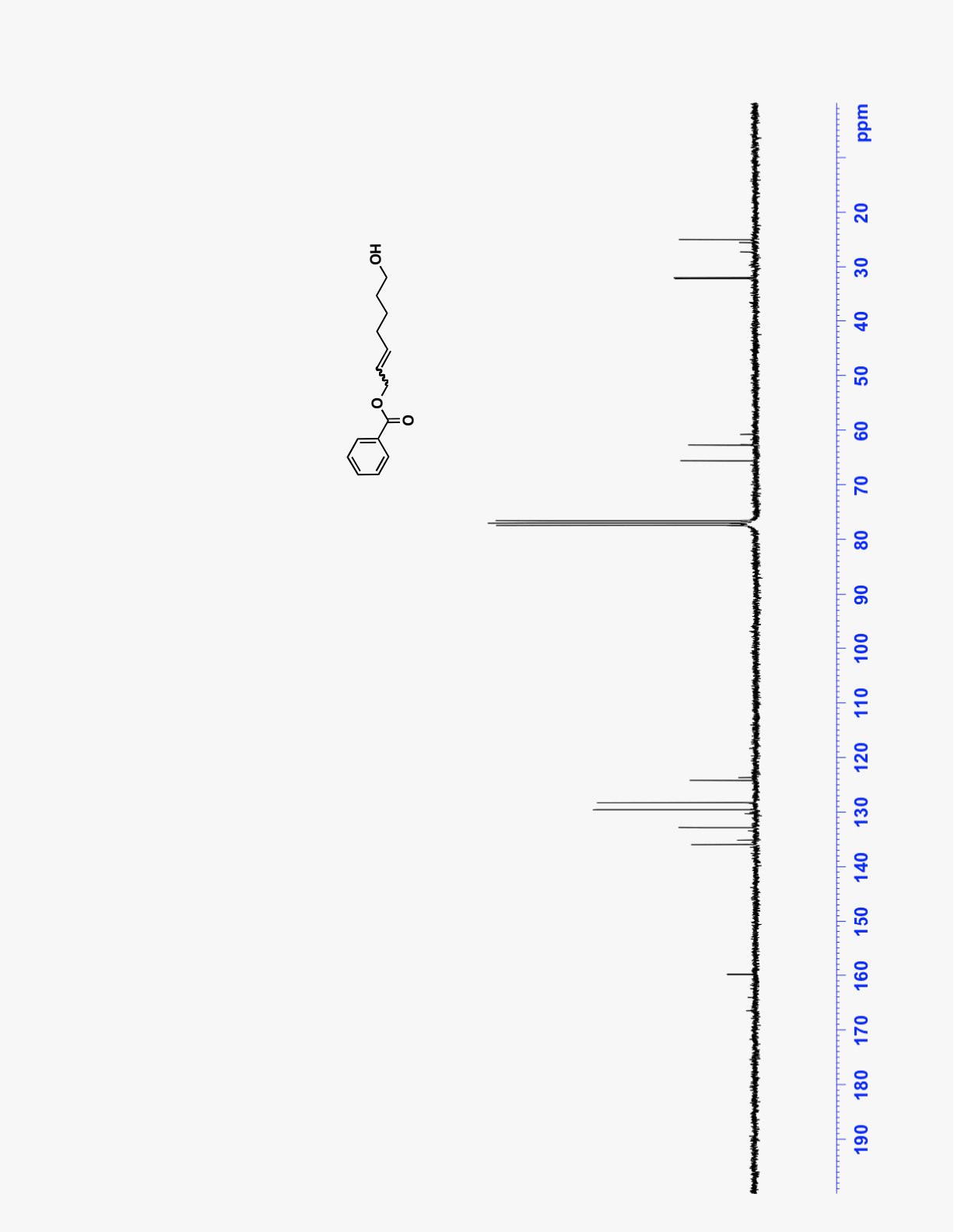

^{1}H NMR spectrum of compound **133**: 1% CD_3OD in $CDCl_3$, 293K, 300 MHz

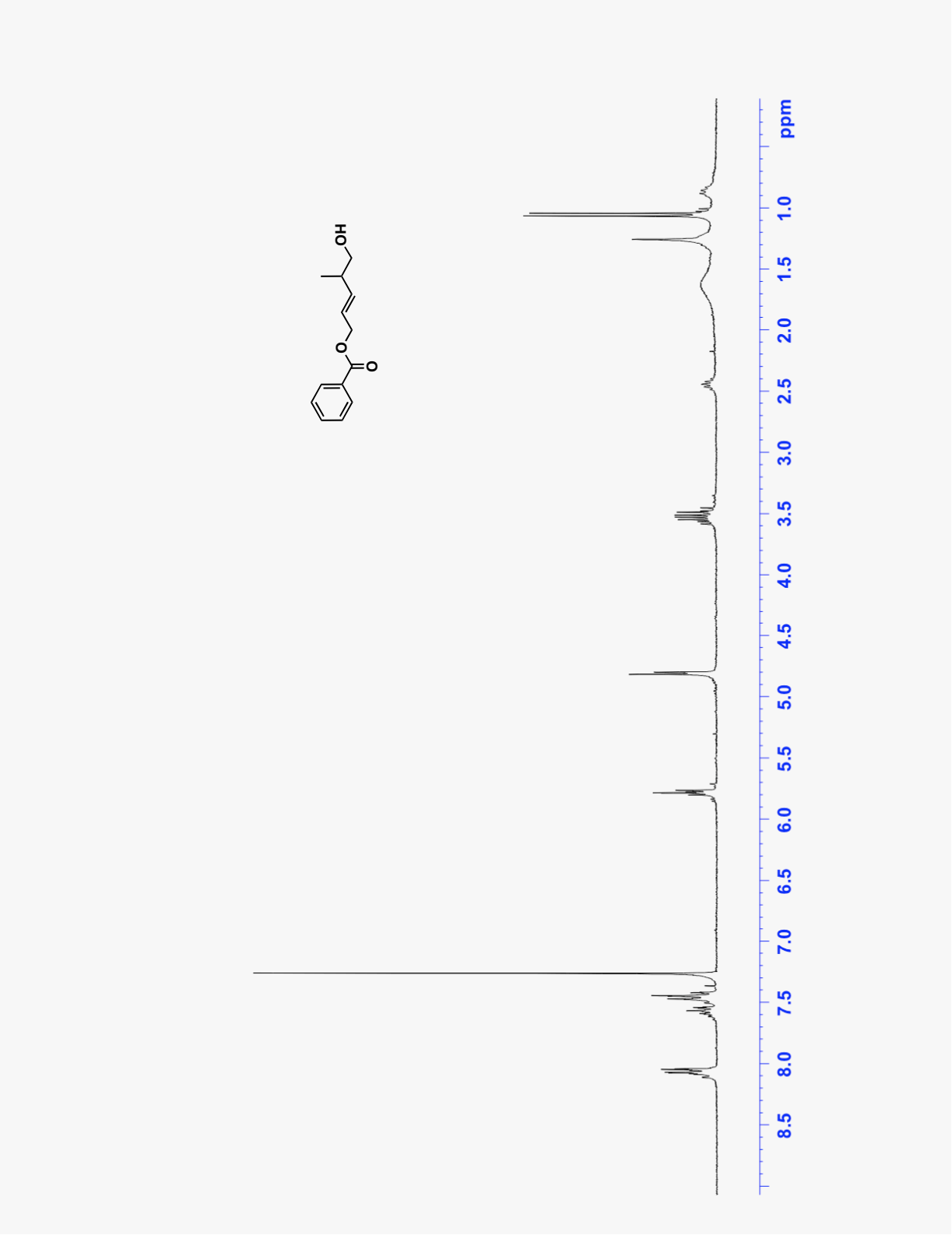

^{13}C NMR spectrum of compound **133**: $CDCl_3$, 293K, 75 MHz

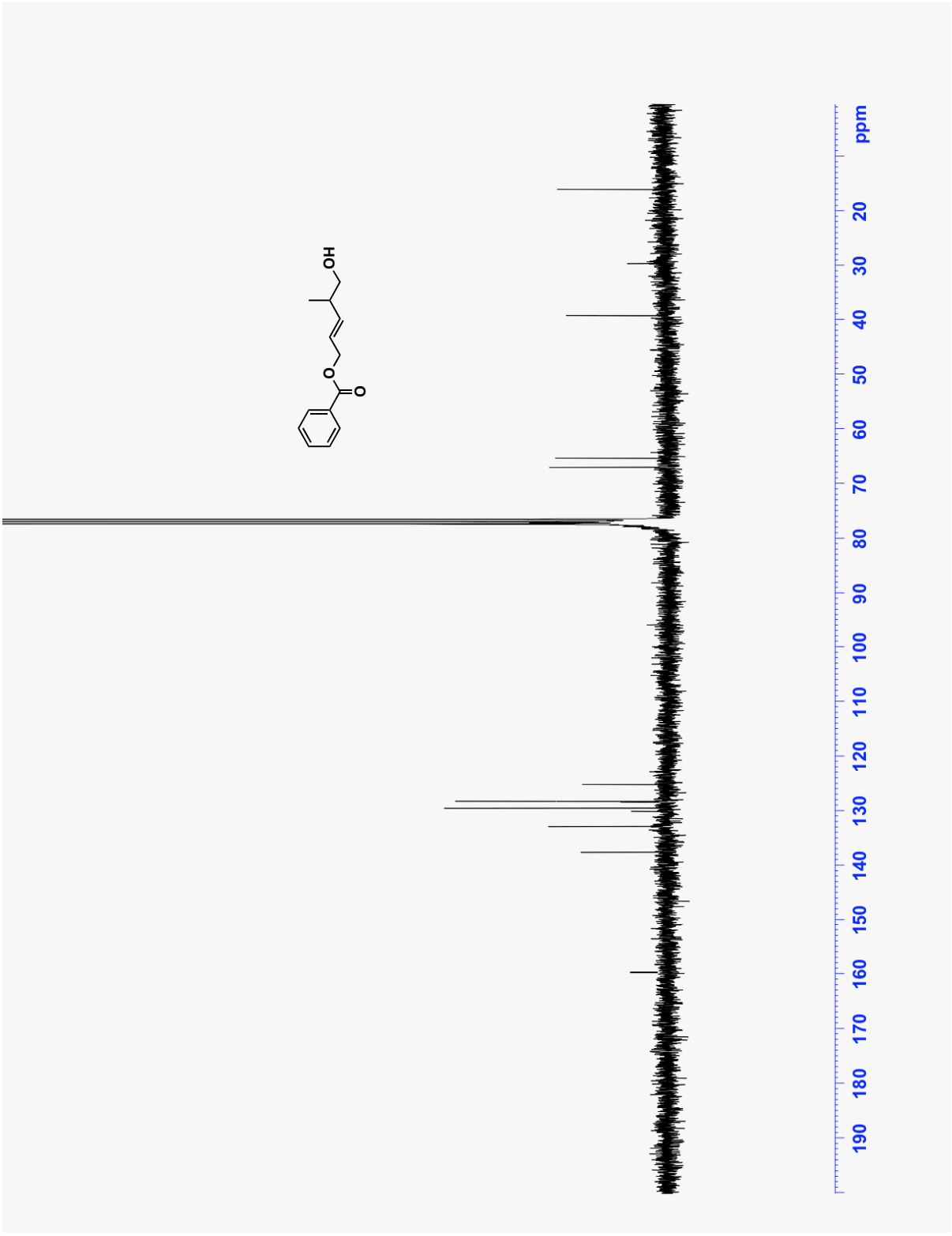

^{1}H NMR spectrum of compound **136**: 1% CD_3OD in $CDCl_3$, 293K, 300 MHz

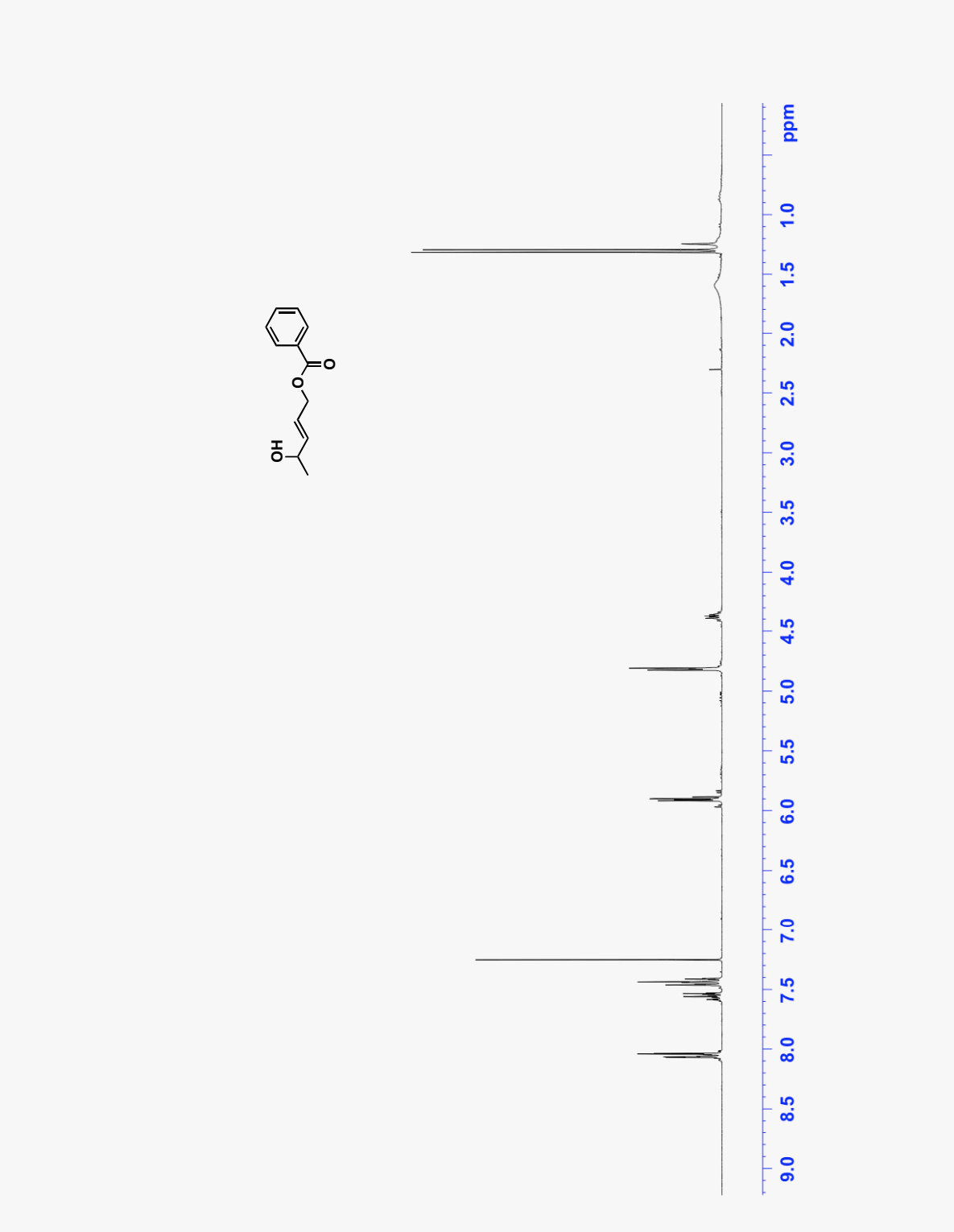

^{13}C NMR spectrum of compound **136**: $CDCl_3$, 293K, 75 MHz

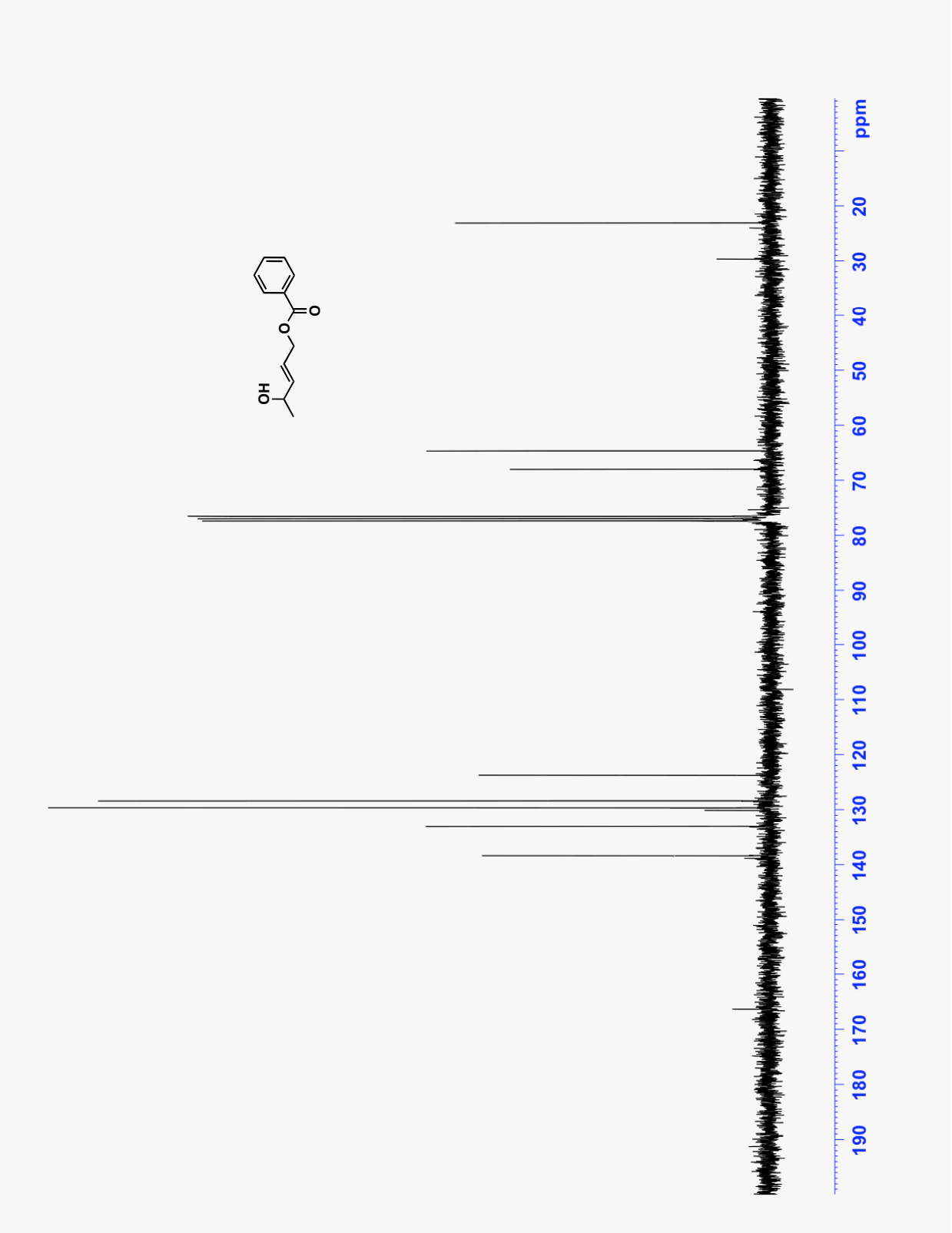

^{1}H NMR spectrum of compound **136** (cis and trans): 1% CD_3OD in $CDCl_3$, 293K, 300 MHz

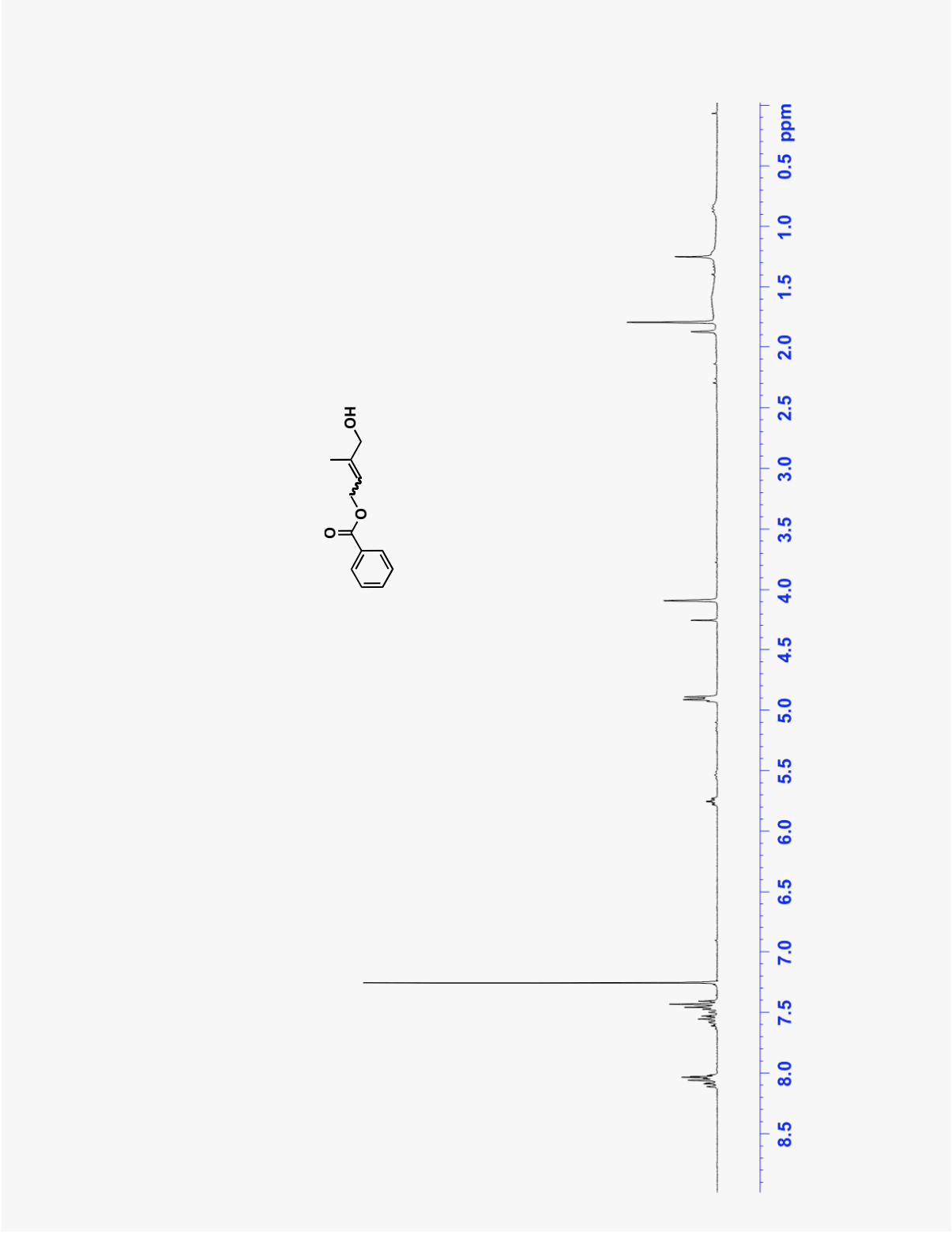

^{1}H NMR spectrum of compound **145**: $CDCl_3$, 293K, 300 MHz

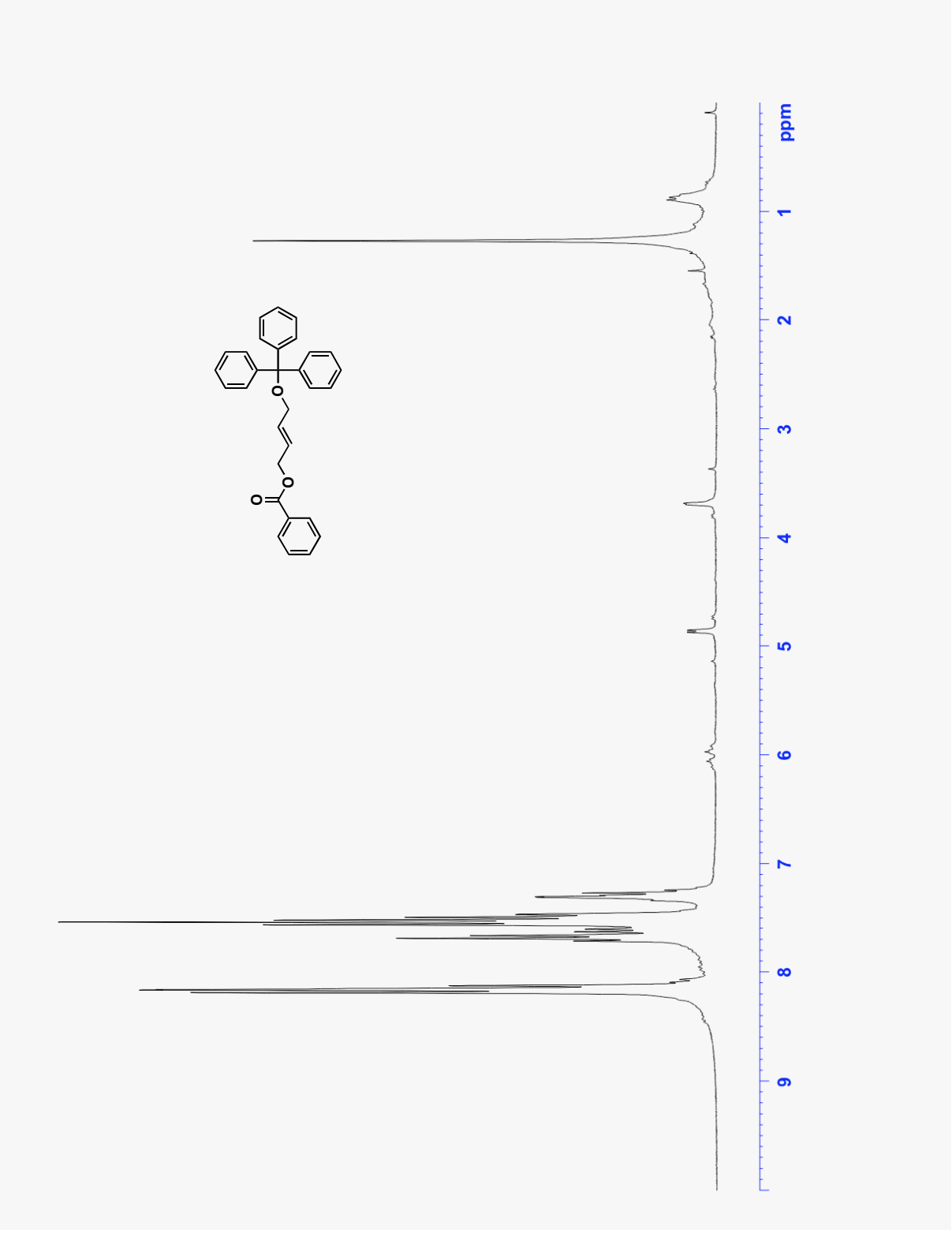

^{1}H NMR spectrum of compound **122**: d_6-DMSO, 293K, 300 MHz

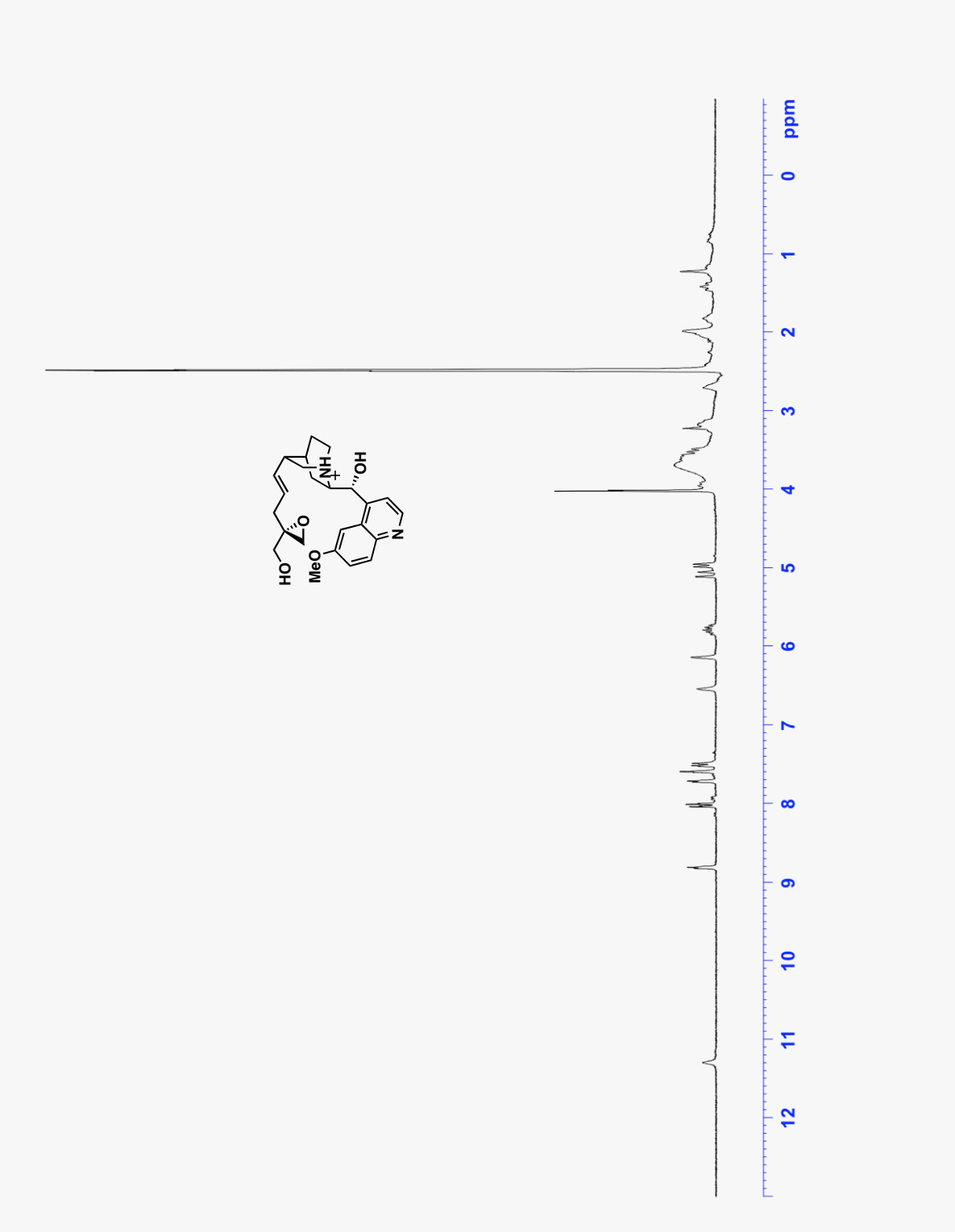

^{13}C NMR spectrum of compound **122**: 1% CD_3OD in $CDCl_3$, 293K, 75 MHz